

[illegible]

[illegible]

Table of Contents

	<u>Page</u>
Introduction.....	1
Body.....	1
Key Research Accomplishments.....	4
Reportable Outcomes.....	4
Conclusion.....	5
References.....	5
Appendices.....	6

Optimizing segmental bone regeneration using functionally graded scaffolds

INTRODUCTION

This project addresses reduction of infection risk of osseointegrated limb interfaces. The overall objective of this project is to develop clinically applicable load-bearing, anti-infective, and osteoinductive functionally graded scaffolds (FGS) as synthetic long bone grafts to treat combat-relevant segmental long bone fractures.

BODY

We propose the following set of tasks to engineer, evaluate and optimize the load bearing, anti-infective, and osteoinductive FGS.

Task 1: To develop an anti-infective CaP / chitosan FGS with multiple antibiotics and sufficient effective period to reduce and prevent infection.

Task 2: To develop an osteoinductive CaP / chitosan FGS with tunable release kinetics to enhance bone regeneration.

Task 3: To develop an anti-infective and osteoinductive CaP / chitosan FGS to reduce infection while enhancing bone regeneration.

As outlined below we have made significant progress in the tasks of the proposal. These aims include:

A photocrosslinkable, elastic chitosan based gel for sustained local delivery of BMP-2 and retaining the bone defect

In our previous studies, our team developed an injectable gel (Kim 2010, 2011, 2012) for cell and bioagent delivery, but the gels are soft and cannot retain themselves in the segmental bone defect. Recently, we have successfully developed a photocrosslinkable, elastic chitosan-based hydrogel platform which is suitable for a critical size segmental bone defect repair. **Figure 1A and B** show that the degradation rates of photocrosslinkable gels can be adjusted by different formulations and UV exposure times. The chitosan-based gel supported the growth and function of human mesenchymal stem cells (hMSCs) (**Figure 1C to F**). **Figure 1F** shows that BMP2 containing 30s-photocrosslinked gels significantly promoted osteogenesis of hMSCs compared to the medium containing the identical initial amount of BMP2. In addition, the 30s-photocrosslinked gels exhibited significantly greater osteogenesis of hMSCs compared to the 300s-photocrosslinked gels at day 5. All the data

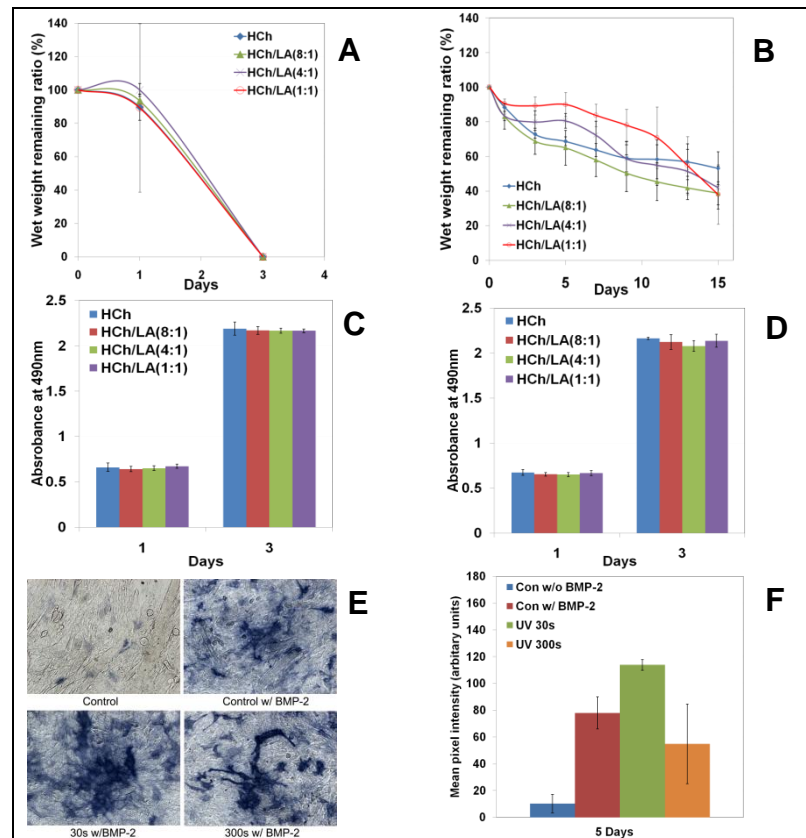


Figure 1. Characterization of a photocrosslinkable chitosan-based gel. (A) Degradation rates of photocrosslinkable gels of different ratio of chitosan to lactide with 30 s UV exposure time in PBS 7.4 with lysozyme (100ug/mL); (B) Degradation rates of photocrosslinkable gels of different ratio of chitosan to lactide with 300 s UV exposure time in PBS 7.4 with lysozyme (100ug/mL); (C) hMSCs viability within photocrosslinkable gels of different ratio of chitosan to lactide with 30 s UV exposure time; (D) hMSCs viability within photocrosslinkable gels of different ratio of chitosan to lactide with 300 s UV exposure time; (E) Alkaline phosphatase staining of hMSCs in BMP2 containing medium and BMP2 containing gels with different UV exposure times; (F) Alkaline phosphatase activity of hMSCs in BMP2 containing medium and BMP2 containing gels with different UV exposure times.

have demonstrated that the photocrosslinkable gels with different formulations and UV exposure times can control release of growth factors and the released growth factor is biologically active.

In vivo evaluation of bone regeneration aided by the promising osteoinductive gels using a load-bearing critical size segmental bone defect model

We are examining the BMP2 dosage effect on bone healing in a load-bearing critical size segmental bone defect. The experiment is on going. Figure 2 shows the radiographs of bone defects and bone healing at 2 weeks after implantation. We will sacrifice animals at 4 weeks after implantation, and then evaluate the bone healing using micro CT scan and histomorphometry.

Cytokine Combination Therapy Prediction for Bone Remodeling and Bone Healing Based on the Intracellular Signaling Pathway

We proposed to use the data generated in our co-administration of growth factor and antibiotic to establish a computation model to predict release dosage and period for improving bone healing and regeneration. Since few quantitative researches have been done to study cytokine combination for bone remodeling and bone healing, in the first step, we focused on and demonstrated a mathematical model to study the cytokine combination therapies based on the intracellular signaling pathway. The underlying molecular mechanism involved in osteoblast differentiation plays a significant role in regulating bone remodeling and bone healing. Runx2 and Osx have been found to be two crucial transcription factors in osteoblast differentiation. Their expressions are stimulated by cytokines including Wnt, BMP2 and TGF β . We developed a systematic model using a system of ODEs to describe the intracellular signaling pathway shown in **Figure 3a**, which was integrated into the dynamic cellular population. Bone regeneration or bone remodeling involves bone resorption by osteoclasts (OC) and the following bone formation by osteoblasts (OB) within basic multicellular units (BMU). Three cytokines were considered: TGF β , Wnt and BMP2. Intracellular signaling pathway consists of Smad2/3, Smad 1/5, β Catenin, and Runx2 and Osx. Runx2 can promote the differentiation of mesenchymal stem cells (MSCs) into pre-osteoblasts (OBp) and can inhibit the differentiation of pre-osteoblasts into active osteoblasts (OBa). Osx also play a promoting role in the later stage of osteoblastic lineage which interacts with osteoclastic lineage through intercellular signaling pathway RANK-RANKL-OPG. The parameters in the intracellular signaling pathways were

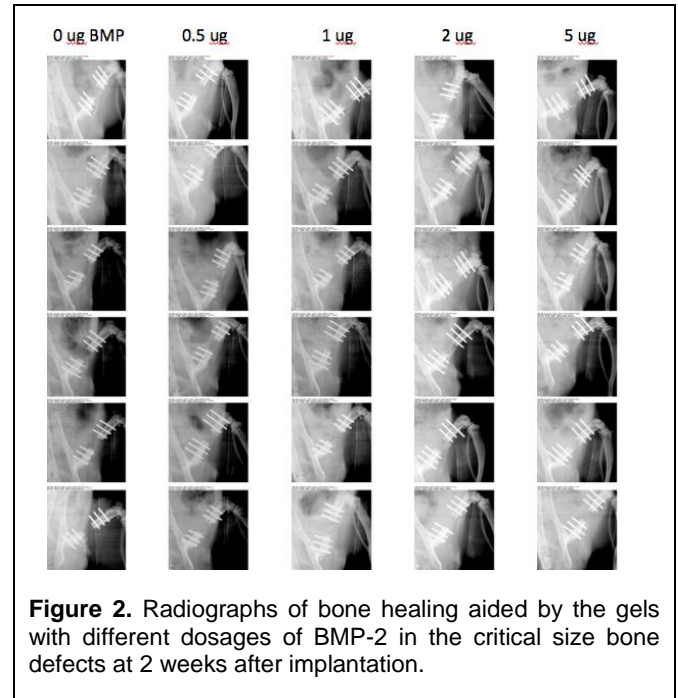


Figure 2. Radiographs of bone healing aided by the gels with different dosages of BMP-2 in the critical size bone defects at 2 weeks after implantation.

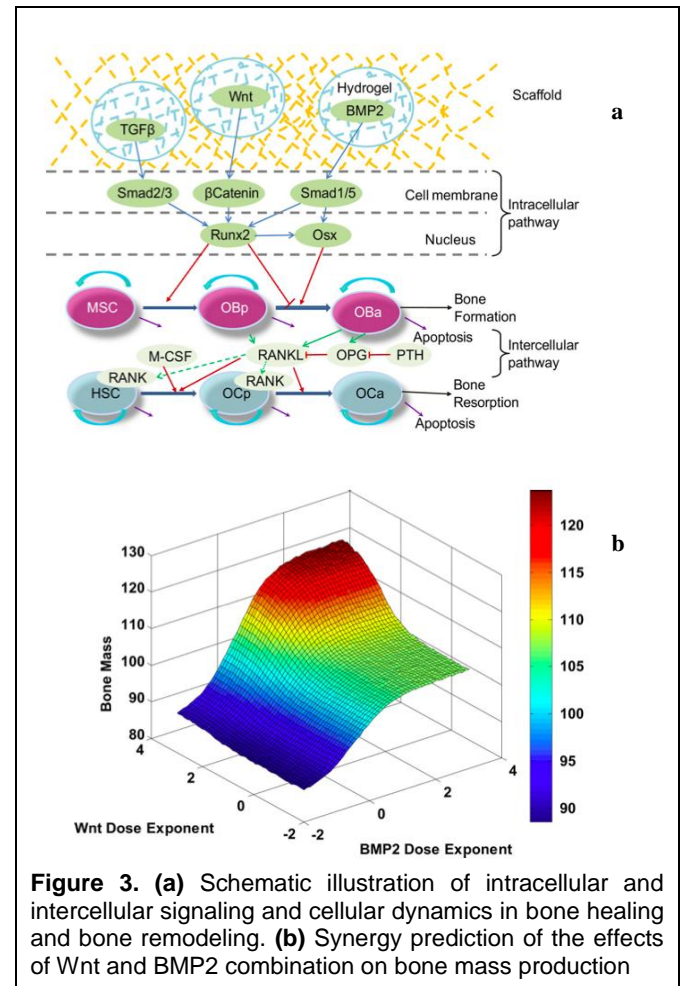


Figure 3. (a) Schematic illustration of intracellular and intercellular signaling and cellular dynamics in bone healing and bone remodeling. **(b)** Synergy prediction of the effects of Wnt and BMP2 combination on bone mass production

estimated by fitting them to the dynamic experimental data from literatures using optimization algorithm. We examined the response of bone volume to the changes of concentration of single and combined cytokines respectively during bone remodeling or bone healing. In **Figure 3b**, our simulations demonstrated that Wnt and BMP2 combination produced a greater effect than any other therapies. Moreover, they performed synergistic effect based on 5% bone growth isobologram (data not shown). Our predictions are potentially helpful to conduct the clinical drug (cytokine) combination experiments.

Synthesis and characterization of novel elastomeric poly(D,L-lactide urethane) maleate composites for use in load-bearing applications

We investigated the synthesis and characterization of a novel 4-arm poly(lactic acid urethane)-maleate (4PLAUMA) elastomer and its composites with nano-hydroxyapatite (nHA) as potential weight-bearing bone void fillers. The 4PLAUMA/nHA ratios of the composites were 1:3, 2:5, 1:2 and 1:1. FTIR and NMR characterization showed urethane and maleate units integrated into the PLA matrix. Energy dispersion and Auger electron spectroscopy confirmed homogeneous distribution of nHA in the polymer matrix.

		Polymer/HA ratio				
		1:3	2:5	1:2	1:1	1:0
Compression	Modulus (MPa)	1973.31 ± 298.53	1675.23 ± 145.83	508.63 ± 107.34	198.64 ± 41.58	-
	Strength (MPa)	78.10 ± 3.82	48.76 ± 10.34	36.37 ± 12.13	22.25 ± 4.45	-
Tension	Modulus (MPa)	3630.46 ± 528.32	1485.31 ± 442.17	822.47 ± 72.81	149.82 ± 53.62	3.70 ± 0.34
	Strength (MPa)	6.23 ± 1.44	4.25 ± 0.22	3.89 ± 0.08	2.11 ± 0.35	1.11 ± 0.16
Bending	Max strain (%)	5.33 ± 1.53	14.34 ± 0.58	22.04 ± 2.39	40.11 ± 2.07	93.33 ± 4.04
	Modulus (MPa)	1810.42 ± 86.10	1479.19 ± 224.91	310.97 ± 106.14	125.56 ± 39.46	-
Torsion	Strength (MPa)	13.00 ± 0.72	6.76 ± 1.68	4.40 ± 0.78	2.03 ± 0.54	-
	Modulus (MPa)	282.46 ± 24.91	223.37 ± 15.36	159.40 ± 38.33	46.28 ± 32.53	0.12 ± 0.01
Torsion	Strength (MPa)	5.20 ± 0.85	5.03 ± 0.33	4.33 ± 0.06	2.67 ± 1.10	0.05 ± 0.01
	Max torsion (°)	78.67 ± 9.07	174.33 ± 10.07	223.66 ± 4.17	244.67 ± 5.51	250.33 ± 11.93

Table 1. Mechanical properties of 4PLAUMA elastomer and composites. Results are given as values ± standard deviation (n=3).

Mechanical properties of the novel elastomer and its composites are shown in **Table 1**. More specifically, maximum moduli and strength of the composites of 4PLAUMA/nHA, respectively, 1973.31 ± 298.53 MPa and 78.10 ± 3.82 MPa for compression, 3630.46 ± 528.32 MPa and 6.23 ± 1.44 MPa for tension, 1810.42 ± 86.10 MPa and 13.00 ± 0.72 for bending, and 282.46 ± 24.91 MPa and 5.20 ± 0.85 MPa for torsion. The maximum tensile strains of the polymer and composites are in the range of 5% to 93%, and their maximum torsional strains vary from 0.26 to 0.90, evidencing elasticity of the material. The composites exhibited very slow degradation rates in aqueous solution shown in **Figure 4A**, from approximately 50% mass remaining for the pure polymer to 75% mass remaining for composites with high nHA contents, after a period of 8 weeks.

Increase in ceramic content increased mechanical properties, but decreased elasticity, degradation rate, and swelling of the composites because ceramic crystals stabilized the polymer network by electrostatic interactions with polar groups in the elastomer. Human bone marrow stem cells and human endothelial cells adhered and proliferated on 4PLAUMA films and degradation products of the composites showed little-to-no toxicity (**Figure 4B**). The new materials will be used for

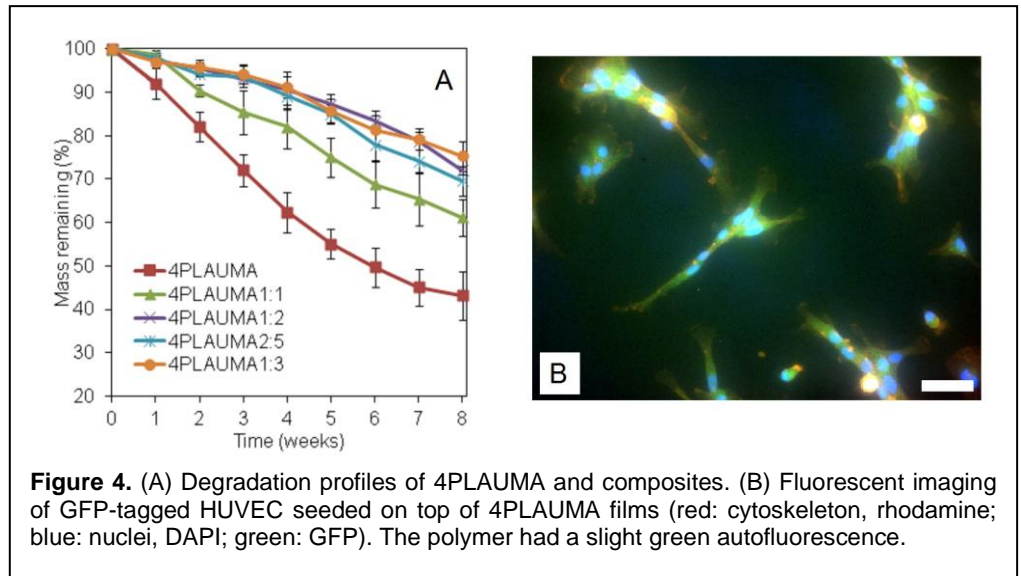


Figure 4. (A) Degradation profiles of 4PLAUMA and composites. (B) Fluorescent imaging of GFP-tagged HUVEC seeded on top of 4PLAUMA films (red: cytoskeleton, rhodamine; blue: nuclei, DAPI; green: GFP). The polymer had a slight green autofluorescence.

weight-bearing bone void fillers and evaluated in vivo.

KEY RESEARCH ACCOMPLISHMENTS

- A novel, photocrosslinkable, elastic chitosan based elastic hydrogel for segmental bone defect repair
- A computation model for prediction of optimized release profiles of multiple bioagents
- A novel elastomer and its nano-hydroxyapatite containing composite for potential load-bearing bone void filler

REPORTABLE OUTCOMES

Publications (6 TOTAL. This list only contains articles NOT included in the last progress report.)

- 1 Sungwoo Kim, Yunqing kang, Chad A. Krueger, Milan Sen, John B. Holcomb, Di Chen, Joseph Wenke, Yunzhi Yang. Sequential delivery of BMP-2 and IGF-1 using a chitosan gel with gelatin microspheres enhances osteoblastic differentiation. *Acta Biomaterialia* 2012; 8: 1768-77 (doi:10.1016/j.actbio.2012.01.009).
- 2 A.H. Nguyen, S. Kim, W. Maloney, J. Wenke, Y. Yang. Effect of co-administration of vancomycin and BMP-2 on co-cultured *Staphylococcus aureus* and W-20-17 mouse bone marrow stromal cells in vitro. *Antimicrobial Agents and Chemotherapy* 2012, 56(7): 3776–3784.
- 3 Sun X, Su J, Bao J, Peng T, Zhang L, Zhang Y, Yang Y, Zhou X. Cytokine Combination Therapy Prediction for Bone Remodeling in Tissue Engineering Based on the Intracellular Signaling Pathway. *Biomaterials*. 2012 Nov;33(33):8265-76. doi:10.1016/j.biomaterials.2012.07.041. Epub 2012 Aug 19
- 4 Yunqing Kang, Sungwoo Kim, Julius Bishop, Ali Khademhosseini, Yunzhi Yang. The osseogenic differentiation of Human Bone Marrow MSC on HUVEC-derived Extracellular Matrix (ECM) and β -TCP Scaffold, *Biomaterials* 2012; 37: 6998-7007 (<http://dx.doi.org/10.1016/j.biomaterials.2012.06.061>)
- 5 Yunqing Kang, Sungwoo Kim, Monica Fahrenholtz, Ali Khademhosseini, Yunzhi Yang. 3D porous β -TCP scaffold influences osteogenic and angiogenic potentials of monocultured and co-cultured hBMSCs and HUVECs, *Acta Biomaterialia* 2012, Aug 16. [Epub ahead of print] PMID: 22902820 (In press)
- 6 Nguyen LH, Annabi N, Nikkhah M, Bae H, Binan L, Park S, Kang Y, Yang Y, Khademhosseini A. [Vascularized bone tissue engineering: approaches for potential improvement](#). *Tissue Eng Part B Rev*. 2012 Oct;18(5):363-82. Epub 2012 Sep 4. PMID: 22765012 [PubMed - in process]

Abstracts (9 TOTAL, This list only contains abstracts NOT included in the last progress report.)

- 1 Andre H. Nguyen¹, Sungwoo Kim^{1,2}, Josh Wenke³, Yunzhi Yang. Effect of co-administration of vancomycin and BMP-2 on co-cultured *S. aureus* and bone cells *in vitro*. at the annual Hinman Student Dental Research Symposium to be held at the Peabody Hotel in Memphis, Tennessee on October 28, 29 & 30, 2011.
- 2 Sungwoo Kim, Yunqing Kang, Won Shik Chu, Monica Fahrenholtz, **Yunzhi Yang**. In vitro evaluation of sequential delivery of BMP-2 and IGF-1 for osteoblastic differentiation using a chitosan gel with gelatin microspheres. Annual conference for ORS, San Francisco, CA, Feb 2-7, 2012
- 3 Andre H. Nguyen¹, Sungwoo Kim^{1,2}, Josh Wenke³, Yunzhi Yang. Effect of co-administration of vancomycin and BMP-2 on co-cultured *S. aureus* and bone cells *in vitro*. Annual conference for ORS, San Francisco, CA, Feb 2-7, 2012.
- 4 Sungwoo Kim, Yunqing kang, Chad A. Krueger, Milan Sen, John B. Holcomb, Di Chen, Joseph Wenke, **Yunzhi Yang**. "A chitosan gel / gelatin microsphere system sequentially delivers BMP-2 and IGF-1 promoting osteoblastic differentiation " has been accepted as an oral presentation at the 9th World Biomaterials Congress (WBC) to be held in Chengdu, China, June 1-5, 2012
- 5 Andre H. Nguyen¹, Sungwoo Kim^{1,2}, Josh Wenke³, **Yunzhi Yang**. Co-administration of

- Vancomycin and BMP-2 on Staphylococcus/Bone Cell Co-culture. AADR Annual Meeting & Exhibition in Tampa, Florida, USA, March 21-24, 2012
- 6 Yang, Y. A chitosan gel / gelatin microsphere system sequentially delivers BMP-2 and IGF-1 promoting osteoblastic differentiation (ID: 2342), the 9th World Biomaterials Congress (9th WBC), Chengdu, China, June 1-5, 2012
 - 7 Sungwoo Kim, **Yunzhi Yang**. Effect of controlled release of growth factors on osteoblast response (Abstract ID#: 160842), Session Title: Cell and Tissue Response to Growth Factors/Osseointegration, 2012 IADR General Session, Iguazu Falls, Brazil, June 20-23, 2012.
 - 8 Kim, S, Kang, Y; Nguyen, A., W. Maloney, Wenke, J., **Yang, Y**. IN VITRO EVALUATION OF CO-ADMINISTRATION OF VANCOMYCIN AND BMP-2 ON CO-CULTURED STAPHYLOCOCCUS AUREUS AND BONE MARROW STROMAL CELLS. The Military Health System Research Symposium (MHSRS), Aug 13-16, Ft. Lauderdale, FL
 - 9 Yunqing Kang, Sungwoo Kim, **Yunzhi Yang**. MSCs and HUVECs Derived ECM Enhances Proliferation and Differentiation of MSCs. EMBC 2012 - 34th Annual International Conference of the IEEE Engineering in Medicine and Biology Society IEEE EMBC 2012, San Diego, Aug 29 to Sept 1, 2012.

Grant Submissions

- | | |
|---|--|
| 1 | <p>Source Army Research Office (ARO) Fiscal Year 2013 Defense University Research Instrumentation Program (DURIP)</p> <p>Title DURIP: Additive manufacturing of functionally graded scaffolds for accelerated regeneration of large segmental bone defects</p> <p>Period 01/01/2013 – 12/31/2013</p> <p>Role Principal Investigator</p> |
| 2 | <p>Source Peer Reviewed Orthopedic Research Program Translational Partner Award</p> <p>Title Synthetic bioactive membrane for accelerated single stage bone repair in large segmental bone defects (OR120016)</p> <p>Period 06/01/2013 – 05/31/2016</p> <p>Role Principal Investigator</p> |

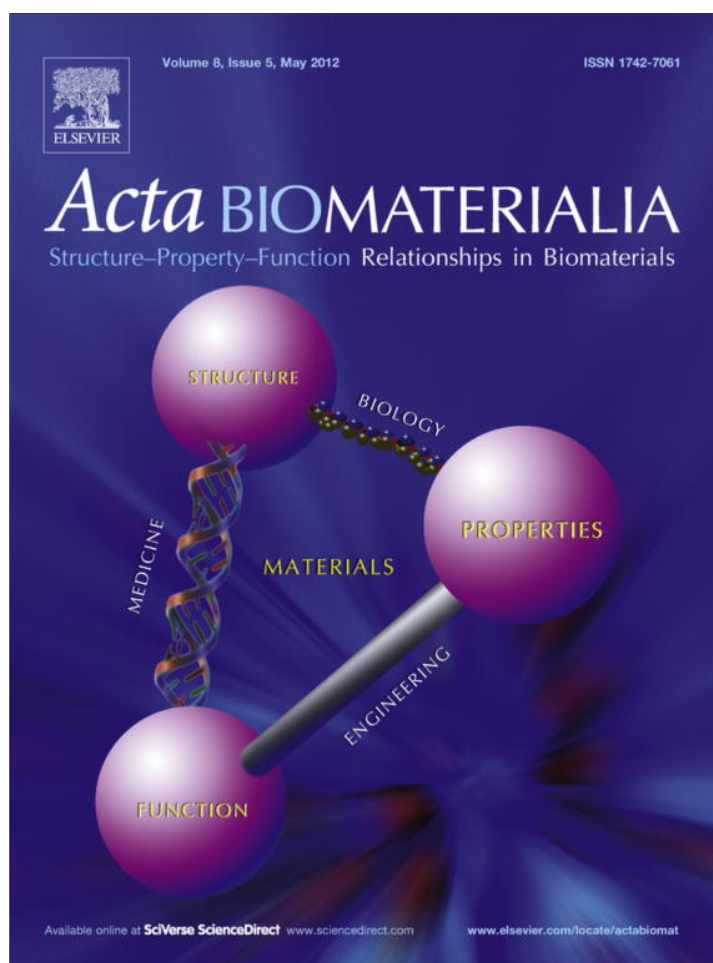
CONCLUSIONS

The project focuses on developing a promising synthetic bone graft with dual delivery characteristic. Our progress includes (1) a promising elastic hydrogel which is suitable for segmental bone defect repair; (2) a valid computation model for prediction of release profiles of multiple bioagents based on intracellular signaling pathways; and (3) development of a novel high mechanical strength, torsion and bending resistant elastomer and composite for load-bearing bone void fillers. If the prototype of the synthetic long bone grafts proves successful, the product will provide a significant benefit to the lives of individuals who have sustained combat-relevant orthopedic injuries. Injured soldiers could fully restore the function of their legs in a much shorter period of time and eventually regenerate the long bone.

REFERENCES

APPENDICES

SUPPORTING DATA
Six papers are attached.



This article appeared in a journal published by Elsevier. The attached copy is furnished to the author for internal non-commercial research and education use, including for instruction at the authors institution and sharing with colleagues.

Other uses, including reproduction and distribution, or selling or licensing copies, or posting to personal, institutional or third party websites are prohibited.

In most cases authors are permitted to post their version of the article (e.g. in Word or Tex form) to their personal website or institutional repository. Authors requiring further information regarding Elsevier's archiving and manuscript policies are encouraged to visit:

<http://www.elsevier.com/copyright>



Sequential delivery of BMP-2 and IGF-1 using a chitosan gel with gelatin microspheres enhances early osteoblastic differentiation

Sungwoo Kim^a, Yunqing Kang^a, Chad A. Krueger^b, Milan Sen^c, John B. Holcomb^d, Di Chen^e, Joseph C. Wenke^b, Yunzhi Yang^{a,*}

^a Department of Orthopedic Surgery, Stanford University, Stanford, CA, USA

^b Extremity Trauma & Regenerative Medicine Task Area, US Army Institute of Surgical Research, San Antonio, TX, USA

^c Department of Orthopedic Surgery, University of Texas Health Science Center at Houston, Houston, TX, USA

^d Center for Translational Injury Research, Department of Surgery, University of Texas Health Science Center at Houston, Houston, TX, USA

^e Department of Biochemistry, Rush University Medical Center, Chicago, IL, USA

ARTICLE INFO

Article history:

Received 25 October 2011

Received in revised form 22 December 2011

Accepted 10 January 2012

Available online 18 January 2012

Keywords:

Chitosan

Gelatin microspheres

Glyoxal

BMP-2

IGF-1

ABSTRACT

The purpose of this study was to develop and characterize a chitosan gel/gelatin microsphere (MSs) dual delivery system for sequential release of bone morphogenetic protein-2 (BMP-2) and insulin-like growth factor-1 (IGF-1) to enhance osteoblast differentiation *in vitro*. We made and characterized the delivery system based on its degree of cross-linking, degradation, and release kinetics. We also evaluated the cytotoxicity of the delivery system and the effect of growth factors on cell response using pre-osteoblast W-20-17 mouse bone marrow stromal cells. IGF-1 was first loaded into MSs, and then the IGF-1-containing MSs were encapsulated into the chitosan gel which contained BMP-2. Cross-linking of gelatin with glyoxal via Schiff bases significantly increased thermal stability and decreased the solubility of the MSs, leading to a significant decrease in the initial release of IGF-1. Encapsulation of the MSs into the chitosan gel generated polyelectrolyte complexes by intermolecular interactions, which further affected the release kinetics of IGF-1. This combinational delivery system provided an initial release of BMP-2 followed by a slow and sustained release of IGF-1. Significantly greater alkaline phosphatase activity was found in W-20-17 cells treated with the sequential delivery system compared with other treatments ($P < 0.05$) after a week of culture.

© 2012 Acta Materialia Inc. Published by Elsevier Ltd. All rights reserved.

1. Introduction

Therapeutic biomacromolecules such as RGD-like peptides and growth factors have been used to enhance the regeneration of damaged tissues by stimulating cellular activities such as cell migration, proliferation, and differentiation [1–6]. However, they have short biological half-lives in physiological conditions due to rapid degradation and deactivation by enzymes and other chemical and physical reactions [1–4]. In addition, the course of wound healing and tissue regeneration is complicated by the interactions of multiple factors [4,7–10]. Local delivery carriers have been developed for the controlled, sustained release of these active proteins [11–14]. Nevertheless, there is a great need for drug delivery systems that allow for improved release kinetics of multiple growth factors in order to enhance their therapeutic efficacy [3,8,11–17].

Recent studies have shown that the combined delivery of bone morphogenetic protein-2 (BMP-2) and insulin-like growth factor-1 (IGF-1) enhances wound healing and tissue regeneration compared

with single growth factor delivery [3,5,11,14,18]. BMP-2 is an FDA-approved growth factor, which plays an important role in the expression of osteogenic markers such as alkaline phosphatase (ALP) and osteocalcin. It is used clinically to help induce osteogenesis [3,5,15,16,19]. IGF-1 is a mitogenic factor affecting the growth of adult cells as well as supporting the growth and differentiation of embryonic cells [17,18,20–24]. It has been used to stimulate osteoblast growth and proliferation, resulting in enhanced osseointegration at the local site [10,17].

Raiche et al. used two layers of glutaraldehyde cross-linked gelatin coatings with different concentrations of growth factors to control the release kinetics of BMP-2 and IGF-1 [14,18]. They found that the sequential release of BMP-2 and IGF-1 resulted in the earliest, most robust elevation of ALP activity of both mouse pluripotent C3H and rat bone marrow stromal cells and that the simultaneous release of BMP-2 and IGF-1 did not promote ALP activity compared with BMP-2 alone. They suggested that treatment with BMP-2 upregulated the expression of the IGF-I receptor, enabling IGF-I to further enhance cell responses [14]. Similarly, Chen et al. reported that the combined delivery of BMP-2 and IGF-1 resulted in the greatest ALP activity of periodontal ligament fibroblasts

* Corresponding author. Tel.: +1 650 723 0772; fax: +1 650 724 5401.

E-mail address: ypyang@stanford.edu (Y. Yang).

(PDLFs) [11]. In their experiments, the release of growth factors was controlled by BMP-2 containing basic gelatin microspheres and IGF-1 containing acidic gelatin microspheres, which were incorporated into glycidyl methacrylated dextran (Dex-GMA) scaffolds.

We have previously developed a thermosensitive injectable chitosan gel to deliver BMP-2. It has been found to significantly enhance the osteoblastic differentiation of mouse osteoblast precursor cells and the mineralization of human embryonic palatal mesenchymal cells [25]. Chitosan gels have been used due to their excellent biocompatibility, enzyme-regulated degradation, and high efficacy of drug therapy [2,3,9,25–28]. Additionally, therapeutic agents are released via the diffusion or biodegradation of the chitosan polymers [5,25–28]. The purpose of this study was to create and characterize a sequential delivery system consisting of a chitosan gel and gelatin microspheres (MSs) to achieve a sequential release of BMP-2 and IGF-1. We hypothesized that an initial release of BMP-2 from the chitosan gel followed by the release of IGF-1 from the gelatin MSs would enhance osteoblastic activity of bone cells. In this study, we made glyoxal cross-linked gelatin MSs for delivery of IGF-1, which were then encapsulated into the chitosan gel formulation. Furthermore, we aimed to characterize the degree of cross-linking, degradation, release rate and cytotoxicity of the delivery system. We also evaluated osteoblastic activity by measuring ALP-specific activity of preosteoblast W-20-17 mouse bone marrow stromal cells.

2. Materials and methods

2.1. Materials

Chitosan (≥ 310 kDa, 75% or greater degree of deacetylation), disodium β -GP (glycerol 2-phosphate disodium salt hydrate; cell culture grade), and glyoxal (40 wt.%) were purchased from Sigma–Aldrich (St Louis, MO). Gelatin type B, olive oil, acetone, and ethanol were all purchased from Fisher Scientific (Fair Lawn, NJ). All other chemicals were reagent grade and were used as received. Human bone morphogenetic protein-2 (BMP-2) was obtained from PeproTech (Rocky Hill, NJ) and recombinant human insulin-like growth factor I (IGF-1) was purchased from R&D Systems (Minneapolis, MN). Fetal bovine serum (FBS), Trypsin–EDTA, L-glutamine, antibiotic–antimycotic, phosphate-buffered saline (PBS), and Dulbecco's modified Eagle's medium (DMEM) were all purchased from Invitrogen™ (Eugene, OR). W-20-17 cells were cultured as per American Type Culture Collection (ATCC) instructions.

2.2. Preparation of gelatin microspheres

Gelatin MSs were prepared using a water-in-oil emulsion technique. Briefly, a gelatin solution was prepared by dissolving 1 g gelatin powder in 10 ml distilled water at 50 °C. The solution was then added dropwise to 60 ml olive oil, which was preheated to 50 °C while stirring at 500 rpm using a straight-blade impeller. The gelatin solution was allowed to emulsify for 10 min. Subsequently, the entire emulsification bath was chilled to 4 °C on ice with continuous stirring at 500 rpm for 40 min, and gelatin MSs were formed. The gelatin MSs were collected by filtration and washed with chilled acetone and ethanol. Finally, the obtained gelatin MSs were freeze-dried overnight.

2.3. Cross-linking of gelatin MSs

The prepared gelatin MSs were dispersed into an aqueous ethanol solution containing different concentrations of glyoxal (10, 20, 50, or 100 mM) and stirred at room temperature for cross-linking for 10 h. The cross-linked gelatin MSs were rinsed twice with

an aqueous ethanol solution to remove the residual cross-linking agent on their surfaces and then freeze-dried overnight. They were then sieved to obtain particles ranging from 50 to 100 μ m.

2.3.1. Fourier transform infrared spectroscopy (FTIR) spectra

In order to investigate chemical structure of both gelatin MSs and cross-linked gelatin MSs, FTIR spectra were obtained using a Nicolet FTIR infrared microscope coupled to a PC with analysis software. Samples were placed in the holder directly in the IR laser beam. All spectra were recorded by transmittance mode (100 times scanning, 650–4000 cm^{-1}).

2.3.2. Degree of cross-linking

Degree of cross-linking of the gelatin MSs was determined by ninhydrin assay, which was used to determine the percentage of free amino groups remaining in the gelatin MSs after cross-linking. The cross-linked gelatin MSs were prepared with different concentrations of glyoxal (10, 20, 50, or 100 mM). The samples were heated in the ninhydrin solution at 100 °C for 10 min, and the light absorbance at 550 nm was recorded using a microplate reader (TECAN Infinite F50). Glycine (Fisher Scientific, Fair Lawn, NJ) was used as an amino acid nitrogen standard at various known concentrations. The degree of cross-linking (D_c) of the samples was calculated following the equation $D_c = [(A-B)/A] \times 100$, where A is mole fraction of free amino group in un-cross-linked gelatin MSs and B is mole fraction of free amino group in cross-linked gelatin MSs.

2.3.3. Swelling of gelatin MSs at different temperatures

To evaluate the effect of cross-linking on water stability of the gelatin MSs, the swelling characteristic of the gelatin MSs was investigated at different temperatures. The swelling of the gelatin MSs and the cross-linked gelatin MSs (50 mM) were observed using a microscope (Nikon ECLIPSE TE-2000-U). The dried samples were placed into a container with PBS (pH 7.4) and incubated at 4 or 37 °C for 3 days. Photomicrographs of the gelatin MSs were processed at 6 h, 1 day, and 3 days of incubation using MetaVue software.

2.3.4. Cytotoxicity

W-20-17 cells were grown and maintained in DMEM media with 10% FBS, 1% antibiotic/antimycotic mixture, 5 ml L-glutamine (200 mM), and sodium pyruvate. This cell line has been used in an ASTM F2131 to evaluate activity of BMP-2 in vitro. Cell culture was achieved in an incubator supplied with 5% CO_2 at 37 °C. The culture medium was changed every 3 days. In order to investigate the cytotoxicity of the gelatin MSs, the W-20-17 cells were cultured in the DMEM media containing the gelatin MSs. Cells were seeded in 24-well plates at a density of 30,000 cells per well and incubated with 10 mg of the gelatin MSs for 3 days. After incubation of 1 and 3 days, the number of viable cells was determined quantitatively using a Cell Titer 96Aqueous One Solution (MTS) assay according to the manufacturer's instructions. Before the assay, the cellular morphology was observed qualitatively using a microscope (Nikon, ECLIPSE TE-2000-U). Photomicrographs of cells were processed using Nikon MetaVue software.

2.4. Gelatin MSs encapsulated chitosan gel composites

A 1.5% (w/v) chitosan solution was prepared by stirring powdered chitosan in 0.75% (v/v) aqueous acetic acid at room temperature overnight. The insoluble particles in the chitosan solution were removed by filtration. A 50% (w/v) β -GP solution was prepared in distilled water and sterilized using PES syringe filters with 0.22 μ m pore size (Millex™, MA) and stored at 4 °C. 50 ml of chitosan solution was dialyzed at room temperature against 1 l of distilled water for 7 days with daily changes of water (1 l) in

an 8 kDa cutoff dialysis membrane to reduce the acetic acid content. The final pH value of the chitosan solution was 6.3. The dialyzed chitosan solution was autoclaved at 121 °C for 20 min, cooled down to room temperature, and stored at 4 °C. The cross-linked gelatin MSs were then encapsulated into the chitosan solution on ice and vortexed. Sterilized, ice-cold β -GP solution (2.31 M) was added drop by drop to the chitosan solution under stirring conditions in an ice bath. The final concentration of β -GP in the chitosan solution was 88 mM, and the final pH value of the chitosan gel formulation was 7.2. Each gel-forming solution was allowed to completely become a gel in an incubator for 3 h at 37 °C.

2.5. Dissolution rate

Gelatin is an amphoteric protein containing both positively charged and negatively charged amino acids. It easily dissolves in water at body temperature, releasing amino acids. In this study, the cross-linked gelatin MSs or the cross-linked gelatin MS-loaded chitosan gel were placed in a container containing 2 ml of PBS (pH 7.4) and incubated at 37 °C for 5 days. At predetermined time points, 500 μ l aliquots of the medium were sampled and the same amount of fresh PBS (pH 7.4) was added into each container. In the collected fractions, the cumulative amounts of dissolved proteins from the gelatin MSs or the combination were determined as a function of time by bicinchoninic acid (BCA) assay (Pierce, Rockford, IL). The optical density of each sample was determined using a microplate reader at 562 nm (TECAN Infinite F50).

2.6. Scanning electron microscopy (SEM)

The surface morphology of the materials was observed to examine compatibility of gelatin MSs with a chitosan gel after implantation at body temperature. Three different materials, i.e. a chitosan gel, an un-cross-linked gelatin MS-loaded chitosan gel, and a cross-linked gelatin MS-loaded chitosan gel, were prepared. They were incubated at 37 °C for 5 h and lyophilized overnight (Freezone, LABCONCO). The samples were sputter-coated with gold and examined under a scanning electron microscope (FEI, USA) operated at 15 kV.

2.7. In vitro release studies

2.7.1. IGF-1 release

In vitro IGF-1 release profiles from cross-linked gelatin MSs or a cross-linked gelatin MS-loaded chitosan gel were examined for 1 week. IGF-1 loading was achieved by a method of adsorption. The cross-linked gelatin MSs were loaded with IGF-1 by swelling in aqueous IGF-1 solutions (IGF-1(MSs)). IGF-1 (isoelectric point (IEP) = 8.6) is positively charged, and therefore, negatively charged type B gelatin forms a polyionic complexation with IGF-1 [23,29–31]. IGF-1 solution was dripped onto the microparticles at a volume of 25 μ l per mg of the cross-linked gelatin MSs. The resulting mixture was vortexed and incubated at 4 °C for 10 h before freeze-drying. Eventually, 50 ng ml⁻¹ of IGF-1 was present within each sample (IGF-1(MSs)). The IGF-1-loaded gelatin MSs were then encapsulated into a chitosan gel formulation (IGF-1(gel + MSs)). The IGF-1 loaded microparticles were added into the chitosan gel formulation on ice and vortexed. 88 mM of cold β -GP solution was added into the mixture to complete the gel-forming solution. Each gel-forming solution was allowed to completely become a gel in an incubator at 37 °C.

IGF-1(MSs) or IGF-1(gel + MSs) was placed in a container containing 2 ml of PBS (pH 7.4) and incubated at 37 °C for a week. At designated time points, 300 μ l aliquots of the release medium were sampled and the same amount of fresh PBS (pH 7.4) was added into each container. In the collected fractions, the cumulative release

amounts of IGF-1 from the materials were determined as a function of time by an IGF-1 ELISA kit (RayBio, GA). Briefly, 100 μ l of the obtained samples were pipetted into a 96-well IGF-1 microplate coated with anti-human IGF-1 and incubated at 4 °C overnight. After washing each well with wash buffer provided by the ELISA kit for a total of four washes, 100 μ l of biotinylated anti-human IGF-1 was added to each well and incubated at room temperature for 1 h. After repeating the washing step, each well was filled with 100 μ l of horseradish peroxidase–streptavidin solution and incubated at room temperature for 45 min. After the washing step, 100 μ l of TMB (3,3',5,5' tetramethylbenzidine) was added to each well and incubated for 30 min at room temperature in the dark. Finally, 50 μ l of stop solution was added into each well. The optical density of each well was determined using a microplate reader at 450 nm (TECAN Infinite F50).

2.7.2. BMP-2 release

The in vitro BMP-2 release profile from the chitosan gel was investigated for 1 week. BMP-2 solution was added directly into the chitosan solution on ice and vortexed. 88 mM of cold β -GP solution was added into the mixture to complete the gel-forming solution. Each gel-forming solution containing BMP-2 was allowed to completely become a gel in an incubator at 37 °C. Eventually, 50 ng ml⁻¹ of BMP-2 was present within each sample (BMP-2 (Gel)).

BMP-2 (Gel) was placed in a container containing 2 ml of PBS (pH 7.4) and incubated at 37 °C for a week. At designated time points, 300 μ l aliquots of the release medium were sampled and the same amount of fresh PBS (pH 7.4) was added into each container. In the collected fractions, the cumulative release amounts of BMP-2 from the chitosan gels were determined as a function of time by a BMP-2 ELISA kit (R&D systems, MN). Briefly, 50 μ l of the obtained supernatant was pipetted into a 96-well BMP-2 microplate coated with a mouse monoclonal antibody and incubated for 2 h at room temperature. After washing each well with wash buffer provided by the ELISA kit for a total of four washes, 200 μ l of BMP-2 conjugate was added to each well and incubated at room temperature for 2 h. After repeating the washing step, each well was filled with 200 μ l of BMP-2 substrate and incubated at room temperature for 30 min in the dark. Finally, 50 μ l of stop solution was added into each well. The optical density of each well was determined using a microplate reader at 450 nm with a correction setting of 540 nm (TECAN Infinite F50).

2.8. In vitro analysis

2.8.1. Effect of growth factors on ALP specific activity of W-20-17

To better evaluate the sequential delivery of growth factors on the cell responses, we first established a growth factor–cell response calibration model. We studied ALP activity as an indicator of early osteoblastic differentiation to designated singular or combination of BMP-2 and IGF-1 listed in Table 1. In this experiment, W-20-17 cells were treated with growth factors (BMP-2, IGF-1, or combinations), and ALP activity and double stranded DNA (dsDNA) of W-20-17 cells were determined. The cells were seeded in 24-well plates at a density of 30,000 cells per well and cultured for 7 days. On days 1 and 3, 50 ng ml⁻¹ of each growth factor or their combination was added into the culture medium as shown in Table 1. The culture medium was changed every 3 days.

At designated time points (5 and 7 days) the medium was removed from the cell culture. The cell layers were washed twice with PBS (pH 7.4) and then lysed with 1 ml of 0.2% Triton X-100 and three freeze–thaw cycles, which consisted of freezing at –80 °C for 30 min immediately followed by thawing at 37 °C for 15 min. 50 μ l aliquots of the cell lysates were sampled and added to 50 μ l of working reagent in a 96-well assay plate. The working reagent contains equal parts (1:1:1) of 1.5 M 2-amino-2-methyl-

Table 1

The group designs for the effect of soluble growth factors on alkaline phosphatase (ALP) specific activity of W-20-17 cells.

	A	B	C	D	E	F	G	H
Day 1	N/A	BMP-2	IGF-1	BMP-2	IGF-1	BMP-2/IGF-1	BMP-2	IGF-1
Day 3	N/A	BMP-2	IGF-1	BMP-2/IGF-1	BMP-2/IGF-1	BMP-2/IGF-1	IGF-1	BMP-2

Table 2

The group designs for the effect of sequential delivery systems on alkaline phosphatase (ALP) specific activity of W-20-17 cells.

	A	B	C	D
Gelatin MSs	N/A	N/A	N/A	IGF-1
Chitosan gel	N/A	BMP-2	BMP-2/IGF-1	BMP-2

1-propanol (Sigma), 20 mM p-nitrophenyl phosphate (Sigma), and 1 mM magnesium chloride. The samples then were incubated for 1 h at 37 °C. After incubation, the reaction was stopped with 100 μ l of 1 N sodium hydroxide on ice. ALP activity was determined from the absorbance using a standard curve prepared from p-nitrophenol stock standard (Sigma). The absorbance was measured at 405 nm using a microplate reader (TECAN Infinite F50).

The cell lysates were then examined for dsDNA to estimate cell number. 50 μ l aliquots of the cell lysates were added in a 96-well assay plate. Each 50 μ l of a 1:200 dilution of PicoGreen (Quant-iT PicoGreen assay kit, Invitrogen) was added to each well and incubated for 5 min in the dark. The assay plate was read at 485 nm excitation and 530 nm emission using a BioTek FLx800 plate reader. The dsDNA content was calculated using a standard curve made by a provided dsDNA standard sample. The ALP activity of cells was then calculated by normalizing to dsDNA content. ALP specific activity was expressed as nmol p-nitrophenol ng⁻¹ dsDNA.

2.8.2. Effect of growth factors by sequential delivery systems on ALP specific activity of W-20-17

The effect of sequential delivery of growth factors on ALP specific activity of W-20-17 was investigated using the chitosan gel or the gelatin MS-loaded chitosan gel as shown in Table 2. Indirect culture via BD BioCoat™ Control Cell Culture inserts was used as a model system to evaluate the cell responses from the materials. The materials loaded with growth factors were placed in the upper chamber of inserts. Cells were seeded in the bottom of 12-well plates at a density of 30,000 cells per well and cultured for 7 days. The culture medium was changed every 3 days. At designated time points (5 and 7 days), the medium was removed from cell culture. ALP activity and dsDNA content were determined as described above.

2.9. Statistical analysis

All data are presented as mean \pm standard deviation. For comparing two groups of data, a Student's *t*-test was performed. For comparing multiple groups of data, one-way ANOVA was performed followed by Dunnett's test. The differences in groups and experimental time points were considered significant if $P < 0.05$.

3. Results

3.1. Cross-linking of gelatin MSs

3.1.1. FTIR spectra of gelatin MSs

The FTIR spectra obtained from the gelatin MSs and the cross-linked gelatin MSs are shown in Fig. 1. The gelatin shows the typical specific amide bands of proteins. The amide I band peaking at

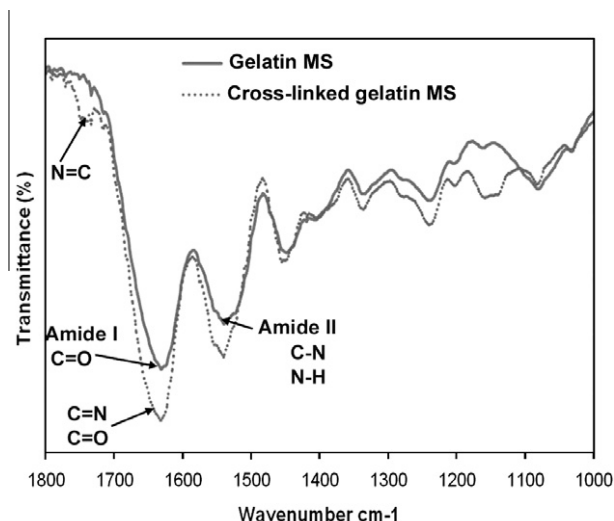


Fig. 1. FTIR spectra of gelatin microspheres and cross-linked gelatin microspheres. The cross-linking occurred through the formation of Schiff base linkage between amino groups of the gelatin and carbonyl groups of glyoxal.

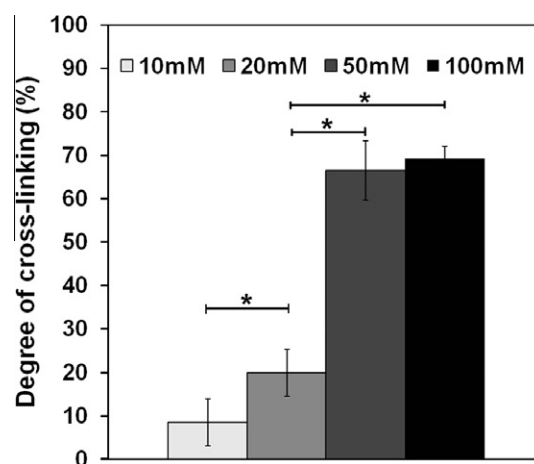


Fig. 2. The degree of cross-linking of the gelatin microspheres. The cross-linked gelatin microspheres were prepared according to different concentrations of glyoxal (10, 20, 50, or 100 mM). The percentage of free amino groups remaining in the gelatin microspheres was determined by a ninhydrin assay at 550 nm after cross-linking. Each value represents the mean \pm SD ($n = 4$). *denotes significant difference between groups ($P < 0.05$).

1620 cm⁻¹ is due to C=O stretching vibration, while the amide II band at 1535 cm⁻¹ is assigned to C-N stretching and N-H bending vibration. In the cross-linked gelatin MSs, the stronger band centered at 1635 cm⁻¹ is due to C=N stretching vibration from Schiff bases, and C=O stretching from the mixture of amide I and unreacted aldehyde groups. The Schiff bases were formed between α -amino groups of the gelatin and carbonyl groups of glyoxal [27,32,33] as a result of cross-linking. The peak at 1540 cm⁻¹ indicates a shift in the amide II band, which becomes stronger after the cross-linking. The absorbance at 1735 cm⁻¹ is due to C=N stretching vibration from Schiff-base reactions.

3.1.2. Degree of cross-linking of gelatin MSs

The gelatin MSs had a dark-yellow color after cross-linking with glyoxal. As shown in Fig. 2, the degree of cross-linking significantly increased with increasing concentration of glyoxal ($P < 0.05$). The degree of cross-linking was 8% at 10 mM, 19% at 20 mM, 66% at 50 mM, and 69% at 100 mM of glyoxal. However, there was no significant difference between 50 and 100 mM of glyoxal ($P = 0.5$).

3.1.3. Swelling of gelatin MSs at different temperatures

Fig. 3 shows the swelling behavior of un-cross-linked gelatin MSs or cross-linked gelatin MSs (50 mM) in PBS solution at 4 °C or 37 °C for 3 days. The swelling behavior of the gelatin MSs changed notably with cross-linking by glyoxal. At 4 °C, a halo of diffuse

material was visible around the un-cross-linked gelatin MSs, indicating that they became swollen and enlarged, while the cross-linked gelatin MSs was much less swollen. At 37 °C, the un-cross-linked gelatin MSs completely dissolved, but the cross-linked gelatin MSs retained their shape.

3.1.4. Cytotoxicity of gelatin MSs

The cytotoxicity of the gelatin MSs on W-20-17 was examined by an MTS assay, and the cell morphology was observed by a microscope for 3 days of incubation. Fig. 4a shows the effect of different concentrations of glyoxal in the gelatin MSs on cell viability via an MTS assay. There were significant increases in activity in W-20-17 cells after 3 days of culture ($P < 0.05$). Cells in all the groups

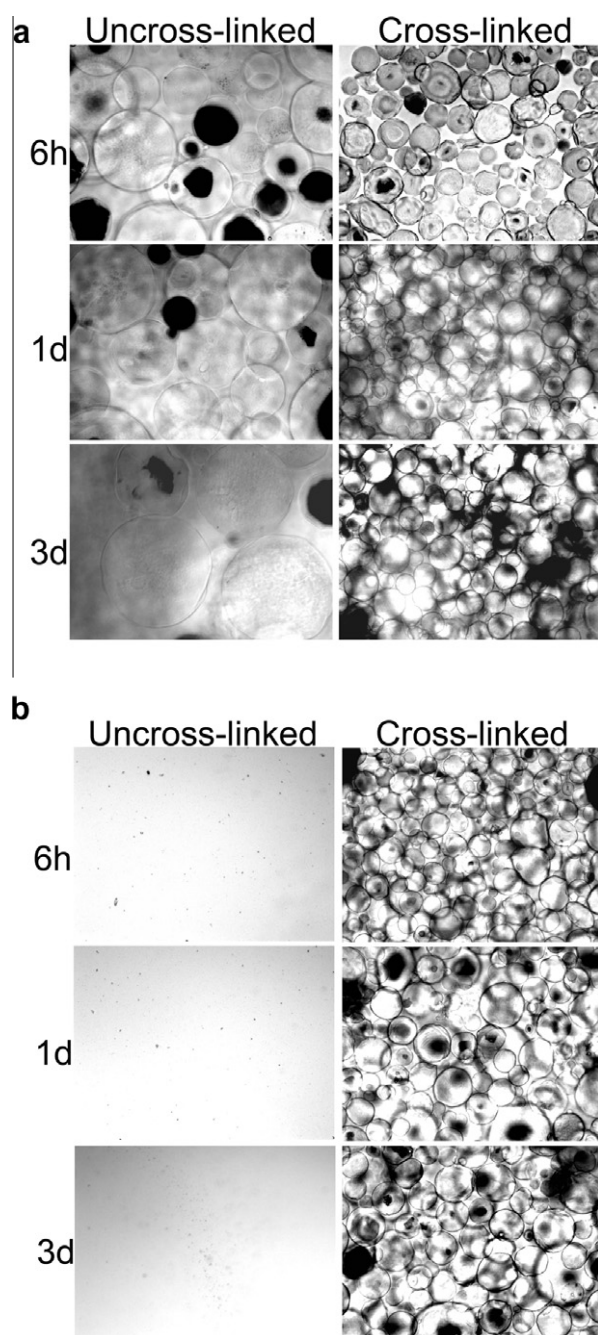


Fig. 3. Swelling behaviors of gelatin microspheres and cross-linked gelatin microspheres at (a) 4 °C and (b) 37 °C. The dried samples were placed into PBS solution, and photomicrographs of the samples were processed at 6 h, 1 day, and 3 days of incubation (magnification is $\times 100$).

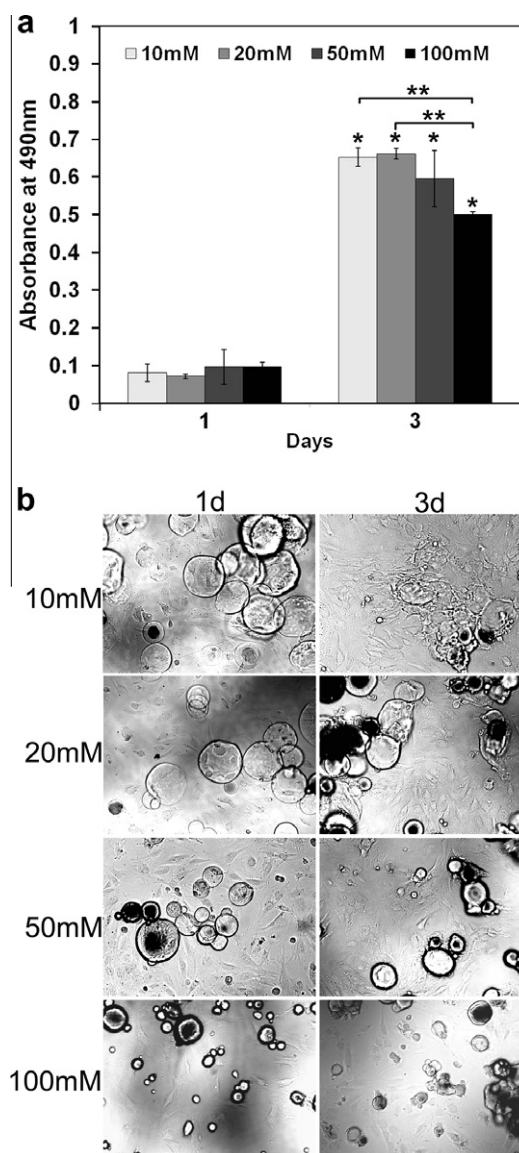


Fig. 4. Cytotoxicity of the cross-linked gelatin microspheres using the preosteoblast mouse stromal cells (W-20-17). (a) The effect of different concentration of glyoxal of gelatin MSs on cell viability via an MTS assay; (b) photomicrographs of cell morphology using a microscope (Nikon ECLIPSE TE-2000-U). Cells were seeded in 24-well plates at a density of 30,000 cells per well and incubated with 10 mg of the gelatin microspheres for 3 days (magnification is $\times 100$). Each value represents the mean \pm SD ($n = 3$). *denotes significant difference compared with 1 day of culture ($P < 0.05$). **denotes significant difference between groups at the same time point ($P < 0.05$).

showed significantly higher metabolic activity at day 3 than at day 1 ($P < 0.05$), indicating that the cells were viable in the presence of the cross-linked gelatin MSs. However, there were significant differences between lower concentrations (10 and 20 mM) and higher concentration (100 mM) of glyoxal ($P < 0.05$). Consistent with an MTS assay, cellular imaging shows that cells in all the groups significantly proliferated for 3 days of culture (Fig. 4b), suggesting the non-cytotoxicity of gelatin MSs.

3.2. Dissolution rate of gelatin MSs

As shown in Fig. 5a, there was an initial burst release of proteins from the gelatin MSs followed by a sustained slow release. However, there was a significant difference between groups for 5 days of incubation ($P < 0.05$). The cumulative amount of proteins released from the gelatin MSs decreased with increasing concentration of glyoxal. In addition, the dissolution rate of gelatin MSs was compared to that of the gelatin MS-loaded chitosan gel (Fig. 5b). Similarly, there was a significant difference in dissolution rate of gelatin MSs with different degrees of cross-linking ($P < 0.05$). The gelatin MSs cross-linked by 50 mM glyoxal showed a significantly lower dissolution rate compared with the other groups after 10 h and 1 day of incubation ($P < 0.05$). However, there was no significant difference between groups after 3 days of incubation.

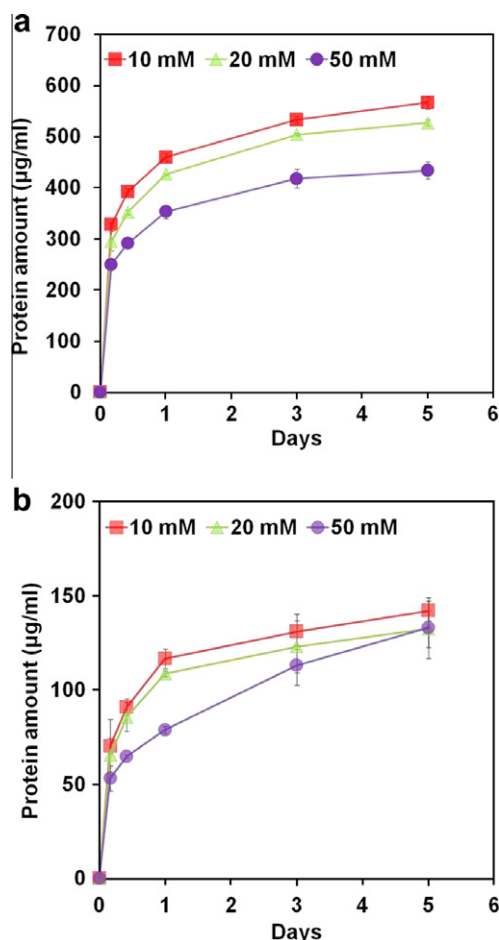


Fig. 5. Dissolution rate of (a) cross-linked gelatin microspheres; (b) cross-linked gelatin microspheres loaded chitosan gel. The samples were placed into PBS solution, and incubated at 37 °C for 5 days. The cumulative amounts of dissolved proteins from gelatin MSs or the combination were determined as a function of time by bicinchoninic acid (BCA) assay at 562 nm. Each value represents the mean \pm SD ($n = 3$).

3.3. SEM images

As shown in Fig. 6, SEM images show surface structures of different materials. The chitosan gel group shows a porous structure formed by some salts and water during the freeze-drying process (Fig. 6a). However, encapsulation of gelatin MSs into the chitosan gel induced a completely different structure. Fig. 6b shows that un-cross-linked gelatin MSs completely dissolved at 37 °C for 5 h. The newly formed structure became less porous compared to the chitosan gel (Fig. 6b), indicating that the chitosan and dissolved gelatin blended well. On the other hand, the cross-linked gelatin MSs did not completely dissolve, but retained their microspherical structure on the surface of the chitosan gel network (Fig. 6c), indicating the enhanced stability of cross-linked gelatin MSs.

3.4. In vitro release studies

The in vitro release behavior of IGF-1 and BMP-2 from the delivery system was interpreted as the cumulative amount of the growth factors over the time. Fig. 7 shows the in vitro release behaviors of IGF-1 from cross-linked gelatin MSs (IGF-1(MSs)) or a chitosan gel encapsulated with the cross-linked gelatin MSs (IGF-1(gel + MSs)) for a week. IGF-1 release behavior from IGF-1(MSs) shows a high initial burst release within 1 day followed by a slow release for 1 week of incubation. The encapsulation of gelatin MSs into the chitosan gel (IGF-1(gel + MSs)) significantly reduced initial release amount of IGF-1 by 48%, resulting in minimal burst release. There was also a moderate and sustained release from IGF-1(gel + MSs) between day 1 and 7. The cumulative BMP-2 release profile from the chitosan gels was compared with IGF-1 release from IGF-1(gel + MSs). The cumulative release amount of BMP-2 was 16.5 ng ml⁻¹ at day 1 and 28.1 ng ml⁻¹ at day 3, while the cumulative release amount of IGF-1 was 8.8 ng ml⁻¹ at day 1 and 10.8 ng ml⁻¹ at day 3. During this period, the amount of BMP-2 released from the chitosan gel was much higher than that of IGF-1. However, during the release periods between day 3 and 7, the release rate of BMP-2 was slower than that of IGF-1, and a greater amount of IGF-1 was released from the delivery system.

3.5. In vitro analysis

3.5.1. Effect of growth factors on ALP specific activity of W-20-17

W-20-17 cells were treated with growth factors (BMP-2, IGF-1, or combinations) as shown in Table 1. The ALP specific activity was determined at days 5 and 7 of incubation by normalizing the ALP amount to the dsDNA content per sample. Fig. 8 shows ALP specific activity of W-20-17 at different conditions. There were significant differences in ALP specific activity among the various growth factor treatments. At 5 days of cell culture, ALP specific activity was considerably increased with BMP-2 treatment, regardless of IGF-I incorporation. Treatments that began with BMP-2 on day 1 followed by BMP-2 alone or in combination with IGF-I on day 3 showed significantly higher ALP activity than any other treatments ($P < 0.05$). However, there was no significant difference between control (no growth factors) and IGF-1 treatment alone, indicating IGF-1 alone did not significantly affect the early osteoblast-associated genes. At 7 days of cell culture, sequential treatment with BMP-2 on day 1 followed by combined BMP-2 and IGF-I on day 3 induced significantly greater ALP activity than any other treatments ($P < 0.05$).

Fig. 9 shows the effect of sequential delivery of growth factors by the chitosan gel/gelatin MSs on ALP specific activity of W-20-17. Different combinations of BMP-2 and IGF-I loading were shown in Table 2. W-20-17 cells showed increased ALP specific activity at 5 days of culture for treatments with all the delivery systems compared with control group. However, there was significant

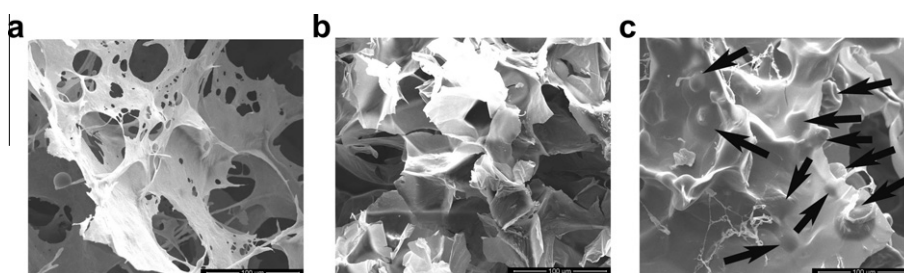


Fig. 6. SEM micrographs on the surface of (a) a chitosan gel; (b) combination of un-cross-linked gelatin microspheres and a chitosan gel; (c) combination of cross-linked gelatin microspheres and a chitosan gel. Samples were incubated at 37 °C for 5 h and lyophilized overnight before the examination under a scanning electron microscope (FEI, USA) operated at 15 kV voltages. Arrows indicate the remaining microspherical structure on the surface of the chitosan gel network (bar = 100 μ m).

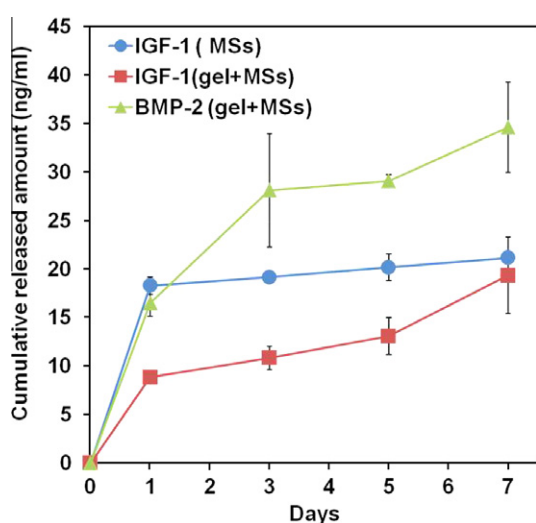


Fig. 7. In vitro cumulative release profiles of growth factors from the materials over a week period. IGF-1 release behavior from cross-linked gelatin MSs (IGF-1(MSs)) was compared with that from cross-linked gelatin MS-loaded chitosan gel (IGF-1(gel + MSs)). BMP-2 release kinetics from a chitosan gel was also compared with IGF-1 release from IGF-1(gel + MSs). The cumulative release amounts of BMP-2 and IGF-1 from the materials were determined as a function of time by either BMP-2 or IGF-1 ELISA kits at 450 nm. Each value represents the mean \pm SD ($n = 3$).

difference between the treatment with BMP-2 from the chitosan gel and with BMP-2 sequentially followed by IGF-1 from the gelatin MS-loaded chitosan gel ($P < 0.05$). At 7 days of cell culture, ALP specific activity was significantly greater for sequential release of BMP-2 followed by IGF-1 from the gelatin MS-loaded chitosan gel than all other treatments ($P < 0.05$). This result indicates the sequential delivery of BMP-2 followed by IGF-1 by the chitosan gel/gelatin MSs induces significantly greater ALP activity of W-20-17 than single BMP-2 delivery or simultaneous delivery of BMP-2 and IGF-1.

4. Discussion

Recent evidence has highlighted the importance of the sequential release of growth factors in order to optimize their efficacy [3,11–18,34,35]. Similarly, this study demonstrates that a sequential release of BMP-2 and IGF-1 significantly enhances osteoblastic differentiation compared to the simultaneous release of BMP-2 and IGF-1. We developed a chitosan gel/gelatin MS-based delivery system for the sequential administration of two model proteins, BMP-2 and IGF-1. This work was first to develop the cross-linked gelatin MSs for delivery of IGF-1, which were then encapsulated into the chitosan gel for sequential release.

Among natural polymers, gelatin, which is a hydrolyzed form of collagen Type I, has been widely studied in the forms of films,

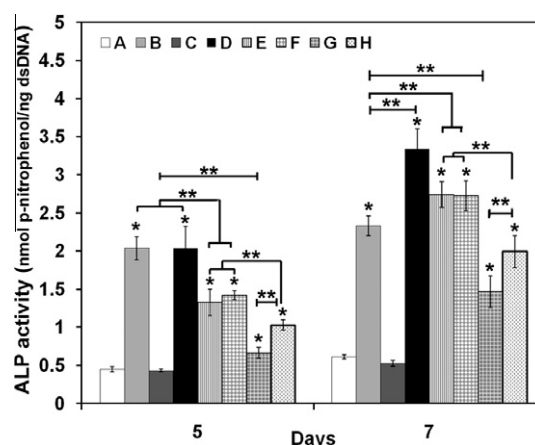


Fig. 8. Effect of growth factors on alkaline phosphatase (ALP) specific activity of W-20-17 cells. The cells were seeded in 24-well plates at a density of 30,000 cells per well and cultured for 7 days. On days 1 and 3, 50 ng ml⁻¹ of each growth factor or their combination was added as shown in Table 1. The culture medium was changed every 3 days. The ALP activity was determined at 5 and 7 days of cultures and normalized for the dsDNA content. ALP activity is expressed as nmol ng⁻¹. Each value represents the mean \pm SD ($n = 3$). *denotes significant increase compared with control group A (no growth factor) at each time point ($P < 0.05$). **denotes significant difference between groups at the same time point ($P < 0.05$). Each group (A–H) is listed in Table 1.

hydrogels, and microspheres [29–33,36–40]. However, gelatin rapidly dissolves in an aqueous environment at body temperature, and exhibits uncontrolled, fast release kinetics of growth factors. For controlled release applications, gelatin MSs have been cross-linked to improve their thermal stability [27,29,30]. In this study, we cross-linked gelatin MSs with glyoxal, which was reported to be less toxic than commonly used cross-linkers, i.e. aldehydes such as formaldehyde, glutaraldehyde, and glyceraldehyde [27,32,37,41–43]. The FTIR spectra revealed the formation of Schiff bases between amide groups of the gelatin and carbonyl groups of glyoxal, which was the result of the cross-linking reaction [29,31]. In this study, the degree of cross-linking significantly increased with increasing concentration of glyoxal ($P < 0.05$) and reached a maximum at 50 mM glyoxal. The cross-linking considerably reduced swellability of the gelatin MSs and enhanced their water stability in an aqueous environment. Cells in all the groups showed significantly increased metabolic activity during 3 days of culture ($P < 0.05$). However, cell growth and proliferation were slower in the gelatin MSs cross-linked with a higher concentration of glyoxal, indicating that optimizing the glyoxal concentration can provide a more suitable for carrier biomaterial. The cross-linking between gelatin molecules and glyoxal increased thermal stability and decreased dissolution, significantly slowing down the release rate of IGF-1. Patel et al. used glutaraldehyde cross-linked gelatin MSs for the controlled release of BMP-2. In their study, gelatin cross-linking

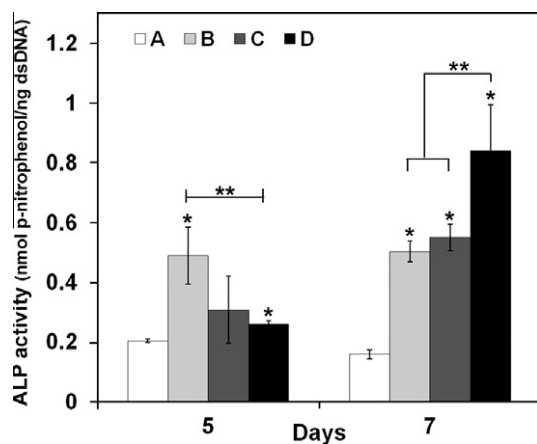


Fig. 9. Effect of sequential delivery systems on alkaline phosphatase (ALP) specific activity of W-20-17 cells. Indirect culture via BD BioCoat™ Control Cell Culture inserts was used as a model system to evaluate the cell responses from the materials. The growth factor loaded materials were placed in the upper chamber of inserts as shown in Table 2. Cells were seeded in the bottom of 12-well plates at a density of 30,000 cells per well and cultured for 7 days. The culture medium was changed every 3 days. The ALP activity was determined at 5 and 7 days of cultures and normalized for the dsDNA content. ALP activity is expressed as nmol ng^{-1} . Each value represents the mean \pm SD ($n = 3$). *denotes significant increase compared with control group A (no growth factor) at each time point ($P < 0.05$). **denotes significant difference between groups at the same time point ($P < 0.05$). Each group (A–D) is listed in Table 2.

and enzymatic degradation significantly reduced the initial burst release and provided linear release kinetics of BMP-2 in vitro thereafter [31]. In another study, Vandelli et al. reported that glycerol-aldehyde cross-linked gelatin MSs showed a decrease in swelling and the in vitro drug release under physiological conditions [37].

We also investigated the dissolution rates of the gelatin MS-loaded chitosan gel. The findings from this study suggest that encapsulation of gelatin MSs into a chitosan gel significantly reduced the initial dissolution rate of gelatin MSs. This is probably because gelatin molecules form polyelectrolyte complexes with chitosan molecules. Chitosan is a cationic biopolymer with a pK_a of 6.5 due to the presence of amino groups [25–28,44]. Gelatin MSs used in this study are negatively charged type B gelatin ($\text{IEP} = 5$) [23,31,44]. Oppositely charged chitosan and gelatin molecules can readily form polyelectrolyte complexes. These intermolecular interactions and cross-linking effects are further suggested by the morphological changes seen by SEM. It was found that the gelatin MSs blended well with the chitosan gel. This is probably due to many functional groups of both gelatin and chitosan [28,44,45]. In addition, Huang et al. reported that a combination of these two biopolymers significantly affects the biological characteristics, and the material's degradation kinetics and mechanical strength [28]. These results suggest that the cross-linking of gelatin MSs and the formation of polyionic complexes by the chitosan and gelatin provide a good medium for controlled release of proteins.

The in vitro release behavior of IGF-1 and BMP-2 from the delivery system showed that the encapsulation of gelatin MSs into a chitosan gel significantly reduced the initial burst release of IGF-1 ($P < 0.05$) and provided a moderate, sustained release. The cumulative amount of BMP-2 released from the chitosan gel was significantly higher than that of the IGF-1 from the gelatin MSs during 3 days of incubation ($P < 0.05$). However, the amount of IGF-1 released was higher than that of BMP-2 during the period between 3 and 7 days of incubation. This result demonstrates that the combination of gelatin MSs and a chitosan gel induces sequential release of BMP-2 followed by IGF-1 over a week.

In addition to the carrier materials' characteristics such as cross-linking and polyionic complexation, interaction between

gelatin and growth factors also affects the product's loading efficiency and release kinetics [23,29,30,37,38]. It is important to minimize the loss of bioactivity resulting from denaturation and deactivation of growth factors during the loading process [29]. Chen et al. investigated the controlled delivery of IGF-1 from dextran-co-gelatin microspheres for periodontal regeneration [23]. Their results showed that a polyion complexation between gelatin and IGF-1 is stable and can be used for the sustained release of numerous charged molecules. In this regard, physical absorption using polyion complexation is a relatively simple and non-destructive method [1,2,30]. In this study, when positively charged IGF-1, with IEP of 8.6, was loaded into the negatively charged gelatin MSs ($\text{IEP} = 5$) [23,24], they formed a polyion complexation. This complex allowed the IGF-1 to be well absorbed into the gelatin MSs while maintaining its bioactivity [23,29–31].

To better evaluate the sequential delivery of growth factors on the cell responses, we first established a growth factor–cell response calibration model. We used ALP activity as an indicator of cell response to BMP-2 and IGF-1. We found that the combination of BMP-2 followed by BMP-2/IGF-1 resulted in the greatest ALP activity of osteoblastic precursor cells. Sustained exposure of cells to BMP-2 significantly increased ALP activity. However, IGF-1 alone did not affect the cell's proliferation or early osteogenic differentiation. Our results are consistent with previous studies [14,18], though they used two layers of gelatin gels cross-linked with glutaraldehyde and two other cell lines. Consequently, we selected four experimental groups and used the newly developed delivery system to release growth factors in a controlled fashion, including sequential and simultaneous delivery groups, to achieve the similar trends of cell response. The cell responses induced by the delivery system were consistent with those by addition of growth factors into medium. A sustained delivery of BMP-2 in addition to a controlled, sequential release of IGF-1 significantly increased the ALP activity of W-20-17 cells.

The recent studies suggested that ideal release strategy for rhBMP-2 includes both a burst and a sustained release for new bone formation [46,47]. For large critical-sized bone defects, a burst release helps to attract osteoprogenitor cells into the delivery system while a sustained release promotes osteoblastic differentiation [46,47]. Brown et al. reported that a burst followed by a sustained release of rhBMP-2 from biodegradable polyurethane (PUR) scaffolds enhanced bone regeneration relative to a sustained release without the burst [46]. The burst release of rhBMP-2 functions as a chemoattractive protein for the recruitment and condensation of osteoprogenitor cells into the scaffold [47]. On the other hand, the sustained delivery of rhBMP-2 enhances bone regeneration by affecting a larger population of osteoprogenitor cells at the fracture and promoting vasculogenesis [46,48]. Our study also showed an initial burst followed by a sustained release of BMP-2 over a week. Consequently, the initial burst release of BMP-2 followed by the sustained releases of both BMP-2 and IGF-1 may synergistically enhance bone regeneration.

One of the weaknesses of this study is that it only evaluated one cell type and one osteoblastic differentiation biomarker. ALP activity is a potent marker of early osteoblastic differentiation, but the ultimate marker or goal of in vitro osteoblastic differentiation is whether or not cells stimulate matrix mineralization. Our previous study showed that the late marker of osteoblastic differentiation such as mineralization and osteocalcin was not dependent on the presence of BMP-2 in W-20-17 cultures [25]. Therefore, we had selected ALP activity as a single early marker of osteoblastic differentiation in this study. Additionally, cell responses are highly variable depending on cell types, species, and different phases of phenotype maturation [25,49,50]. As the goal of this study was to develop and characterize a sequential delivery system of growth factors, the aforementioned variables were not adjusted and future research

should be undertaken to determine the long term effects of the delivery system with regard to release profile, degradation behavior, and calcium mineral deposition.

5. Conclusions

In this study we have synthesized and characterized a chitosan gel/gelatin MS-based delivery system. We also demonstrated a sequential administration of two model proteins, BMP-2 and IGF-1 by this delivery system. The controlled releases of these two proteins are regulated by the degree of cross-linking of gelatin MSs, the encapsulation of gelatin MSs into the chitosan gel, and the interactions between proteins and carriers. The enhanced effect of sequential administration of BMP-2 and IGF-1 on early osteoblastic differentiation marker activity was clearly validated by the addition of growth factors to the medium and the experimental delivery system. The advantage of this protocol is that the delivery effect can be validated and can be extended to other delivery systems and proteins.

Acknowledgments

We acknowledge the grant supports from DOD W81XWH-10-1-0966, Airlift Research Foundation, Wallace H. Coulter Foundation, March of Dimes Birth Defect Foundation, NIH R01AR057837 from NIAMS and NIH R01DE021468 from NIDCR.

Appendix A. Figures with essential colour discrimination

Certain figure in this article, particularly Figs. 5 and 7, is difficult to interpret in black and white. The full colour image can be found in the on-line version, at doi:10.1016/j.actbio.2012.01.009.

References

- [1] Tayalia P, Mooney DJ. Controlled growth factor delivery for tissue engineering. *Adv Mater* 2009;21:3269–85.
- [2] Tabata Y. Tissue regeneration based on growth factor release. *Tissue Eng* 2003;9(Suppl 1):S5–S15.
- [3] Lee K, Silva EA, Mooney DJ. Growth factor delivery-based tissue engineering: general approaches and a review of recent developments. *J R Soc Interf* 2011;6(8(55)):153–70.
- [4] Hing KA. Bone repair in the twenty-first century: biology, chemistry or engineering? *Philos Trans A Math Phys Eng Sci* 2004;362(1825):2821–50.
- [5] Salgado AJ, Coutinho OP, Reis RL. Bone tissue engineering: state of the art and future trends. *Macromol Biosci* 2004;4(8):743–65.
- [6] Pallu S, Fricain JC, Barelille R, Bourget C, Dard M, Sewing A, et al. Cyclo-DfKRG peptide modulates in vitro and in vivo behavior of human osteoprogenitor cells on titanium alloys. *Acta Biomater* 2009;5(9):3581–92.
- [7] Li B, Davidson JM, Guelcher SA. The effect of the local delivery of platelet-derived growth factor from reactive two-component polyurethane scaffolds on the healing in rat skin excisional wounds. *Biomaterials* 2009;30(20):3486–94.
- [8] Richardson TP, Peters MC, Ennett AB, Mooney DJ. Polymeric system for dual growth factor delivery. *Nat Biotechnol* 2001;19:1029–34.
- [9] Ito Y. Covalently immobilized biosignal molecule materials for tissue engineering. *Soft Matter* 2008;4:46–56.
- [10] Di Silvio L, Kayser MV, Downes S. Validation and optimization of a polymer system for potential use as a controlled drug-delivery system. *Clin Mater* 1994;16(2):91–8.
- [11] Chen FM, Chen R, Wang XJ, Sun HH, Wu ZF. In vitro cellular responses to scaffolds containing two microencapsulated growth factors. *Biomaterials* 2009;30(28):5215–24.
- [12] Basmanav FB, Kose GT, Hasirci V. Sequential growth factor delivery from complexed microspheres for bone tissue engineering. *Biomaterials* 2008;29(31):4195–204.
- [13] Arosarena OA, Puleo DA. In vitro effects of combined and sequential bone morphogenetic protein administration. *Arch Facial Plast Surg* 2007;9(4):242–7.
- [14] Raiche AT, Puleo DA. In vitro effects of combined and sequential delivery of two bone growth factors. *Biomaterials* 2004;25(4):677–85.
- [15] Yilgor P, Hasirci N, Hasirci V. Sequential BMP-2/BMP-7 delivery from polyester nanocapsules. *J Biomed Mater Res A* 2010;93(2):528–36.
- [16] Yilgor P, Tuzlakoglu K, Reis RL, Hasirci N, Hasirci V, et al. Incorporation of a sequential BMP-2/BMP-7 delivery system into chitosan-based scaffolds for bone tissue engineering. *Biomaterials* 2009;30(21):3551–9.
- [17] Jaklenec A, Hincckfuss A, Bilgen B, Ciombor DM, Aaron R, Mathiowitz E. Sequential release of bioactive IGF-I and TGF-beta 1 from PLGA microsphere-based scaffolds. *Biomaterials* 2008;29(10):1518–25.
- [18] Raiche AT, Puleo DA. Cell responses to BMP-2 and IGF-1 released with different time-dependent profiles. *J Biomed Mater Res Part A* 2004;69A(2):342–50.
- [19] De Groot J. Carriers that concentrate native bone morphogenetic protein in vivo. *Tissue Eng* 1998;4(4):337–41.
- [20] Meinel L, Zoidis E, Zapf J, Hassa P, Hottiger MO, von Rechenberg B, et al. Localized insulin-like growth factor I delivery to enhance new bone formation. *Bone* 2003;33(4):660–72.
- [21] Meinel L, Illi OE, Zapf J, Malfanti M, Peter Merkle H, Gander B. Stabilizing insulin-like growth factor-I in poly(D,L-lactide-co-glycolide) microspheres. *J Control Release* 2001;70(1–2):193–202.
- [22] Worster AA, Brower-Toland BD, Fortier LA, Bent SJ, Williams J, Nixon AJ. Chondrocytic differentiation of mesenchymal stem cells sequentially exposed to transforming growth factor-beta1 in monolayer and insulin-like growth factor-I in a three-dimensional matrix. *J Orthop Res* 2001;19(4):738–49.
- [23] Chen FM, Zhao YM, Wu H, Deng ZH, Wang QT, Jin Y. Enhancement of periodontal tissue regeneration by locally controlled delivery of insulin-like growth factor-I from dextran-co-gelatin microspheres. *J Control Release* 2006;114(2):209–22.
- [24] Holland TA, Tabata Y, Mikos AG. Dual growth factor delivery from degradable oligo(poly(ethylene glycol) fumarate) hydrogel scaffolds for cartilage tissue engineering. *J Control Release* 2005;101(1–3):111–25.
- [25] Kim S, Tsao H, Kang Y, Sen M, Wenke J, Yang Y, et al. In vitro evaluation of an injectable chitosan gel for sustained local delivery of BMP-2 for osteoblastic differentiation. *J Biomed Mater Res B: Appl Biomater* 2011;99(2):380–90.
- [26] Hoemann CD, Chenite A, Sun J, Hurtig M, Serreque A, Buschmann MD, et al. Cytocompatible gel formation of chitosan-glycerol phosphate solutions supplemented with hydroxyl ethyl cellulose is due to the presence of glyoxal. *J Biomed Mater Res A* 2007;83(2):521–9.
- [27] Gupta KC, Jabrail FH. Glutaraldehyde and glyoxal cross-linked chitosan microspheres for controlled delivery of centchroman. *Carbohydr Res* 2006;341(6):744–56.
- [28] Huang Y, Onyeri S, Siewe M, Moshfeghian A, Madhally SV. In vitro characterization of chitosan-gelatin scaffolds for tissue engineering. *Biomaterials* 2005;26(36):7616–27.
- [29] Young S, Wong M, Tabata Y, Mikos AG. Gelatin as a delivery vehicle for the controlled release of bioactive molecules. *J Control Release* 2005;109(1–3):256–74.
- [30] Ikada Y, Tabata Y. Protein release from gelatin matrices. *Adv Drug Deliv Rev* 1998;31(3):287–301.
- [31] Patel ZS, Yamamoto M, Ueda H, Tabata Y, Mikos AG. Biodegradable gelatin microparticles as delivery systems for the controlled release of bone morphogenetic protein-2. *Acta Biomater* 2008;4(5):1126–38.
- [32] Farris S, Song J, Huang Q. Alternative reaction mechanism for the cross-linking of gelatin with glutaraldehyde. *J Agric Food Chem* 2010;58(2):998–1003.
- [33] Stancu IC. Gelatin hydrogels with PAMAM nanostructured surface and high density surface-localized amino groups. *React Funct Polym* 2010;70(5):314–24.
- [34] Pei M, Seidel J, Vunjak-Novakovic G, Freed LE. Growth factors for sequential cellular de- and re-differentiation in tissue engineering. *Biochem Biophys Res Commun* 2002;294(1):149–54.
- [35] Martin I, Suetterlin R, Baschong W, Heberer M, Vunjak-Novakovic G, Freed LE. Enhanced cartilage tissue engineering by sequential exposure of chondrocytes to FGF-2 during 2D expansion and BMP-2 during 3D cultivation. *J Cell Biochem* 2001;83(1):121–8.
- [36] Solorio L, Zwolinski C, Lund AW, Farrell MJ, Stegemann JP. Gelatin microspheres crosslinked with genipin for local delivery of growth factors. *J Tissue Eng Regen Med* 2010;4(7):514–23.
- [37] Vandelli MA, Rivasi F, Guerra P, Forni F, Arletti R. Gelatin microspheres crosslinked with D,L-glyceraldehyde as a potential drug delivery system: preparation, characterisation, in vitro and in vivo studies. *Int J Pharm* 2001;215(1–2):175–84.
- [38] Wei HJ, Yang HH, Chen CH, Lin WW, Chen SC, Sung HW. Gelatin microspheres encapsulated with a nonpeptide angiogenic agent, ginsenoside Rg1, for intramyocardial injection in a rat model with infarcted myocardium. *J Control Release* 2007;120(1–2):27–34.
- [39] Liang HC, Chang WH, Lin KJ, Sung HW. Genipin-crosslinked gelatin microspheres as a drug carrier for intramuscular administration: in vitro and in vivo studies. *J Biomed Mater Res A* 2003;65(2):271–82.
- [40] de Carvalho RA, Grosso CRF. Properties of chemically modified gelatin films. *Braz J Chem Eng* 2006;23(1):45–53.
- [41] Yang Q, Dou F, Liang B, Shen Q. Studies of cross-linking reaction on chitosan fiber with glyoxal. *Carbohydr Polym* 2005;59(2):205–10.
- [42] Vaz CM, van Doeveren PF, Yilmaz G, de Graaf LA, Reis RL, Cunha AM. Processing and characterization of biodegradable soy plastics: Effects of crosslinking with glyoxal and thermal treatment. *J Appl Polym Sci* 2005;97(2):604–10.
- [43] de Carvalho RA, Grosso CRF. Characterization of gelatin based films modified with transglutaminase, glyoxal and formaldehyde. *Food Hydrocolloids* 2004;18(5):717–26.

- [44] Mao J, Kondu S, Ji HF, McShane MJ. Study of the near-neutral pH-sensitivity of chitosan/gelatin hydrogels by turbidimetry and microcantilever deflection. *Biotechnol Bioeng* 2006;95(3):333–41.
- [45] Mao J, Kondu S, Ji HF, McShane MJ. Study on physical properties and nerve cell affinity of composite films from chitosan and gelatin solutions. *Biomaterials* 2003;24(17):2871–80.
- [46] Brown KV, Li B, Guda T, Perrien DS, Guelcher SA, Wenke JC. Improving bone formation in a rat femur segmental defect by controlling bone morphogenetic protein-2 release. *Tissue Eng Part A* 2011;17(13–14):1735–46.
- [47] Fiedler J, Roderer G, Gunther KP, Brenner RE. BMP-2, BMP-4, and PDGF-bb stimulate chemotactic migration of primary human mesenchymal progenitor cells. *J Cell Biochem* 2002;87:305–12.
- [48] Kolambkar YM, Dupont KM, Boerckel JD, Huebsch N, Mooney DJ, Guldberg RE, et al. An alginate-based hybrid system for growth factor delivery in the functional repair of large bone defects. *Biomaterials* 2011;32:65–74.
- [49] Diefenderfer DL, Osyczka AM, Garino JP, Leboy PS. Regulation of BMP-induced transcription in cultured human bone marrow stromal cells. *J Bone Joint Surg Am* 2003;85A(Suppl 2):19–28.
- [50] Osyczka AM, Diefenderfer DL, Bhargava G, Leboy PS. Different effects of BMP-2 on marrow stromal cells from human and rat bone. *Cells Tissues Organs* 2004;176(1–3):109–19.

9 ZYWicZ7 cUXa]b]ghfU]cb'cZJ UbWta nW]b
UbX'6 AD!&'cb'7 cW`h fYX'GHUd\ mēcWtVW g'
U fYi g'UbX'K !&\$!%+`Aci gY'6 cbY'A Uffck
Glfca U'7 Y`g' *In Vitro*

5 "<"B[i mYbžG"?]a žK ">"A UcbYmž>"7 "K Yb_YUbX'M"
Mub[
Antimicrob. Agents Chemother. &\$%&ž) *fl-L' ++* "8 C=
%\$"%8&, #5 57 '\$\$%/% !%&"
Di V`]g\ YX'5\ YUX'cZDf]b]h+`A Umi&\$%&"`

Updated information and services can be found at:
<http://aac.asm.org/content/56/7/3776>

These include:

F9: 9F9B79G

This article cites 50 articles, 16 of which can be accessed free
at: <http://aac.asm.org/content/56/7/3776#ref-list-1>

7CBH9BH5 @FHG

Receive: RSS Feeds, eTOCs, free email alerts (when new
articles cite this article), [more»](#)

Information about commercial reprint orders: \ Htd.#ci fbUg"Uga "cf[#]hY#]gW#Ydf]b]g"1\ ha`
To subscribe to to another ASM Journal go to: \ Htd.#ci fbUg"Uga "cf[#]hY#gi VgW]d]h]cbg#

Effect of Coadministration of Vancomycin and BMP-2 on Cocultured *Staphylococcus aureus* and W-20-17 Mouse Bone Marrow Stromal Cells *In Vitro*

A. H. Nguyen,^a S. Kim,^{a,b} W. J. Maloney,^b J. C. Wenke,^c and Y. Yang^{a,b}

Department of Restorative Dentistry and Biomaterials, University of Texas Health Science Center at Houston, Houston, Texas, USA^a; Department of Orthopedic Surgery, Stanford University, USA^b; and United States Army Institute of Surgical Research, Fort Sam Houston, Texas, USA^c

In this study, we aimed to establish an *in vitro* bacterium/bone cell coculture model system and to use this model for dose dependence studies of dual administration of antibiotics and growth factors *in vitro*. We examined the effect of single or dual administration of the antibiotic vancomycin (VAN) at 0 to 16 µg/ml and bone morphogenetic protein-2 (BMP-2) at 0 or 100 ng/ml on both methicillin-sensitive *Staphylococcus aureus* and mouse bone marrow stromal cells (W-20-17) under both mono- and coculture conditions. Cell metabolic activity, Live/Dead staining, double-stranded DNA (dsDNA) amounts, and alkaline phosphatase activity were measured to assess cell viability, proliferation, and differentiation. An interleukin-6 (IL-6) enzyme-linked immunosorbent assay (ELISA) kit was used to test the bone cell inflammation response in the presence of bacteria. Our results suggest that, when delivered together in coculture, VAN and BMP-2 maintain their primary functions as an antibiotic and a growth factor, respectively. Most interestingly, this dual-delivery type of approach has shown itself to be effective at lower concentrations of VAN than those required for an approach relying strictly on the antibiotic. It may be that BMP-2 enhances cell proliferation and differentiation before the cells become infected. In coculture, a dosage of VAN higher than that used for treatment in monoculture may be necessary to effectively inhibit growth of *Staphylococcus aureus*. This could mean that the coculture environment may be limiting the efficacy of VAN, possibly by way of bacterial invasion of the bone cells. This report of a coculture study demonstrates a potential beneficial effect of the coadministration of antibiotics and growth factors compared to treatment with antibiotic alone.

The regeneration of contaminated bony tissue defects poses itself as one of the major areas of concern in the field of bone tissue engineering, especially with regard to war traumas in extremities, where infection of open type III fractures is all but certain (10, 33). These bacterial infections complicate the already strenuous repair process, often resulting in slower union rates or even amputation (7, 22). At the present, standard clinical care is a two-phase process. First, antibiotics are administered to stop any ongoing infection of the bony tissue if present. Second, a bone graft is implanted, and bone growth factors are delivered to facilitate the regrowth of natural bone tissue by using the patient's resident osteoblasts. While this treatment protocol is designed to prevent contamination and promote bone growth, recurrent infection following implantation of the graft continues to be a major barrier to generating consistently positive outcomes (2, 19, 29, 48).

One suggested approach to combating this issue is to use a specialized synthetic bone graft material capable of delivering both antibiotics and growth factors locally after implantation (9, 16, 25, 31, 46, 47, 50). While antibiotic integration into bone grafts has been proven successful, less work has been done to deliver an antibiotic and a growth factor together (either in series or parallel) (24, 25). As a result of limiting the need for the antibiotic to travel systemically, there are higher antibiotic levels at the site of the wound and systemically safe levels, thus paving the way for resident osteoblasts to penetrate into the graft well before the offending bacteria are able to reach high confluence and form biofilms (38). Moreover, combined treatment with bone growth factors such as bone morphogenetic protein-2 (BMP-2) can accelerate the healing process in a simple, streamlined delivery approach (14,

20, 23, 28, 34, 37). With the emergence of these complex dual-purpose grafts, the need for a flexible *in vitro* test system highly representative of *in vivo* conditions is of paramount importance in helping to smooth the natural transition into animal studies. Such a model system would allow more realistic assessment of different clinical treatment options in a rapid, cost-efficient, and safe manner, especially with regard to testing possibly host-toxic therapies.

Here, we aimed to establish an *in vitro* bacterium/bone cell coculture model system and to use this model for dose dependence studies of the dual administration of antibiotics and growth factors *in vitro*. We examined the interactions between our two tested model cell lines (W-20-17 mouse bone marrow stromal cells [mBMSCs] and methicillin-sensitive *S. aureus* ATCC 6538) as well as their responses to various treatments with vancomycin (VAN) at 0 to 16 µg/ml and BMP-2 at 0 or 100 ng/ml both in mono- and coculture (13). *S. aureus* is a highly infectious Gram-positive bacterium known for its ability to internalize itself within mammalian cells and is the predominant cause of bone graft failures (2, 3, 8, 9, 11, 12, 15, 19, 29, 30, 32, 36, 44, 48). W-20-17 is derived from mouse bone marrow stromal cells and has been used as an ASTM (F2131) standard test for *in vitro* biological activity of

Received 18 January 2012 Returned for modification 28 February 2012

Accepted 16 April 2012

Published ahead of print 7 May 2012

Address correspondence to Y. Yang, ypyang@stanford.edu.

Copyright © 2012, American Society for Microbiology. All Rights Reserved.

doi:10.1128/AAC.00114-12

BMP-2. Previous studies showed that BMP-2 significantly stimulated alkaline phosphatase (ALP) activity in W-20-17 in a dose-dependent manner (26). With so many antibiotics available for treatment of infections by Gram-positive bacterial strains such as our chosen methicillin-sensitive *S. aureus* (MSSA) strain, vancomycin presents itself as one of the most aggressive antibiotics available for clinical use and has been proven to work very well against methicillin-resistant *S. aureus* (MRSA) while still being effective against MSSA (21, 38, 39, 41, 43). While toxicity of the drug is often considered a deterrent for its use, vancomycin is only toxic at levels well above the MIC for nonresistant *S. aureus* (21, 43). Regardless, we also assessed whether or not concentrations of vancomycin well above our suspected working levels (up to 200 µg/ml) would be toxic to our W-20-17 cells. Because of the many complications involved in performing cocultures of this nature, we utilized a modified version of a previously created system in order to establish our model (the details of which are explained below) (6, 13). Note that the design of our system is fairly modular, allowing the substitution of different cell lines and substances in order to meet the demands of multiple experimental conditions.

We hypothesized that BMP-2 and VAN would maintain their respective primary functions on their target cell lines when delivered together in our coculture system. To test this, cell viability, proliferation, and differentiation under an array of conditions and across a number of time points were measured. Our findings show that even when delivered together in coculture, VAN and BMP-2 do not lose their functionality as an antibiotic and a growth factor, respectively. Moreover, some evidence suggests that the addition of BMP-2 can reduce the amount of VAN necessary to inhibit bacterial growth and thus allow more rapid bone cell proliferation and differentiation.

MATERIALS AND METHODS

Culture of bacteria. A clinical strain of *S. aureus* (ATCC 6538) was propagated according to the guidelines provided by the vendor. Briefly, cells were grown in 200 ml of tryptic soy broth (TSB) in a 1-liter Erlenmeyer flask and incubated at 37°C in a humidified incubator. Once cells reached an optical density at 600 nm (OD₆₀₀) of ~0.5, they were centrifuged (10 min at 4,300 × g and 4°C) and resuspended in a 20% glycerol solution. Aliquots of this suspension were then frozen in liquid nitrogen and stored at -80°C until needed for culture.

Culture of mouse bone cells. W-20-17 cells (ATCC) were propagated according to the guidelines provided by the vendor. Briefly, cells were grown and maintained in Dulbecco's modified Eagle's medium (DMEM) with 10% fetal bovine serum (FBS), a 1% antibiotic/antimycotic mixture, 5 ml of L-glutamine (200 mM), and sodium pyruvate. This cell line is an ASTM standard to evaluate activity of BMP-2 *in vitro*. The cells were cultured in an incubator supplied with 5% CO₂ at 37°C. Medium was replaced every 3 days. To prevent oversaturation of the flask, cultures were periodically subjected to passage prior to the cells reaching high confluence.

Preparation of VAN and BMP-2 treatments. Vancomycin treatments were prepared by dissolving dry vancomycin hydrochloride (Acros Organics) in phosphate-buffered saline (PBS). Serial dilutions were performed to create stocks with concentrations of 160, 80, 40, 20, and 10 µg of VAN/ml (1, 5, 17, 21, 40, 43). These stocks were then run through a sterile filter and refrigerated until use. BMP-2 stocks (R&D Inc.) were similarly suspended in PBS and stored at -20°C until use.

Experimental design. For monocultures, *S. aureus* bacteria were grown in 24-well plates. Appropriate volumes of TSB, VAN, BMP-2, and phosphate-buffered saline (PBS) were added to each well such that the

final volume was 500 µl (1,000 µl for cultures used in ALP and double-stranded DNA [dsDNA] assays). Cells from thawed frozen stock were seeded to a final concentration of 10⁵ CFU/ml and incubated at 37°C in a humidified incubator (5% CO₂). Tested final concentrations of VAN were 0, 1, 2, 4, 8, and 16 µg/ml, while tested concentrations of BMP-2 were 0 and 100 ng/ml. W-20-17 cells were also grown in monoculture in 24-well plates. Cells were seeded to a final concentration of 15,000 cells per well in DMEM and incubated at 37°C in a humidified incubator (5% CO₂). Tested final concentrations of VAN were 0, 1, 2, 4, 8, and 16 µg/ml, while tested concentrations of BMP-2 were 0 and 100 ng/ml. For treatments requiring either zero VAN or zero BMP-2, the appropriate volume of PBS was added instead. For culture growth for longer times, culture medium and treatments were replaced with fresh medium and the appropriate amounts of each VAN or BMP-2 treatment every 3 days. All concentrations were kept constant throughout the culture period.

Bacterial cells used for coculture were taken from a growing liquid culture. A 125-ml flask containing 10 ml of TSB was inoculated with *S. aureus* bacteria and allowed to grow overnight in a humidified incubator (37°C, 5% CO₂), with shaking at 200 rpm. The following day, the culture was centrifuged (10 min at 4,300 × g and 4°C) and the pellet was washed with 10 ml of Hank's balanced salt solution (HBSS) and resuspended in 10 ml of DMEM-p (DMEM, 10% FBS, 0% penicillin, 5 ml of L-glutamine [200 mM], and sodium pyruvate). Cocultures of *S. aureus* and W-20-17 cells were performed through a series of incubations, washes, and medium changes. First, W-20-17 cells were cultured overnight as described previously. After incubation, culture wells were aspirated and rinsed twice with 500 µl of HBSS before replacement of the medium with 480 µl of DMEM-p. Next, the mouse cell cultures were infected with 20 µl of *S. aureus* suspension for an approximate final concentration of 10⁷ CFU/ml, a concentration higher than that used for monocultures in order to aid in the differentiation of treatment groups by using a more stringent set of conditions. This coculture was then incubated for 45 min at 37°C. Following the 45-min infection period, cell culture wells were aspirated and washed twice with 500 µl of HBSS to remove as much of the extracellular bacteria as possible and incubated at 37°C in 400 µl of DMEM-p and 100 µl of a predetermined treatment combination of VAN (0, 1, 2, 4, 8, or 16 µg/ml) and BMP-2 (0 or 100 ng/ml).

Measurement of metabolic activity. Metabolic activity was measured using Promega CellTiter96 Aqueous One solution (MTS [3-(4,5-dimethylthiazol-2-yl)-5-(3-carboxymethoxyphenyl)-2-(4-sulphophenyl)-2H-tetrazolium, inner salt]) as directed by the supplier. At predetermined time points, the number of viable cells was determined quantitatively according to the manufacturer's instructions. For monocultures, the metabolic activity of *S. aureus* or W-20-17 cells was tested separately (in TSB or DMEM, respectively). For cocultures, the metabolic activity of W-20-17 cells was evaluated by culturing a *S. aureus* monoculture (10⁷ CFU/ml) in parallel with the coculture (using the same treatments and under the same conditions) and subtracting the monoculture background from the coculture measurement. To remove as much of the residual bacteria as possible, culture medium was aspirated, washed twice with 500 µl of HBSS, supplied with 400 µl of fresh DMEM-p and 100 µl of the treatment, and incubated for 30 min before the reagent was added. Assays began with 100 µl of the reagent being added to each well of the 24-well plate. Cultures were then placed in a humidified incubator at 37°C for 1 h. Finally, 100 µl of each well was transferred to a 96-well assay plate and measured at 490 nm in a microplate reader (TECAN Infinite F50).

Staining and visualization of cells. Qualitative analysis of cell cultures was accomplished using Invitrogen Live/Dead (L/D) cell viability kits as directed by the supplier. Bacterial monocultures were visualized using a Live/Dead BacLight Bacterial Viability kit, whereas W-20-17 monocultures and cocultures were visualized using a Live/Dead Mammalian Cell Viability kit. Photomicrographs of cells were documented using a microscope (Nikon Eclipse TE-2000-U) and processed using MetaVue software (Nikon MetaVue) after 1, 2, and 3 days of W-20-17 monoculture, 3 days of *S. aureus* monoculture, and 1, 3, and 7 days of coculture.

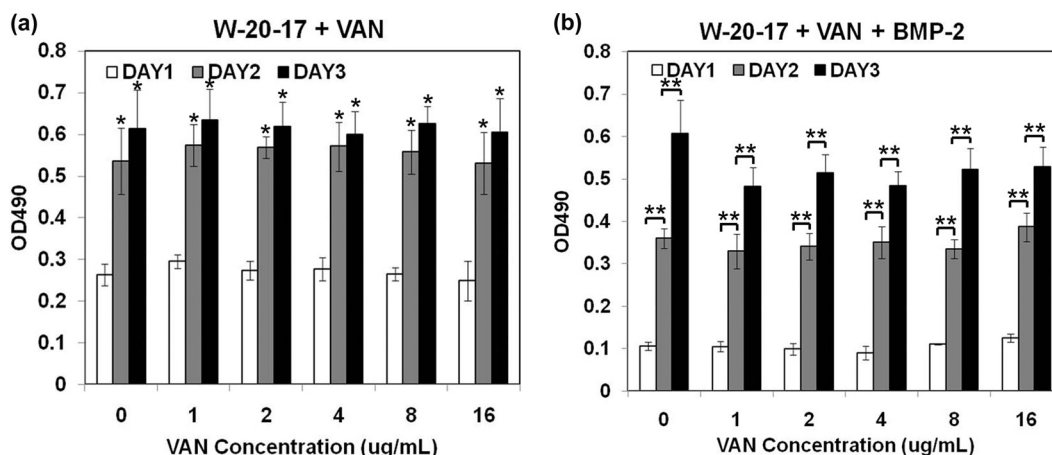


FIG 1 Measure of metabolic activity of W-20-17 treated with 0 to 16 µg/ml VAN in combination with (a) 0 ng/ml BMP-2 or (b) 100 ng/ml BMP-2 over 3 days using an MTS colorimetric assay. Higher OD₄₉₀ values indicate greater metabolic activity. The initial cell density was 15,000 cells per well for 3 days. The absorbance is expressed as a measure of the cell viability via cell culture media for 3 days of incubation. Each value represents the mean ± SD (*n* = 3). *, statistically significant difference compared with 1 day of culture (*P* < 0.05). **, statistically significant difference between different time points (*P* < 0.05).

Preparation of cell culture lysate for ALP and dsDNA. At the designated time, the medium was removed from the cell culture. The cell layers of W-20-17 were washed twice with PBS (pH 7.4) and then lysed with 1 ml of 0.2% Triton X-100 by three freeze-thaw cycles, which consisted of freezing at −80°C for 30 min immediately followed by thawing at 37°C for 15 min. The cell lysates were used to determine ALP activity and double-stranded DNA levels.

Preparation of bacterial cell culture lysate for ALP and dsDNA. At the designated time, the samples in each well were mixed and transferred to microcentrifuge tubes and centrifuged for 15 min at 10,000 × *g* and 4°C. The supernatant was removed, and the pellet was then resuspended in 1,000 µl of 0.2% Triton X-100. Lysis was achieved by performing four freeze-thaw cycles, which consisted of freezing at −80°C for 30 min immediately followed by thawing at 37°C for 15 min. The cell lysates were used to determine ALP activity and double-stranded DNA levels.

Measurement of ALP activity. The cell lysates were assayed for the presence of ALP, an important marker for determining osteoblast phenotype. Aliquots (50 µl) of the cell lysates were sampled and added to 50 µl of working reagent in a 96-well assay plate. The working reagent contained equal parts (1:1:1) of 1.5 M 2-amino-2-methyl-1-propanol (Sigma), 20 mM *p*-nitrophenyl phosphate (Sigma), and 1 mM magnesium chloride. The samples then were incubated for 1 h at 37°C. After incubation, the reaction was stopped with 100 µl of 1 N sodium hydroxide on ice. ALP activity was determined from the absorbance using a standard curve prepared from *p*-nitrophenol stock standard (Sigma). The absorbance was measured at 405 nm using a microplate reader (Bio-Rad model 680). The ALP activity of cells was then calculated by normalizing to double-stranded DNA (dsDNA). ALP activity was expressed as nanomoles per nanogram.

Measurement of dsDNA amount. The cell lysates were examined for double-stranded DNA to estimate cell numbers. Aliquots (50 µl) of the cell lysates were added in a 96-well assay plate. A 50-µl volume of a 1:200 dilution of PicoGreen (Quant-iT PicoGreen assay kit; Invitrogen) was added to each well and incubated for 5 min in the dark. The assay plate was read (485-nm excitation and 530-nm emission) using a BioTek FLx800 plate reader. The double-stranded DNA content was calculated using a standard curve made using a provided dsDNA standard sample. Amounts of dsDNA were measured using a PicoGreen fluorescence assay to standardize ALP production measurements.

Measurement of IL-6 response. Interleukin-6 (IL-6) production by W-20-17 in coculture was measured using an Invitrogen IL-6 enzyme-linked immunosorbent assay (ELISA) kit with minor modifications to the

sampling protocol provided by the supplier. Samples tested were prepared from the supernatant of each culture. Briefly, *S. aureus*/W-20-17 cocultures and W-20-17 monocultures were performed as described previously. After 3 days of incubation, the medium from each well was transferred to individual microcentrifuge tubes and centrifuged for 5 min at 300 × *g* and 4°C. The resulting supernatant was then stored at −20°C until measurement using the ELISA kit. The assay was performed as written in the kit's instructions. Briefly, the collected samples were added to the assay well plate in duplicate. The prescribed series of reagent additions, washes, and incubations were performed as instructed. Following the addition of stop solution, absorbance was measured using a Tecan Infinite F50 microplate reader set to 450 nm.

Statistical analysis. All data are presented as means ± standard deviations. For comparing two groups of data, a Student *t* test was performed. For comparing multiple groups of data, one-way analysis of variance (ANOVA) was performed followed by Tukey's test. The differences in data for groups and experimental time points were considered statistically significant when *P* < 0.05.

RESULTS

Mouse cell metabolic activity in monoculture. MTS assays were performed to measure cell metabolic activity at various concentrations of antibiotic VAN (between 0 and 16 µg/ml) and BMP-2 (either 0 or 100 ng/ml) over a 3-day period. The results were used to determine effectiveness at the bacterial concentration tested in coculture (Fig. 1). W-20-17 cells showed significantly higher metabolic activity at day 3 than at day 1 (*P* < 0.05), indicating that the cells were able to grow and proliferate in the presence of VAN. Our results indicate that VAN had little to no measurable effect on overall cell metabolic activity regardless of concentration, BMP-2 presence, or culture duration. Worth noting is that all groups treated with BMP-2 (Fig. 1b) showed lower metabolic activity relative to their BMP-2-free counterparts (Fig. 1a). This suggests that BMP-2 may reduce the overall metabolic activity of W-20-17 cell cultures (possibly by reducing cell proliferation in favor of cell differentiation). Live/Dead fluorescence staining also showed that in all treatment groups, W-20-17 cells were viable and maintained their normative spindle-like shapes (Fig. 2). Furthermore, visual assessment indicates an increase in cell proliferation over the 3 days of culture across all treatments of VAN and BMP-2.

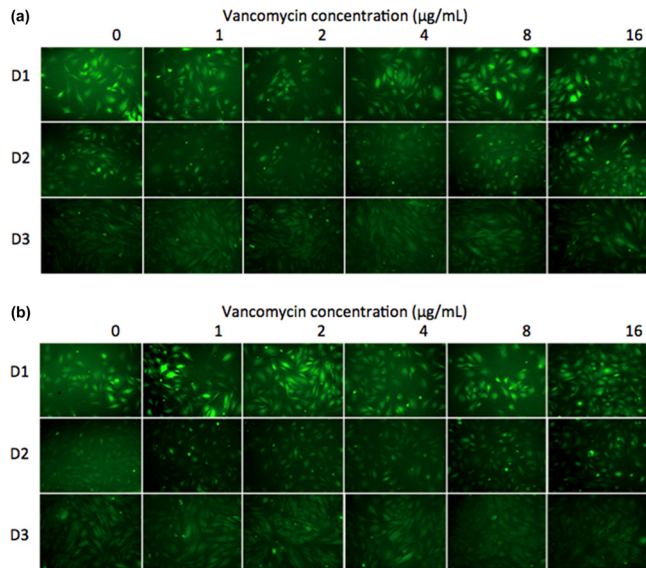


FIG 2 Live/Dead fluorescence staining of W-20-17 treated with 0 to 16 µg/ml VAN and either (a) 0 ng/ml BMP-2 or (b) 100 ng/ml BMP-2 in monoculture in DMEM. Photos were taken at $\times 100$ magnification after up to 3 days of culture (D1, day 1; D2, day 2; D3, day 3). Green indicates live bone cells, and red indicates dead cells.

Mouse cell osteoblastic differentiation in monoculture. ALP assays were performed to measure osteogenic activity of W-20-17 cells at various concentrations of antibiotic VAN (between 0 and 16 µg/ml) and BMP-2 (either 0 or 100 ng/ml) over a 7-day period. Our results indicate that VAN had no clear effect on ALP-specific activity (ALP normalized to dsDNA per unit) regardless of concentration, BMP-2 presence, or day (Fig. 3). The results suggest that BMP-2 was able to maintain its ability to increase overall ALP activity at all concentrations of VAN. dsDNA levels were measured in order to normalize ALP activity. Results indicate little overall difference in dsDNA levels at day 7, but there was a consistent trend of reduced dsDNA levels at day 5 in the BMP-2-treated groups relative to their BMP-2-free counterparts. Regardless, a statistically significant difference existed between the 0

ng/ml and 100 ng/ml BMP-2 groups in terms of ALP-specific activity.

Bacterial metabolic activity in monoculture. MTS assays were performed to measure cell metabolic activity at various concentrations of VAN antibiotic (between 0 and 16 µg/ml) and BMP-2 (either 0 or 100 ng/ml) over a 24-h period (Fig. 4). Our results indicate that at every measurement time, all treatment groups with VAN at ≥ 1 µg/ml showed highly suppressed *S. aureus* growth (for all intents and purposes, *S. aureus* metabolic activity was practically zero in these groups). The treatment group with no VAN showed dramatic increases in metabolic activity by 6 h and immeasurably high levels by 24 h. Overall, our data suggest that even at concentrations of 1 µg/ml, VAN was effective at hindering the growth of our strain of *S. aureus* when seeded at 10^5 CFU/ml. However, because this result proved incapable of distinguishing the levels of efficacy of our treatments, the assays used for Live/Dead fluorescence staining of *S. aureus* as well as all coculture assays were seeded with bacteria at 10^7 CFU/ml. At this higher concentration, L/D staining also confirmed that *S. aureus* lost their viability after treatment with VAN at a concentration of at least 2 µg/ml regardless of the presence or absence of BMP-2 (Fig. 5). Visually, there was a decrease in bacterial cell proliferation within the 3 days of culture across all treatments performed with VAN.

Bacterial ALP production in monoculture. Bacterial ALP production was measured to assess whether or not the amount of ALP produced by the tested *S. aureus* strain was significant compared to W-20-17 cell results. Therefore, a high concentration of *S. aureus* cells (10^9 CFU) was cultured in 1 ml of DMEM-p in a shaking incubator for 3 h. ALP activity was measured as described previously. Results indicated that *S. aureus* strain ATCC 6538 produced about 0.045 nmol of ALP per ng of dsDNA. This is more than 10-fold less than the ALP-specific activity of W-20-17 cultured under similar conditions and is over 100-fold less than the ALP-specific activity of W-20-17 cultured with BMP-2. Despite this difference, the possibility cannot be ruled out that ALP production of *S. aureus* affects measurements taken from coculture. To suppress the possibly confounding variable of gross bacterial ALP production, ALP-specific activity (gross ALP data normal-

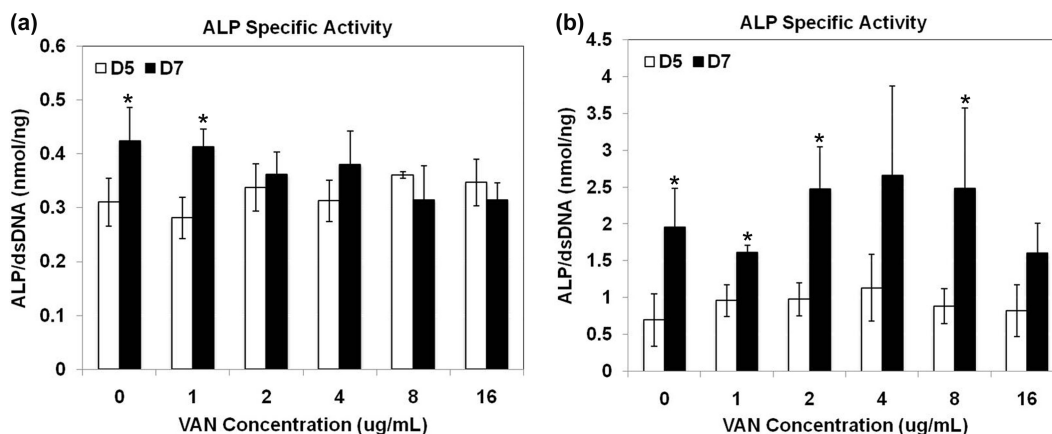


FIG 3 Measure of early osteoblastic differentiation of W-20-17 treated with 0 to 16 µg/ml VAN in combination with (a) 0 ng/ml BMP-2 or (b) 100 ng/ml BMP-2 in monoculture using an ALP assay. The ALP activity was determined at 5 and 7 days of culture and normalized for the dsDNA content. ALP activity is expressed as nanomoles per nanogram. Each value represents the mean \pm SD ($n = 3$). *, statistically significant difference compared with 5 days of culture ($P < 0.05$).

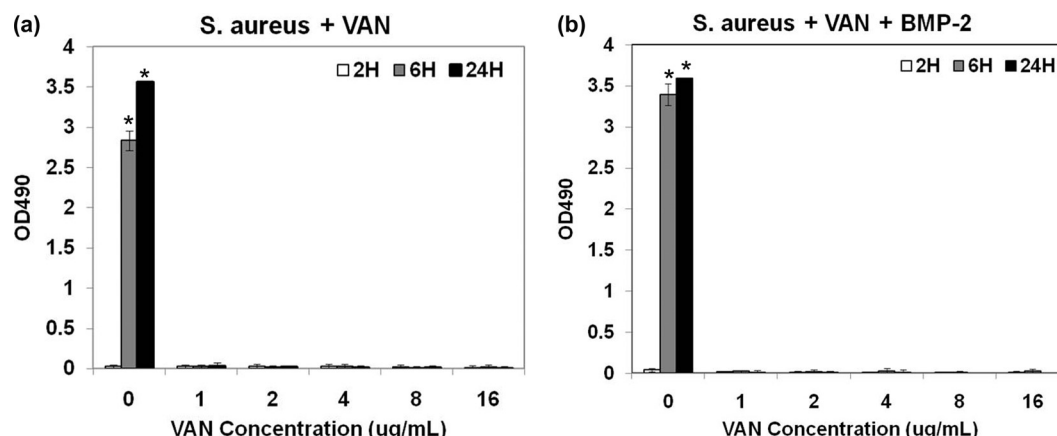


FIG 4 Measure of metabolic activity of *S. aureus* treated with 0 to 16 $\mu\text{g/ml}$ VAN in combination with (a) 0 ng/ml BMP-2 or (b) 100 ng/ml BMP-2 over 24 h using an MTS colorimetric assay. The initial concentration of *S. aureus* was 10^5 CFU/ml. Higher OD₄₉₀ values indicate greater metabolic activity. The absorbance is expressed as a measure of the cell viability via cell culture media for 24 h of incubation. Each value represents the mean \pm SD ($n = 3$). *, statistically significant difference compared with 2 h of culture ($P < 0.05$).

ized to dsDNA levels) was used for coculture assessment rather than raw ALP measurements.

Metabolic activity of mouse cells in coculture. MTS assays were performed to measure cell metabolic activity at various concentrations of VAN antibiotic (between 0 and 16 $\mu\text{g/ml}$) and BMP-2 (either 0 or 100 ng/ml) over a 7-day period (Fig. 6). L/D staining imaging was also performed to investigate viabilities of cells (Fig. 7). The results indicated that treatments with VAN at greater than 4 $\mu\text{g/ml}$ were effective at stopping bacterial growth in a coculture over a 7-day period. However, it was also found that treatment with VAN at between 1 and 2 $\mu\text{g/ml}$ represented the minimum concentration range required to effectively combat bacterial growth after 4 h in monoculture when bacteria were seeded at 10^7 CFU/ml (Fig. 5). Note that the MTS assay cannot distinguish between the metabolic activities of residual bacteria and those of growing W-20-17 cells when grown in coculture. Given the qualitative staining results, it is clear that the large increases in OD₄₉₀ values in groups treated with VAN at less than 8 $\mu\text{g/ml}$ can primarily be attributed to *S. aureus* growth. Groups treated with VAN at $\geq 8 \mu\text{g/ml}$ showed metabolic activity that was likely attributable to the W-20-17 cells. Note that treatment with VAN at 16 $\mu\text{g/ml}$ was sufficient for both concentrations of BMP-2 tested. However, a significant decrease in metabolic activity by day 7 was evident in groups treated with VAN at only 8 $\mu\text{g/ml}$ whereas there was an increase in activity in the comparable treatment group with BMP-2 at 100 ng/ml. This suggests that treatment with

8 $\mu\text{g/ml}$ VAN may not be sufficient to retain W-20-17 growth unless coupled with BMP-2 at 100 ng/ml. As shown in Fig. 7, the minimum VAN concentration that allowed W-20-17 growth increased at each time point regardless of BMP-2 treatment (red arrows). Staining results showed that with BMP-2 at both 0 and 100 ng/ml, 2 $\mu\text{g/ml}$ VAN was effective for 1 day, 4 $\mu\text{g/ml}$ for 3 days, and 8 $\mu\text{g/ml}$ for 7 days. Qualitatively, treatments with higher concentrations of VAN showed greater W-20-17 proliferation and reduced bacterial growth. When W-20-17 growth was evident, treatments with BMP-2 showed greater growth than those without.

Osteoblastic differentiation of mouse cells in coculture. ALP-specific activity was measured in order to assess the osteoblastic differentiation of W-20-17 cells in response to different vancomycin doses in a coculture environment over a 7-day period (Fig. 8). Treatments with VAN at 4 $\mu\text{g/ml}$ or a lower concentration were ineffective at inhibiting bacterial growth (as indicated by low or decreasing measurements of ALP-specific activity) regardless of the BMP-2 concentration. By day 7, ALP-specific activities showed a marked increase over day 3 activities in groups treated with VAN at 8 $\mu\text{g/ml}$ in combination with BMP-2 at 100 ng/ml but not in groups without BMP-2. This suggests that the combination of BMP-2 and VAN allows enhanced osteoblastic differentiation when cells are challenged with the parasitic *S. aureus* bacteria in coculture. ALP-specific activities in the coculture with VAN at 8 $\mu\text{g/ml}$ and 16 $\mu\text{g/ml}$ were similar to those seen with the monoculture. As expected, BMP-2-treated cultures that survived the 7-day period exhibited significantly greater ALP production than those without BMP-2, suggesting that BMP-2 maintains its effectiveness in coculture.

dsDNA amounts were primarily measured to assess ALP-specific activity. As a whole, though, dsDNA levels act as a general measure of cell proliferation. A progressive increase in dsDNA levels over the 7-day culture was evident, despite staining evidence suggesting the presence of very few W-20-17 cells in the cultures with low VAN concentrations. This was likely the result of bacterial dsDNA influencing measurements. To correct for this, we have reported only ALP-specific activity. Because we know that bacterial cells produce much lower concentrations of ALP than

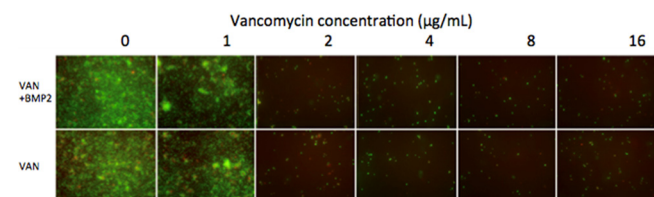


FIG 5 Live/Dead fluorescence staining of *S. aureus* treated with 0 to 16 $\mu\text{g/ml}$ VAN in monoculture and 0 or 100 ng/ml BMP-2 in TSB medium. Photos were taken at $\times 100$ magnification after 4 h of culture. Green indicates live bacterial cells, whereas red indicates dead cells. A visual decrease in cell viability over the 3 days of culture across all treatments of VAN is evident.

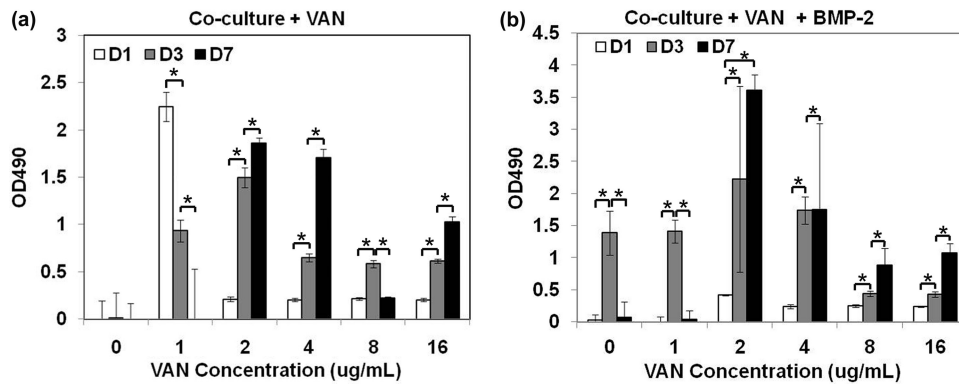


FIG 6 Measure of metabolic activity of W-20-17 in coculture treated with 0 to 16 µg/ml VAN in combination with (a) 0 ng/ml BMP-2 or (b) 100 ng/ml BMP-2 over 7 days using an MTS colorimetric assay. Higher OD₄₉₀ values indicate greater metabolic activity. The initial cell density was 15,000 cells per well. The absorbance is expressed as a measure of the cell viability via cell culture media for 7 days of incubation. Each value represents the mean \pm SD ($n = 3$). *, statistically significant difference between different time points ($P < 0.05$).

W-20-17 cells per capita, we expect that cocultures with high bacterial concentrations would show low ALP-specific activities whereas those with high numbers of W-20-17 would show values closer to that of the W-20-17 monoculture.

IL-6 production of cells in coculture. Interleukin-6 (IL-6) is a protein found to be secreted by human and mouse osteoblasts at elevated levels in response to infection by bacteria (specifically *S. aureus*) (6). Our results indicate that IL-6 production was significantly increased only upon exposure to bacteria in groups with VAN treatment at 16 µg/ml (Fig. 9). VAN treatments at ≤ 1 µg/ml resulted in a reduction in the amount of IL-6 produced. This is likely attributable to a decrease in the raw numbers of W-20-17 cells in culture. Treatments with VAN at 2 to 8 µg/ml showed no

significant change in IL-6 production. Groups treated with VAN at 16 µg/ml showed an increase in the amount of IL-6 produced. This suggests a greater number of cells combating infection by *S. aureus*.

DISCUSSION

The goals of this study were to establish an *in vitro* coculture model system to better represent the *in vivo* scenario of dual drug delivery and to gain a better understanding of the interactions between two specific compounds of choice: vancomycin antibiotic and bone morphogenetic protein 2. Briefly, we treated mouse bone marrow stromal cells (W-20-17) and *S. aureus* cells (ATCC 6538) with various concentrations of VAN (0 to 16 µg/ml) and BMP-2 (0 or 100 ng/ml) in both mono- and cocultures. In order to assess cell proliferation, differentiation, morphology, and inflammation response, an array of assays were performed for each treatment group across cultures grown for periods ranging from 1 h to 7 days. We selected the W-20-17 cell line because it has been used for an ASTM (F2131) standard test for *in vitro* biological activity of BMP-2. *S. aureus* was chosen for both its clinical origin and its high prevalence in bone graft failures (2, 4, 19, 29). If desired, modification of the system we establish here could accommodate testing of other antibiotic or growth factor compounds across a wide array of mammalian/bacterial cell cocultures. Similarly, the utilization of other antimicrobials such as silver ions should also be considered in order to complement the activities of substances such as VAN and BMP-2 (42, 49).

With regard to the efficacy of VAN antibiotic, we found that in coculture, VAN behaved differently than expected based on our monoculture findings. Staining results showed that in cocultures with BMP-2 at both 0 and 100 ng/ml, 2 µg/ml VAN was effective for 1 day, 4 µg/ml for 3 days, and 8 µg/ml for 7 days. This suggests that while bacteria were kept in check by some concentrations of VAN early on, concentrations below 8 µg/ml were not effective at reducing bacterial growth for extended periods of time. Compared to *S. aureus* monoculture L/D staining, coculture MTS results showed that in coculture, a higher dosage of VAN (8 µg/ml versus 2 µg/ml) was necessary to effectively inhibit bacterial growth for the same treatment group in monoculture (Fig. 5 and 6). By day 7, it would be expected that the *S. aureus* monocultures treated with at least 2 µg/ml VAN would continue to show little to

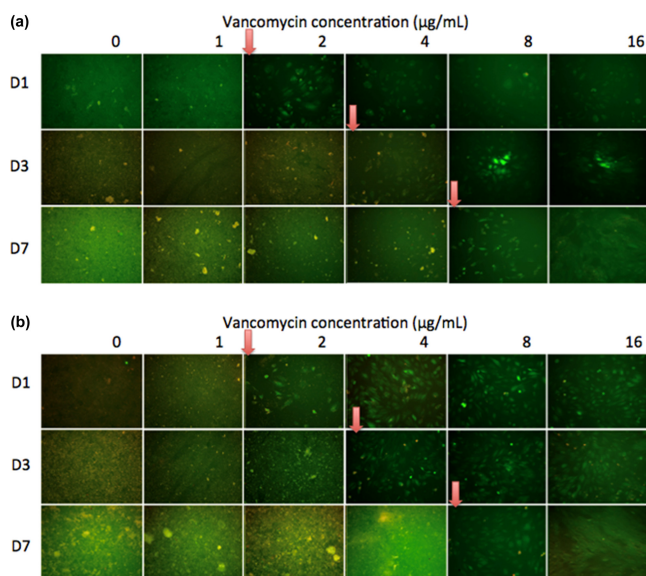


FIG 7 Live/Dead fluorescence staining of *S. aureus* and W-20-17 coculture treated with 0 to 16 µg/ml VAN in combination with (a) 0 ng/ml BMP-2 or (b) 100 ng/ml BMP-2 in DMEM-p medium. Photos were taken at $\times 100$ magnification after 1, 3, and 7 days of culture. Green indicates live cells, whereas red indicates dead cells. Smaller, spherical shapes are indicative of bacteria, while larger, more irregular shapes are W-12-17 cells. Red arrows indicate effective dosage of VAN.

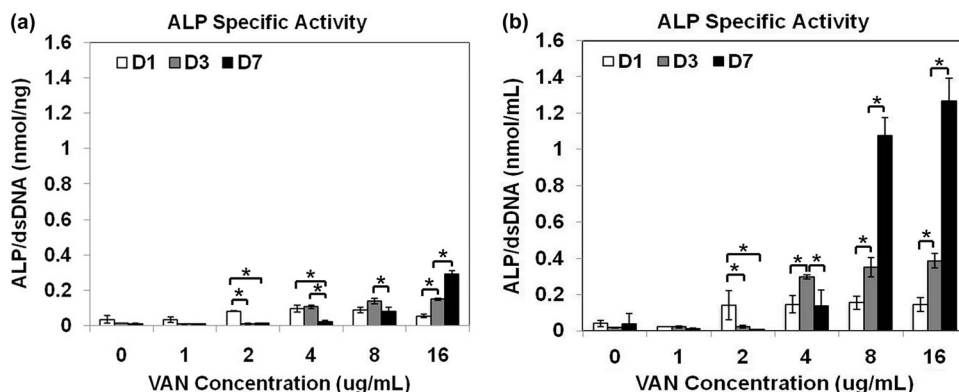


FIG 8 Measure of early osteoblastic differentiation of W-20-17/*S. aureus* coculture treated with 0 to 16 µg/ml VAN in combination with (a) 0 ng/ml BMP-2 or (b) 100 ng/ml BMP-2 using an ALP assay. Measurements were taken after 1, 3, and 7 days in culture and normalized for the dsDNA content. ALP activity is expressed as nanomoles per nanogram. Each value represents the mean ± SD ($n = 3$). *, statistically significant difference between different time points ($P < 0.05$). VAN treatments had a significant effect on ALP-specific activity. Higher concentrations of VAN were correlated with higher ALP-specific activities, suggesting that most of the activity was being generated by mBMSCs in culture, as opposed to *S. aureus*, which showed significantly lower ALP-specific activity (see Fig. 7). Treatment with 100 ng/ml BMP-2 yielded significantly higher ALP-specific activity than treatment without BMP-2. These results suggest that in coculture, both VAN and BMP-2 are able to maintain their respective functions.

no bacterial growth, but the accuracy of this approximation requires further testing. Still, this suggests that monocultures may not be a representative model for antibiotic dose dependence in our coculture model. Furthermore, this suggests that the coculture environment may limit the efficacy of VAN. It has been proposed that internalization of the *S. aureus* by the osteoblasts allows the bacteria to evade any vancomycin in solution, thus reducing the efficacy of the drug (13). However, further investigation is required to elucidate this mechanism, either through mechanistic study or through testing of alternative cell lines and compounds.

In both mono- and cocultures, we found that for all concentrations tested (0 to 16 µg/ml), VAN had no evident effect on the growth of mouse bone cells. Even at VAN concentrations of up to 200 µg/ml (data not shown), we found that the antibiotic had no detrimental effect on W-20-17 proliferation, differentiation, or morphology. This result holds true for both for the cultures that received only VAN and the cultures that also received BMP-2. Clearly, VAN is a good candidate as the antibiotic of choice in our

proposed dual-delivery system in that it is effective against *S. aureus*, the primary offender in bone graft failure, and has no evident toxicity to host osteoblasts at effective concentrations. Furthermore, our results are consistent with the available literature (35).

The second prong of our proposed dual-delivery system, BMP-2, showed that it is capable of creating a significant increase in ALP production (an early marker of osteoblastic differentiation) in both mono- and cocultures. In our qualitative L/D staining assessment, cultures treated with BMP-2 at 100 ng/ml showed better growth than those without BMP-2 treatment. This qualitative result is backed by the quantitative MTS and ALP assay results. ALP-specific activity was used to differentiate between bacterial proliferation (low ALP-specific activity) and mBMSC proliferation (high ALP-specific activity). On average, treatment with BMP-2 resulted in a statistically significant increase in ALP-specific activity (from less than 0.5 nmol/ml to as much as 2.5 nmol/ml). This pattern is also evident in coculture, suggesting that BMP-2 maintains its functionality in both mono- and cocultures. BMP-2 showed little to no effect both qualitatively and quantitatively on the monocultures of ATCC 6538 *S. aureus* within the 24-h time frame tested. This remained true for all concentrations of VAN tested, further positing that BMP-2 can maintain its positive effect on mouse bone cells while generating little to no positive effect on bacterial cells.

While BMP-2 and VAN behaved as expected when delivered in coculture, their combined effects on both the W-20-17 and *S. aureus* have, to our knowledge, never been established before despite their dual delivery previously having been explored (18, 27, 45). It is important to emphasize that across all concentrations of VAN tested, BMP-2 had no measurable detrimental effect on the drug's action against the Gram-positive bacteria. In fact, we found that some assays indicated that in treatments with BMP-2, a lower concentration of vancomycin was able to achieve almost complete suppression of bacterial growth compared to treatments without BMP-2 (VAN at 8 µg/ml in cocultures with BMP-2 versus 16 µg/ml in cocultures without BMP-2). The true mechanism behind this result cannot be determined due to the limitations of our assays, but we believe that it may have been a result of

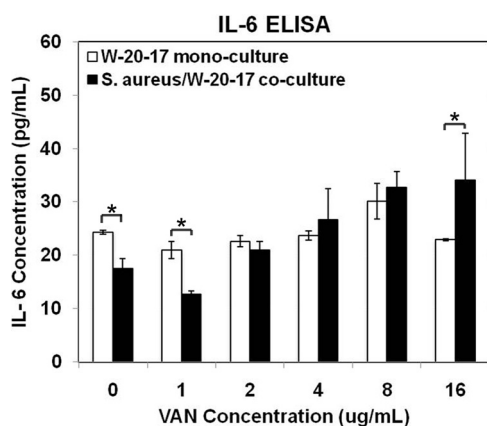


FIG 9 Measurement of W-20-17 inflammation response in coculture with *S. aureus* and treated with 0 to 16 µg/ml VAN and 100 ng/ml BMP-2 using an IL-6 ELISA kit. *, statistically significant difference between monoculture and coculture ($P < 0.05$).

BMP-2 conferring a competitive advantage upon the mBMSCs over the bacteria. It is suggested that BMP-2 allows improved cell growth and differentiation by day 7, thus allowing bone cell growth to outpace the capacity of the bacteria to infect and proliferate. Because this effect has not been observed before, further investigation into this interaction is necessary. If found to be true, this type of interaction would be suspected to be observed in treatments with other combinations of antibiotics and growth factors capable of maintaining function when delivered together. Such a finding could very well bring the study of prohost/antimicrobial compound dual delivery to the forefront of anti-infection research.

Here we begin an attempt to bridge the two major avenues of study in bone tissue repair: accelerated growth and improved treatment success rates. While each of these concepts has already been implemented in standard clinical care in the form of antibiotic and bone growth factor delivery, there still remains a need for refinement in their execution. This is the first of many studies aimed at creating a streamlined dual-delivery system that is capable of delivering both antibiotic drugs and bone growth factors to achieve those aforementioned goals. We have established an mBMSC/*S. aureus* coculture model system that is aimed at mimicking the *in vivo* conditions of bone graft infection and giving consistent, predictable results. From this model system, we have begun to characterize the interactions of two drugs of interest: VAN antibiotic and BMP-2 growth factor. Our findings indicate that, individually, they maintain their expected functionality as an antibiotic and growth factor, respectively, but that, in combination, their combined effects may result in a lower demand for the use of toxic, expensive VAN. As a whole, these results pave the way for future study in the dual delivery of antibiotics and growth factors. We plan to begin testing both delivery timing and more material-focused studies regarding the actual mechanistic approach to delivering said components using the coculture model system established here.

ACKNOWLEDGMENTS

We acknowledge the support from DOD (W81XWH-10-1-0966 and W81XWH-10-2-0010), Airlift Research Foundation, Wallace H. Coulter Foundation, NIH R01AR057837 from NIAMS, and NIH R01DE021468 from NIDCR.

REFERENCES

- Ackerman BH, Vannier AM, Eudy EB. 1992. Analysis of vancomycin time-kill studies with *Staphylococcus* species by using a curve stripping program to describe the relationship between concentration and pharmacodynamic response. *Antimicrob. Agents Chemother.* 36:1766–1769.
- Ako-Nai AK, Ikem IC, Daniel FV, Ojo DO, Oginni LM. 2009. A comparison of superficial and deep bacterial presence in open fractures of the lower extremities. *Int. J. Low. Extrem. Wounds* 8:197–202.
- Alexander EH, Hudson MC. 2001. Factors influencing the internalization of *Staphylococcus aureus* and impacts on the course of infections in humans. *Appl. Microbiol. Biotechnol.* 56:361–366.
- Allen RT, Lee YP, Stimson E, Garfin SR. 2007. Bone morphogenetic protein-2 (BMP-2) in treatment of pyogenic vertebral osteomyelitis. *Spine (Phila Pa 1976)* 32:2996–3006.
- Barna JC, Williams DH. 1984. The structure and mode of action of glycopeptide antibiotics of the vancomycin group. *Annu. Rev. Microbiol.* 38:339–357.
- Bost KL, et al. 1999. *Staphylococcus aureus* infection of mouse or human osteoblasts induces high levels of interleukin-6 and interleukin-12 production. *J. Infect. Dis.* 180:1912–1920.
- Boyce T, Edwards J, Scarborough N. 1999. Allograft bone. The influence of processing on safety and performance. *Orthop. Clin. North Am.* 30:571–581.
- Ciampolini J, Harding KG. 2000. Pathophysiology of chronic bacterial osteomyelitis. Why do antibiotics fail so often? *Postgrad. Med. J.* 76:479–483.
- Cornell CN, Tyndall D, Waller S, Lane JM, Brause BD. 1993. Treatment of experimental osteomyelitis with antibiotic-impregnated bone graft substitute. *J. Orthop. Res.* 11:619–626.
- Covey DC, et al. 2008. Orthopaedic war injuries: from combat casualty care to definitive treatment: a current review of clinical advances, basic science, and research opportunities. *Instr. Course Lect.* 57:65–86.
- Ellington JK, Elhofy A, Bost KL, Hudson MC. 2001. Involvement of mitogen-activated protein kinase pathways in *Staphylococcus aureus* invasion of normal osteoblasts. *Infect. Immun.* 69:5235–5242.
- Ellington JK, et al. 2006. Intracellular *Staphylococcus aureus* and antibiotic resistance: implications for treatment of staphylococcal osteomyelitis. *J. Orthop. Res.* 24:87–93.
- Ellington JK, et al. 1999. Mechanisms of *Staphylococcus aureus* invasion of cultured osteoblasts. *Microb. Pathog.* 26:317–323.
- Elsalanty ME, et al. 2008. Recombinant human BMP-2 enhances the effects of materials used for reconstruction of large cranial defects. *J. Oral Maxillofac. Surg.* 66:277–285.
- Garzoni C, Kelley WL. 2009. *Staphylococcus*: new evidence for intracellular persistence. *Trends Microbiol.* 17:59–65.
- Ginebra P, Traykova T, Planell JA. 2006. Calcium phosphate cements as bone drug delivery systems: a review. *J. Control Release* 113:102–110.
- Graziani AL, Lawson LA, Gibson GA, Steinberg MA, MacGregor RR. 1988. Vancomycin concentrations in infected and noninfected human bone. *Antimicrob. Agents Chemother.* 32:1320–1322.
- Guelcher SA, et al. 2011. Dual-purpose bone grafts improve healing and reduce infection. *J. Orthop. Trauma* 25:477–482.
- Gustilo RB, Anderson JT. 1976. Prevention of infection in the treatment of one thousand and twenty-five open fractures of long bones: retrospective and prospective analysis. *J. Bone Joint Surg. Am.* 58:453–458.
- Hanada K, Dennis JE, Caplan AI. 1997. Stimulatory effects of basic fibroblast growth factor and bone morphogenetic protein-2 on osteogenic differentiation of rat bone marrow-derived mesenchymal stem cells. *J. Bone Miner. Res.* 12:1606–1614.
- Hidayat LK, Hsu DI, Quist R, Shriner KA, Wong-Beringer A. 2006. High-dose vancomycin therapy for methicillin-resistant *Staphylococcus aureus* infections: efficacy and toxicity. *Arch. Intern. Med.* 116:2138–2144.
- Johnson EN, Burns TC, Hayda RA, Hospenthal DR, Murray CK. 2007. Infectious complications of open type III tibial fractures among combat casualties. *Clin. Infect. Dis.* 45:409–415.
- Kemp DH, et al. 2008. Retention of in vitro and in vivo BMP-2 bioactivities in sustained delivery vehicles for bone tissue engineering. *Biomaterials* 29:3245–3252.
- Ketonis C, et al. 2010. Antibiotic modification of native grafts: improving upon nature's scaffolds. *Tissue Eng. Part A* 16:2041–2049.
- Ketonis C, et al. 2011. Vancomycin bonded to bone grafts prevents bacterial colonization. *Antimicrob. Agents Chemother.* 55:487–494.
- Kim S, et al. 2011. In vitro evaluation of an injectable chitosan gel for sustained local delivery of BMP-2 for osteoblastic differentiation. *J. Biomed. Mater. Res. B Appl. Biomater.* 99:380–390.
- Liu SJ, et al. 2007. Novel solvent-free fabrication of biodegradable polylactic-glycolic acid (PLGA) capsules for antibiotics and rhBMP-2 delivery. *Int. J. Pharm.* 330:45–53.
- Liu Y, Huse RO, de Groot K, Buser D, Hunziker EB. 2007. Delivery mode and efficacy of BMP-2 in association with implants. *J. Dent. Res.* 86:84–89.
- Lord CF, Gebhardt MC, Tomford WW, Mankin HJ. 1988. Infection of bone allografts. *J. Bone Joint Surg. Am.* 70:369–376.
- Menzies BE, Kourteva I. 1998. Internalization of *Staphylococcus aureus* by endothelial cells induces apoptosis. *Infect. Immun.* 66:5994–5998.
- Murray CK, et al. 2011. Prevention of infections associated with combat-related extremity injuries. *J. Trauma* 71(Suppl. 2):S235–S257.
- Nair SP, Williams RJ, Henderson B. 2000. Advances in our understanding of the bone and joint pathology caused by *Staphylococcus aureus* infection. *Rheumatology (Oxford)* 39:821–834.
- Owens BD, et al. 2008. Combat wounds in operation Iraqi Freedom and operation Enduring Freedom. *J. Trauma* 64:295–299.
- Raiche AT, Puleo DA. 2004. Cell responses to BMP-2 and IGF-1 released

- with different time-dependent profiles. *J. Biomed. Mater. Res. A* 69:342–350.
35. Rathbone CR, Cross JD, Brown KV, Murray CK, Wenke JC. 2011. Effect of various concentrations of antibiotics on osteogenic cell viability and activity. *J. Orthop. Res.* 29:1070–1074.
36. Reilly SS, Hudson MC, Kellam JF, Ramp WK. 2000. In vivo internalization of *Staphylococcus aureus* by embryonic chick osteoblasts. *Bone* 26:63–70.
37. Riew KD, Wright NM, Cheng S, Avioli LV, Lou J. 1998. Induction of bone formation using a recombinant adenoviral vector carrying the human BMP-2 gene in a rabbit spinal fusion model. *Calcif. Tissue Int.* 63:357–360.
38. Rose WE, Poppens PT. 2009. Impact of biofilm on the in vitro activity of vancomycin alone and in combination with tigecycline and rifampicin against *Staphylococcus aureus*. *J. Antimicrob. Chemother.* 63:485–488.
39. Smith TL, et al. 1999. Emergence of vancomycin resistance in *Staphylococcus aureus*. Glycopeptide-Intermediate *Staphylococcus aureus* Working Group. *N. Engl. J. Med.* 340:493–501.
40. Soriano A, et al. 2008. Influence of vancomycin minimum inhibitory concentration on the treatment of methicillin-resistant *Staphylococcus aureus* bacteremia. *Clin. Infect. Dis.* 46:193–200.
41. Sorrell TC, Packham DR, Shanker S, Foldes M, Munro R. 1982. Vancomycin therapy for methicillin-resistant *Staphylococcus aureus*. *Ann. Intern. Med.* 97:344–350.
42. Stinner DJ, Waterman SM, Masini BD, Wenke JC. 2011. Silver dressings augment the ability of negative pressure wound therapy to reduce bacteria in a contaminated open fracture model. *J. Trauma* 71(Suppl.):S147–S150.
43. Tenover FC, Moellering RC, Jr. 2007. The rationale for revising the Clinical and Laboratory Standards Institute vancomycin minimal inhibitory concentration interpretive criteria for *Staphylococcus aureus*. *Clin. Infect. Dis.* 44:1208–1215.
44. Tucker KA, Reilly SS, Leslie CS, Hudson MC. 2000. Intracellular *Staphylococcus aureus* induces apoptosis in mouse osteoblasts. *FEMS Microbiol. Lett.* 186:151–156.
45. Wang Y, et al. 2011. Assessing the character of the rhBMP-2 and vancomycin-loaded calcium sulphate composites in vitro and in vivo. *Arch. Orthop. Trauma Surg.* 131:991–1001.
46. Wenke JC, Guelcher SA. 2011. Dual delivery of an antibiotic and a growth factor addresses both the microbiological and biological challenges of contaminated bone fractures. *Expert Opin. Drug Deliv.* 8:1555–1569.
47. Winkler H, Janata O, Berger C, Wein W, Georgopoulos A. 2000. In vitro release of vancomycin and tobramycin from impregnated human and bovine bone grafts. *J. Antimicrob. Chemother.* 46:423–428.
48. Younger EM, Chapman MW. 1989. Morbidity at bone graft donor sites. *J. Orthop. Trauma* 3:192–195.
49. Zheng Z, et al. 2010. The use of BMP-2 coupled-Nanosilver-PLGA composite grafts to induce bone repair in grossly infected segmental defects. *Biomaterials* 31:9293–9300.
50. Zilberman M, Elsner JJ. 2008. Antibiotic-eluting medical devices for various applications. *J. Control Release* 130:202–215.



Cytokine combination therapy prediction for bone remodeling in tissue engineering based on the intracellular signaling pathway

Xiaoqiang Sun^{a,b}, Jing Su^{a,1}, Jiguang Bao^b, Tao Peng^a, Le Zhang^{e,f}, Yuanyuan Zhang^{c,*}, Yunzhi Yang^{d,*}, Xiaobo Zhou^{a,*}

^a Department of Radiology, The Methodist Hospital Research Institute, Weil Cornell Medical College, Houston, TX 77030, USA

^b School of Mathematical Science, Beijing Normal University, Beijing, 100875, PR China

^c Wake Forest Institute for Regenerative Medicine, Wake Forest University School of Medicine, Medical Center Blvd., Winston-Salem, NC 27157, USA

^d Department of Orthopedic Surgery, Stanford University, 300 Pasteur Drive, Edwards R155, Stanford, CA 94305, USA

^e Department of Mathematical Sciences, Michigan Technological University, Houghton, MI 49931, USA

^f College of Computer and Information Science, Southwest University, Chongqing, 400715, PR China

ARTICLE INFO

Article history:

Received 18 May 2012

Accepted 20 July 2012

Available online 19 August 2012

Keywords:

Bone tissue engineering
Bone remodeling
Cytokine combination therapy
Systems biology
Osteogenic differentiation
Signaling pathway

ABSTRACT

The long-term performance of tissue-engineered bone grafts is determined by a dynamic balance between bone regeneration and resorption. We proposed using embedded cytokine slow-releasing hydrogels to tune this balance toward a desirable final bone density. In this study we established a systems biology model, and quantitatively explored the combinatorial effects of delivered cytokines from hydrogels on final bone density. We hypothesized that: 1) bone regeneration was driven by transcription factors Runx2 and Osterix, which responded to released cytokines, such as Wnt, BMP2, and TGFβ, drove the development of osteoblast lineage, and contributed to bone mass generation; and 2) the osteoclast lineage, on the other hand, governed the bone resorption, and communications between these two lineages determined the dynamics of bone remodeling. In our model, Intracellular signaling pathways were represented by ordinary differential equations, while the intercellular communications and cellular population dynamics were modeled by stochastic differential equations. Effects of synergistic cytokine combinations were evaluated by Loewe index and Bliss index. Simulation results revealed that the Wnt/BMP2 combinations released from hydrogels showed best control of bone regeneration and synergistic effects, and suggested optimal dose ratios of given cytokine combinations released from hydrogels to most efficiently control the long-term bone remodeling. We revealed the characteristics of cytokine combinations of Wnt/BMP2 which could be used to guide the design of *in vivo* bone scaffolds and the clinical treatment of some diseases such as osteoporosis.

© 2012 Elsevier Ltd. All rights reserved.

1. Introduction

Bone remodeling in tissue engineering is a long-term physiological process that dynamically balances osteogenesis and bone resorption and re-distributes bone mass to match the external mechanical changes [1–3]. This complex biological event involves

intracellular signaling, stem cell driven lineage developing, and intercellular communications among various cellular phenotypes. A variety of systematic and local factors play important roles in such multi-scale signaling [4]. Bone remodeling is especially critical to the success of tissue-engineered bone grafts. Failure to accumulate bone mass according to the physiological needs of mechanical strength will cause post-implantation bone fractures and poor outcomes. Personalized tuning of bone remodeling process is another challenge. For example, osteoporosis patients are often victims of bone fractures, and in their bone scaffolds the osteogenesis should be enhanced to overcome the patient hormone and cytokine environments that promote bone resorption. A flexible and tunable infrastructure which allows fine tuning of the bone remodeling process is required to meet the clinical needs.

This challenge can be potentially addressed by cytokine combination therapy which encapsulates multiple cytokines (or

Abbreviations: BMP2, bone morphogenetic protein 2; TGFβ, transforming growth factor β; Osx, Osterix; Runx2, Runt-related transcription factor 2; BMU, basic multi-cellular unit; MSC, mesenchymal stem cell; OBpy, pre-osteoblasts; OBa, active osteoblasts; HSC, hematopoietic stem cells; OCp, pre-osteoclasts; OCa, active osteoclasts; ODEs, ordinary differential equations; SDEs, stochastic differential equations; OPG, osteoprotegerin.

* Corresponding authors.

E-mail addresses: yzhang@wfubmc.edu, xsun@tmhs.org (Y. Zhang), ypyang@stanford.edu (Y. Yang), XZhou@tmhs.org (X. Zhou).

¹ Co-first author.

growth factors) into polymer nanospheres, expected to produce a better effect than the single factor. Recently our group [5–8] and others [9–11] have shown the capabilities of accurately and independently controlling drug release rates of individual growth factors and cytokines from the delayed slow-release hydrogels embedded in artificial bone scaffolds. Hydrogels are highly absorbent natural (e.g. hyaluronic acid) or synthetic polymers (e.g. polyvinyl alcohol, sodium polyacrylate, and acrylate polymers) that may possess a degree of flexibility very similar to normal tissue because of their considerable water. When used as scaffolds for bone tissue regeneration, hydrogels often contain human primary cells (e.g. osteocytes and endothelial cells) and growth factors or cytokines to repair bone tissue. Cytokines (e.g. BMP2, TGF β and Wnt ligands) play an important role in osteogenic differentiation of MSC and bone remodeling. Ideally key cytokines can be programmatically released into the micro-environments of the bone graft and guide desired bone remodeling [12,13]. This study addresses the effects of optimally-combined cytokines after released from hydrogels on bone regeneration.

Osteoblast and osteoclast lineages are responsible for two competing but coordinated processes, bone formation and resorption, respectively, and thus profile the dynamic of bone remodeling. These two processes occur in a structure called basic multi-cellular units (BMU) [14] at multiple sites in the skeleton as well as artificial scaffolds [1]. Bone marrow mesenchymal stem cells (MSC) differentiate to pre-osteoblast, then osteogenic lineages, which are responsible for bone formation; while hematopoietic stem cells (HSC) differentiate to the pre-osteoclasts, and then osteoclasts, which govern bone resorption.

A number of mathematical models have been developed to describe the bone remodeling in recent years. Komarova et al. [15] constructed a mathematical model to calculate cell population dynamics and changes in bone mass at a discrete site of bone remodeling, considering the autocrine and paracrine interactions among osteoblasts and osteoclasts. Lemaire et al. [16] proposed

another cell population model to explain the interactions between osteoblasts and osteoclasts by establishing the intercellular signaling pathway RANK-RANKL-OPG. Then Pivonka et al. [17] extended this pathway to study and theoretically explore the functional implications of particular RANK/OPG expression profiles on bone mass. Furthermore, Pivonka et al. [17,18] used such models to investigate the possible therapeutic intervention to restore bone mass due to the imbalance of RANK-RANKL-OPG regulation [18].

However, previous studies have often lacked an intracellular signaling and fell short on representing the intracellular molecular mechanism. Several molecular signals and mechanisms involved in the bone healing or remodeling have been revealed from *in vitro* and/or *in vivo* experiments. The osteoblast commitment, differentiation and functions are controlled by several transcription factors resulting in the expression of genes responsible for the osteoblastic lineage from MSC to pre-osteoblasts and then to active osteoblasts [19], as described in Fig. 1. Runx-related transcription factor 2 (Runx2) and Osterix (Osx) have been generally demonstrated to be two crucial transcription factors in osteogenic differentiation [19]. Various cytokines, such as BMP2, TGF β and Wnt ligands, can stimulate the expression of Runx2 and Osx through a variety of pathways [19–22]. After the pathway is activated, Runx2 and Osx play different particular roles in different stages of osteoblastic lineage. Both Runx2 and Osx can promote the differentiation of MSC into pre-osteoblasts [19,23], whereas Runx2 can inhibit the differentiation of pre-osteoblasts into active osteoclasts [19,24].

Moreover, only a few mathematical models have been developed to investigate the effect of cytokine therapy, especially cytokine combination therapy, for bone healing. Particularly, we are concerned with the following questions in the bone healing therapy. First, are the effects of cytokine combination better than those of single cytokine? Second, how do we evaluate the synergism of the cytokine combination therapies? Third, what are the most efficient dose and ratio of specific cytokine combination to achieve expected bone remodeling goals? To answer these

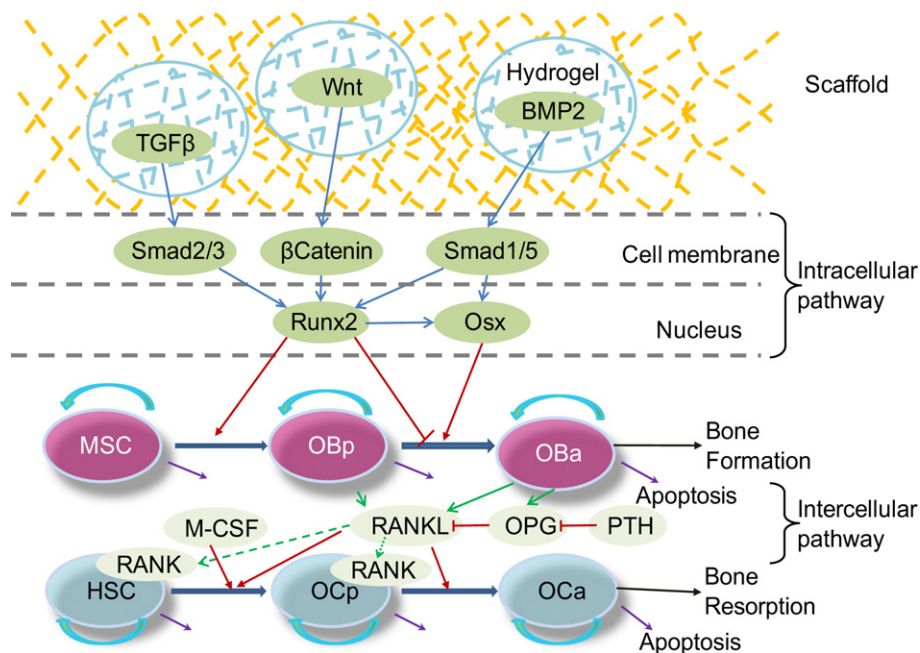


Fig. 1. Schematic illustration of intracellular and intercellular signaling and cellular dynamics in bone healing and bone remodeling. Bone regeneration or bone remodeling involves bone resorption by osteoclasts (OC) and the following bone formation by osteoblasts (OB) within basic multi-cellular units (BMU). Three cytokines were considered: TGF β , Wnt and BMP2. Intracellular signaling pathway consists of Smad2/3, Smad1/5, β -Catenin, and Runx2 and Osx. Runx2 can promote the differentiation of mesenchymal stem cells (MSCs) into pre-osteoblasts (OBp) and can inhibit the differentiation of pre-osteoblasts into active osteoblasts (OBa). Osx also play a promoting role in the later stage of osteoblastic lineage which interacts with osteoclastic lineage through intercellular signaling pathway RANK-RANKL-OPG.

questions, numerous candidate conditions should be examined for this complex system of multiple cell type, various cytokine candidates, and multiple time scales. Traditional biological experiments are expensive and time-consuming. Therefore, a systems biological model is required to best utilize our current knowledge of the bone remodeling process to explore *in silico* candidate conditions, screen out critical factors and key cytokines of the system, and guide the biological experiments.

This work was designed to build up a computational systematic model to study the combination effects of cytokines released from hydrogels including Wnt, BMP2, and TGFβ for controlling the balance of bone formation and resorption of implanted bone scaffolds based on the intracellular signaling pathway. We firstly developed a systematic model composed of a system of ordinary differential equations (ODEs) to describe the intracellular signaling pathway to regulate osteogenic differentiation. And then, we combined the intracellular signaling pathway with intercellular signaling pathway to control osteoclast differentiation. Next, we integrated the intracellular and intercellular signaling pathways into the cellular population dynamics described by a set of stochastic differential equations (SDEs) to simulate bone healing and remodeling. The unknown coefficients in the intracellular signaling pathway were estimated by fitting them to the dynamic experimental data [21,25,26] using optimization algorithm. Finally, we investigated the response of cellular population dynamics to therapies of single or combined cytokines as well as quantitatively evaluated the combination effect of cytokines by Loewe and Bliss indexes.

2. Methods

As shown in Fig. 2, our model encompasses four relevant biological scales: intracellular, intercellular, cellular and bone tissue scales. We are going to introduce the details of the four scales in the followings.

2.1. Intracellular signaling pathway construction

Runx-related transcription factor 2 (Runx2) and Osterix (Osx) have been found as two crucial transcription factors in osteoblast differentiation [19]. Wnt signaling directly regulates the expression of Runx2 through β-Catenin [19,27]. BMP2 and TGFβ can activate or phosphorylate Smad1/5 and Smad2/3 respectively [20,21]. These Smads can interact with co-Smad (Smad4) or other transcription factors to stimulate the expression of Runx2 [19,20]. Runx2, as well as Smad1/5 activated by BMP2, can stimulate the expression of downstream Osx [19,22].

We used a system of ODEs to describe the time dynamics of concentration for each component in intracellular pathway (Fig. 1) by Michaelis–Menten Law [28].

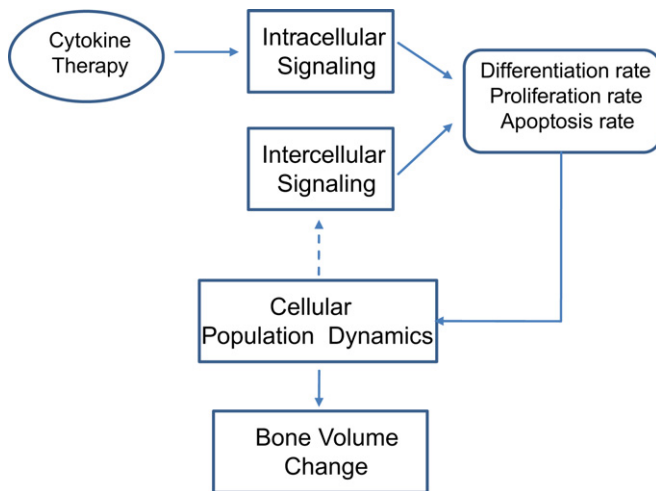


Fig. 2. Multi-scale model for bone regeneration or bone remodeling system. Our systematic model encompasses four relevant biological scales: intracellular, intercellular, cellular and bone tissue scales. See details of the modeling in main text.

Hill function [28,29] was employed to model the regulatory relationship between the proteins and/or transcription factors.

Smad1/5 can be phosphorylated by BMP2 [20]. The concentration change of phosphorylated Smad1/5 ([S1]) depends on the concentration of BMP2 ([BMP2]), unphosphorylated Smad1/5 ([TotalS1] – [S1]), and dephosphorylation of itself. Equation (1) describes the phosphorylation and dephosphorylation of Smad1/5.

$$\frac{d[S1]}{dt} = \frac{V_1 \cdot [BMP2]}{K_1 + [BMP2]} \cdot ([TotalS1] - [S1]) - d_1 \cdot [S1]. \quad (1)$$

Smad2/3 can be phosphorylated by TGFβ [26]. The change of the concentration of phosphorylated Smad2/3 ([S2]) depends on the concentration of TGFβ ([TGFβ]), unphosphorylated Smad2/3 ([TotalS2] – [S2]), and dephosphorylation of itself. Equation (2) describes the phosphorylation and dephosphorylation of Smad2/3.

$$\frac{d[S2]}{dt} = \frac{V_2 \cdot [TGF\beta]}{K_2 + [TGF\beta]} \cdot ([TotalS2] - [S2]) - d_2 \cdot [S2]. \quad (2)$$

β-Catenin is one of the key proteins in Wnt signaling pathway [23,27], the change of the concentration of β-Catenin have been modeled by Equation (3) [30,31].

$$\frac{d[\beta - Catenin]}{dt} = a - \left(\left(\frac{[Wnt] + b}{c \cdot [Wnt] + d} \right) \cdot \left(\frac{e}{e + [\beta - Catenin]} \right) + f \right) \cdot [\beta - Catenin]. \quad (3)$$

Runx2 has been found to be a crucial transcription factor in osteogenic differentiation [19,23]. Its expression and activation can be promoted by BMP2 through Smad1/5, and also by TGFβ through Smad2/3, and by Wnt ligands through β-Catenin and other proteins [27]. Equation (4) describes the expression and degradation of Runx2.

$$\frac{d[Runx2]}{dt} = \frac{V_4 \cdot [S1]}{K_4 + [S1]} + \frac{V_5 \cdot [S2]}{K_5 + [S2]} + \frac{V_6 \cdot [\beta - Catenin]}{K_6 + [\beta - Catenin]} - d_4 \cdot [Runx2]. \quad (4)$$

Osx is also a critical transcription factor in osteoblast differentiation, acting as downstream of Runx2 and Smad1/5. Equation (5) describes the expression and degradation of Osx.

$$\frac{d[Osx]}{dt} = \frac{V_7 \cdot [S1]}{K_7 + [S1]} + \frac{V_8 \cdot [Runx2]}{K_8 + [Runx2]} - d_5 \cdot [Osx]. \quad (5)$$

2.2. Intercellular signaling pathway

The intercellular signaling pathway in bone remodeling, known as RANK-RANKL-OPG system, is important in cell–cell communication, which can explain how the osteoblast lineage regulates the osteoclast differentiation and activation [32]. Because RANK-RANKL-OPG pathway has been well investigated by previous studies [17,18], here we just listed the detailed equations describing the intercellular pathway in the supplementary files (Text S2).

2.3. Integrating the intracellular and intercellular signaling pathways into cellular population dynamics

We assumed that the binding and/or dissociation reactions in intracellular signaling pathway are much faster than both cellular phenotypic switches and cellular population changes [17,33], so we derived the quasi-steady state of intracellular signaling pathway (as listed in Text S1) and then we integrated it into cellular population dynamics. As described in Fig. 1, the differentiation of MSC into pre-osteoblasts is promoted by Runx2 and Osx [19,23]. This regulation was described by Equation (6).

$$\dot{D}_{MSC} = D_{MSC} \cdot H_{act, MSC}^{Runx2} \cdot (1 + H_{act, MSC}^{Osx}), \quad (6.1)$$

$$H_{act, MSC}^{Runx2} = \frac{V_{D1, Runx2} \cdot [Runx2]}{K_{D1, Runx2} + [Runx2]}, \quad (6.2)$$

$$H_{act, MSC}^{Osx} = \frac{V_{D1, Osx} \cdot [Osx]}{K_{D1, Osx} + [Osx]}. \quad (6.3)$$

where D_{MSC} is the differentiation rate of mesenchymal stem cells; $K_{D1, Runx2}$ and $K_{D1, Osx}$ are regulation coefficients regarding Runx2 and Osx; $V_{D1, Runx2}$ and $V_{D1, Osx}$ are Hill regulatory factors.

The differentiation of pre-osteoblasts into active osteoblasts is inhibited by Runx2 and promoted by Osx [19,24] as Equation (7).

$$\dot{D}_{OBp} = D_{OBp} \cdot (H_{rep, OBp}^{Runx2} + H_{act, OBp}^{Osx}), \quad (7.1)$$

$$H_{rep, OBp}^{Runx2} = \frac{1}{1 + [Runx2]/K_{D2, Runx2}}, \quad (7.2)$$

$$H_{act, OBp}^{Osx} = \frac{V_{D2, Osx} \cdot [Osx]}{K_{D2, Osx} + [Osx]}. \quad (7.3)$$

where D_{OBp} is the differentiation rate of pre-osteoclasts; $K_{D2,Runx2}$ and $K_{D2,Osx}$ are regulation coefficients regarding Runx2 and Osx; $V_{D2,Osx}$ are Hill regulatory factors.

Differentiation and activation of hematopoietic stem cells into pre-osteoclasts, as well as differentiation of pre-osteoclasts into active osteoblasts, requires the binding of RANKL released by osteoblasts to RANK on the surface of osteoclasts, which is inhibited by OPG that can bind to RANKL. The intercellular pathway can be incorporated into cellular population dynamics with Equation (8) [17,18].

$$\bar{D}_{HSC} = D_{HSC} \cdot H_{act,HSC}^{CSF1}, \quad (8.1)$$

$$\bar{D}_{OCp} = D_{OCp} \cdot \left(H_{act,OCp}^{CSF1} \cdot H_{act,OCp}^{RANKL} \right), \quad (8.2)$$

$$H_{act,OCp}^{RANKL} = \frac{[RANKL]}{K_{D3,RANKL} + [RANKL]}, \quad (8.3)$$

where D_{HSC} is the differentiation rate of hematopoietic stem cells; D_{OCp} is the differentiation rate of pre-osteoclasts; $K_{D3,RANKL}$ is the regulation coefficient regarding RANKL; $H_{act,HSC}^{CSF1}$ and $H_{act,OBp}^{CSF1}$ are illustrated in Table S2.

2.4. Cellular population dynamics

As described in Fig. 1, our model considered 6 types of bone cells in 2 lineages. The osteoblastic lineage consists of MSC, pre-osteoblasts and active osteoblast. And osteoclastic lineage is comprised of HSC, pre-osteoclasts and active osteoclasts cell types. Since MSC and HSC outnumber other cell types [17], this model sets the numbers of these two cell types as constant (n_{MSC} , n_{HSC}).

We employed a set of stochastic differential equations (SDEs) [34] to model the cellular population dynamics during bone remodeling or bone healing as follows.

$$dX_{OBp} = \bar{D}_{MSC} \cdot n_{MSC} dt + (P_{OBp} - \bar{D}_{OBp} - d_{OBp}) \cdot X_{OBp} dt + X_{OBp} \cdot \sigma_1 dW_1, \quad (9)$$

$$dX_{OBa} = \bar{D}_{OBp} \cdot X_{OBp} dt + (P_{OBa} - d_{OBa}) \cdot X_{OBa} dt + X_{OBa} \cdot \sigma_2 dW_2, \quad (10)$$

$$dX_{OCp} = \bar{D}_{HSC} \cdot n_{HSC} dt + (P_{OCp} - \bar{D}_{OCp} - d_{OCp}) \cdot X_{OCp} dt + X_{OCp} \cdot \sigma_3 dW_3, \quad (11)$$

$$dX_{OCa} = \bar{D}_{OCp} \cdot X_{OCp} dt + (P_{OCa} - d_{OCa}) \cdot X_{OCa} dt + X_{OCa} \cdot \sigma_4 dW_4. \quad (12)$$

where X_{OBp} , X_{OBa} , X_{OCp} and X_{OCa} are random variables representing the concentration of pre-osteoblasts, active osteoblasts, pre-osteoclasts and active osteoclasts,

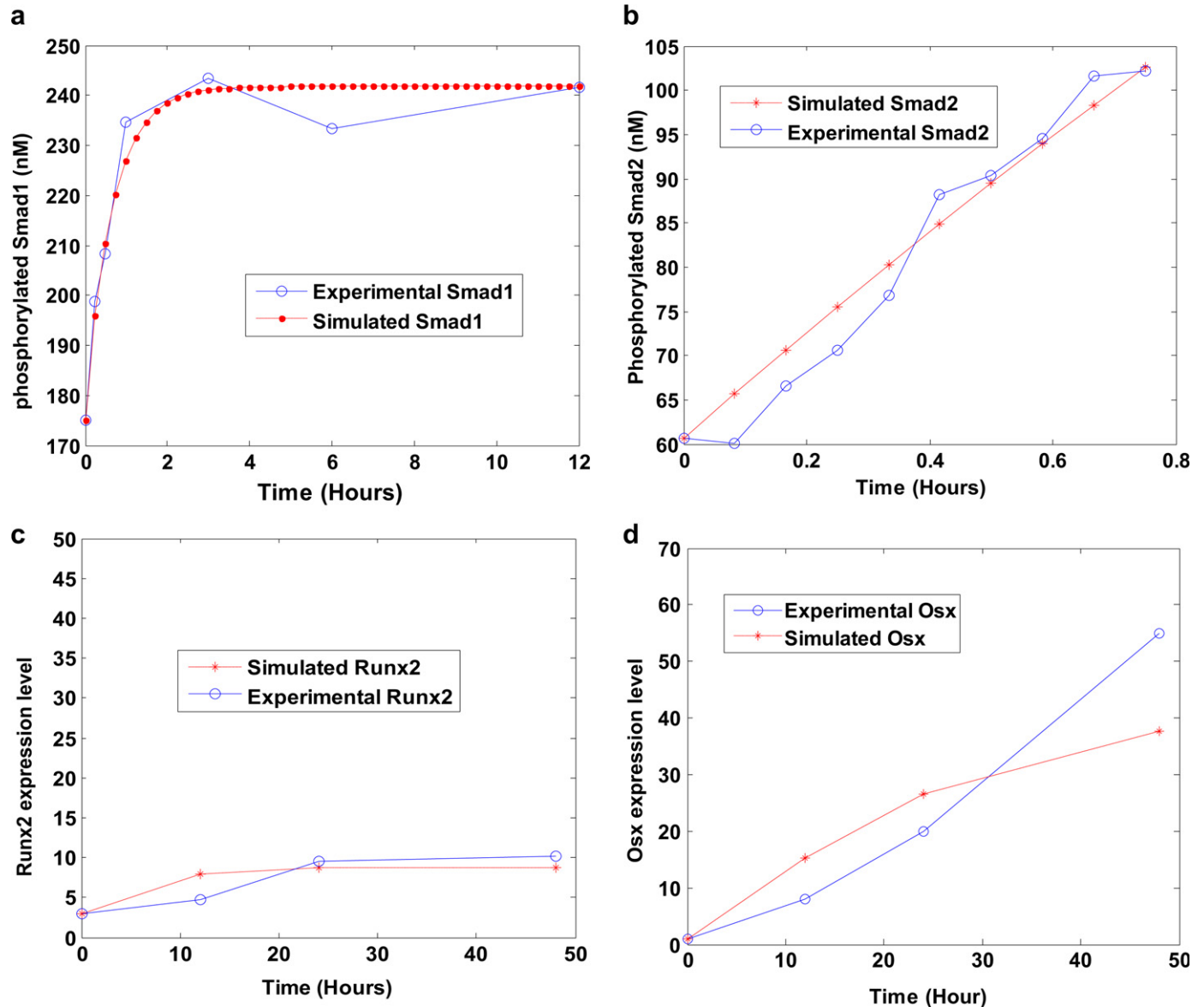


Fig. 3. Fitness results between the simulated dynamic data and the experimental data. X axis represents time. Y axis represents the concentrations of (a) phosphorylated Smad1/5, (b) phosphorylated Smad2/3, and the expression levels of (c) Runx2 and (d) Osx, respectively.

respectively. W_i ($i = 1, 2, 3, 4$) is Wiener process or also called standard Brownian motion to simulate local diffusion of cell population, i.e. migration and/or immigration in a basic multi-cellular unit as well as the stochastic regulation of signaling pathway. σ_i ($i = 1, 2, 3, 4$) represents diffusion coefficient. D_{MSC} , D_{OBp} , D_{HSC} , and D_{OCp} stand for differentiation rates of MSC, pre-osteoblasts, HSC, and pre-osteoclasts, respectively. P_{OBp} , P_{OBa} , P_{OCp} , and P_{OCa} are proliferation rates (or self renew rates) of corresponding cell types. d_{OBp} , d_{OBa} , d_{OCp} , and d_{OCa} are apoptosis rates of considered cell types, respectively.

Bone mass change is determined by bone formation due to osteoblasts and bone resorption due to osteoclasts. We assumed that bone deposition and bone resorption rate is proportional to the number of active osteoblasts and active osteoclasts respectively [17,18], so the change rate of bone mass is proportional positively to the number of active osteoblasts and negatively proportional to the number of active osteoclasts, which can be described by Equation (13).

$$dM = k_{form} \cdot X_{OBa} dt - k_{rep} \cdot X_{OCa} dt, \quad (13)$$

where M represents the bone mass normalized to the initial value. k_{form} and k_{rep} are bone formation and resorption rates respectively. The bone mass change is chosen as an output in our systematic model.

Most of above parameters of cellular population dynamics were well studied by previous researches [17,18], and listed in Table S2. The unknown parameters were computed and assumed to ensure the requirement of stability of the system in the normal steady state [18], please refer to Text S3.

The system of nonlinear ODEs was numerically solved using implicit Euler method [35], the stochastic differential equations were solved by Euler–Maruyama method [36]. The program was performed in MATLAB R2007b (MathWorks).

3. Results

This study developed a systematic model for bone regeneration and bone remodeling based on the intracellular signaling pathway of osteogenic differentiation. We firstly developed the intracellular signaling pathway and estimated its unknown coefficients. Secondly, we investigated the responses of cellular population to therapies of single cytokine or combined cytokines released from hydrogels. Finally, we quantitatively evaluated the combination effect of cytokines by applying Loewe and Bliss indexes [26,27].

3.1. Intracellular pathway parameter estimation

After having described the intracellular signaling pathway by a mathematical model, we have to estimate the unknown coefficients of the model. There are totally 18 unknown coefficients in

Equations (1), (2), (4) and (5). The coefficients of Equation (3) have been validated by previous study [30]. Among these 18 unknown coefficients, V_1 , V_2 , V_4 , V_5 , V_6 , V_7 and V_8 are maximum activation velocities of corresponding reactions; K_1 , K_2 , K_4 , K_5 , K_6 , K_7 and K_8 are Michealis–Menten constants; d_1 , d_2 , d_4 and d_5 are degradation rates of Smad1/5, Smad2/3, Runx2 and Osx, respectively.

We did parameter fitting regarding the dynamic experimental data [21,25,26] by genetic algorithm [37]. Our experimental data [21,25,26] consist of 4 sets of data with 24 different time points, which are listed in Fig. S1. Equation (14) was employed for parameter estimation by minimizing the fitness error between the experimental and simulated data,

$$\hat{\theta} = \arg \min_{\theta \in \Theta} \sum_{i=1}^n (y_{t_i}^{\text{sim}}(\theta) - y_{t_i}^{\text{exp}}(\theta))^2, \quad (14)$$

where $y_{t_i}^{\text{sim}}(\theta)$ and $y_{t_i}^{\text{exp}}(\theta)$ represent the simulated and experimental data with time point t_i and parameters θ , respectively. Θ stands for the parameter space, in which the search space for each parameter was preset in a range according to previous studies [21,25,26] along with Michealis–Menten kinetics. Genetic algorithm [37] was adopted to minimize the cost function in Equation (14).

Fig. 3 shows that simulated dynamic data fit well to the dynamic experimental data as previously reported [21,25,26]. The mean squared error between the simulated data and experimental data is 0.2553. The speed of the whole estimation algorithm is comparably fast and the total programming running time in the parameter estimation is 16.95 min.

The coefficient of variation is used to determine if the parameter is identifiable or not. Coefficient of variation is defined as the ratio of the standard deviation to the mean of the estimated values. For a given parameter, if its coefficient of variation is greater than 1, then it is unidentifiable; otherwise it is identifiable. To compute the coefficient of variation for each unknown parameters, we applied bootstrap strategy [38] to re-sample 24 experimental time point data 24 times by “leave one out” technique [39]. After that, we can have 24 sets of experimental data and calculate the coefficient of variation for each parameter. Fig. 4 shows that only the coefficients of variation of V_7 and K_7 are greater than 1, indicating that only

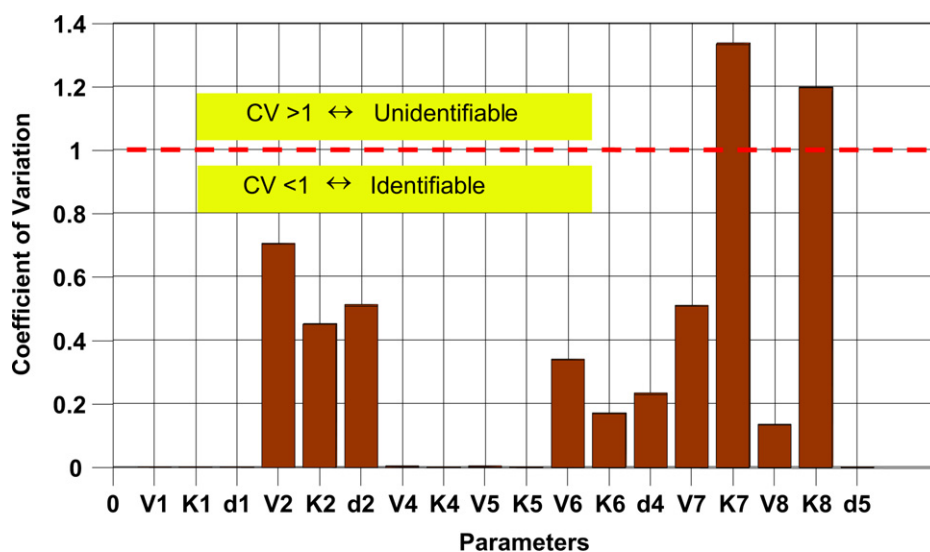


Fig. 4. Coefficient of variation of parameters. Only the coefficients of variation of V_7 and K_7 are larger than 1, indicating that only 11.11% of parameters are unidentifiable and other 88.89% of parameters are identifiable.

11.11% of parameters are unidentifiable whereas 88.89% of parameters are identifiable.

Parameter sensitivity analysis is a tool to examine whether the system is preserved to the modest parameter changes and quantitatively explores the sensitive parameters. In this work, local parameter sensitivity analysis was employed to study the relationship between the expression of Runx2 (and Osx) and the variations for each parameter value. The sensitivity coefficient (S) was calculated according to the following formula:

$$S_i = \frac{\partial[\text{Runx2}]}{\partial P_i} \bigg/ \frac{[\text{Runx2}]}{P_i} \approx \frac{\Delta[\text{Runx2}]}{[\text{Runx2}]} \bigg/ \frac{\Delta P_i}{P_i}, \text{ for small } \Delta P_i. \quad (15)$$

where P_i is one of the 18 estimated parameters and ΔP_i is a small change of the corresponding parameter. Each parameter was increased (or decreased) by 1% from its estimated value, and then we can obtain the percentage changes of the concentrations of Runx2 and Osx, respectively. Fig. 5 shows that the expression of Runx2 is sensitive to V_6 , K_6 and d_4 and the expression of Osx is

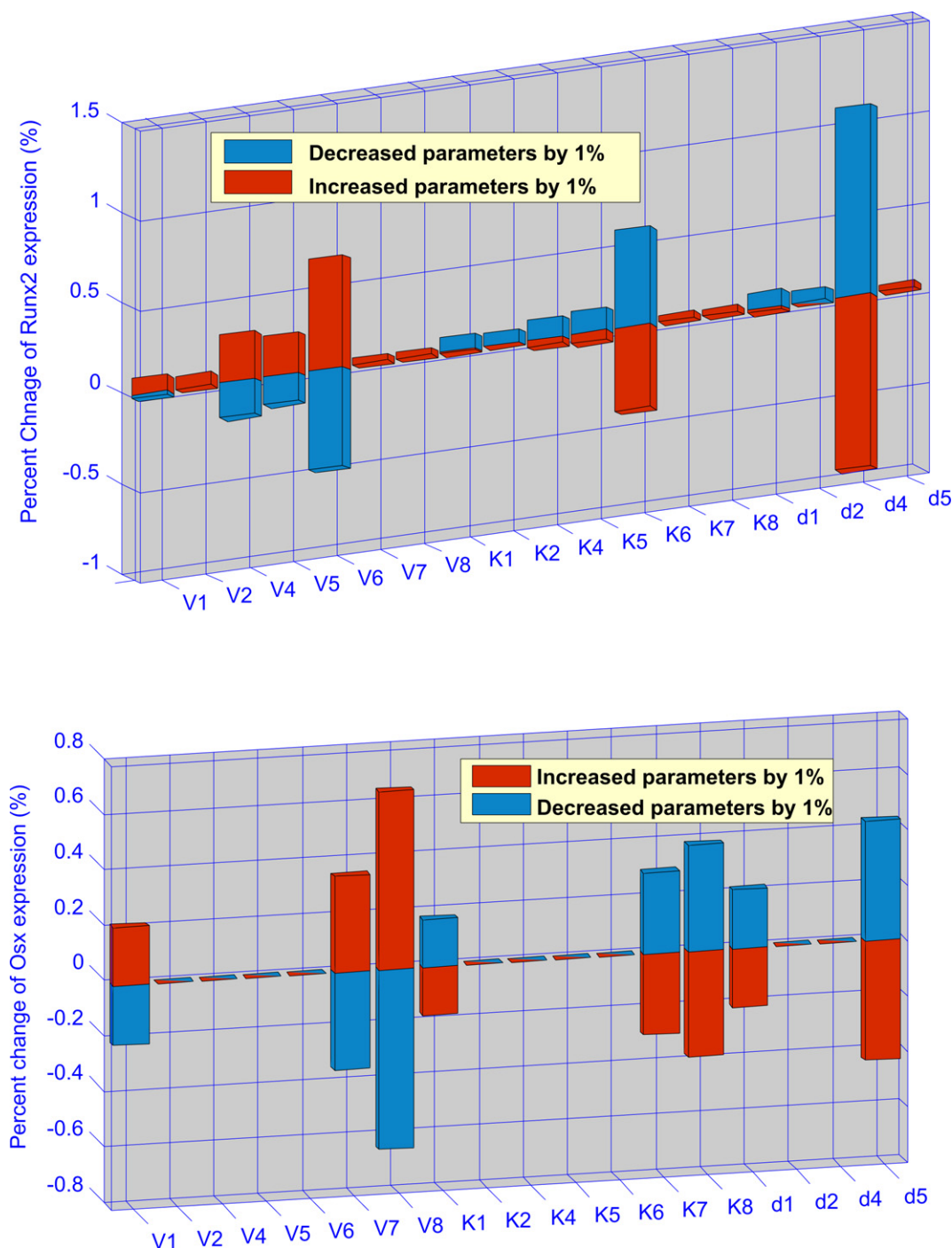


Fig. 5. Parameter sensitivity analysis of the intracellular pathway model. Above subfigure shows that the expression of Runx2 is more sensitive to V_6 , K_6 and d_4 . Below subfigure shows that the expression of Osx is more sensitive to V_8 , K_8 and d_8 , as well as to V_1 , K_1 , d_1 and V_7 , K_7 . These results show us which kinetic parameters and molecules are more important in the system and also demonstrate that the developed intracellular pathway system is robust.

sensitive to V_1 , V_7 , V_8 , K_1 , K_7 , K_8 , d_1 and d_8 . However, the maximum sensitivity of parameter for the expression of Runx2 and Osx is 1.2% and 0.7%, respectively. Our sensitive analysis (Fig. 5) turns out that our intracellular pathway system is rather robust.

3.2. The response of cellular population dynamics to the cytokine therapies

Fig. 6 shows the cellular population and bone mass response to the concentration change of each of three cytokines including BMP2, TGF β and Wnt. We increased the concentration of Wnt, BMP2 and TGF β 10 folds to their normal or initial *in vivo* concentration during the period from the 50th day to the 150th day and the results were evaluated on the 200th day. (1) Fig. 6a shows if the concentration of Wnt was increased, both concentrations of pre-

osteoblasts and active osteoblasts increased rapidly; whereas the concentration of active osteoclasts increased firstly, then decreased at the end of the treatment and finally converged to its steady state; the concentration of pre-osteoclasts was almost invariant. (2) If the concentration of BMP2 was increased, Fig. 6b shows that the concentration of active osteoblasts increased significantly and the concentration of osteoclasts decreased greatly whereas both concentrations of pre-osteoblasts and pre-osteoclasts were almost invariant. (3) When we increased the concentration of TGF β (Fig. 6c) a much lower response was observed. (4) Fig. 6d shows that the increase of bone mass induced by BMP2 was the greatest, whereas the increase of bone mass induced by TGF β was the least.

Then we examined how combined cytokines influence the cellular population and bone mass. We checked all of the combinations of cytokines, i.e. Wnt/BMP2, BMP2/TGF β , Wnt/TGF β , and

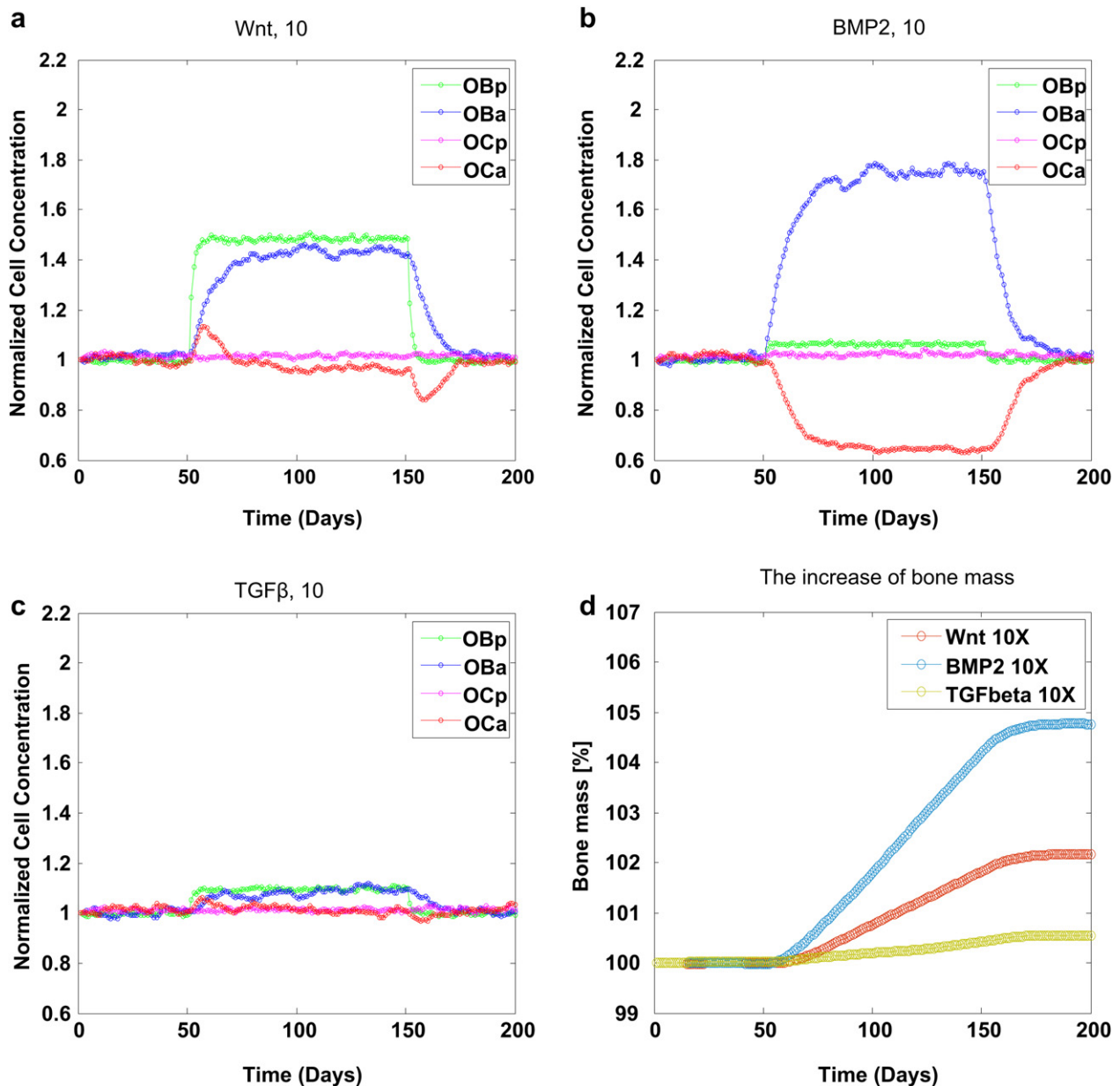


Fig. 6. The responses of cell population and bone mass to the change of single cytokine concentration. (a) increased Wnt, (b) increased BMP2 and (c) increased TGF β by 10 folds respectively from the 50th day to the 150th day. (a) When the concentration of Wnt was increased, both concentrations of pre-osteoblasts and active osteoblasts increased rapidly; whereas the concentration of pre-osteoclasts was almost invariant. (b) When the concentration of BMP2 was increased, the concentration of active osteoblasts increased significantly and the concentration of osteoclasts decreased greatly whereas both concentrations of pre-osteoblasts and pre-osteoclasts were almost invariant. (c) When the concentration of TGF- β was increased a much lower response was observed. (d) The bone mass increased most when the concentration of BMP2 was increased.

Table 1
Responses of bone mass to different cytokine therapies.

Cytokine therapy	Bone mass (%)	
	150 days	200 days
BMP	103.6	104.6
Wnt	102.4	102.7
TGFβ	100.4	100.8
BMP2/Wnt	104.7	105.8
BMP2/TGFβ	103.5	104.3
Wnt/TGFβ	101.7	101.9
BMP2/Wnt/TGFβ	103.8	104.5

The combined BMP₂ and Wnt promoted the bone mass formation greatest within 200 days are shown in bold.

Wnt/BMP2/TGFβ. The responses of cellular population dynamics are demonstrated in the [Supplementary Fig. S2](#). [Table 1](#) lists the percentage increases of bone mass under different cytokine therapies. We increased the concentration of Wnt/BMP2 as a combination 5*Wnt + 5*BMP2 simultaneously during the period from the 50th day to the 150th day, and the results were evaluated on the 200th day. The percentage increase of bone mass showed that combined effect was greater than both of the effects of single Wnt and BMP2. Additionally, [Table 1](#) shows insignificant improvement of the combined effect of BMP2/TGFβ compared to the effect of single BMP2. Other combination effects can also be seen from [Table 1](#).

We then changed the concentration of single cytokine or combined cytokines in a large range from 10^{-2} to 10^3 with respect to their initial values to investigate the response of bone mass. [Fig. 7](#) indicates that the combination of Wnt and BMP2 always affected

the change of bone mass more than other single or combined cytokines, especially when the dose multiple exponent of the combined Wnt/BMP2 was higher than 1. However, when the dose multiple exponent of combined Wnt and BMP2 was less than 0.3, the combined Wnt/BMP2 resulted in the decrease of the bone mass compared to its initial state.

3.3. Cytokine combination therapy evaluations

[Fig. 7](#) reveals that the combination of Wnt and BMP2 greatly affected the change of bone mass than others. [Fig. 8](#) shows that the flexible tuning of the bone mass percentage was controlled by Wnt and BMP2 combination. And then, we adopted the Loewe additivity [40,41] and Bliss independence [41–43] to evaluate and examine whether the combination effect of Wnt and BMP2 is synergy or not.

The combination index of Loewe synergy is defined as a ratio of total effective cytokine dose (combination versus single cytokines) required to achieve a given effect as follows:

$$CI_{\text{Loewe}} = \frac{d_1}{GC_x^{(1)}} + \frac{d_2}{GC_x^{(2)}}, \quad (16)$$

where d_1 (Wnt) and d_2 (BMP2) are the cytokine combination dose located in the combination isobologram with respect to the bone mass increasing x percentage. $GC_x^{(1)}$ or $GC_x^{(2)}$ represents the concentration of single cytokine Wnt or BMP2 with respect to the bone mass increasing by x percentage, respectively. $CI_{\text{Loewe}} < 1$, $CI_{\text{Loewe}} > 1$ and $CI_{\text{Loewe}} = 1$ indicate Loewe synergy, antagonism and additivity, respectively.

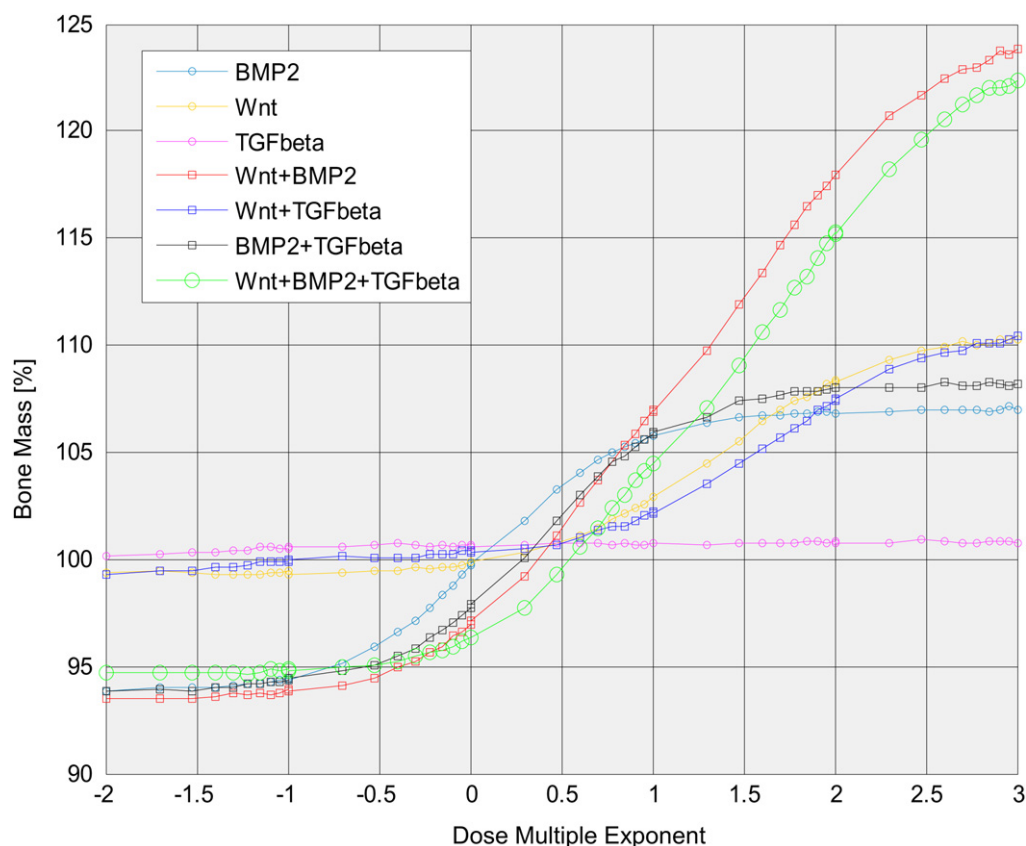


Fig. 7. The responses of bone mass to the change of concentration of cytokines in a large range from 10^{-2} to 10^3 with respect to their initial values. X axis represents the dose multiple exponent in different therapies, Y axis represents the corresponding bone mass percentages. The combination of Wnt and BMP2 can influence the change of bone mass more than other single or combined cytokines. We also note that when the dose multiple exponent of combined Wnt and BMP2 was less than 0.3, the combined Wnt and BMP2 resulted in the decrease of the bone mass compared to its initial state.

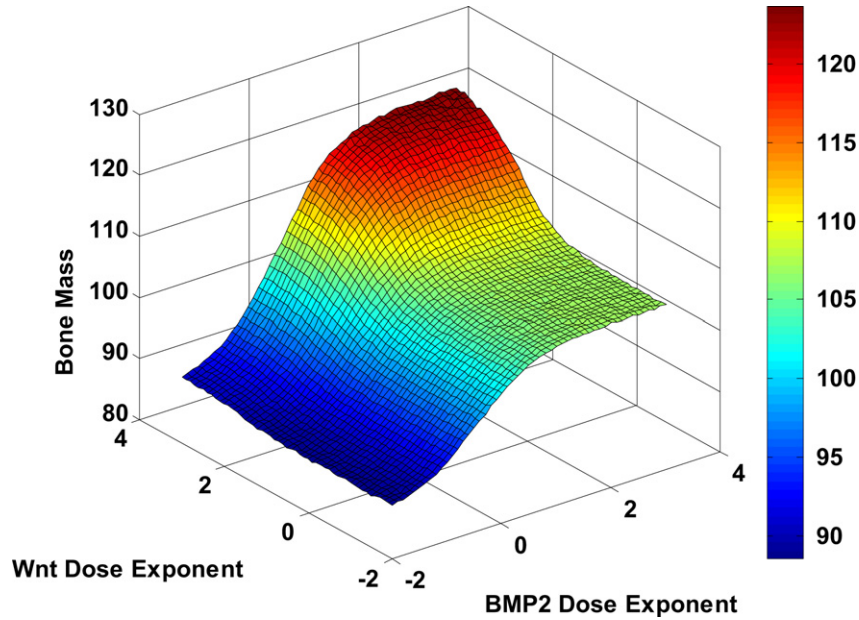


Fig. 8. Prediction of bone mass production by Wnt and BMP2 combination. The flexible tuning of the bone mass percentage was controlled by Wnt and BMP2 combination.

Fig. 9 shows that 5% isobologram of Wnt and BMP2 (green curve) bows inward indicating $CI_{\text{Loewe}} < 1$ in this case. Therefore the combination of Wnt and BMP2 is synergistic regarding the 5% bone growth isobologram. Also the optimal combination to achieve 5% bone growth was marked on the isobologram as a red dot, at which point the isobologram was tangent to the equivalent total dose line (the black dashed line).

Another famous synergy quantification method for combination therapy is Bliss independence [41–43], which is defined as

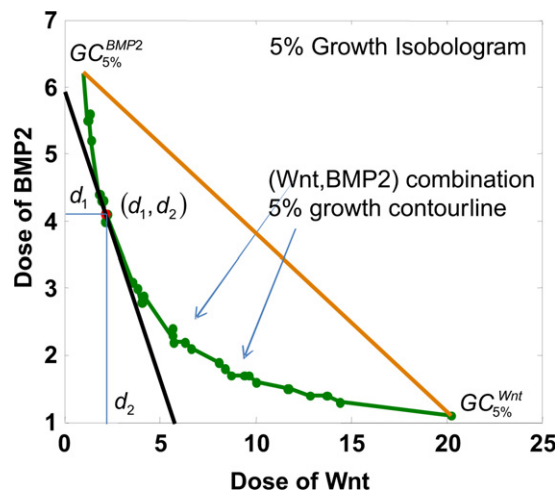
$$CI_{\text{Bliss}}(x, y) = \frac{R_1(x) + R_2(y) - R_1(x)R_2(y)}{R_{12}(x, y)}, \quad (17.1)$$

where $R_i(x)$ is response level defined as follows

$$R_i(x) = O_{\text{cytokine}}(x)/O_{\text{initial}}. \quad (17.2)$$

O_{initial} and O_{cytokine} are the initial bone mass and the bone mass under treatment of corresponding cytokine, respectively. $R_1(x) + R_2(y) - R_1(x)R_2(y)$ in Equation (17.1) is the expected response effect, and $R_{12}(x, y)$ is the actual combination effect. Hence, if $CI_{\text{Bliss}} < 1$, Bliss index considers the combination of the cytokines has synergistic effect; if $CI_{\text{Bliss}} > 1$, Bliss index considers the combination of the drugs has antagonistic effect; otherwise, Bliss index considers the combination of the drugs has additive effect.

We then employed Bliss index to explore more information and characteristics of the combination effect of Wnt and BMP2. As visualized in Fig. 10, our results exhibited that BMP2 levels governed the synergism. When the BMP2 level was higher than 0, the two drugs were synergistic, otherwise antagonistic. We also found that Wnt at high levels showed opposite effects in terms of synergism at different BMP2 levels. When BMP2 level was high, increasing Wnt level promoted the synergistic effects of the two



“Loewe combination index”

$$CI = \frac{d_1}{GC_x^{(1)}} + \frac{d_2}{GC_x^{(2)}}$$

$$CI < 1 \Leftrightarrow \text{Synergy}$$

$$CI > 1 \Leftrightarrow \text{Antagonism}$$

$$CI = 1 \Leftrightarrow \text{Additive}$$

Fig. 9. Synergy prediction on Wnt and BMP2 combination based on Loewe combination index. 5% isobologram of Wnt and BMP2 (green curve) bows inward indicating $CI < 1$, therefore the combination of Wnt and BMP2 is synergy. The optimal combination of Wnt and BMP2 in terms of the minimum total dose to achieve 5% bone mass growth was marked in red at (d_1, d_2) (For interpretation of the references to colour in this figure legend, the reader is referred to the web version of this article.)

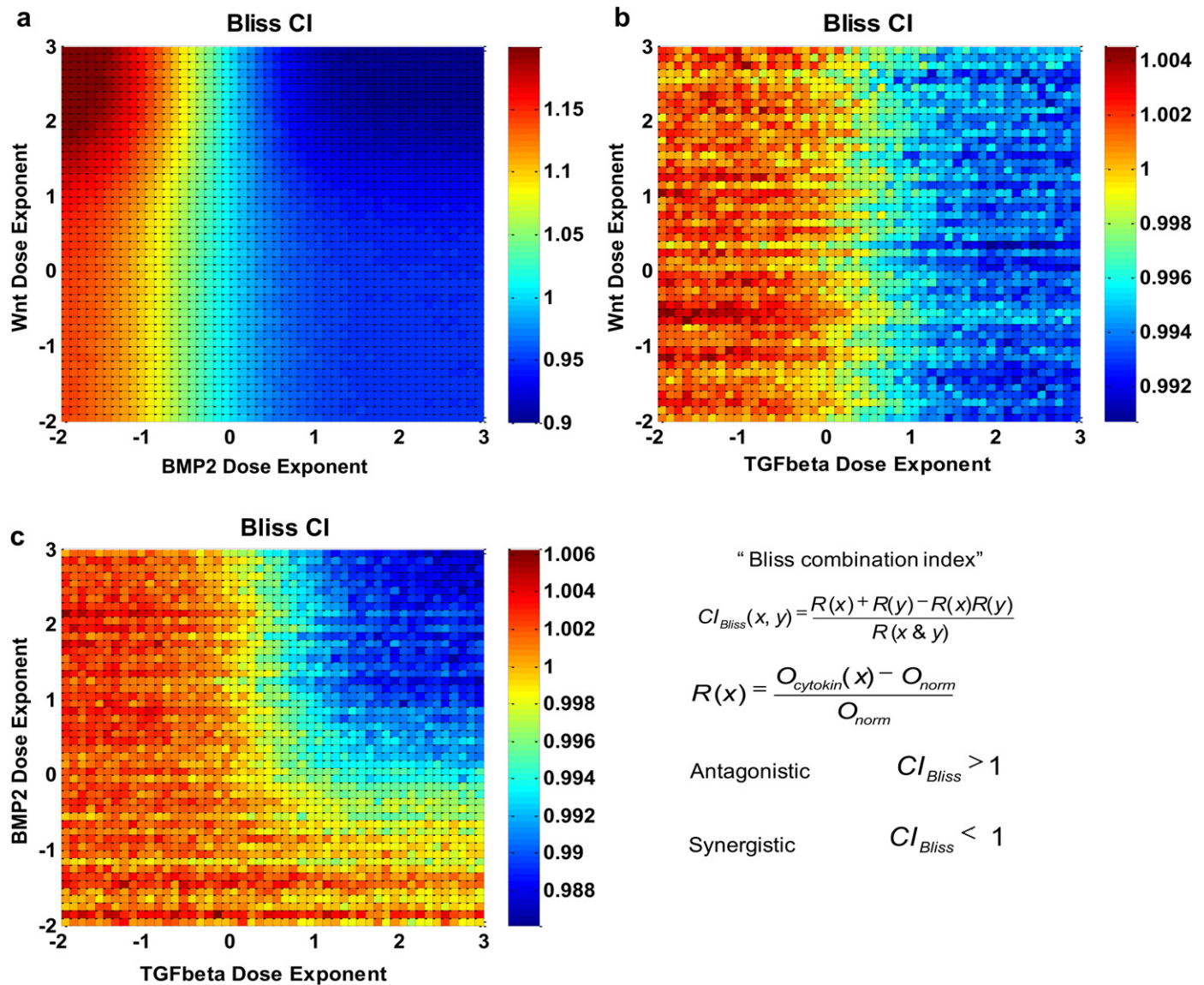


Fig. 10. Synergy prediction on dual combinations of Wnt, BMP2, and TGFβ based on Bliss combination index. Wnt and BMP2 perform dose-dependent synergism. (a) BMP2 levels governed the synergism. When the BMP2 level was higher than 0, the two drugs were synergistic, otherwise antagonistic. We also found that Wnt at high levels showed opposite effects in terms of synergism at different BMP2 levels. When BMP2 level was high, increasing Wnt level promoted the synergistic effects of the two drugs. In contrast, when BMP2 level was low, the more the Wnt was introduced, the stronger the antagonistic effect was. (b) Wnt/TGFβ and (c) BMP2/TGFβ combinations also showed dose-dependent synergism but much lower responses.

drugs. In contrast, when BMP2 level was low, the more the Wnt was introduced, the stronger the antagonistic effect was.

Additionally, Fig. 10 demonstrates that the combinations of Wnt/TGFβ and BMP2/TGFβ also produced dose-dependent synergisms yet much lower responses.

4. Discussion

Our quantitative study evaluated the combinatorial effects of cytokines including Wnt, BMP2, and TGFβ released from hydrogels on bone mass regeneration based on the latest knowledge of intra- and inter-cellular signaling during bone regeneration and remodeling. We established a multi-scale systematic model by integrating the intracellular signaling pathways of interests for each cell phenotypes along with intercellular communications into the stochastic cellular population dynamics. Parameters of the intracellular signaling pathways were estimated by fitting the model to

the dynamic experimental data [21,25,26] using genetic algorithm [37]. We then explored *in silico* dose effects and synergism of various cytokine combinations, which provided insights into the critical control mechanisms of the dynamic bone remodeling process. Synergisms were evaluated using Loewe index [40,41] and Bliss index [41–43].

Our modeling strategy successfully captured key kinetic features of the underlying intra- and inter-cellular signaling pathways, given that less critical molecular details were lumped into Hill functions ([44,45]). The simulation results (Fig. 3) were consistent with experimental data (Fig. S1), which suggested the fundamental signaling networks used in this work were reliable. The estimation of parameters was confident as most parameters were well covered by experimental data, with only 2 out of 18 parameters were unidentifiable (Fig. 4). Parameter sensitivity test (Fig. 5) proved that the model was robust against the inaccuracy of parameter estimation, which is crucial to the simulation of complex bio-systems.

The simulations of dose effects revealed that the sensitivities and dynamics of different types of bone cells to the doses of each cytokine were significantly different. Though all three cytokines promoted the populations of active osteoblasts and pre-osteoblasts (Fig. 6a–c), BMP2 promoted the population of active osteoblasts greatest and also significantly suppressed that of active osteoclasts (Fig. 6b). Other groups also observed similar effects of BMP2 [46,47]. This finding may be useful for the clinical treatment of osteoporosis, that is, growth factors, such as BMP2, can be potentially used to not only promote the bone formation but also inhibit the bone resorption for osteoporosis patients. It was also interesting to observe that TGF β , one of the most abundant cytokines in bone tissues, showed few effects on bone remodeling, which was consistent with results from peers [48] that the major role of TGF β during bone remodeling is to promote migration of bone MSC instead of directly regulating the balance between bone formation and resorption.

The *in silico* exploring of drug (cytokine) combinations cast new light on the design strategies of engineered bone scaffolds, such as hydrogels carrying cytokines or growth factors and cells. Regarding the cytokines encapsulated in the hydrogels, the combinations of Wnt and BMP2 surpassed all the other choices with dramatic enhance merit of both total bone mass production (Fig. 7) and the most significant synergistic effects (Fig. 10a). This results are consistent with published works [49,50] but, in addition, we demonstrate here that the effects of Wnt were BMP2-dependent. When the BMP2 level was low, Wnt alone could not initiate significant bone mass production, and also showed antagonistic effects. TGF β showed similar trends. As for prevention of over-generation of bone mass and the consequential hyperostosis, reduction of any single cytokines of TGF β or Wnt could not suppress bone over-generation, while any of their combinations as well as single or combined BMP2 performed equally well.

Optimal doses of cytokine combinations released from the hydrogels for most efficiently tuning bone remodeling could be achieved from the growth isobolograms of specific goals of tuning. For example, as shown in Fig. 9, if the overall bone regeneration in the artificial scaffolds should be boosted by 5% to meet the clinical need of a bone fracture patient who also suffers from osteoporosis, the most efficient cytokine delivery doses should be around BMP2 of 4.1 and Wnt of 2.2. Such results will provide very useful guidelines for the designs of the cytokine releasing devices.

The major purpose of this work was to explore the possible strategies of long-term delivering of cytokines to guide the bone remodeling of the engineered bone grafts and promote the prognosis, therefore we did not explicitly simulate those processes that were also crucial for bone tissue engineering but not for bone remodeling, which including initial vascularization, inflammatory effects. Mechanical cues that are sensed and processed by osteocytes in the regulation of bone formation and resorption [51] are also important but beyond the scope of this work. Actual intra- and inter-cellular signaling mechanisms involved in bone remodeling and healing are extensively complicated [19,52]. As the first attempt, we focused on several well known major mechanisms [19–24,27,50] and combined the detailed reactions of the signaling pathways (i.e. ligand–receptor reaction, protein binding and disassociation) using Hill functions. The parameter estimation was based on the current available *in vitro* dynamic experimental data [21,25,26], as the reliable *in vivo* dynamic data are not yet available. Other growth factors and cytokines, such as IGF1, FGF2, VEGF and etc. released from hydrogels, along with mechanosensor cells, osteocytes, will be examined in a follow up study. Intensive *in vivo* studies guided by this work will provide necessary data for further extending our current model to a quantitative, personalized simulation system to develop proper treatment plan for each patient.

5. Conclusions

This study showed the dominating role of BMP2 in bone regeneration and remodeling, predicted that the combination of Wnt and BMP2 can achieve best control of bone remodeling and best bone mass regeneration among tested combinations, and suggested optimal dose ratios of given cytokine combinations released from hydrogels to most efficiently control the long-term bone remodeling. The analysis of simulation results brings insights into the underlying molecular and cellular mechanisms for the combination effects of cytokines. This model as well as the quantitative synergism evaluation of cytokine combinations in terms of bone formation has significantly narrowed the candidates of cytokine delivery conditions for the designs of biological experiments, and will guide the design of *in vivo* bone scaffolds and the clinical treatment of some diseases such as osteoporosis.

Acknowledgments

We would like to acknowledge the members of Translational Biosystems Lab in Cornell Medical School and Dr. Huiming Peng for the valuable discussions. This work was supported by Funding: NIH R01LM010185-03 (Zhou), NIH U01HL111560-01 (Zhou), NIH 1R01DE022676-01 (Zhou), U01 CA166886-01 (Zhou) and DODW81XWH-11-2-0168-P4 (Zhou & Yang) and DODW81XWH-10-1-0966 (Yang).

Appendix A. Supplementary material

Supplementary data related to this article can be found online at <http://dx.doi.org/10.1016/j.biomaterials.2012.07.041>.

References

- [1] Chang YS, Oka M, Kobayashi M, Gu HO, Li ZL, Kitsugi T, et al. Bone formation and remodeling around implanted materials under load-bearing conditions. *Clin Mater* 1994;17:181–7.
- [2] O'Keefe RJ, Mao J. Bone tissue engineering and regeneration: from discovery to the clinic – an overview. *Tissue Eng Part B* 2011;17:389–92.
- [3] Schindeler A, McDonald MM, Bokko P, Little DG. Bone remodeling during fracture repair: the cellular picture. *Semin Cell Dev Biol* 2008;19:459–66.
- [4] Kalfas IH. Principles of bone healing. *Neurosurg Focus* 2001;10:1–4.
- [5] Sadr N, Zhu M, Osaki T, Kakegawa T, Yang Y, Moretti M, et al. SAM-based cell transfer to photopatterned hydrogels for microengineering vascular-like structures. *Biomaterials* 2011;32:7479–90.
- [6] Kim S, Nishimoto SK, Bumgardner JD, Haggard WO, Gaber MW, Yang Y. A chitosan/[beta]-glycerophosphate thermo-sensitive gel for the delivery of ellagic acid for the treatment of brain cancer. *Biomaterials* 2010;31:4157–66.
- [7] Kang Y, Kim S, Khademhosseini A, Yang Y. Creation of bony microenvironment with CaP and cell-derived ECM to enhance human bone-marrow MSC behavior and delivery of BMP-2. *Biomaterials* 2011;32:6119–30.
- [8] Kim S, Kang Y, Krueger CA, Sen M, Holcomb JB, Chen D, et al. Sequential delivery of BMP-2 and IGF-1 using a chitosan gel with gelatin microspheres enhances early osteoblastic differentiation. *Acta Biomater* 2012;8:1768–77.
- [9] Koutsopoulos S, Zhang S. Two-layered injectable self-assembling peptide self hydrogels for long-term sustained release of human antibodies. *J Control Release* 2012;160:451–8.
- [10] Yang J-A, Kim H, Park K, Hahn SK. Molecular design of hyaluronic acid hydrogel networks for long-term controlled delivery of human growth hormone. *Soft Matter* 2011;7:868–70.
- [11] Wei L, Cai C, Lin J, Chen T. Dual-drug delivery system based on hydrogel/micelle composites. *Biomaterials* 2009;30:2606–13.
- [12] Dimitriou R, Tsiridis E, Giannoudis PV. Current concepts of molecular aspects of bone healing. *Injury* 2005;36:1392–404.
- [13] Ai-Aql Z, Alagl A, Graves D, Gerstenfeld L, Einhorn T. Molecular mechanisms controlling bone formation during fracture healing and distraction osteogenesis. *J Dent Res* 2008;87:107–18.
- [14] Jilka RL. Biology of the basic multicellular unit and the pathophysiology of osteoporosis. *Med Pediatr Oncol* 2003;41:182–5.
- [15] Komarova SV, Smith RJ, Dixon SJ, Sims SM, Wahl LM. Mathematical model predicts a critical role for osteoclast autocrine regulation in the control of bone remodeling. *Bone* 2003;33:206–15.

- [16] Lemaire V, Tobin FL, Greller LD, Cho CR, Suva LJ. Modeling the interactions between osteoblast and osteoclast activities in bone remodeling. *J Theor Biol* 2004;229:293–309.
- [17] Pivonka P, Zimak J, Smith DW, Gardiner BS, Dunstan CR, Sims NA, et al. Model structure and control of bone remodeling: a theoretical study. *Bone* 2008;43: 249–63.
- [18] Pivonka P, Zimak J, Smith DW, Gardiner BS, Dunstan CR, Sims NA, et al. Theoretical investigation of the role of the RANK-RANKL-OPG system in bone remodeling. *J Theor Biol* 2010;262:306–16.
- [19] Gordeladze JO, Reseland JE, Duroux-Richard I, Apparailly F, Jorgensen C. From stem cells to bone: phenotype acquisition, stabilization, and tissue engineering in animal models. *ILAR J* 2009;51:42–61.
- [20] Afzal F, Pratap J, Ito K, Ito Y, Stein JL, Van Wijnen AJ, et al. Smad function and intranuclear targeting share a Runx2 motif required for osteogenic lineage induction and BMP2 responsive transcription. *J Cell Physiol* 2005;204:63–72.
- [21] Miyoshi K, Nagata H, Horiguchi T, Abe K, Arie Wahyudi I, Baba Y, et al. BMP2-induced gene profiling in dental epithelial cell line. *J Med Invest* 2008;55: 216–26.
- [22] Ryoo HM, Lee MH, Kim YJ. Critical molecular switches involved in BMP-2-induced osteogenic differentiation of mesenchymal cells. *Gene* 2006;366:51–7.
- [23] Crockett JC, Rogers MJ, Coxon FP, Hocking LJ, Helfrich MH. Bone remodelling at a glance. *J Cell Sci* 2011;124:991–8.
- [24] Komori T. Regulation of bone development and maintenance by Runx2. *Front Biosci* 2008;13:898–903.
- [25] Tohmonda T, Miyauchi Y, Ghosh R, Yoda M, Uchikawa S, Takito J, et al. The IRE1[alpha]-XBP1 pathway is essential for osteoblast differentiation through promoting transcription of Osterix. *EMBO Rep* 2011;12:451–7.
- [26] Schmierer B, Tournier AL, Bates PA, Hill CS. Mathematical modeling identifies Smad nucleocytoplasmic shuttling as a dynamic signal-interpreting system. *Proc Natl Acad Sci U S A* 2008;105:6608–13.
- [27] Yavropoulou MP, Yovos JG. The role of the Wnt signaling pathway in osteoblast commitment and differentiation. *Hormones* 2007;6:279–94.
- [28] Klipp E, Liebermeister W, Wierling C, Kowald A, Lehrach H, Herwig R. Systems biology: a textbook. p. 13–27. Weinheim: Wiley-VCH; 2009.
- [29] Chou TC. Derivation and properties of Michaelis–Menten type and Hill type equations for reference ligands. *J Theor Biol* 1976;59:253–76.
- [30] Lee E, Salic A, Krüger R, Heinrich R, Kirschner MW. The roles of APC and Axin derived from experimental and theoretical analysis of the Wnt pathway. *PLoS Biol* 2003;1:e10.
- [31] Murray PJ, Kang JW, Mirams GR, Shin SY, Byrne HM, Maini PK, et al. Modelling spatially regulated [beta]-catenin dynamics and invasion in intestinal crypts. *Biophys J* 2010;99:716–25.
- [32] Boyce BF, Xing L. Functions of RANKL/RANK/OPG in bone modeling and remodeling. *Arch Biochem Biophys* 2008;473:139–46.
- [33] Lee JM, Gianchandani EP, Eddy JA, Papin JA. Dynamic analysis of integrated signaling, metabolic, and regulatory networks. *PLoS Comput Biol* 2008;4: e1000086.
- [34] Øksendal BK. Stochastic differential equations: an introduction with applications. p. 61–72. 5th ed. New York: Springer Verlag; 2003.
- [35] Holmes MH. Introduction to numerical methods in differential equations. p. 5–23. New York: Springer Verlag; 2007.
- [36] Higham DJ. An algorithmic introduction to numerical simulation of stochastic differential equations. *SIAM Rev* 2001;525–46.
- [37] Katara S, Bhan A, Caruthers JM, Delgass WN, Venkatasubramanian V. A hybrid genetic algorithm for efficient parameter estimation of large kinetic models. *Comput Chem Eng* 2004;28:2569–81.
- [38] Davison AC, Hinkley DV. Bootstrap methods and their application. p. 11–22. New York: Cambridge Univ Pr; 1997.
- [39] Lee JM, Zhang J, Su AI, Walker JR, Wiltshire T, Kang K, et al. A novel approach to investigate tissue-specific trinucleotide repeat instability. *BMC Syst Biol* 2010;4:29.
- [40] Straetmans R, O'Brien T, Wouters L, Van Dun J, Janicot M, Bijns L, et al. Design and analysis of drug combination experiments. *Biom J* 2005;47: 299–308.
- [41] Fitzgerald JB, Schoeberl B, Nielsen UB, Sorger PK. Systems biology and combination therapy in the quest for clinical efficacy. *Nat Chem Biol* 2006;2: 458–66.
- [42] Peng H, Wen J, Li H, Chang J, Zhou X. Drug inhibition profile prediction for NFkB pathway in multiple myeloma. *PLoS One* 2011;6:e14750.
- [43] Bliss C. The toxicity of poisons applied jointly. *Ann Appl Biol* 1939;26: 585–615.
- [44] Novak B, Tyson JJ. Design principles of biochemical oscillators. *Nat Rev Mol Cell Biol* 2008;9:981–91.
- [45] Mather W, Bennett MR, Hasty J, Tsimring LS. Delay-induced degrade-and-fire oscillations in small genetic circuits. *Phys Rev Lett* 2009;102:068105.
- [46] Yilgor P, Tuzlakoglu K, Reis RL, Hasirci N, Hasirci V. Incorporation of a sequential BMP-2/BMP-7 delivery system into chitosan-based scaffolds for bone tissue engineering. *Biomaterials* 2009;30:3551–9.
- [47] Kempen DHR, Lu L, Hefferan TE, Creemers LB, Maran A, Classic KL, et al. Retention of in vitro and in vivo BMP-2 bioactivities in sustained delivery vehicles for bone tissue engineering. *Biomaterials* 2008;29:3245–52.
- [48] Tang Y, Wu X, Lei W, Pang L, Wan C, Shi Z, et al. TGF- β 1-induced migration of bone mesenchymal stem cells couples bone resorption with formation. *Nat Med* 2009;15:757–65.
- [49] Sato MM, Nakashima A, Nashimoto M, Yawaka Y, Tamura M. Bone morphogenetic protein-2 enhances Wnt/ β -catenin signaling-induced osteoprotegerin expression. *Genes Cells* 2009;14:141–53.
- [50] Nakashima A, Katagiri T, Tamura M. Cross-talk between Wnt and bone morphogenetic protein 2 (BMP-2) signaling in differentiation pathway of C2C12 myoblasts. *J Biol Chem* 2005;280:37660–8.
- [51] Jacobs CR, Temiyasathit S, Castillo AB. Osteocyte mechanobiology and pericellular mechanics. *Annu Rev Biomed Eng* 2010;12:369–400.
- [52] Hughes FJ, Turner W, Belibasakis G, Martuscelli G. Effects of growth factors and cytokines on osteoblast differentiation. *Periodontol* 2000 2006;41:48–72.

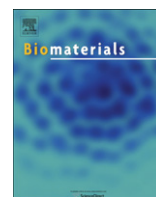


This article appeared in a journal published by Elsevier. The attached copy is furnished to the author for internal non-commercial research and education use, including for instruction at the authors institution and sharing with colleagues.

Other uses, including reproduction and distribution, or selling or licensing copies, or posting to personal, institutional or third party websites are prohibited.

In most cases authors are permitted to post their version of the article (e.g. in Word or Tex form) to their personal website or institutional repository. Authors requiring further information regarding Elsevier's archiving and manuscript policies are encouraged to visit:

<http://www.elsevier.com/copyright>



The osteogenic differentiation of human bone marrow MSCs on HUVEC-derived ECM and β -TCP scaffold

Yunqing Kang^a, Sungwoo Kim^a, Julius Bishop^a, Ali Khademhosseini^{b,c,d}, Yunzhi Yang^{a,*}

^a Department of Orthopedic Surgery, Stanford University, 300 Pasteur Drive, Edwards R155, Stanford, CA 94305, USA

^b Center for Biomedical Engineering, Department of Medicine, Brigham and Women's Hospital, Harvard Medical School, Cambridge, MA 02139, USA

^c Harvard-MIT Division of Health Sciences and Technology, Massachusetts Institute of Technology, Cambridge, MA 02139, USA

^d Wyss Institute for Biologically Inspired Engineering, Harvard University, Boston, MA 02115, USA

ARTICLE INFO

Article history:

Received 31 May 2012

Accepted 22 June 2012

Available online 15 July 2012

Keywords:

Extracellular matrix

HUVEC

hMSC

Osteogenesis

β -TCP

ABSTRACT

Extracellular matrix (ECM) serves a key role in cell migration, attachment, and cell development. Here we report that ECM derived from human umbilical vein endothelial cells (HUVEC) promoted osteogenic differentiation of human bone marrow mesenchymal stem cells (hMSC). We first produced an HUVEC-derived ECM on a three-dimensional (3D) beta-tricalcium phosphate (β -TCP) scaffold by HUVEC seeding, incubation, and decellularization. The HUVEC-derived ECM was then characterized by SEM, FTIR, XPS, and immunofluorescence staining. The effect of HUVEC-derived ECM-containing β -TCP scaffold on hMSC osteogenic differentiation was subsequently examined. SEM images indicate a dense matrix layer deposited on the surface of struts and pore walls. FTIR and XPS measurements show the presence of new functional groups (amide and hydroxyl groups) and elements (C and N) in the ECM/ β -TCP scaffold when compared to the β -TCP scaffold alone. Immunofluorescence images indicate that high levels of fibronectin and collagen IV and low level of laminin were present on the scaffold. ECM-containing β -TCP scaffolds significantly increased alkaline phosphatase (ALP) specific activity and up-regulated expression of osteogenesis-related genes such as *runx2*, *alkaline phosphatase*, *osteopontin* and *osteocalcin* in hMSC, compared to β -TCP scaffolds alone. This increased effect was due to the activation of MAPK/ERK signaling pathway since disruption of this pathway using an ERK inhibitor PD98059 results in down-regulation of these osteogenic genes. Cell-derived ECM-containing calcium phosphate scaffolds is a promising osteogenic-promoting bone void filler in bone tissue regeneration.

© 2012 Elsevier Ltd. All rights reserved.

1. Introduction

Extracellular matrix (ECM) is a fibrillar basement network of secreted proteins that is composed mainly of collagens and proteoglycans. ECM provides appropriate microenvironment to support cell adhesion and direct cell behaviors such as proliferation, and differentiation [1–3]. *In vivo*, ECM is initially produced by cells and subsequently formed into a three-dimensional (3D) network [3].

In an attempt to engineer similar microenvironments in tissue engineered scaffolds for regenerative medicine applications, previous studies have utilized decellularized ECM derived from human or animal tissues and organs, typically urinary bladder, heart valves or small intestine [4–6], to produce biological scaffolds. However, potential pathogen transmission and the

dimensions of the original tissue limit the application of decellularized ECM from human or animal tissue [4,5,7]. In contrast, the use of synthetic scaffolds carries little to no risk of infectious disease transmission and has the added advantage of easy formulation. However, these synthetic scaffolds rarely provide the necessary biological stimulus for appropriate tissue development.

In order to reproduce ECM-like function in synthetic scaffolds, previous studies have utilized ECM proteins such as vitronectin, collagen, laminin and fibronectin to coat the surface of polymers, ceramics, and hydrogels [8–13,14]. Kundu and Putnam demonstrated that vitronectin and collagen I coated onto PLGA polymer film regulated the osteogenic behavior of hMSC through MAPK/ERK signaling pathway [12,13] while Klees et al. reported that laminin-5 stimulated the osteogenic differentiation of hMSC [15]. Although these studies demonstrate that ECM proteins can enhance cell attachment and differentiation, it is difficult to reproduce the exact composition and function of native ECM using protein-coating methods alone [16].

* Corresponding author. Tel.: +1 650 723 0772; fax: +1 650 724 5401.
E-mail address: ypyang@stanford.edu (Y. Yang).

Therefore, creating a native ECM on a synthetic scaffold may facilitate cell development by combining biological cues with three-dimensional (3D) mechanical support. Cell-derived ECM fabricated onto 3D scaffolds has recently garnered increased attention with several studies showing promising results [17–20,21]. Mikos and colleagues showed that titanium fiber meshes containing ECM derived from rat marrow stromal cells increased bone matrix deposition *in vitro* when compared to those directly grown on titanium fiber mesh or polymeric scaffold alone [22–24,25]. Chen and colleagues demonstrated that bone marrow cell-derived ECM facilitates expansion of mesenchymal colony-forming units *in vitro* while maintaining their stem cell properties [26]. These results suggest that cell-derived ECM creates a micro-environment conducive to osteoblastic cell differentiation. Therefore, we hypothesize that HUVEC-derived ECM-containing porous ceramic scaffolds can promote osteogenic differentiation of hMSC.

There were three goals of this study. The first was to investigate the feasibility of depositing HUVEC-derived ECM on the surface of a porous β -TCP bioceramic scaffold. The second was to see if HUVEC-derived ECM would enhance osteogenic differentiation of hMSC, and the third was to assess the function of the MAPK/ERK signaling pathway in the osteogenic process. We first established the protocol of HUVEC-derived ECM on porous β -TCP scaffolds and characterized it using scanning electron microscope (SEM), Fourier transmission infrared spectrum (FTIR), X-ray photoelectron spectroscopy (XPS), and immunofluorescence staining. Then osteogenic differentiation of hMSC was investigated through evaluation of alkaline phosphatase (ALP) specific activity and gene expression of osteogenic genes, including alkaline phosphatase (*alp*), runt-related transcription factor 2 (*runx2*), osteopontin (*opn*) and osteocalcin (*oc*). Finally, an osteogenic signaling pathway MAPK/ERK was also studied.

2. Materials and methods

2.1. Materials

β -TCP powder (specific surface area: 17 m²/g) was obtained from Nanocerox, Inc. (Ann Arbor, Michigan). Paraffin granules purchased from Fisher Scientific (Pittsburgh, USA) were used to fabricate small beads as porogen.

An MSCGM™ BulletKit™, EBM™ (endothelial basal medium), and an EGM™ (endothelial growth media) SingleQuots™ Kit were purchased from Lonza, Inc. Anti-human laminin monoclonal antibody (MAB1921) was obtained from Millipore (Billerica, MA). Mouse anti-human monoclonal antibodies to collagen IV (ab6311) and to fibronectin (ab26245) were purchased from Abcam. Mouse monoclonal osteocalcin antibody (sc73464) was purchased from Santa Cruz Biotechnology (Santa Cruz, CA). Rabbit anti-human polyclonal antibody ERK1/2 and phospho-ERK1/2 (Thr202/Tyr204), and the secondary antibody Alexa Fluor® 594 (goat anti-mouse, 2 mg/mL) were purchased from Invitrogen (Carlsbad, CA). Anti-rabbit IgG (H + L) HRP conjugate was purchased from Promega. MEK1/2 inhibitor PD98059 was purchased from Sigma–Aldrich.

2.2. Preparation of β -TCP scaffolds

The process to fabricate β -TCP scaffolds using a template-casting method was described in previous studies [27,28]. In short, β -TCP powder, dispersant (Darvan® C), surfactant (Surfonal®), and carboxymethyl cellulose powder were mixed in distilled water to form slurry. Paraffin beads with designed size were packed into a customized mold and heated to partially melt the beads and form the template. The β -TCP ceramic slurry was then cast onto the template. The slurry can thoroughly fill the template under vacuum environment. The as-cast template was solidified for two days and then dehydrated in a series of graded ethanol solutions. After the dehydration, the dehydrated ceramic green body was put in an alumina dish and sintered at 1250 °C for 3 h. The morphology of β -TCP scaffolds was characterized by scanning electron microscopy. The diameter of the scaffolds used for this study was 7–8 mm and the height was 5–6 mm. The porosity of the scaffolds was 82.5 ± 0.1% and the pore size ranged from 350 μ m to 500 μ m [29].

2.3. Cell culture

HUVEC was provided from the laboratory of the late Dr. J. Folkman (Children's Hospital, Boston). hMSC was provided by Dr. Melero-Martin from Children's

Hospital, Boston. The hMSC can differentiate into adipogenic, chondrogenic, and osteogenic lineages [30]. The hMSC were cultured in MSCBM, which is a non-differentiating growth medium containing 10% fetal bovine serum (FBS) and 1 × glutamine–penicillin–streptomycin (GPS; Invitrogen). HUVEC were cultured in EBM-2 containing supplements from EGM-2 kit and 10% FBS. The cell medium was changed every 3 days. Cells below passage 9 were used in all the experiments.

2.4. Production of ECM on β -TCP scaffolds

HUVEC were cultured in EBM-2 and trypsinized after confluence. 1 × 10⁵ cells suspended in 100 μ l medium were seeded onto scaffolds and then incubated for 1 h for cell attachment on the surface of scaffolds; afterwards, additional culture medium was added to culture cells on the scaffold for 14 days. Medium was changed every 3 days. At the designed time points, cell/scaffolds were washed in PBS and then HUVEC were stripped off from the scaffolds in a mixture solution of 0.5% Triton X-100 and 20 mM NH₄OH for 5 min according to previously reported methods [31,32], leaving structurally-intact ECM exposed and uniformly attached on the surface of inner walls of scaffolds. Finally, ECM-deposited scaffold surfaces were gently washed 5 times using PBS and air-dried in the biological hood for further use.

2.5. Identification and characterization of ECM deposited on β -TCP scaffolds

2.5.1. Scanning electron microscope (SEM)

The surface morphology of β -TCP scaffold and ECM/ β -TCP scaffold were examined using an SEM (FEI, USA). The scaffolds were sputter-coated with gold before imaging. The operated voltage was set at a 15 kV.

2.5.2. Immunofluorescent staining of matrix

To study the protein components and distribution pattern of HUVEC-derived ECM on β -TCP scaffolds, immunofluorescent staining was performed. Three proteins, collagen IV, fibronectin and laminin as biomarkers of ECM components, were immunofluorescent stained. After decellularization, ECM/ β -TCP scaffolds were washed three times in PBS. A 5% BSA–PBS buffer solution was used to block the samples for 1 h at room temperature, and then primary antibodies, including mouse anti-human collagen IV (dilution 1:200), fibronectin (dilution 1:100), and laminin (dilution 1:100) in 1% BSA–PBS, were added into the sample followed by incubation overnight at 4 °C. After washing with PBS, a secondary antibody (Alexa Fluor® 594, 2 μ g/mL, Invitrogen) in 1% BSA–PBS was added into the samples and incubated in the dark for 1 h at room temperature. Finally, the cell nuclei were counterstained with DAPI (5 μ g/mL) for 1 min and then extensively washed with PBS. The fluorescent staining was imaged by confocal microscopy (CSLM, Olympus IX81).

2.5.3. Fourier transmission infrared spectrum (FTIR)

FTIR analysis was carried out to determine components of ECM/ β -TCP using an attenuated total reflection system on a Nicolet spectrometer. FTIR spectra were recorded with 100 scans at 4.0 cm^{−1} resolution. Spectra were normalized to a background spectrum. A dry system was used to prevent atmospheric moisture.

2.5.4. X-ray photoelectron spectroscopy (XPS)

XPS was conducted to investigate the surface elements of ECM on β -TCP (detectable depth 3–5 nm). A focused monochromatic Al-K α X-ray (1486.6 eV) was used as excitation source. To bombard the sample, X-rays were set to 40 W of power, a running voltage of 15 kV and a sampling area of 200 μ m in diameter. The binding energy (1100–0 eV) was recorded in survey scan spectra at 0.5 eV steps, and the pass energy was set at 140 eV. Elemental spectra of C1s, O1s, N1s, Ca2s, P2p were scanned at a high resolution with 0.1 eV intervals. The percentages of each major element were automatically calculated by equipment-associated Multipak software. Binding energies of elemental spectra were autoshift-scaled to the spectra of C1s peak which was set at 284.7 eV. A control sample consisting of decellularized ECM collected from culture plates was also measured.

2.6. Proliferation and osteogenic differentiation assays

hMSC were seeded at a density of 1 × 10⁵ cells/scaffold on ECM/ β -TCP and β -TCP scaffolds in MSCBM non-differentiation medium, and then the culture medium was changed to hMSC osteogenic media, which contains 10% FBS, 10 mM β -glycerophosphate, 10 nM dexamethasone, and 50 μ g/mL ascorbic acid. For the experimental groups involving the inhibitor PD98059, fresh osteogenic media containing inhibitor PD98059 at a final concentration of 50 μ M were added. On each media change, fresh inhibitor was added into the fresh media. At each time point, cells were harvested from scaffolds. After rinsing the samples in PBS, the samples were frozen at −20 °C.

Concentration of double-stranded DNA (dsDNA), which represents cell proliferation, was quantified in a fluorometric assay. At the determined time point, Cells were lysed in a 0.2% Triton X-100 solution followed by three freeze/thaw cycles. During each cycle, cells/scaffolds were frozen to −80 °C for 20 min followed by thawing to 37 °C for another 20 min. To homogenize cell lysates solution, samples were finally sonicated on ice for 1 min. Lysates were then placed on 96-well plates. A PicoGreen assay kit (Invitrogen) was used to measure the absorbance. A BioTek FL800 instrument was used for sample reading at 480/520 nm (ex/em) wavelengths.

Table 1
Sequences of primers used for real-time PCR analysis.

Genes	Sequences
GAPDH	For: 5'-AAC AGC GAC ACC CAC TCC TC Rev: 5'-CAT ACC AGG AAA TGA GCT TGA CAA
<i>runx2</i>	For: 5'-AGA TGA TGA CAC TGC CAC CTC TG Rev: 5'-GGG ATG AAA TGC TTG GGA ACT
<i>alp</i>	For: 5'-ACC ATT CCC ACG TCT TCA CAT TT Rev: 5'-AGA CAT TCT CTC GTT CAC CGC C
<i>opn</i>	For: 5'-ATG AGA TTG GCA GTG ATT Rev: 5'-TTC AAT CAG AAA CCT GGA A
<i>oc</i>	For: 5'-TGT GAG CTC AAT CCG GAC TGT Rev: 5'-CCG ATA GGC CTC CTG AAG C

DNA concentrations were then determined by comparing values to a standard curve constructed with values for solutions with known DNA concentrations.

To determine alkaline phosphatase activity (ALP), a working solution containing p-nitrophenyl phosphate (p-NPP) was added into samples and then incubated for 30 min at 37 °C. After incubation, the reaction was stopped by placing samples on ice and adding 100 µL of 1 M sodium hydroxide. The absorbance values of samples were obtained on a microplate reader (BioTek) at 405 nm wavelength. The ALP concentration of samples was calculated through a standard curve. The ALP specific activity was determined by normalizing ALP value of each sample to its dsDNA concentration.

2.7. Real-time PCR

Cellular total RNA was extracted after 7 and 14 days of incubation using an RNeasy mini Kit (QIAGEN). RNA concentration was determined on an Eppendorf Bio-photometer. RNA samples were then reversed-transcribed into cDNA using an iScript cDNA synthesis kit (BIO-RAD). Real-time PCR was run on an ABI 7900HT Sequence Detection system (ABI, Foster city, CA) using a cDNA product template, specific primers, and iQ SYBR Green supermix (BIO-RAD) in a total volume of 10 µL. Primer sequences as shown in Table 1 for *runx2*, *alp*, osteopontin (*opn*), osteocalcin (*oc*), and glyceraldehyde 3-phosphate dehydrogenase (GAPDH) were purchased from Invitrogen and used to evaluate gene expression [33–35]. The relative genes expression levels were analyzed using the $2^{-\Delta\Delta C_t}$ method [36] by normalizing with the housekeeping gene GAPDH as an endogenous control and calibrating with efficiency, where $\Delta\Delta C_t$ is calculated from $(C_{t,\text{sample}} - C_{t,\text{control}})_{\text{target gene}} - (C_{t,\text{sample}} - C_{t,\text{control}})_{\text{GAPDH}}$.

2.8. Western blot

For Western blot analysis, hMSC were seeded on the β -TCP and ECM/ β -TCP scaffolds for 24 h. Cells/scaffolds were then lysed with cold RIPA buffer containing a phosphatase inhibitor cocktail and Halt™ protease (Thermo Scientific, Rockford, IL, USA) for 10 min, and then cell lysates were centrifuged at 15,000 rpm for 15 min at 4 °C to pellet the cell debris. An aliquot of each lysate was taken out to measure protein concentration using a BCA protein assay kit (Thermo Scientific, Rockford, IL, USA). Five µg proteins in a 2× Laemmli loading buffer were heated at 95 °C for 5 min, and separated on 4–15% Mini-Protean TGXTM gels (BIO-RAD). Each lane was loaded with equal protein amounts. A Spectra™ multicolor broad range protein ladder (Fermentas) was run in parallel lanes. After electrophoresis, a PVDF membrane (Millipore, Billerica, MA) was used to transfer the proteins from gels in a buffer (192 mM glycine, 25 mM Tris, and 20% v/v methanol (pH 8.3)) and then washed in 1× TBST washing buffer. The membrane was blocked in 1× TBST with 5% BSA for 1 h at room temperature. Primary antibodies for ERK1/2 and phospho-ERK1/2 (1:1000, Invitrogen) in 1× TBST containing 1% BSA were added onto the PVDF membranes and then incubated overnight at 4 °C. The membranes were rinsed three times in TBST, and the secondary anti-rabbit IgG HRP conjugate (1:2500, Promega) was added and incubated for 1 h at room temperature, followed by another three washes in TBST. The protein bands on the PVDF membrane were visualized in an All-PRO Imaging X-ray film processor (Hicksville, New York) after immersing in ECL Western blotting detection reagents (GE Healthcare, UK) for short time.

2.9. Statistical analysis

In this study all the experimental groups were carried out in triplicate and a Student's *t*-test was used to statistically analyze the difference between groups. Difference was considered significant if the *p* value was less than 0.05.

3. Results

3.1. Characterization of ECM on β -TCP scaffolds

3.1.1. SEM morphologies of ECM

To establish the protocol of producing ECM and the efficacy of decellularization (Fig. 1A), HUVEC were initially seeded on tissue culture plates and decellularized. Light microscopy images of the same field show the morphology of HUVEC after reaching

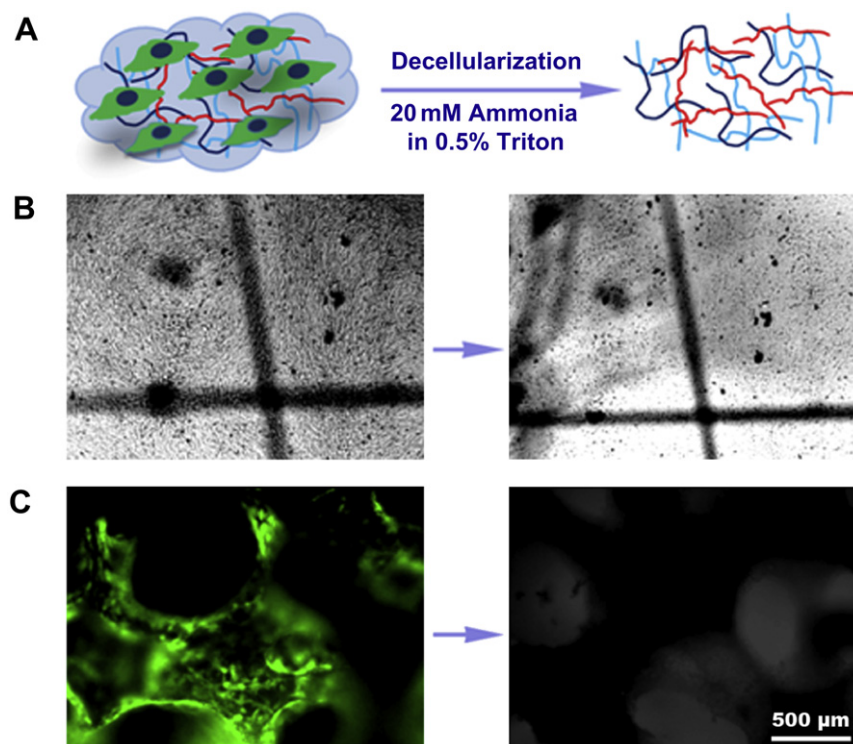


Fig. 1. (A) The schematic of HUVEC-derived ECM production. Left: lines depict ECM, and cells are on the ECM basement; right: ECM after the extraction procedure. (B) Light microscopy images of HUVEC cultured on a tissue culture plate for 14 days after confluence before (left) and after (right) decellularization (right). Location “+” marked identical fields. (C) Fluorescent image of HUVEC cultured on the β -TCP scaffold for 14 days before (left) and after (right) decellularization (magnification: 4×).

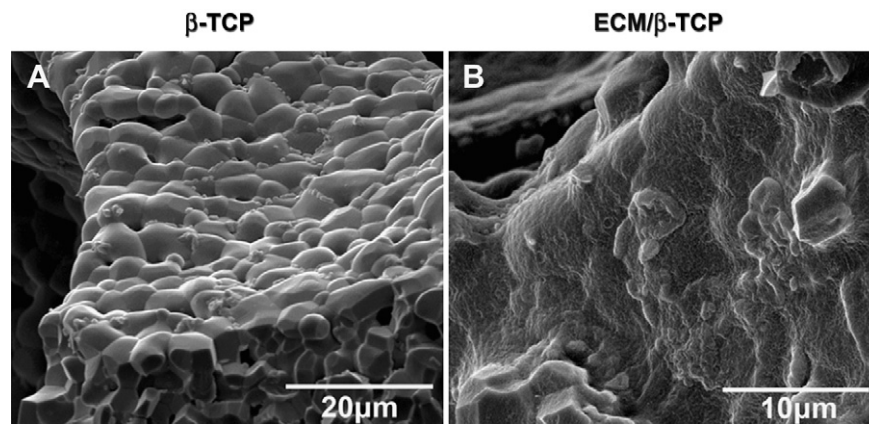


Fig. 2. SEM images of β -TCP scaffold before seeding the HUVEC (left) and of the ECM layer on the β -TCP scaffold after decellularization (right).

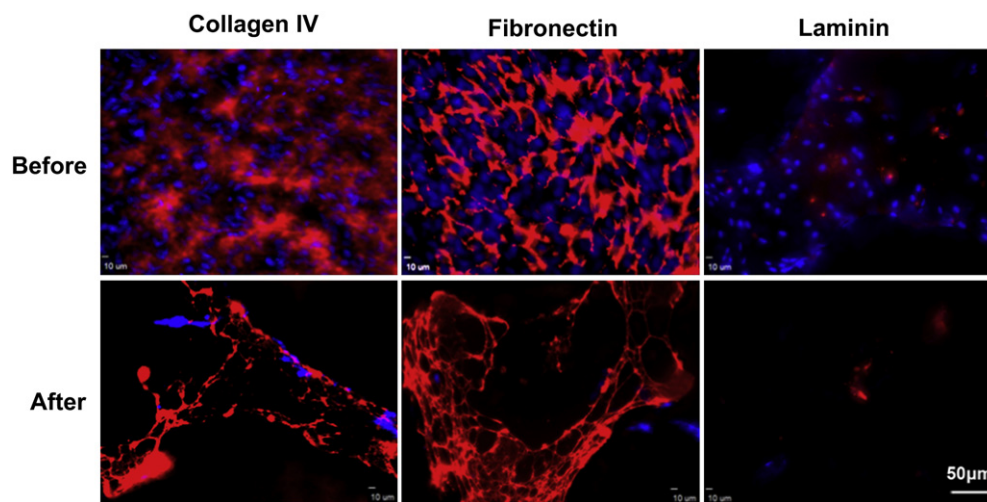


Fig. 3. Immunofluorescent staining images of collagen type IV, fibronectin, and laminin before and after decellularization. Red: Alexa Fluor[®] 594 goat anti-mouse antibody; Blue: DAPI. (For interpretation of color in this figure legend, the reader is referred to web version of the article.)

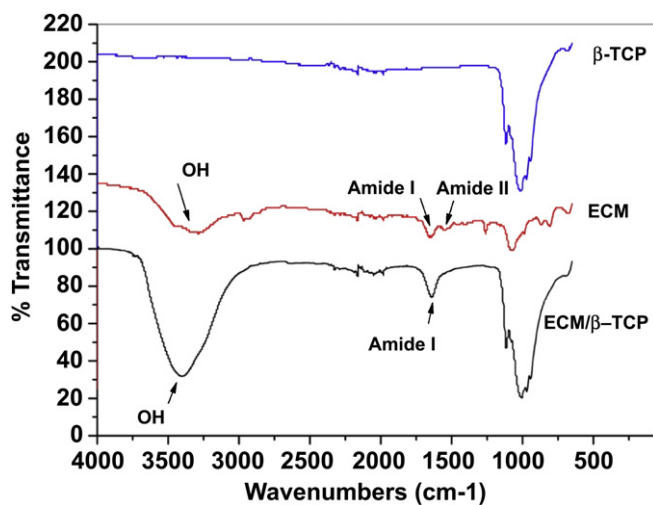


Fig. 4. ATR-FTIR transmission spectra of the β -TCP, ECM from tissue culture plate, and ECM/ β -TCP. The characteristic peaks of amide and hydroxyl groups are shown on the ECM and ECM/ β -TCP spectrum, respectively.

confluence and the decellularized extracellular matrix (Fig. 1B). Having demonstrated the feasibility of producing decellularized ECM *in vitro*, HUVEC cells/scaffolds were cultured for 14 days on β -TCP scaffolds, and subsequently decellularized. Fig. 1C shows that green GFP-tagged HUVEC cells covered all the surface of the scaffold after culturing for 14 days. No green fluorescence was observed on the scaffold after decellularization. Fig. 2 shows the SEM morphology of the surface of the scaffolds. Surfaces of untreated β -TCP scaffold (β -TCP only) surfaces showed ceramic micrograins and micropores whereas the surfaces of HUVEC ECM-containing β -TCP scaffolds (ECM/ β -TCP) contained a dense and heterogeneous coating.

3.1.2. Immunofluorescent staining of collagen IV, laminin and fibronectin

The presence of the ECM on the scaffold was demonstrated using immunofluorescent staining of collagen type IV, laminin, and fibronectin. Results shown in Fig. 3 show that collagen IV and fibronectin produced strong fluorescence intensity, suggesting abundance within the HUVEC ECM, whereas laminin was expressed a relatively low level in a sparse dot-like morphology. After decellularization, the majority of HUVEC were removed, although several nuclei were observed in fluorescent images before and after decellularization. Similarly, these three matrix proteins were present before and after decellularization.

3.1.3. FTIR analysis

Results for FTIR analysis are shown in Fig. 4. The wide bands in the range of $900\text{--}1200\text{ cm}^{-1}$ were assigned to characteristic bands of phosphate in β -TCP [37]. These were not observed in the ECM-only spectrum. In the spectra from ECM group, which was harvested from tissue plate after decellularization, two absorption peaks at $1500\text{--}1580\text{ cm}^{-1}$ and $1580\text{--}1750\text{ cm}^{-1}$ were present and assigned to amide I and amide II. The FTIR spectra of ECM/ β -TCP showed two new adsorption bands at 1642.4 cm^{-1} and 3389.3 cm^{-1} , which were absent from the β -TCP only spectrum. As discussed in previous work [38], these peaks corresponded to amide I and hydroxyl groups, respectively. The amide group was assigned to the presence of collagen, while proteoglycans might be

responsible for the high hydroxyl group signal [39]. Neither peak was observed in the spectrum of β -TCP only.

3.1.4. XPS analysis

The elements in the ECM/ β -TCP scaffolds and the ECM harvested from tissue culture plates were measured by XPS. Result in Fig. 5 showed that there is a new peak (binding energy, 400 eV) in the ECM/ β -TCP and ECM-only spectra, corresponding to the amino groups in the peptide bond [32,39]. This peak corresponding to N1s was not observed for ECM-free β -TCP scaffolds. Signal intensity for the C1s peak, at 284.7 eV, was larger for the construct, compared to that of β -TCP only. Table 2 further indicated that the nitrogen atomic percentage in β -TCP only groups was zero, while ECM/ β -TCP

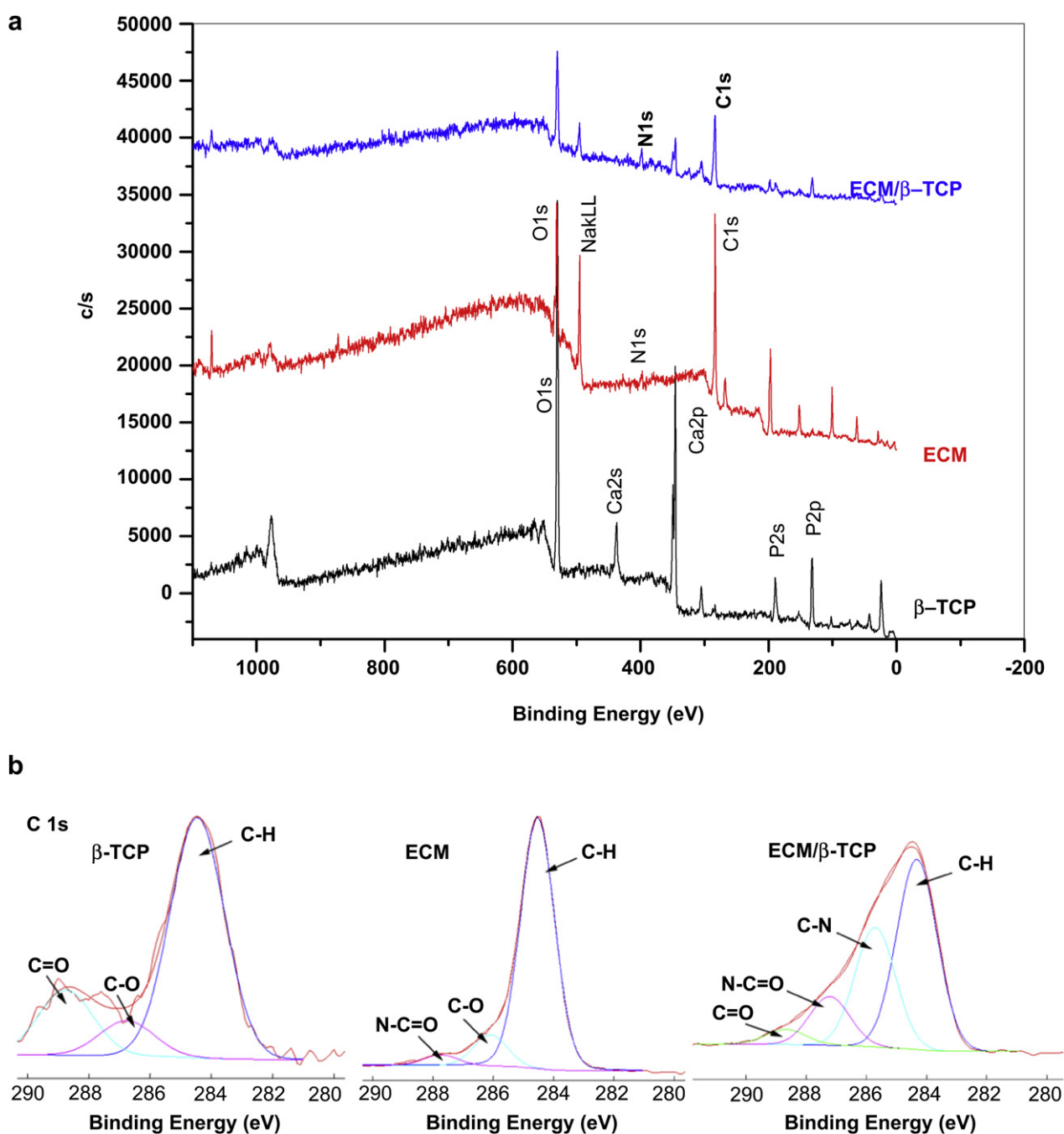


Fig. 5. XPS survey scan spectra (a) and XPS C1s core level spectra (b) for β -TCP, ECM from tissue culture plate, and ECM/ β -TCP.

groups contained 1.7%. The carbon atomic percentage in ECM/ β -TCP groups was also significantly higher than β -TCP only groups: up to 55.5% in the ECM/ β -TCP and 5% in the β -TCP. Trace amounts of carbon in the β -TCP only group were probably attributed to chemical reagents containing carbon during sample processing or from measurement environment. The C1s spectra of β -TCP only, ECM decellularized from tissue culture plates, and ECM/ β -TCP groups are demonstrated in Fig. 5b–d, respectively. For the β -TCP only groups, two minor components (286.5 eV (C–O) and 288.8 eV (C=O)) and a main neutral carbon (C–H) component (284.6 eV) were present. For the spectrum of ECM and ECM/ β -TCP groups (Fig. 5c, d), two new peaks corresponded to C–N (285.7 eV) and O=C–N (287.6 eV) was shown [39]. These functional groups mainly result from ECM protein biomolecules deposited on the scaffolds.

3.2. Proliferation and osteogenic differentiation of hMSC on β -TCP and ECM/ β -TCP scaffolds

3.2.1. dsDNA and ALP

To investigate the effect of ECM on hMSC proliferation and early differentiation, hMSC were seeded on β -TCP only and ECM/ β -TCP scaffolds for 3, 7, and 14 days, and the dsDNA content and ALP activity was analyzed. Results in Fig. 6a, b showed no significant difference in dsDNA contents between the β -TCP only and ECM/ β -TCP scaffold groups, suggesting that HUVEC-deposited ECM did not alter the proliferation of hMSC. However, the early osteogenic differentiation marker ALP indicates higher activity level in ECM/ β -TCP scaffolds than that in β -TCP only scaffolds. This result indicated that ECM deposited on the scaffolds significantly promotes the early differentiation of hMSC.

3.2.2. Real-time PCR

hMSC were seeded on β -TCP only scaffolds and ECM/ β -TCP scaffolds for 7 and 14 days, and real-time PCR was performed to analyze the osteogenic gene expression. The results indicated that hMSC cultured in ECM/ β -TCP scaffolds showed significantly higher gene expression level of osteogenic transcription factor (*runx2*), early differentiation gene *alp*, and bone extracellular matrix proteins (*opn* and *oc*) after 7 and 14 days, compared to the β -TCP scaffolds (Fig. 7). For *runx2*, hMSC cultured in ECM/ β -TCP scaffolds were expressed 5.2-fold higher than that in β -TCP scaffolds after 7 days and 38-fold after 14 days. For *alp*, it was expressed 4.7 and 2.2-fold at 7 and 14 days, respectively. Similarly, *opn* and *oc* genes were also expressed higher fold in ECM/ β -TCP scaffolds group than that in β -TCP only scaffolds. Together, these gene expression results demonstrate that HUVEC-derived ECM-containing β -TCP scaffolds significantly up-regulated the expression of osteogenic-related genes.

3.2.3. Immunofluorescence staining of osteocalcin matrix protein

To further verify the significant role of ECM in promoting the osteogenic potential of hMSC, a late-stage extracellular matrix protein of hMSC (osteocalcin) was immunostained. Confocal images showed that the fluorescent density is significantly higher in ECM/ β -TCP groups than in the β -TCP only group after culturing for 14 and 21 days (Fig. 8). In β -TCP only group, osteocalcin was

sparsely distributed on the scaffold, while it was homogeneously dispersed on the ECM/ β -TCP scaffold at a high-density. These immunofluorescence results demonstrate that HUVEC-derived ECM-containing β -TCP scaffolds increased deposition of osteogenic ECM in hMSC.

3.3. Osteogenic induction of hMSC via MAPK/ERK pathway

To study whether ECM has an effect on the osteogenic differentiation of hMSC through the MAPK/ERK signaling pathway, an inhibitor of the MAPK/ERK signaling pathway, PD98059, was used and its effects on hMSC differentiation were investigated by measuring ALP activity, osteogenic gene expression, and phosphorylated ERK1/2 levels. ALP activity measurements indicated that the inhibitor did not significantly inhibit the ALP activity of hMSC when seeded on β -TCP only scaffolds, whereas ALP activity level of hMSC when seeded on ECM/ β -TCP scaffolds was (Fig. 9). Gene expression results indicate that PD98059 inhibitor significantly reduced the expression level of genes *runx2*, *alp*, and *opn*

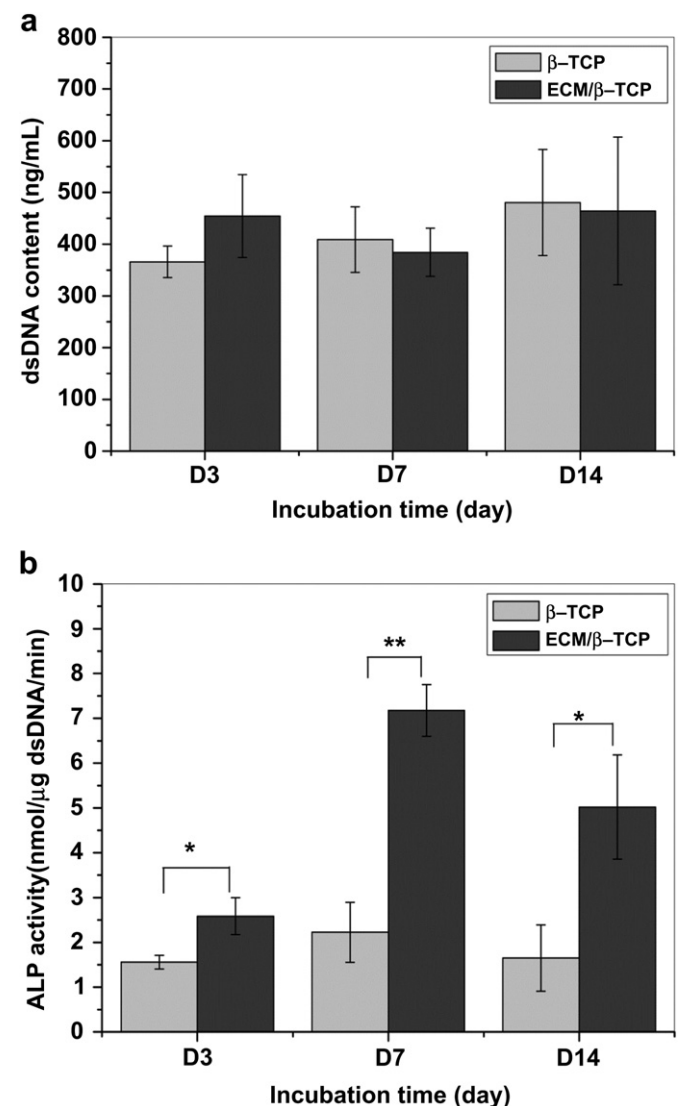


Fig. 6. The amount of dsDNA content synthesized by hMSC grown over time on β -TCP and ECM/ β -TCP scaffolds (a). ALP activity of the hMSC on β -TCP and ECM/ β -TCP scaffolds (b) ($n = 3$). An * and ** are marked to show significant differences between groups (* $p < 0.05$, ** $p < 0.01$).

Table 2

The atomic percent of individual elements on the surface of the scaffolds automatically calculated by the software Multipak associated with the equipment.

Groups	Ca2p	P2p	O1s	C1s	N1s	Na1s	Cl2p
β -TCP	18.4	14.3	52.2	5	0	0	0
ECM	0	0	23.2	68.7	5.4	<0.1	2.7
ECM/ β -TCP	3.4	7.1	30.8	55.5	1.7	1.2	0.8

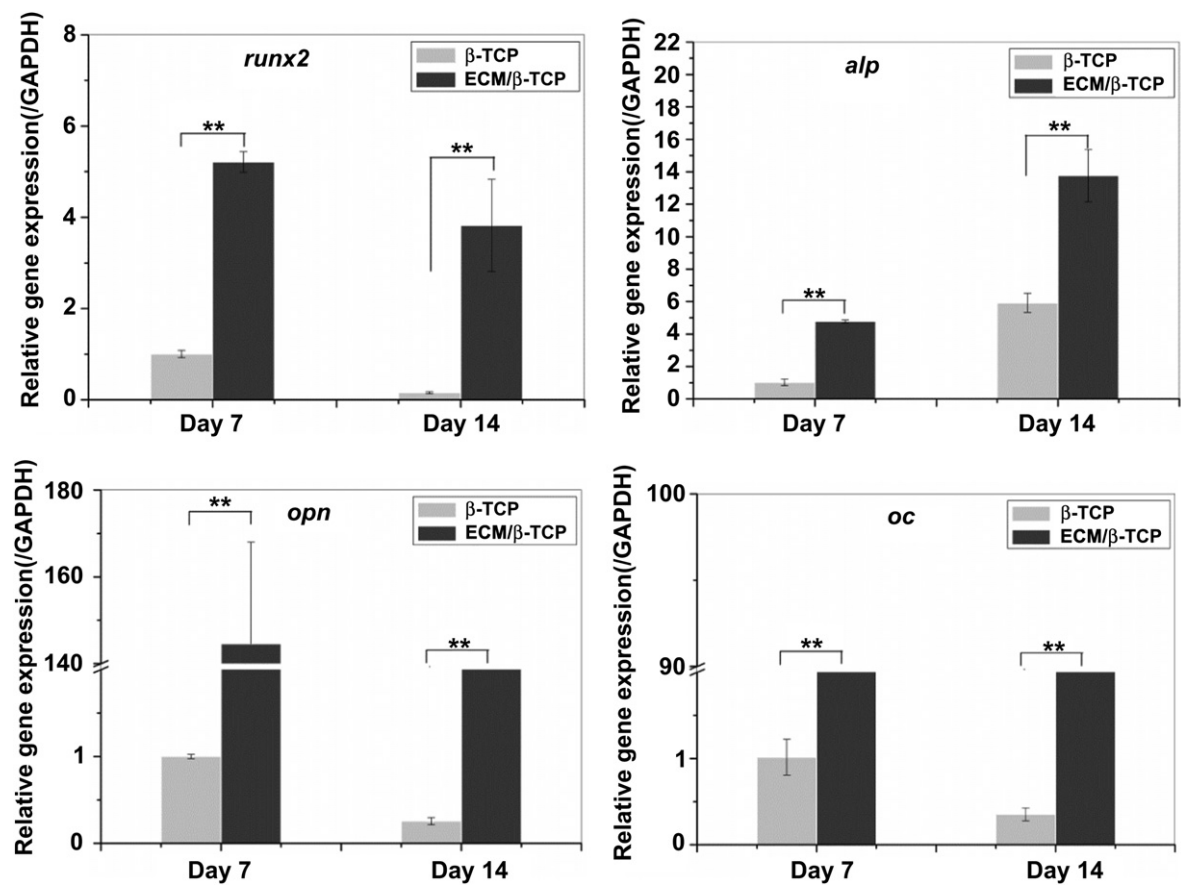


Fig. 7. Related osteogenic gene expression levels in hMSC cultured on β -TCP and ECM/ β -TCP scaffolds. *Runx2*, *alp*, *opn* and *oc* gene expression levels were assessed by real-time PCR at days 7 and 14. GAPDH expression was also determined as an internal control. Significant difference between the two groups are shown as * and ** (* p < 0.05, ** p < 0.01).

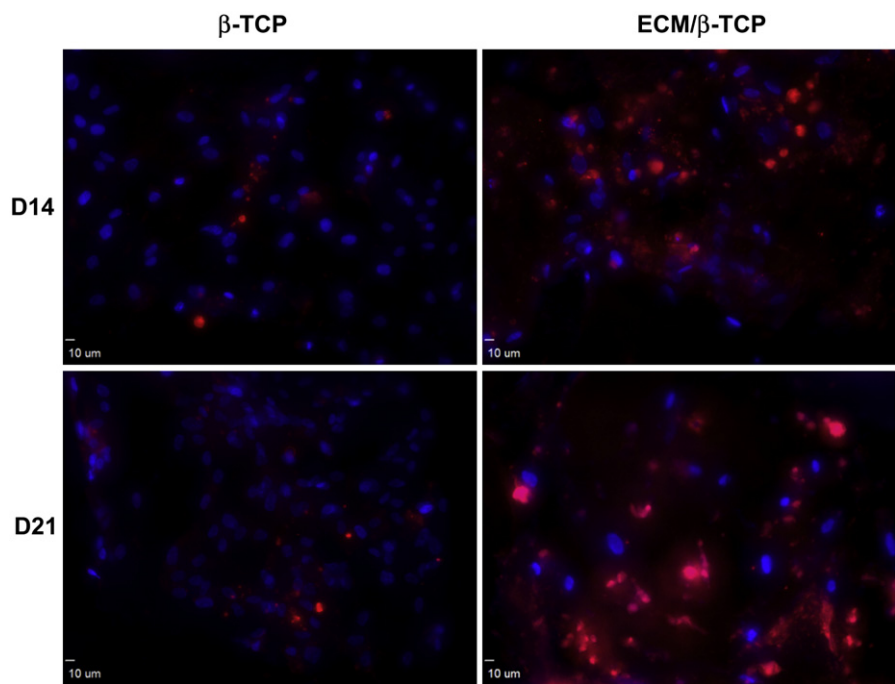


Fig. 8. Confocal microscope images of osteocalcin in hMSC cultured on β -TCP and ECM/ β -TCP scaffolds for 14 and 21 days. Red: Alexa Fluor[®] 594 goat anti-mouse; Blue: DAPI. [For interpretation of color in this figure legend, the reader is referred to web version of the article.]

when hMSC were seeded on ECM/ β -TCP scaffold at 7 and 14 days, while it did not inhibit the gene expression of hMSC on β -TCP scaffolds (Fig. 10 for *runx2*, *alp*, *opn*). In addition, Western blot analysis indicated that PD98059 inhibited the expression of phosphorylated protein ERK1/2 24 h after treatment (Fig. 11). Together, these results suggest that ECM increased osteogenic differentiation in hMSC via MAPK/ERK signaling.

4. Discussion

A microenvironment with appropriate spatial and temporal signals will promote tissue regeneration. Porous β -TCP ceramic scaffolds have been developed to provide structural support in bone regeneration; however, these scaffolds lack bioactive components on the surface. ECM can serve as a source of growth factors, cytokines, chemokines and other biological signals, providing bioactive cues for cell proliferation and differentiation. As such, deposition of cell-derived ECM on a 3D porous β -TCP ceramic scaffold potentially creates a biomimetic microenvironment that promotes cellular development by combining biological cues and structural support.

In our previous study, we produced hMSC-derived ECM deposited on CaP scaffolds [27]. In this study, we grew HUVEC on 3D porous β -TCP ceramic scaffolds and then decellularized the construct to generate HUVEC-derived ECM. This was followed by characterization using SEM, FTIR, XPS and immunochemistry. The results demonstrated the presence of ECM components on the surface of CaP scaffolds. It has been reported that endothelial derived ECM is enriched in proteoglycans laminin, collagen IV, and fibronectin. Fibronectin, collagen IV and laminin are thought to be important ECM protein components for cell adhesion, proliferation and differentiation [15,31,32,40–42]. We further used these proteins as biomarkers for the presence of ECM. Our immunofluorescent staining experiments have shown the presence of collagen IV, fibronectin, and laminin on the β -TCP scaffolds.

After the characterization of ECM on the ceramic scaffold, we evaluated whether this HUVEC-derived ECM microenvironment of ECM/ β -TCP composite scaffold can promote the osteogenic differentiation of hMSC *in vitro*. We seeded hMSC on the ECM/ β -TCP and β -TCP only scaffolds. dsDNA content and ALP activity were measured to determine the extent of cell proliferation and differentiation while the expression of osteogenic genes was determined using real-time PCR. Our study did not demonstrate a significant difference between the ECM/ β -TCP and β -TCP scaffold groups in

dsDNA content, which provides an indirect measure of cell proliferation. Therefore, the presence of ECM on the scaffold did not significantly promote cell proliferation compared to the plain scaffold condition with incubation time. This may be because we used osteogenic medium, which promotes cells to differentiate but not to proliferate.

Our results do suggest that ECM plays a significant role in cell differentiation. ALP activity expression levels in ECM/ β -TCP scaffolds were significantly higher than those in β -TCP only scaffolds. Bone-related genes were up-regulated in ECM/ β -TCP groups compared to β -TCP only groups. The immunofluorescent staining for osteocalcin, a component of bone matrix, was shown to occur at a higher density within ECM/ β -TCP scaffolds relative to β -TCP only scaffolds. These results imply that HUVEC-derived ECM promotes early osteogenic differentiation of hMSC *in vitro*. This may be attributable to collagen, fibronectin and laminin proteins in HUVEC-derived ECM, which have previously been reported to stimulate osteogenic differentiation [12,13,15]. However, Kaigler et al. reported that ECM derived from human dermal microvascular endothelial cells did not have any effect on hMSC's osteogenic differentiation. In their experiments, they removed endothelial cells using urea from culture plates and immediately seeded hMSC on the remaining ECM [43]. Villars et al. also reported that HUVEC-derived ECM had no effect on the ALP activity of hMSC [44]. They used glycerol solution to remove cell materials and scraped ECM for dialysis, and then dialyzed ECM solution was homogenously coated for seeding hMSC. Our method is distinct in that we seeded HUVEC on scaffolds and decellularized the constructs using 0.5% Triton solution to remove cells and deposit ECM on the scaffolds. Our finding that HUVEC-derived ECM significantly promoted the osteogenic differentiation of hMSC is distinct from previous studies and this difference may be a result of the unique combination of ECM architecture and CaP scaffolds in a 3D spatial structure.

The early differentiation of hMSC may be mediated by the activation of the MAPK/ERK osteogenic signal pathway [12,15,45,46]. HUVEC-derived ECM deposited on the surface of a scaffold provides new bioactive components, which may activate ERK1/2 expression through the MAPK/ERK signaling pathway mediated by integrins on the cell membrane of hMSC. To determine if the ECM activates the osteogenic differentiation of hMSC through the MAPK/ERK signaling pathway, we used the inhibitor PD98059 to block this MAPK/ERK signaling pathway. ALP activity and gene expression results showed that ALP activity was significantly inhibited and the osteogenic genes were significantly down-regulated in ECM/ β -TCP group after PD98059 treatment. This inhibition did not occur in β -TCP group. Similarly, protein expression from Western blotting also showed that the phosphorylated ERK1/2 level in ECM/ β -TCP group was significantly inhibited while protein expression in the β -TCP group was not. These results implicate the MAPK/ERK signaling pathway in activating hMSC osteogenic differentiation. ECM components activated this signaling pathway via integrins on the hMSC membrane, thus down-streaming the osteogenic differentiation pathway of hMSC [15,45,46]. This implies that ECM provides important biological cues for the differentiation of hMSC.

This study reinforces our understanding of cell–matrix interaction in ceramic scaffold-based tissue regeneration techniques. A biomimetic microenvironment provides bioactive cues, regulating the osteogenic behaviors of hMSC. Therefore, through the *in vitro* generation of a cell-derived ECM, the cellular function of a ceramic scaffold can be improved without any additional chemical modification or growth factor binding. This technique could also be used to enhance other tissue regeneration scaffolds. We believe that the clinical impact of this technique could be significant, as the treatment of significant bone defects remains an unsolved problem in

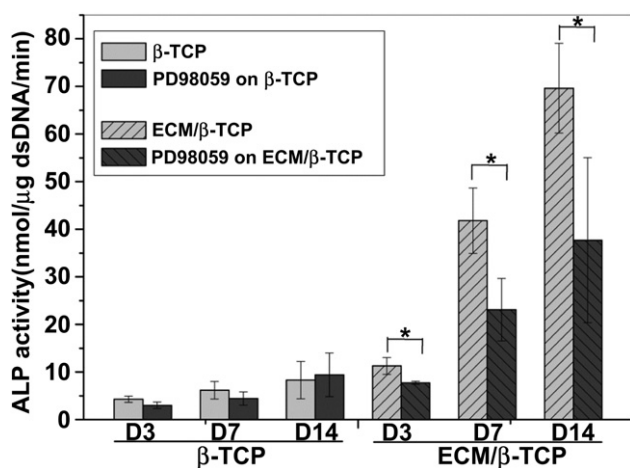


Fig. 9. ALP activity of the hMSC on β -TCP and ECM/ β -TCP scaffolds before and after the addition of inhibitor PD98059.

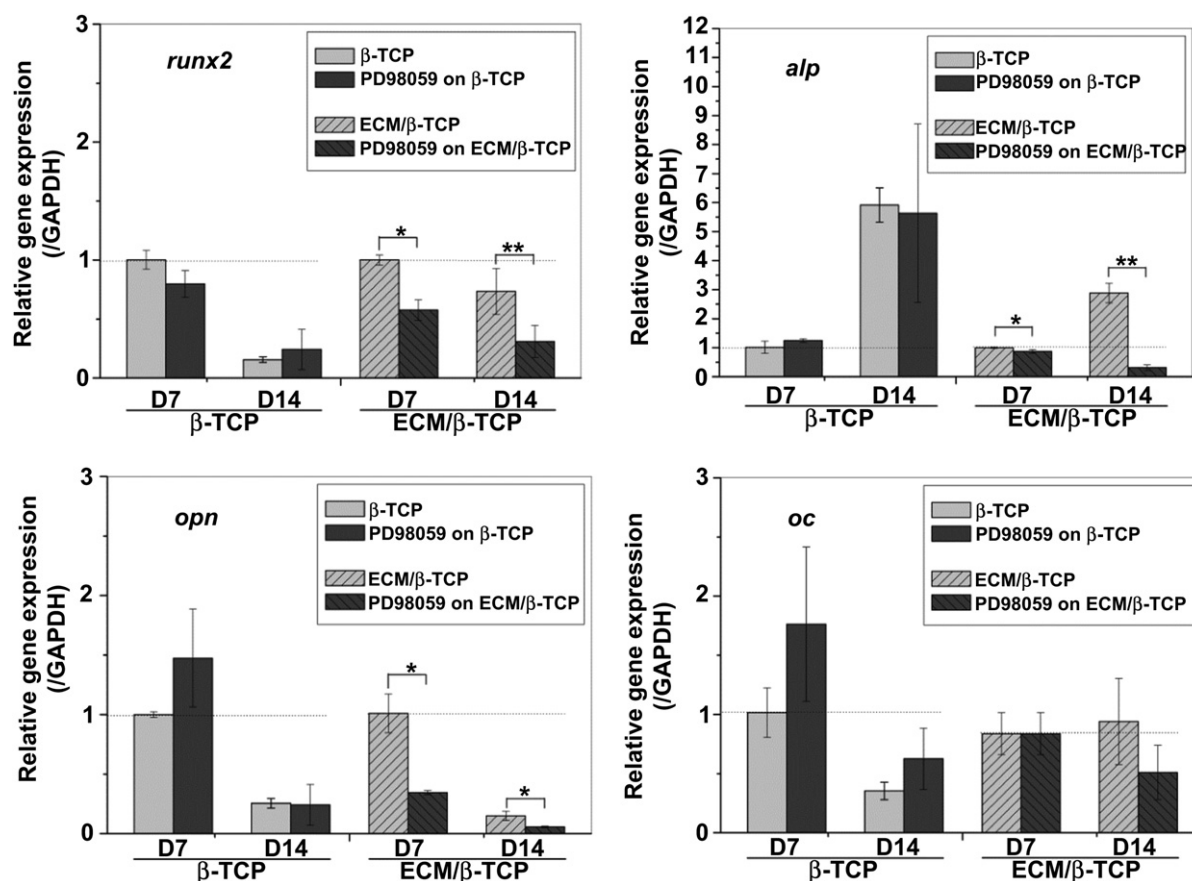


Fig. 10. Related osteogenic gene expression levels in hMSC cultured on ECM/ β -TCP scaffolds with and without the presence of inhibitor PD98059. *Runx2*, *alp*, *opn* and *oc* gene expression levels were inhibited by the addition of PD98059. Significant difference between the two groups are shown as * and ** (* $p < 0.05$, ** $p < 0.01$).

modern medicine. Our ECM-modified scaffold can be tailored to defects of various shapes and sizes, is easily handled and stored in a clinical setting, and avoids the potential risk of infectious disease.

It is worth noting that in our previous experiments, we seeded hMSC onto 3D porous β -TCP scaffold and generated hMSC-derived ECM-containing porous β -TCP scaffolds [27]. In these studies, we did not observe enhancement of early osteogenic differentiation of hMSC by the hMSC-derived ECM. The difference is that we used an osteogenic medium for the first time in our current study and this

combination of HUVEC-derived ECM and osteogenic medium may promote early osteogenic differentiation of hMSC. In the future, we will need to determine if the HUVEC-derived ECM alone will promote early osteogenic differentiation of hMSC in non-osteogenic medium and if the HUVEC-derived ECM will better promote early osteogenic differentiation of hMSC as compared to hMSC-derived ECM in osteogenic medium. Additional research is also indicated to investigate the *in vivo* behaviors of this ECM/scaffold.

5. Conclusion

We fabricated an HUVEC-derived ECM-containing interconnected porous biodegradable β -TCP scaffold. hMSC seeded on this HUVEC ECM-deposited β -TCP scaffold showed increased osteogenic differentiation due to the activation of MAPK/ERK signal pathway. This porous β -TCP with cell-derived ECM provides a promising platform not only for providing mechanical support in a porous structure, but also for mimicking the native cellular microenvironment with biological cues to promote stem cell differentiation.

Acknowledgments

This work was supported by grants from the following agencies: NIH R01AR057837 (NIAMS), NIH R01DE021468 (NIDCR), DOD W81XWH-10-1-0966 (PRORP), W81XWH-10-200-10 (Airlift Research Foundation), W81XWH-11-2-0168-P4 (Alliance of Nano-Health) and Wallace H. Coulter Foundation.

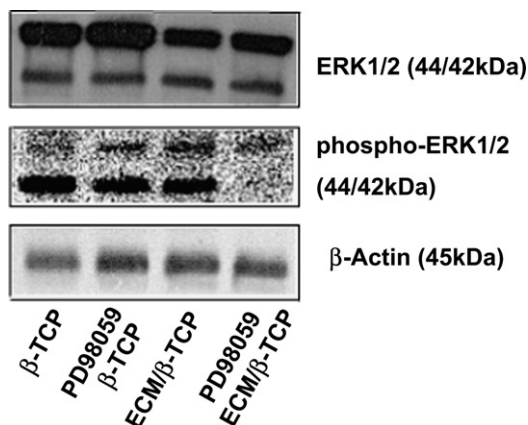



Fig. 11. Protein expression levels of phosphorylated ERK1/2 and total ERK1/2 were evaluated by Western blotting. Blocking MAPK/ERK signaling inhibits the osteogenic differentiation of hMSC on ECM/ β -TCP scaffolds. Cell lysates were generated after 24 h. The concentration of total protein was assayed by BCA assay.

References

- [1] Badylak SF, Freytes DO, Gilbert TW. Extracellular matrix as a biological scaffold material: structure and function. *Acta Biomater* 2009;5:1–13.
- [2] Kleinman HK, Luckenbill-Edds L, Cannon FW, Sephel GC. Use of extracellular matrix components for cell culture. *Anal Biochem* 1987;166:1–13.
- [3] Reilly GC, Engler AJ. Intrinsic extracellular matrix properties regulate stem cell differentiation. *J Biomech* 2010;43:55–62.
- [4] Flynn LE, Prestwich GD, Semple JL, Woodhouse KA. Proliferation and differentiation of adipose-derived stem cells on naturally derived scaffolds. *Biomaterials* 2008;29:1862–71.
- [5] Bhrany AD, Beckstead BL, Lang TC, Farwell DG, Giachelli CM, Ratner BD. Development of an esophagus acellular matrix tissue scaffold. *Tissue Eng* 2006;12:319–30.
- [6] Crapo PM, Gilbert TW, Badylak SF. An overview of tissue and whole organ decellularization processes. *Biomaterials* 2011;32:3233–43.
- [7] Badylak S, Liang A, Record R, Tullius R, Hodde J. Endothelial cell adherence to small intestinal submucosa: an acellular bioscaffold. *Biomaterials* 1999;20:2257–63.
- [8] Li WJ, Tuli R, Huang X, Laquerriere P, Tuan RS. Multilineage differentiation of human mesenchymal stem cells in a three-dimensional nanofibrous scaffold. *Biomaterials* 2005;26:5158–66.
- [9] Mauney JR, Kirker-Head C, Abrahamson L, Gronowicz G, Volloch V, Kaplan DL. Matrix-mediated retention of in vitro osteogenic differentiation potential and in vivo bone-forming capacity by human adult bone marrow-derived mesenchymal stem cells during ex vivo expansion. *J Biomed Mater Res A* 2006;79:464–75.
- [10] Mistry AS, Mikos AG. Tissue engineering strategies for bone regeneration. *Adv Biochem Eng Biotechnol* 2005;94:1–22.
- [11] Khademhosseini A, Vacanti JP, Langer R. Progress in tissue engineering. *Sci Am* 2009;300:64–71.
- [12] Kundu AK, Khatiwala CB, Putnam AJ. Extracellular matrix remodeling, integrin expression, and downstream signaling pathways influence the osteogenic differentiation of mesenchymal stem cells on poly(lactide-co-glycolide) substrates. *Tissue Eng Part A* 2009;15:273–83.
- [13] Kundu AK, Putnam AJ. Vitronectin and collagen I differentially regulate osteogenesis in mesenchymal stem cells. *Biochem Biophys Res Commun* 2006;347:347–57.
- [14] Ku Y, Chung C-P, Pang J-H. The effect of the surface modification of titanium using a recombinant fragment of fibronectin and vitronectin on cell behavior. *Biomaterials* 2005;26:5153–7.
- [15] Klees RF, Salaszyk RM, Kingsley K, Williams WA, Boskey A, Plopper GE. Laminin-5 induces osteogenic gene expression in human mesenchymal stem cells through an ERK-dependent pathway. *Mol Biol Cell* 2005;16:881–90.
- [16] Hoshida T, Lu H, Kawazoe N, Chen G. Decellularized matrices for tissue engineering. *Expert Opin Biol Ther* 2010;10:1717–28.
- [17] Cheng HW, Tsui YK, Cheung KM, Chan D, Chan BP. Decellularization of chondrocyte-encapsulated collagen microspheres: a three-dimensional model to study the effects of acellular matrix on stem cell fate. *Tissue Eng Part C Methods* 2009;15:697–706.
- [18] Choi KH, Choi BH, Park SR, Kim BJ, Min BH. The chondrogenic differentiation of mesenchymal stem cells on an extracellular matrix scaffold derived from porcine chondrocytes. *Biomaterials* 2010;31:5355–65.
- [19] Liao J, Guo X, Grande-Allen KJ, Kasper FK, Mikos AG. Bioactive polymer/extracellular matrix scaffolds fabricated with a flow perfusion bioreactor for cartilage tissue engineering. *Biomaterials* 2010;31:8911–20.
- [20] Wolchok JC, Tresco PA. The isolation of cell derived extracellular matrix constructs using sacrificial open-cell foams. *Biomaterials* 2010;31:9595–603.
- [21] Silva EA, Mooney DJ. Synthetic extracellular matrices for tissue engineering and regeneration. In: *Current topics in developmental biology*. Academic Press; 2004. p. 181–205.
- [22] Pham QP, Kasper FK, Scott Baggett L, Raphael RM, Jansen JA, Mikos AG. The influence of an in vitro generated bone-like extracellular matrix on osteoblastic gene expression of marrow stromal cells. *Biomaterials* 2008;29:2729–39.
- [23] Datta N, Holtorf HL, Sikavitsas VI, Jansen JA, Mikos AG. Effect of bone extracellular matrix synthesized in vitro on the osteoblastic differentiation of marrow stromal cells. *Biomaterials* 2005;26:971–7.
- [24] Datta N, Pham QP, Sharma U, Sikavitsas VI, Jansen JA, Mikos AG. In vitro generated extracellular matrix and fluid shear stress synergistically enhance 3D osteoblastic differentiation. *Proc Natl Acad Sci U S A* 2006;103:2488–93.
- [25] Thibault RA, Scott Baggett L, Mikos AG, Kasper FK. Osteogenic differentiation of mesenchymal stem cells on pregenerated extracellular matrix scaffolds in the absence of osteogenic cell culture supplements. *Tissue Eng Part A* 2010;16:431–40.
- [26] Chen XD, Dusevich V, Feng JQ, Manolagas SC, Jilka RL. Extracellular matrix made by bone marrow cells facilitates expansion of marrow-derived mesenchymal progenitor cells and prevents their differentiation into osteoblasts. *J Bone Miner Res* 2007;22:1943–56.
- [27] Kang Y, Kim S, Khademhosseini A, Yang Y. Creation of bony microenvironment with CaP and cell-derived ECM to enhance human bone-marrow MSC behavior and delivery of BMP-2. *Biomaterials* 2011;32:6119–30.
- [28] Liu Y, Kim JH, Young D, Kim S, Nishimoto SK, Yang Y. Novel template-casting technique for fabricating beta-tricalcium phosphate scaffolds with high interconnectivity and mechanical strength and in vitro cell responses. *J Biomed Mater Res A* 2010;92:997–1006.
- [29] Kang Y, Scully A, Young DA, Kim S, Tsao H, Sen M, et al. Enhanced mechanical performance and biological evaluation of a PLGA coated beta-TCP composite scaffold for load-bearing applications. *Eur Polym J* 2011;47:1569–77.
- [30] Melero-Martin JM, De Obaldia ME, Kang SY, Khan ZA, Yuan L, Oettgen P, et al. Engineering robust and functional vascular networks in vivo with human adult and cord blood-derived progenitor cells. *Circ Res* 2008;103:194–202.
- [31] Matsubara T, Tsutsumi S, Pan H, Hiraoka H, Oda R, Nishimura M, et al. A new technique to expand human mesenchymal stem cells using basement membrane extracellular matrix. *Biochem Biophys Res Commun* 2004;313:503–8.
- [32] Xue X, Wang J, Zhu Y, Tu Q, Huang N. Biocompatibility of pure titanium modified by human endothelial cell-derived extracellular matrix. *Appl Surf Sci* 2010;256:3866–73.
- [33] Yim EK, Wan AC, Le Visage C, Liao IC, Leong KW. Proliferation and differentiation of human mesenchymal stem cell encapsulated in polyelectrolyte complexation fibrous scaffold. *Biomaterials* 2006;27:6111–22.
- [34] Anderson JM, Vines JB, Patterson JL, Chen H, Javed A, Jun HW. Osteogenic differentiation of human mesenchymal stem cells synergistically enhanced by biomimetic peptide amphiphiles combined with conditioned medium. *Acta Biomater* 2011;7:675–82.
- [35] Hofmann A, Ritz U, Verrier S, Eglin D, Alini M, Fuchs S, et al. The effect of human osteoblasts on proliferation and neo-vessel formation of human umbilical vein endothelial cells in a long-term 3D co-culture on polyurethane scaffolds. *Biomaterials* 2008;29:4217–26.
- [36] Livak KJ, Schmittgen TD. Analysis of relative gene expression data using real-time quantitative PCR and the 2[−][Delta][Delta]CT method. *Methods* 2001;25:402–8.
- [37] Coelho PG, Coimbra ME, Ribeiro C, Fancio E, Higa O, Suzuki M, et al. Physico/chemical characterization and preliminary human histology assessment of a [beta]-TCP particulate material for bone augmentation. *Mater Sci Eng C* 2009;29:2085–91.
- [38] Yang MC, Wang SS, Chou NK, Chi NH, Huang YY, Chang YL, et al. The cardiomyogenic differentiation of rat mesenchymal stem cells on silk fibroin-polysaccharide cardiac patches in vitro. *Biomaterials* 2009;30:3757–65.
- [39] Wen F, Chang S, Toh YC, Teoh SH, Yu H. Development of poly (lactic-co-glycolic acid)-collagen scaffolds for tissue engineering. *Mater Sci Eng C* 2007;27:285–92.
- [40] Kleinman HK, Philp D, Hoffman MP. Role of the extracellular matrix in morphogenesis. *Curr Opin Biotech* 2003;14:526–32.
- [41] Cagliero E, Roth T, Roy S, Lorenzi M. Characteristics and mechanisms of high-glucose-induced overexpression of basement membrane components in cultured human endothelial cells. *Diabetes* 1991;40:102–10.
- [42] Beltramo E, Pomeroy F, Allione A, D'Alu F, Ponte E, Porta M. Pericyte adhesion is impaired on extracellular matrix produced by endothelial cells in high hexose concentrations. *Diabetologia* 2002;45:416–9.
- [43] Kaigler D, Krebsbach PH, West ER, Horger K, Huang YC, Mooney DJ. Endothelial cell modulation of bone marrow stromal cell osteogenic potential. *FASEB J* 2005;19:665–7.
- [44] Villars F, Bordenave L, Bareille R, Amedee J. Effect of human endothelial cells on human bone marrow stromal cell phenotype: role of VEGF? *J Cell Biochem* 2000;79:672–85.
- [45] Xiao G, Jiang D, Thomas P, Benson MD, Guan K, Karsenty G, et al. MAPK pathways activate and phosphorylate the osteoblast-specific transcription factor, Cbfa1. *J Biol Chem* 2000;275:4453–9.
- [46] Osyczka AM, Leboy PS. Bone morphogenetic protein regulation of early osteoblast genes in human marrow stromal cells is mediated by extracellular signal-regulated kinase and phosphatidylinositol 3-kinase signaling. *Endocrinology* 2005;146:3428–37.

AUTHOR QUERY FORM

	Journal: ACTBIO Article Number: 2336	Please e-mail or fax your responses and any corrections to: E-mail: corrections.essd@elsevier.sps.co.in Fax: +31 2048 52799
---	---	---

Dear Author,

Please check your proof carefully and mark all corrections at the appropriate place in the proof (e.g., by using on-screen annotation in the PDF file) or compile them in a separate list. Note: if you opt to annotate the file with software other than Adobe Reader then please also highlight the appropriate place in the PDF file. To ensure fast publication of your paper please return your corrections within 48 hours.

For correction or revision of any artwork, please consult <http://www.elsevier.com/artworkinstructions>.

Any queries or remarks that have arisen during the processing of your manuscript are listed below and highlighted by flags in the proof. Click on the 'Q' link to go to the location in the proof.

Location in article	Query / Remark: click on the Q link to go Please insert your reply or correction at the corresponding line in the proof
Q1 Q2	<p>Please confirm that given names and surnames have been identified correctly.</p> <p>Please check what does S.1, S.3a, S.3b refer to?</p> <div data-bbox="416 1868 981 1970"><p>Please check this box if you have no corrections to make to the PDF file</p><input data-bbox="868 1885 940 1949" type="checkbox"/></div>

Thank you for your assistance.



Contents lists available at SciVerse ScienceDirect

Acta Biomaterialia

journal homepage: www.elsevier.com/locate/actabiomat



Osteogenic and angiogenic potentials of monocultured and co-cultured human-bone-marrow-derived mesenchymal stem cells and human-umbilical-vein endothelial cells on three-dimensional porous beta-tricalcium phosphate scaffold

Yunqing Kang^a, Sungwoo Kim^a, Monica Fahrenholtz^b, Ali Khademhosseini^{c,d,e}, Yunzhi Yang^{a,*}

^a Department of Orthopedic Surgery, Stanford University, 300 Pasteur Drive, Stanford, CA 94305, USA

^b Department of Bioengineering, Rice University, 6100 Main St., Houston, TX 77030, USA

^c Center for Biomedical Engineering, Department of Medicine, Brigham and Women's Hospital, Harvard Medical School, Cambridge, MA 02139, USA

^d Harvard-MIT Division of Health Sciences and Technology, Massachusetts Institute of Technology, Cambridge, MA 02139, USA

^e Wyss Institute for Biologically Inspired Engineering, Harvard University, Boston, MA 02115, USA

ARTICLE INFO

Article history:

Received 14 April 2012

Received in revised form 23 July 2012

Accepted 8 August 2012

Available online xxxx

Keywords:

β-TCP

hBMSCs

HUVECs

Osteogenesis

Angiogenesis

ABSTRACT

The use of biodegradable beta-tricalcium phosphate (β-TCP) scaffolds holds great promise for bone tissue engineering. However, the effects of β-TCP on bone and endothelial cells are not fully understood. This study aimed to investigate cell proliferation and differentiation of mono- or co-cultured human-bone-marrow-derived mesenchymal stem cells (hBMSCs) and human-umbilical-vein endothelial cells (HUVECs) on a three-dimensional porous, biodegradable β-TCP scaffold. In co-culture studies, the ratios of hBMSCs:HUVECs were 5:1, 1:1 and 1:5. Cellular morphologies of HUVECs, hBMSCs and co-cultured HUVECs/hBMSCs on the β-TCP scaffolds were monitored using confocal and scanning electron microscopy. Cell proliferation was monitored by measuring the amount of double-stranded DNA (dsDNA) whereas hBMSC and HUVEC differentiation was assessed using the osteogenic and angiogenic markers, alkaline phosphatase (ALP) and PECAM-1 (CD31), respectively. Results show that HUVECs, hBMSCs and hBMSCs/HUVECs adhered to and proliferated well on the β-TCP scaffolds. In monoculture, hBMSCs grew faster than HUVECs on the β-TCP scaffolds after 7 days, but HUVECs reached similar levels of proliferation after 14 days. In monoculture, β-TCP scaffolds promoted ALP activities of both hBMSCs and HUVECs when compared to those grown on tissue culture well plates. ALP activity of cells in co-culture was higher than that of hBMSCs in monoculture. Real-time polymerase chain reaction results indicate that *runx2* and *alp* gene expression in monocultured hBMSCs remained unchanged at days 7 and 14, but *alp* gene expression was significantly increased in hBMSC co-cultures when the contribution of individual cell types was not distinguished.

© 2012 Acta Materialia Inc. Published by Elsevier Ltd. All rights reserved.

1. Introduction

Tissue engineering holds great promise for regenerating functional tissues and organs. One important component of tissue engineered materials is the scaffold, which is an artificial extracellular matrix (ECM) that serves as a temporary support structure and imparts the necessary biophysical, biomechanical and biochemical cues required for cell attachment, proliferation and differentiation to form tissue [1]. In particular, it is highly desirable for scaffolds to possess an interconnected and open macroporous structure to facilitate cellular in-growth and neovascularization of regenerated tissue in vivo.

Calcium phosphate (CaP) bioceramics have been widely used in clinical settings for bone repair and reconstruction [2,3]. Hydroxyapatite (HA) and beta-tricalcium phosphate (β-TCP) are the most popular bioceramics due to their close resemblance to natural bone, excellent biocompatibility and biodegradability. Bone-marrow-derived mesenchymal stem cells (BMSCs) have been used in combination with CaP scaffolds in bone tissue engineering [4–7]. Many studies involving the use of BMSC-seeded bioceramics have shown promising results in the context of bone regeneration [8–11]; however, most of these investigations have highlighted the osteogenic potential of BMSCs on these CaP bioceramics.

Bone tissue contains multiple cell types, including osteogenic cells and endothelial cells. A number of studies in bone repair and regeneration have highlighted the intimate interactions between endothelial cells and osteoprogenitor cells [12,13]. Indeed,

* Corresponding author. Tel.: +1 650 723 0772; fax: +1 650 724 5401.

E-mail address: ypyang@stanford.edu (Y. Yang).

it has been well established that angiogenesis is a prerequisite for osteogenesis *in vivo* [14]. For example, insufficient neovascularization of bone constructs/tissues after scaffold implantation resulted in hypoxia and cellular necrosis [15–19]. Thus, a key factor in repairing large bone defects is vascularization of the scaffold. Within this context, it is important to characterize the effects of bioceramic scaffolds with regards to osteogenic and endothelial differentiation. It has been reported that co-cultured human endothelial cells with human osteoblast cells on porous HA, β -TCP or Ca-deficient HA containing polycaprolactone supported the formation of capillary-like structures [20,21]. Zhou et al. pre-vascularized β -TCP scaffold by co-seeding MSCs and MSC-derived endothelial cells (ECs) and used it to promote the repair of segmental bone defects in rabbits [22].

In this study, we investigated the effect of a porous, biodegradable β -TCP scaffold on the behavior of mono- or co-cultured human-bone-marrow-derived mesenchymal stem cells (hBMSCs) and human-umbilical-vein endothelial cells (HUVECs). We hypothesize that different cell ratios of hBMSCs and HUVECs may behave differently on a porous, biodegradable β -TCP scaffold. In this experiment, interconnected porous β -TCP scaffolds were prepared by a template-casting method [23–25]. Cell proliferation was monitored by measuring the amount of double-stranded DNA (dsDNA), whereas hBMSC and HUVEC differentiation was assessed using the osteogenic and angiogenic markers alkaline phosphatase (ALP) and PECAM-1 (CD31), respectively.

2. Materials and methods

2.1. Materials

β -TCP powder with a specific surface area of $17 \text{ m}^2 \text{ g}^{-1}$ was purchased from Nanocerox, Inc. (Ann Arbor, Michigan). Carboxymethyl cellulose powder, paraffin beads and ethyl alcohol were purchased from Fisher Scientific (Pittsburgh, USA).

Dulbecco's modified Eagle's medium (DMEM), fetal bovine serum (FBS) and L-glutamine, $100 \times$ antibiotic-antimycotic solution were purchased from Invitrogen Co. (Grand Island, NY, CA). EBMTM endothelial basal medium containing EGMTM endothelial growth medium and a Single QuotsTM kit were purchased from Lonza, Inc. Alexa Fluor[®] 594 goat anti-mouse secondary antibody (2 mg ml^{-1}) was purchased from Invitrogen Inc. An RNeasy mini kit for extracting RNA was purchased from QIAGEN (Valencia, CA, USA).

2.2. Preparation of β -TCP scaffolds

Porous β -TCP scaffolds were fabricated using a template-casting method as previously described [23–25]. Briefly, β -TCP powder, carboxymethyl cellulose powder, surfactant (Surfonal[®]) and dispersant (Darvan[®] C) were mixed in distilled water to form a ceramic slurry. Paraffin beads were packed into a customized mold and heated to induce partially melting and formation of a template. The β -TCP ceramic slurry was then cast into the mold under vacuum, solidified and subsequently dehydrated in a series of ethyl alcohol solutions (70%, 90% and 95%). After removing the dehydrated green body from the mold, the green body was dried in an oven for 2 h, and then placed into an electric high temperature furnace and sintered at 1250°C for 3 h. The morphology of β -TCP scaffolds was characterized by scanning electron microscopy. The average pore size of scaffold was obtained from scanning electron microscopy (SEM) images and at least six pores were measured. The interconnected pore structure of scaffold was scanned using micro-computed tomography (micro-CT; Imtek Micro CAT II, Knoxville, TN) at a resolution of $80 \mu\text{m}$. Raw images were further reconstructed

and analyzed by GE microView software (General Electric Co.). The scaffolds used in this study were 7–8 mm in diameter and 5–6 mm in height.

2.3. Cell culture of hBMSCs and HUVECs

hBMSCs were purchased from Lonza Inc. (Allendale, NJ) [26]. According to the manufacturer's certificate of analysis, the cells are more than 90% positive for CD105, CD166, CD29 and CD44, and less than 10% positive for CD14, CD34 and CD45. The cells were cultured in basal medium consisting of DMEM, (Invitrogen, USA) with 10% FBS, 1% L-glutamine (200 mM) and 1% antibiotic-antimycotic solution under standard conditions (5% CO_2 , 95% humidity, and 37°C). Passages 6–8 were used for all the experiments.

Immortalized HUVECs constitutively expressing green fluorescent protein (GFP) were a generous gift from the late Dr. J. Folkman, Children's Hospital, Boston. HUVECs were cultured in endothelial basal medium (EBM-2, Lonza) with endothelial growth supplement Single Quots (EGM-2, Lonza) in a 5% CO_2 atmosphere at 37°C .

A preliminary study was performed to test the culture medium for co-culture experiments (Supplementary Fig. S1). In this study, the medium used in all co-culture experiments was a 1:1 mixture of EBM-2 and DMEM.

When the cells reached ~85–90% confluence in flasks, they were subcultured using 0.25% trypsin-EDTA (Invitrogen, USA) and resuspended in culture medium. Next, 100,000 cells in $100 \mu\text{l}$ medium were gently seeded into the sterilized β -TCP scaffolds and incubated at 37°C for 1 h to allow cells to attach onto the inner construct surface of the scaffold. New medium was then added for further incubation. The medium was changed every 3 days. To investigate the reciprocal effect of the two cell types on osteogenesis and angiogenesis, three mixture ratios (1:5, 1:1, 5:1) of hBMSCs and HUVECs were seeded and co-cultured on the scaffolds. In mono- and co-culture experiments, the seeding density (100,000 cells per scaffold) was held constant regardless of cell mixture ratios. To indicate the cell distribution in the scaffolds, scaffolds with seeded HUVEC-GFP cells were recaptured using a fluorescent microscope (Nikon 2000) and shown in Supplementary Fig. S2.

2.4. Morphologies of HUVECs, hBMSCs and co-cultured cells on the β -TCP scaffolds

The morphology of HUVECs on β -TCP scaffolds was monitored using a confocal laser scanning microscope (CLSM; Olympus IX81) after 1, 3 and 7 days of incubation in EBM-2 medium. Morphologies of HUVECs, hBMSCs and hBMSC/HUVEC mixtures seeded on the β -TCP scaffolds were also observed under a scanning electron microscope (SEM, FEI Quanta 400). HUVECs and hBMSCs in monoculture were incubated in EBM-2 and DMEM, respectively, and hBMSC/HUVEC mixture cells (50%:50%) were co-cultured in EBM-2:DMEM mixture medium (1:1) for 3 days. Following this, scaffolds were fixed with 2.5% glutaraldehyde for 2 h, followed by graded dehydration using a series of ethanol solutions (generally 70%, 80%, 90% and 100%). Samples were then dried in a hood and sputtered with gold before observation under an SEM (FEI Quanta 400) at 20 kV.

2.5. Visualization of F-actin

F-actin was stained by rhodamine phalloidin to assess cytoskeletal organization on the β -TCP scaffold. After 7 days of incubation in the same medium as used in the experiments for SEM, cells/scaffolds were rinsed twice using phosphate buffered saline (PBS) and then fixed by 4% paraformaldehyde solution (PFA) for 15 min at

room temperature. The fixed cells were further permeabilized in 0.5% Triton X-100 and incubated in 100 nM rhodamine phalloidin working solution (Cytoskeleton Inc., USA) at room temperature for 2 h. After a brief rinse with PBS, DAPI solution (5 $\mu\text{g ml}^{-1}$) was added to counterstain cell nuclei. After a thorough washing with PBS, cells on scaffolds were visualized with a CLSM.

2.6. Immunofluorescent staining of PECAM-1

Platelet-endothelial cell adhesion molecule (PECAM-1, or CD31) is an endothelial-specific adhesion protein and a specific marker of HUVECs. It was assessed by immunofluorescent staining. The effect of β -TCP scaffolds on PECAM-1 expression of HUVECs in monoculture or co-culture with hBMSCs in various ratios (1:5, 1:1, 5:1) were investigated at 7 and 14 days. They were cultured in a 1:1 mixture of EBM-2 and DMEM, and then rinsed twice with PBS and fixed in a solution of 4% PFA for 15 min at room temperature. After washing three times in PBS, the fixed cells/scaffolds were placed in 3% bovine serum albumin (BSA)/PBS blocking buffer for 1 h, and then were incubated with mouse anti-human CD31 primary antibody (1:3000, Cell Signaling Technology) in 1% BSA/PBS overnight at 4 $^{\circ}\text{C}$. The cells/scaffolds were then washed three times using PBS, and incubated in an anti-mouse secondary antibody Alexa Fluor[®]594 (1:1000; 2 $\mu\text{g ml}^{-1}$, Invitrogen) for 1 h at room temperature. After a brief rinse using PBS, the cell nuclei were counterstained with DAPI solution (5 $\mu\text{g ml}^{-1}$) for 1 min. The scaffold samples were then extensively washed with PBS, and visualized with a CLSM.

2.7. Osteogenic differentiation assay of hBMSCs

The effect of β -TCP scaffolds on the early osteogenic differentiation of hBMSCs in monoculture and co-culture was assessed through ALP specific activity. hBMSCs were co-cultured with various ratios of HUVECs (5:1, 1:1, 1:5) on the scaffolds. Monocultured hBMSCs and HUVECs were used as controls. The medium used in these co-culture experiments was a 1:1 mixture of EBM-2 and DMEM, as determined in our preliminary study (S.1).

At the end of each time point, cells/scaffolds were washed twice with PBS and preserved at -80°C . Cells/scaffolds experiencing three freeze/thaw cycles in $-80^{\circ}\text{C}/37^{\circ}\text{C}$, were then lysed in 500 μl of 0.2% Triton X-100 in PBS, and finally homogenized by sonication for 30 s on ice. The ALP activity was assayed using a colorimetric p-NPP method [23,24]. The absorbance was measured on a microplate reader (TECAN) at 405 nm after 30 min incubation at 37 $^{\circ}\text{C}$. ALP specific activity levels were quantified with a standard curve and normalized to the amount of total cellular dsDNA from the same sample. dsDNA content was determined using a Pico Green assay (Molecular Probe, Invitrogen). A 50 μl volume of working reagent was added to the 50 μl cell lysate of the sample. The sample was read at 485/528 nm (excitation/emission) on a fluorescence spectrophotometer (Biotek, Flx800, USA). The amount of dsDNA was calculated by comparing the standard curves of the known dsDNA sample according to the manufacturer's instruction.

2.8. Quantitative real-time polymerase chain reaction (PCR)

Total RNA of cells was extracted from the monocultured and co-cultured cells after incubation of 7 and 14 days using an RN easy mini Kit (QIAGEN) following the manufacturer's protocol. RNA concentration was determined on an Eppendorf Biophotometer. To reverse-transcribe RNA of the samples into cDNA, an iScript cDNA synthesis kit (BIO-RAD) was used according to the manufacturer's protocols. Using cDNA product template, specific primers and iQ-SYBR Green supermix (BIO-RAD), real-time PCR was performed on an ABI 7900HT Sequence Detection system (ABI, Foster city,

Table 1
Sequences of primers used for real-time PCR analysis.

Genes	Sequences
GAPDH	For: 5'-AACAGCGACACCCACTCCTC Rev: 5'-CATACCAGGAATGAGCTTGACAA
<i>runx-2</i>	For: 5'-AGATGATGACACTGCCACCTCTG Rev: 5'-GGGATGAAATGCTTGGGAACT
<i>alp</i>	For: 5'-ACATTCACACGCTCTTCACATT Rev: 5'-AGACATTCTCTCGTTCACCGCC
<i>opn</i>	For: 5'-ATGAGATTGGCAGTGATT Rev: 5'-TTCAATCAGAACTGGAA
<i>oc</i>	For: 5'-TGTGAGCTCAATCCGACTGT Rev: 5'-CCGATAGGCTCTCTGAAGC
<i>bsp</i>	For: 5'-ATGGCTGTGCTTTCTCAATG Rev: 5'-GGATAAAGTAGGCATGCTTG
<i>bmp-2</i>	For: 5'-GCCCTTTCTCTGCGCTAT Rev: 5'-TTGACCAACGCTGAACAATGG
<i>cd31</i>	For: 5'-GAGTCTGCTGACCCCTTCTG Rev: 5'-CACTCTCTCCACCAACACCT

USA). The total reaction volume was 10 μl . Primer sequences are shown in Table 1, including runt-related transcription factor 2 (*runx2*), alkaline phosphatase (*alp*), osteopontin (*opn*), osteocalcin (*oc*), bone sialoprotein (*bsp*), bone morphogenetic protein-2 (*bmp-2*), *cd31* and glyceraldehyde 3-phosphate dehydrogenase (GAPDH). These primers were purchased from Invitrogen Co. and used to evaluate gene expression [27–29]. The relative expression levels of genes were analyzed using the $2^{-\Delta\Delta\text{Ct}}$ method [30] by normalizing with the housekeeping gene GAPDH as an endogenous control and calibrating with efficiency, where $\Delta\Delta\text{Ct}$ is calculated from $(C_{\text{t, target}} - C_{\text{t, control}})_{\text{target gene}} - (C_{\text{t, target}} - C_{\text{t, control}})_{\text{GAPDH}}$.

2.9. Statistical analysis

All the groups in the experiments were performed in triplicate, and the statistical significance was analyzed by Student's *t*-test. If the *p*-values obtained from the *t*-test were less than 0.05, the difference was considered to be significant.

3. Results

3.1. Porous morphologies of the β -TCP scaffold

Representative morphology of a β -TCP scaffold is shown in Fig. 1. The porous structure and interconnected pores of a β -TCP scaffold is shown in Fig. 1A at a lower magnification. The pores size of the scaffold is in the range of 350–500 μm and the average pore size measured from SEM images is $\sim 396 \pm 49 \mu\text{m}$. Fig. 1B indicates a local strut of the scaffold at a higher magnification. The strut surface appears dense and consists of microscale grains. Fig. 1C–E shows the representative three-dimensional (3-D) and two-dimensional (2-D) reconstructed micro-CT images. The interconnected pores are observed across the scaffold in Fig. 1C–E.

3.2. Cell morphologies on the β -TCP scaffold

Morphologies of GFP-tagged HUVECs on the β -TCP scaffold were observed with a CLSM. Fig. 2 shows cell morphology changes on a β -TCP scaffold over time. Fluorescent images in Fig. 2A show that HUVECs adhered and spread well on the surface of struts and inner pores of the scaffold at day 1, and cells exhibited a cobblestone-like morphology. HUVECs proliferated well on the scaffold with increasing culture time. At day 3, HUVECs covered the majority of the strut surface (Fig. 2B) and a dense endothelial layer

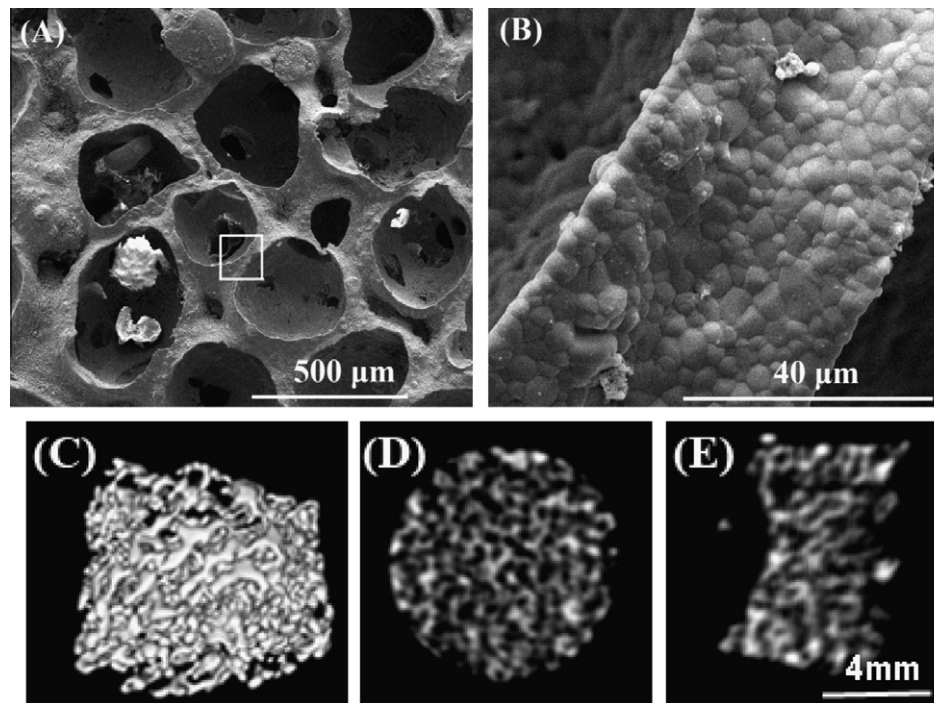


Fig. 1. SEM morphologies of the β -TCP scaffold with different magnifications: (A) interconnected pores at low magnification (50 \times), and (B) the local strut surface at high magnification of the square area in (A) (3000 \times). Micro-CT images indicate the interconnected pores of scaffold in 3-D (C), and 2-D reconstruction (D) and (E).

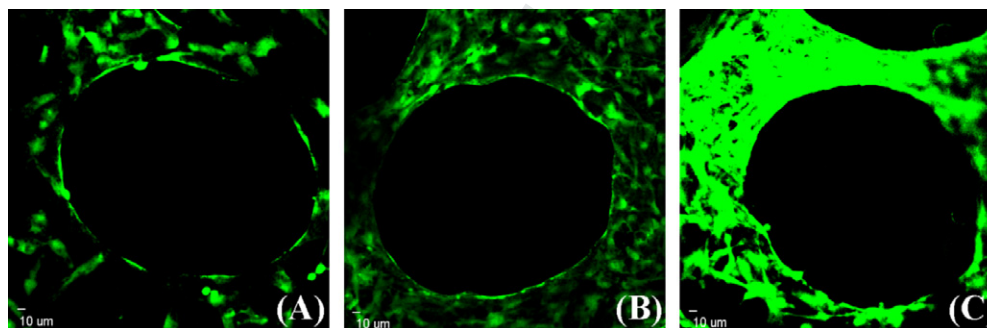


Fig. 2. HUVEC adhesion and spread morphology on the struts of a β -TCP scaffold observed by confocal laser scanning microscopy. HUVECs are observed to attach and grow well on the scaffold for (A) 1 day, (B) 3 days and (C) 7 days. Images were captured on the same site of one scaffold.

was formed by day 7 (Fig. 2C). In this study, SEM was used to further investigate cell morphologies of hBMSCs and HUVECs on the β -TCP scaffolds. Results showed that both hBMSCs and HUVECs can adhere well on the scaffolds (Fig. 3). In monocultures, HUVECs exhibited cobblestone-like morphology and formed a flattened endothelial cell layer (Fig. 3A), while hBMSCs exhibited a typical spindle-like morphology (Fig. 3B). In co-culture of hBMSCs and HUVECs, both spindle-like cells and cobble-like cells could be observed, suggesting the co-existence of both cell types on the scaffold (Fig. 3C).

3.3. Visualization of F-actin filament of cells

In HUVEC and hBMSC monocultures, an abundance of actin fibers was observed in the cytoplasm of the cells (Fig. 4A, G and C, H). The fluorescent image in Fig. 4B shows cobblestone-like morphology. In hBMSC monocultures, the rhodamine phalloidin/DAPI staining of hBMSCs in Fig. 4C indicated a homogenous distribution of actin fibers and filament elongation of cells on the scaffold. Additionally, as shown in Fig. 4D, hBMSCs were GFP-negative, distin-

guishing them from the GFP-positive HUVECs. In co-cultures, comparing the rhodamine phalloidin/DAPI staining image in Fig. 4E with the GFP fluorescent image in Fig. 4F, the distribution of hBMSCs in co-culture can be distinguished from that of GFP-tagged HUVECs. Contacting zones or overlapping growths were observed. Fig. 4G and H shows the F-actin staining of HUVECs and hBMSCs at a higher magnification, respectively. Obvious actin fiber bundles can be observed in the cytoplasm.

3.4. Immunofluorescent staining of PECAM-1

In HUVECs monocultures, immunofluorescent images show the expression of PECAM-1 at the cell–cell interface after 7 days of culture (Fig. 5). With increasing culture time, PECAM-1 expression of HUVECs became more pronounced and cells were observed forming network after 14 days. For both the 1:5 hBMSCs/HUVECs and HUVEC alone groups, PECAM-1 expression increased with culture time. The higher magnification images in the inserts showed the formation of small sprouts (Fig. 5). In the 5:1 and 1:1 hBMSC/HU-

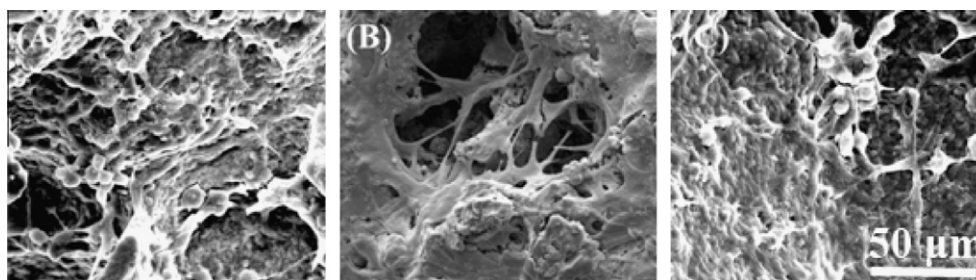


Fig. 3. Scanning electron micrographs showing cells growing on the β -TCP scaffolds after 3 days of culture: (A) HUVECs, (B) hBMSCs and (C) co-cultured hBMSCs/HUVECs (1:1 ratio).

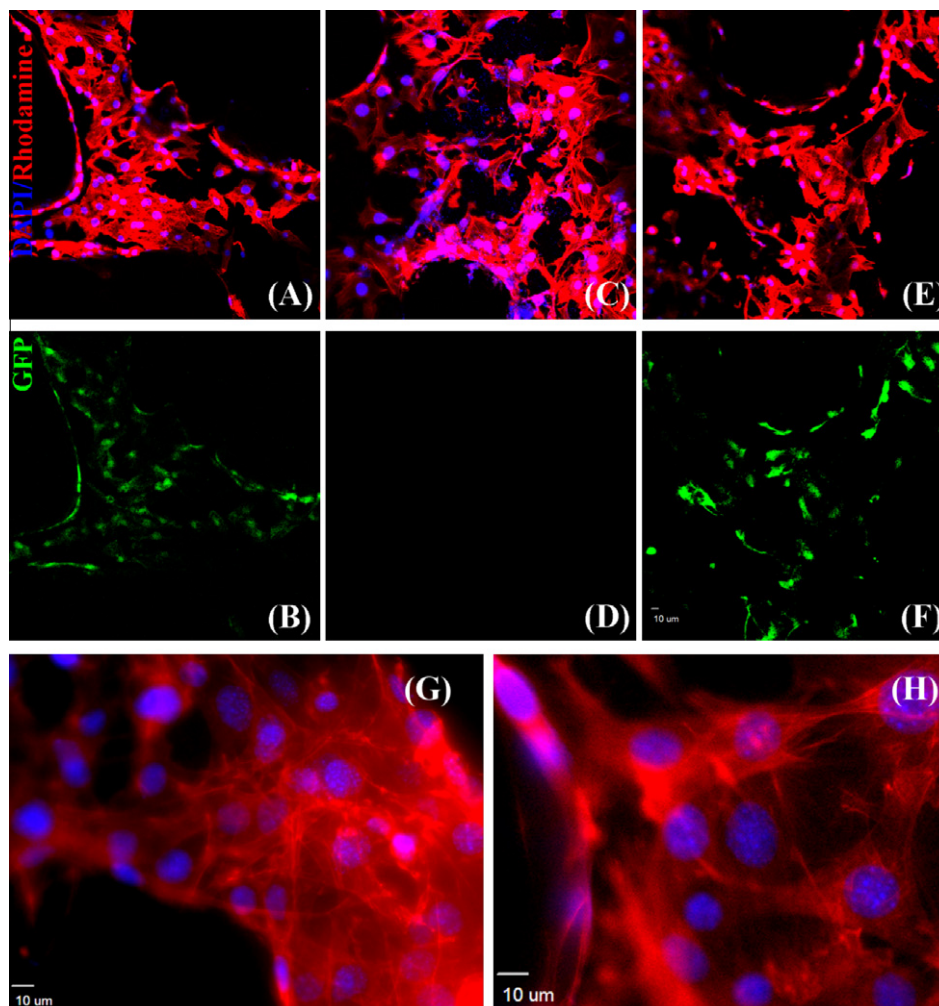


Fig. 4. Cytoskeletal organization of cells grown on the β -TCP scaffolds at day 7, as observed under a CLSM and demonstrated by rhodamine phalloidin/DAPI staining for F-actin/cell nuclei (A, C, E) and endogenous GFP (B, D, F). An abundance of F-actin fiber is observed in HUVECs (A, B), hBMSCs (C, D) and co-cultured hBMSCs/HUVECs (E, F), indicating a homogenous distribution of F-actin. (G) and (H) show F-actin staining of HUVECs and hBMSCs at a higher magnification, respectively.

VEC groups, these network structures were not apparent due to the lower proportion of HUVECs present.

3.5. Cell proliferation and ALP activity of hBMSCs

The proliferation of hBMSCs and HUVECs on the β -TCP scaffolds is shown in Fig. 6a. For hBMSC monocultures, cell proliferation increased from day 3 to day 7. After 7 days, cellular dsDNA content started to decrease. For HUVEC monocultures, cellular dsDNA amount increased from day 3 to day 14. The growth rate of HUVECs

was slower compared to that of hBMSCs, but reached the same level of proliferation within 14 days of incubation. Compared to monocultures, the total cellular dsDNA amount in co-culture was proportional to the cell ratios and growth rates (Fig. 6a).

To evaluate the effect of HUVECs on the ALP activity of hBMSCs, hBMSCs were co-cultured with HUVECs at various ratios in non-osteogenic medium. The ALP activity of cells in monoculture and co-culture is shown in Fig. 6b. Results show that, in both mono- and co-culture, the ALP activity level of hBMSCs continually increased over 14 days (Fig. 6b). For the 5:1 and 1:1 hBMSC/HUVEC

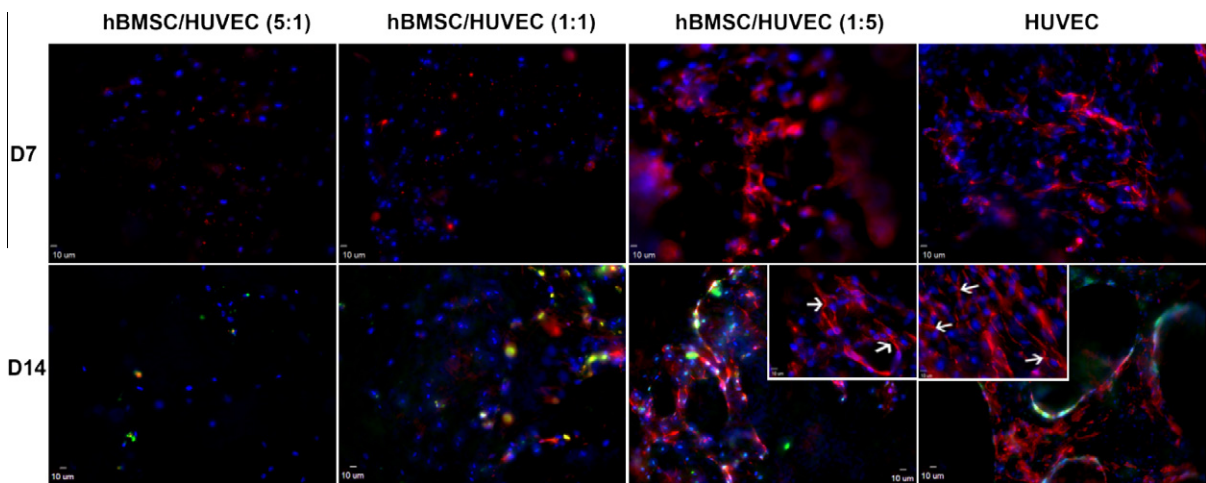


Fig. 5. CLSM images showing expression of endothelial marker, PECAM-1 (CD31), by HUVECs in monoculture and co-culture with hBMSCs at day 7 and day 14 on β -TCP scaffolds. Confocal images through a z-stack demonstrated the expression of CD31. Insert images represent CD31 expression of hBMSC/HUVEC (1:5) and HUVEC groups on day 14 at a higher magnification. Formation of small sprouts can be observed (white arrows). CD31 is in red (labeled with Alexa Fluor 594), and nuclei are in blue (labeled with DAPI).

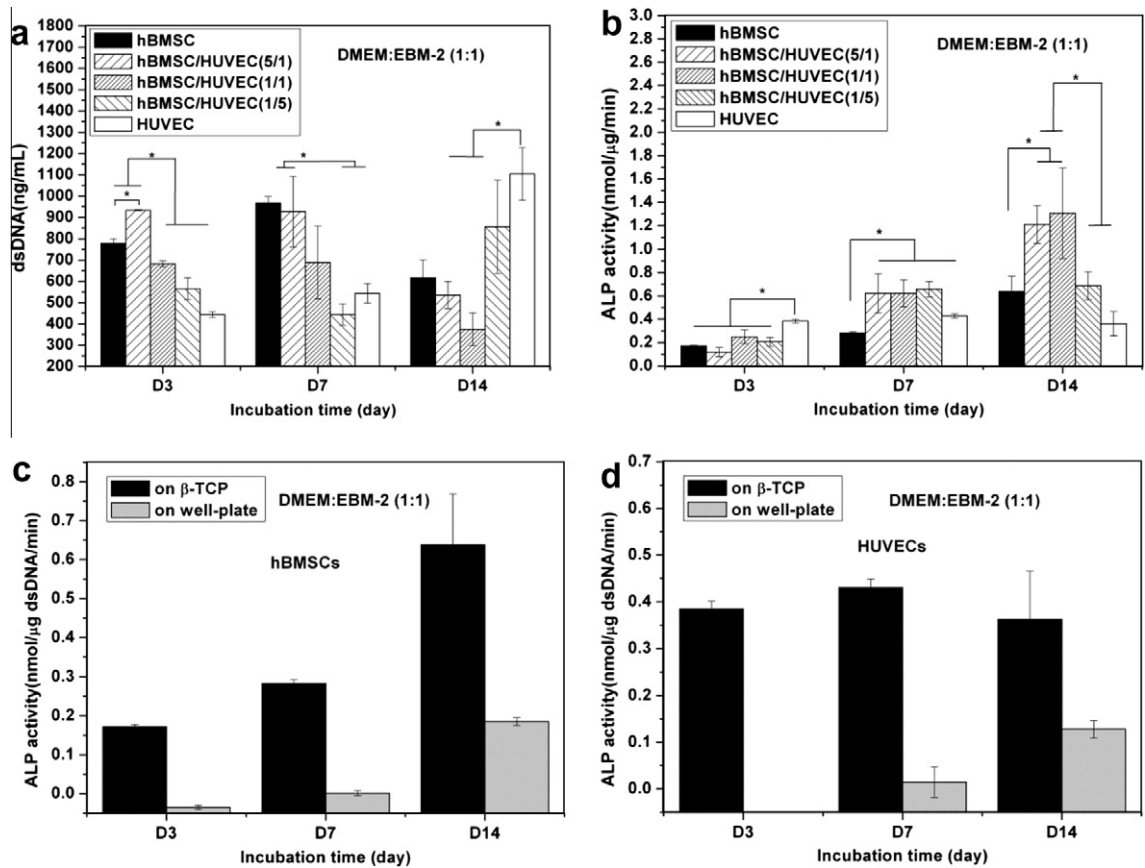


Fig. 6. dsDNA contents of cells in monocultured hBMSCs and HUVECs, and co-cultured hBMSCs/HUVECs at various ratios on the β -TCP scaffolds (a), and ALP activity expression in hBMSCs on the β -TCP scaffolds in monocultures and co-culture after 3, 7 and 14 days of incubation (b). ALP activity in monoculture hBMSCs (c) and HUVECs (d) on well plate and β -TCP scaffolds. An asterisk is used to indicate significant difference ($p < 0.05$).

groups, the ALP activity of co-cultured cells was significantly higher compared to those in monoculture ($p < 0.05$), except for the 1:5 hBMSC/HUVEC groups at day 14. ALP expression of HUVECs was higher than that in other groups at day 3, and it remained constant during 14 days of culture. ALP expression of hBMSCs or HUVECs alone on well plates was also investigated, and the results show that ALP activity could not be detected until day 14 (Fig. 6c and

d), but the cells on the β -TCP scaffolds produced detectable ALP activity level at days 3 and 7 (Fig. 6b).

3.6. Gene expression

Quantitative real-time PCR was performed to evaluate the expression of osteogenic and endothelial markers. Fig. 7 shows

the osteogenic gene expression of hBMSCs and the endothelial gene expression of HUVECs in monoculture and co-culture. All gene expression was normalized to the expression levels of monocultured hBMSCs at day 7 (reference value set to 1).

For monocultures, the expression of *runx2* of hBMSCs did not change at 7 and 14 days of incubation. In the co-culture, *runx2* down-regulation increased with a decrease in the hBMSC/HUVEC ratio. *Alp* expression did not significantly change for monocultured hBMSCs, but it was significantly increased in the 5:1 hBMSC/HUVEC ratio group at day 7 and in the 5:1 and 1:1 hBMSC/HUVEC ratio groups at day 14. In monocultures, hBMSCs increased the expressions of *bsp* and *opn*, two early bone matrix genes, and reduced the expression of *oc*, a late bone matrix gene between day 7 and day 14 [31–33]. The addition of HUVECs significantly decreased the expression of the three genes in all co-culture groups. Additionally, these early osteogenic differentiation genes and bone matrix genes including *runx2*, *alp*, *bsp* and *opn* were detected at very low levels in HUVECs. In contrast, HUVECs expressed higher levels of *bmp-2* and *cd31*, when compared to hBMSCs. The expression of these two genes was detected in hBMSC monocultures. The expression of these two genes in co-culture groups increased as the hBMSC/HUVEC ratio decreased.

4. Discussion

β -TCP bioceramics have been widely used in clinical settings for bone repair and reconstruction [2,3]. In bone tissue engineering, it is common to merge biodegradable, biomimetic, porous CaP scaffolds with stem cells such as MSCs to regenerate bone tissue [4,8–11]. However, most of these works focused mainly on the osteogenic potential of MSCs on bioceramic scaffolds. It is well known that osteogenic and angiogenic processes are interdependent via the intimate interaction between bone-forming cells and endothelial cells [34–36]. An increasing number of studies have focused on the reciprocal effects between mesenchymal stem cells and endothelial cells or their corresponding precursors [37–40]. Although these studies provide new insights into the relationship between bone-forming cells and endothelial cells, the influence of the porous β -TCP ceramic scaffolds on the osteogenic and angiogenic potentials of hBMSCs and HUVECs in monoculture or co-culture is still not well understood.

In this study we investigated the cell behavior of HUVECs, hBMSCs and co-cultured hBMSCs/HUVECs on β -TCP scaffolds, including cell attachment, proliferation, and cell-specific marker expression. In co-culture, we mixed two types of cells in suspension and then seeded them on the β -TCP scaffolds. In this model, the interactions between two types of cells occurred by direct cell–cell contacts and diffusible paracrine signaling [38,41]. In these experiments, one major factor impacting cell behavior is the co-culture medium. Different culture media may lead to stem cell differentiation towards osteogenic, chondrogenic, endothelial, adipogenic and vascular smooth muscle phenotypes [42]. To select the appropriate co-culture medium in this study, we first co-cultured the two types of cells on well plates using three different media, including EBM-2, DMEM, and a 1:1 mixture of both. We found that the morphology of hBMSCs changed from spindle shape in DMEM to a slightly long, narrow spindle shape in EBM-2. In the mixture medium, the morphology of hBMSCs did not show this kind of change (S.1). For HUVECs, we found that they hardly survived or proliferated in DMEM. In a 1:1 mixture, the co-cultured cells can both display normal cell morphology as in their own preferred monoculture medium, regardless of their co-culture ratio (5:1, 1:1, 1:5; see S.1). To take into consideration the behavior of both cell types, the combined medium DMEM:EBM-2 (1:1) was selected to culture the cells on scaffolds. In this study, we were inter-

ested in the effect of β -TCP scaffolds on hBMSC and HUVEC monoculture and co-culture. Therefore, we used non-osteogenic medium in all experiments to exclude the medium effect on osteogenic activity level of hBMSCs.

The morphological observations by the confocal and SEM in Figs. 2 and 3 clearly indicate that the cells, in either monoculture or co-culture, can attach and proliferate well on the highly interconnected porous scaffolds. Cytoskeletal organization of cells on the scaffolds in Fig. 4 was also clearly observed. Cytoskeletal proteins such as actin have been used to illustrate spreading and attachment of cells on substrates [43]. Our F-actin labeling results show that HUVECs and hBMSCs exhibit uniform and homogenous distribution of actin in cytoplasm. These results indicate that the cells can attach and spread on the scaffolds. Previous studies have reported that biomaterial coated with extracellular matrix proteins significantly enhances attachment of endothelial cells to biomaterials and in some cases protein coating is a prerequisite for attachment of endothelial cells [20,44,45]. In this study, β -TCP scaffolds without pre-coating also supported attachment and spreading of endothelial cells.

The ALP activity level produced by hBMSCs on β -TCP scaffolds was significantly higher than that on well plates (Fig. 6c). This result implies that β -TCP scaffolds significantly promote early differentiation of hBMSCs. This may be attributed to the release of calcium and phosphate ions from β -TCP scaffolds. Our results indicated that Ca and P concentrations increased with the incubation time (S.3a). It has been indicated from previous studies that extracellular Ca^{2+} and inorganic P released by CaP biomaterials favor osteoblast differentiation, proliferation and matrix mineralization through activating Ca-sensing receptors in osteoblast cells [46–48]. Surprisingly, HUVECs seeded on β -TCP scaffolds also expressed ALP activity, although it remained constant over 14 days of incubation (Fig. 6b). Furthermore, HUVECs on well plates also exhibited ALP activity at day 14 (Fig. 6d). The HUVECs used in this study is a GFP transfected, immortalized cell line. The reason that HUVECs have a detectable ALP activity may be related to the mixture medium employed in this study or due to the release of Ca and P ions, which can alter the pH to a weak alkaline environment (S.3b). Alternatively, the change of pH from 7.4 to 7.9 due to the release of Ca and P ions may have induced ALP activity (S.3b). Wang et al. have also reported ALP expression in HUVECs in vitro [49]. Although the reasons remain unknown, it is clear that β -TCP scaffolds stimulated higher ALP activity in HUVECs on β -TCP scaffolds compared to those on well plates. This suggests that culture on a 3-D porous β -TCP bioceramic may change the behavior of HUVECs. More mechanistic studies to investigate the effects of 3-D structures on the morphology and calcium chemistry of cells should be performed to address these questions.

Our results further indicated that early ALP activities of the 5:1 and 1:1 co-culture groups were significantly higher than that of hBMSCs in monoculture. This may be a result of the BMP-2 secreted by HUVECs [49]. In real-time PCR, *bmp-2* gene expression was significantly higher in HUVECs when compared to hBMSCs, which further implies the possibility of HUVECs releasing soluble BMP-2 into the co-culture medium [49].

Additionally, the total dsDNA content of co-cultured cells was not the same as that of cells in monoculture, as shown in the dsDNA results (Fig. 6a). The proliferation rate of co-cultured mixture cells did not exceed that in monocultured hBMSCs but significantly exceeds that in monocultured HUVECs. This result could be explained by the dynamic change of percentage of both cell types in co-culture, as the growth rate of hBMSCs and HUVECs is different. hBMSCs grown in monoculture showed a clearly higher cell growth rate as compared with HUVECs in monoculture at an early stage (Fig. 6a). These results collectively suggested the interactions between hBMSCs and HUVECs in co-culture changed the individual

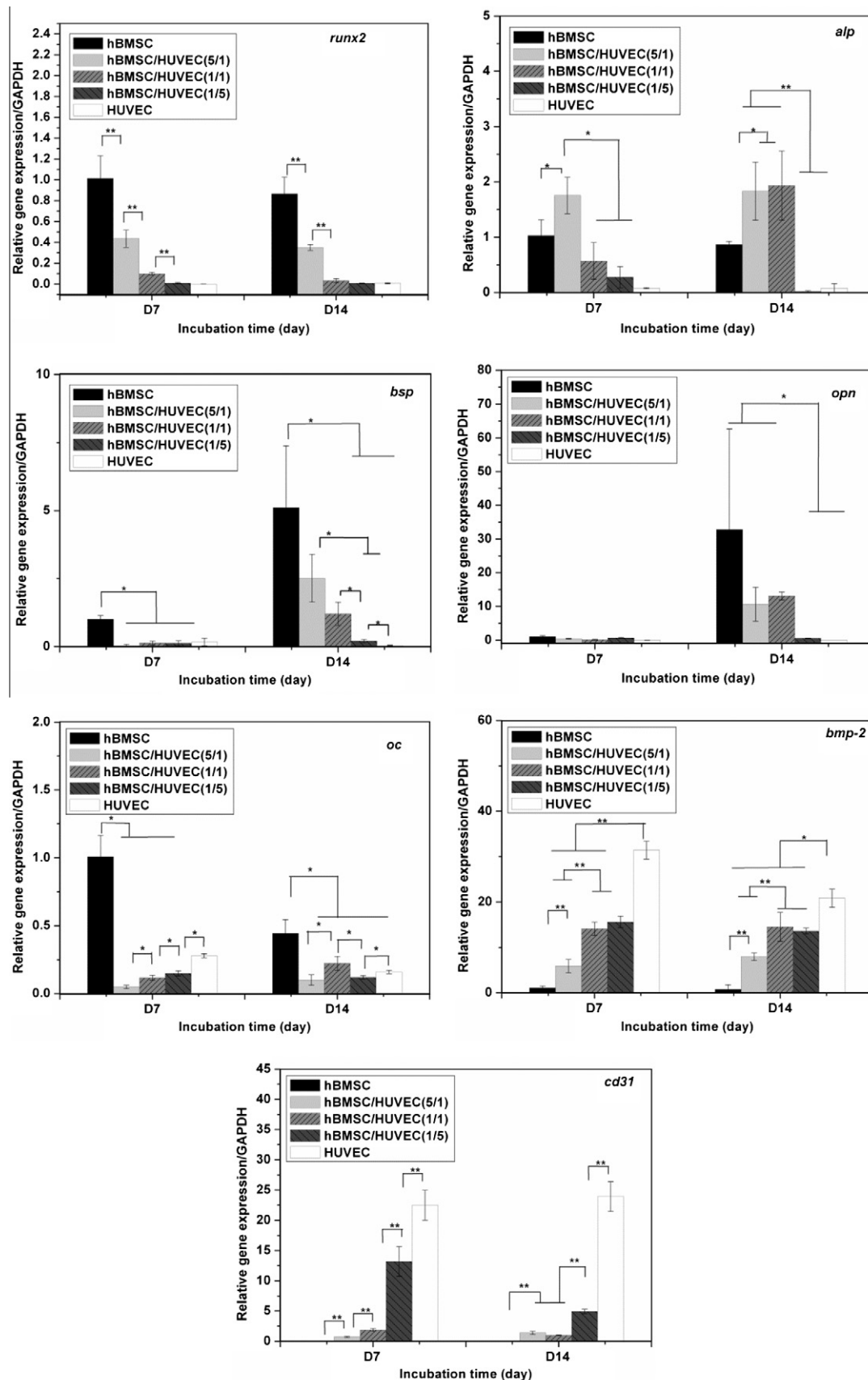


Fig. 7. Osteogenesis-related gene expression of hBMSCs on the β -TCP scaffolds in monoculture and co-culture after 7 and 14 days. One and two asterisks are used to show significant difference ($p < 0.05$ and 0.01 , respectively).

growth rate of HUVECs and hBMSCs. This result further implied that the HUVECs in co-culture may not stimulate hBMSCs proliferation; meanwhile, hBMSCs could suppress HUVEC expansion due to their high proliferative capacity in co-culture.

We further investigated the angiogenic potential of co-cultured cells in vitro on the β -TCP ceramic scaffolds. Cell adhesion molecule PECAM-1 expression at the cell–cell interface could be used to indicate the microcapillary-like structure or lumina. Cell adhesion molecule PECAM-1 expressed by HUVECs is known to be crucial for vessel formation and maintenance [50]. Our results show that in the HUVEC monoculture, a large amount of PECAM-1 expression can be clearly observed on the scaffolds shown in Fig. 5. Some elongated networks but no obvious lumina were observed during this experimental period. The ability of HUVECs to form lumina may depend on the properties of the extracellular matrix, which can affect the migration of HUVECs [51]. Co-culturing endothelial cells with bone-forming cells may facilitate the tube formation in vitro on scaffolds since the bone-forming cells can produce cytokines and angiogenic growth factors such as VEGF [52,53]. Also, the extracellular matrix produced by bone-forming cells may promote the formation of microcapillary-like structure when the cells co-cultured in direct contact [20,54]. Our data in co-culture did not show that hBMSCs promoted the tube formation of HUVECs on the scaffolds. Unlike the continuous PECAM-1 expression by the monocultured HUVECs at day 14 of incubation, a lower, scattered PECAM-1 expression can be observed in the groups of lower ratio of HUVECs (1:5 and 1:1). This is probably a result of decreased HUVEC population and the separation of HUVECs by hBMSCs. In the co-culture groups, hBMSCs and HUVECs were loaded simultaneously onto the porous scaffolds. A higher ratio of hBMSCs (5:1) in the mixed cell suspension could separate individual HUVECs, leading to the inability of HUVECs to contact and form a microcapillary-like structure.

The real-time PCR studies indicated that ALP gene expression levels in the co-culture group were significantly increased, but most of other genes were decreased. It is worth noting that we are unable to distinguish the contribution of individual cell type because gene expression in this study came from the total mRNA of two types of cells. As the expression level of hBMSCs is a part of the total expression level in the co-culture, therefore gene expression of all these osteogenic markers of hBMSCs specifically in co-culture could be higher [29]. Although further evaluation and new strategies will be needed to investigate the interactions between mesenchymal stem cells and endothelial cells on the biodegradable β -TCP, these present results implied that β -TCP scaffold with 3-D spatial features could be a useful platform to further investigate the interactions between the two cell types in 3-D structures for better understanding of bone regeneration, as this β -TCP ceramic scaffold can provide biocompatible and suitable surface properties for hBMSC and HUVEC development.

5. Conclusions

In the present study we examined the effect of an interconnected, macroporous, biodegradable β -TCP scaffold on cell behaviors of HUVECs and hBMSCs in both monoculture and co-culture. Our results demonstrate that β -TCP scaffolds supported the attachment and proliferation of HUVECs and hBMSCs in both monocultures and co-cultures. β -TCP scaffolds stimulated ALP activity of both hBMSCs and HUVECs. In co-cultures, HUVECs enhanced the very early osteogenic differentiation of hBMSCs. Meanwhile, the formation of an elongated network-like structure was observed in vitro on the β -TCP scaffolds. This β -TCP scaffold could provide a 3-D platform for studying interactions between multiple cells involved in bone regeneration. In particular, vascularization and

osteogenesis of biodegradable β -TCP scaffolds can be promoted by manipulating structural and biological cues.

Acknowledgements

This work was supported by grants from the following agencies: NIH R01AR057837 (NIAMS), NIH R01DE021468 (NIDCR), DOD W81XWH-10-1-0966 (PRORP), W81XWH-10-200-10 (Airlift Research Foundation), W81XWH-11-2-0168-P4 (Alliance of Nano Health), and Wallace H. Coulter Foundation.

Appendix A. Figures with essential colour discrimination

Certain figures in this article, particularly Figs. 2, 4, and 5, are difficult to interpret in black and white. The full colour images can be found in the on-line version, at <http://dx.doi.org/10.1016/j.actbio.2012.08.008>.

Appendix B. Supplementary data

Supplementary data associated with this article can be found, in the online version, at <http://dx.doi.org/10.1016/j.actbio.2012.08.008>.

References

- [1] Dietmar WH. Scaffolds in tissue engineering bone and cartilage. *Biomaterials* 2000;21:2529–43.
- [2] Kalita SJ, Bhardwaj A, Bhatt HA. Nanocrystalline calcium phosphate ceramics in biomedical engineering. *Mater Sci Eng C* 2007;27:441–9.
- [3] Descamps M, Duhoo T, Monchau F, Lu J, Hardouin P, Hornez JC, et al. Manufacture of macroporous [beta]-tricalcium phosphate bioceramics. *J Eur Ceram Soc* 2008;28:149–57.
- [4] Pittenger MF, Mackay AM, Beck SC, Jaiswal RK, Douglas R, Mosca JD, et al. Multilineage potential of adult human mesenchymal stem cells. *Science* 1999;284:143–7.
- [5] Chai YC, Roberts SJ, Desmet E, Kerckhofs G, van Gestel N, Geris L, et al. Mechanisms of ectopic bone formation by human osteoprogenitor cells on CaP biomaterial carriers. *Biomaterials* 2012;33:3127–42.
- [6] Kasten P, Vogel J, Luginbühl R, Niemeyer P, Tonak M, Lorenz H, et al. Ectopic bone formation associated with mesenchymal stem cells in a resorbable calcium deficient hydroxyapatite carrier. *Biomaterials* 2005;26:5879–89.
- [7] Krut MC, de Bruijn JD, Wilson CE, Oner FC, van Blitterswijk CA, Verbout AJ, et al. Viable osteogenic cells are obligatory for tissue-engineered ectopic bone formation in goats. *Tissue Eng* 2003;9:327–36.
- [8] Arinze TL, Tran T, McAlary J, Daculsi G. A comparative study of biphasic calcium phosphate ceramics for human mesenchymal stem-cell-induced bone formation. *Biomaterials* 2005;26:3631–8.
- [9] Dong J, Uemura T, Shirasaki Y, Tateishi T. Promotion of bone formation using highly pure porous β -TCP combined with bone marrow-derived osteoprogenitor cells. *Biomaterials* 2002;23:4493–502.
- [10] Grynias MD, Pilliar RM, Kandel RA, Renlund R, Filiaggi M, Dumitriu M. Porous calcium polyphosphate scaffolds for bone substitute applications in vivo studies. *Biomaterials* 2002;23:2063–70.
- [11] Jafarian M, Eslaminejad MB, Khojasteh A, Mashhadi Abbas F, Dehghan MM, Hassanizadeh R, et al. Marrow-derived mesenchymal stem cells-directed bone regeneration in the dog mandible: a comparison between biphasic calcium phosphate and natural bone mineral. *Oral Surg Oral Med O* 2008;105:e14–24.
- [12] Gerber HP, Vu TH, Ryan AM, Kowalski J, Werb Z, Ferrara N. VEGF couples hypertrophic cartilage remodeling, ossification and angiogenesis during endochondral bone formation. *Nat Med* 1999;5:623–8.
- [13] Grelhier M, Bordenave L, Amedee J. Cell-to-cell communication between osteogenic and endothelial lineages: implications for tissue engineering. *Trends Biotechnol* 2009;27:562–71.
- [14] McCarthy I. The physiology of bone blood flow: a review. *J Bone Joint Surg Am* 2006;88(Suppl. 3):4–9.
- [15] Rose FR, Cyster LA, Grant DM, Scotchford CA, Howdle SM, Shakesheff KM. In vitro assessment of cell penetration into porous hydroxyapatite scaffolds with a central aligned channel. *Biomaterials* 2004;25:5507–14.
- [16] Ishaug SL, Crane GM, Miller MJ, Yasko AW, Yaszemski MJ, Mikos AG. Bone formation by three-dimensional stromal osteoblast culture in biodegradable polymer scaffolds. *J Biomed Mater Res* 1997;36:17–28.
- [17] Rouwkema J, Rivron NC, van Blitterswijk CA. Vascularization in tissue engineering. *Trends Biotechnol* 2008;26:434–41.
- [18] Smith MK, Peters MC, Richardson TP, Garbarn JC, Mooney DJ. Locally enhanced angiogenesis promotes transplanted cell survival. *Tissue Eng* 2004;10:63–71.
- [19] Klenke FM, Liu Y, Yuan H, Hunziker EB, Siebenrock KA, Hofstetter W. Impact of pore size on the vascularization and osseointegration of ceramic bone substitutes in vivo. *J Biomed Mater Res A* 2008;85:777–86.

- [20] Unger RE, Sartoris A, Peters K, Motta A, Migliaresi C, Kunkel M, et al. Tissue-like self-assembly in cocultures of endothelial cells and osteoblasts and the formation of microcapillary-like structures on three-dimensional porous biomaterials. *Biomaterials* 2007;28:3965–76.
- [21] Yu H, VandeVord PJ, Mao L, Matthew HW, Wooley PH, Yang SY. Improved tissue-engineered bone regeneration by endothelial cell mediated vascularization. *Biomaterials* 2009;30:508–17.
- [22] Zhou J, Lin H, Fang T, Li X, Dai W, Uemura T, et al. The repair of large segmental bone defects in the rabbit with vascularized tissue engineered bone. *Biomaterials* 2010;31:1171–9.
- [23] Liu Y, Kim JH, Young D, Kim S, Nishimoto SK, Yang Y. Novel template-casting technique for fabricating beta-tricalcium phosphate scaffolds with high interconnectivity and mechanical strength and in vitro cell responses. *J Biomed Mater Res A* 2010;92:997–1006.
- [24] Kang Y, Kim S, Khademhosseini A, Yang Y. Creation of bony microenvironment with CaP and cell-derived ECM to enhance human bone-marrow MSC behavior and delivery of BMP-2. *Biomaterials* 2011;32:6119–30.
- [25] Kang Y, Scully A, Young DA, Kim S, Tsao H, Sen M, et al. Enhanced mechanical performance and biological evaluation of a PLGA coated beta-TCP composite scaffold for load-bearing applications. *Eur Polym J* 2011;47:1569–77.
- [26] Zhao J, Zhang N, Prestwich GD, Wen X. Recruitment of endogenous stem cells for tissue repair. *Macromol Biosci* 2008;8:836–42.
- [27] Yim EK, Wan AC, Le Visage C, Liao IC, Leong KW. Proliferation and differentiation of human mesenchymal stem cell encapsulated in polyelectrolyte complexation fibrous scaffold. *Biomaterials* 2006;27:6111–22.
- [28] Anderson JM, Vines JB, Patterson JL, Chen H, Javed A, Jun HW. Osteogenic differentiation of human mesenchymal stem cells synergistically enhanced by biomimetic peptide amphiphiles combined with conditioned medium. *Acta Biomater* 2011;7:675–82.
- [29] Hofmann A, Ritz U, Verrier S, Eglin D, Alini M, Fuchs S, et al. The effect of human osteoblasts on proliferation and neo-vessel formation of human umbilical vein endothelial cells in a long-term 3D co-culture on polyurethane scaffolds. *Biomaterials* 2008;29:4217–26.
- [30] Livak KJ, Schmittgen TD. Analysis of relative gene expression data using real-time quantitative PCR and the 2- $[\Delta\Delta CT]$ method. *Methods* 2001;25:402–8.
- [31] Pham QP, Kurtis Kasper F, Scott Baggett L, Raphae RM, Jansen JA, Mikos AG. The influence of an in vitro generated bone-like extracellular matrix on osteoblastic gene expression of marrow stromal cells. *Biomaterials* 2008;29:2729–39.
- [32] Sommer B, Bickel M, Hofstetter W, Wetterwald A. Expression of matrix proteins during the development of mineralized tissues. *Bone* 1996;19:371–80.
- [33] Arafat MT, Lam CXF, Ekaputra AK, Wong SY, Li X, Gibson I. Biomimetic composite coating on rapid prototyped scaffolds for bone tissue engineering. *Acta Biomater* 2011;7:809–20.
- [34] Kanczler JM, Oreffo RO. Osteogenesis and angiogenesis: the potential for engineering bone. *Eur Cell Mater* 2008;15:100–14.
- [35] Towler DA. The osteogenic-angiogenic interface: novel insights into the biology of bone formation and fracture repair. *Curr Osteoporos Rep* 2008;6:67–71.
- [36] Finkenzeller G, Arabatzis G, Geyer M, Wenger A, Bannasch H, Stark GB. Gene expression profiling reveals platelet-derived growth factor receptor alpha as a target of cell contact-dependent gene regulation in an endothelial cell-osteoblast co-culture model. *Tissue Eng* 2006;12:2889–903.
- [37] Choong CS, Hutmacher DW, Triffitt JT. Co-culture of bone marrow fibroblasts and endothelial cells on modified polycaprolactone substrates for enhanced potentials in bone tissue engineering. *Tissue Eng* 2006;12:2521–31.
- [38] Guillotin B, Bareille R, Bourget C, Bordenave L, Amedee J. Interaction between human umbilical vein endothelial cells and human osteoprogenitors triggers pleiotropic effect that may support osteoblastic function. *Bone* 2008;42:1080–91.
- [39] Scherberich A, Galli R, Jaquiere C, Farhadi J, Martin I. Three-dimensional perfusion culture of human adipose tissue-derived endothelial and osteoblastic progenitors generates osteogenic constructs with intrinsic vascularization capacity. *Stem Cells* 2007;25:1823–9.
- [40] Rouwkema J, de Boer J, Van Blitterswijk CA. Endothelial cells assemble into a 3-dimensional prevascular network in a bone tissue engineering construct. *Tissue Eng* 2006;12:2685–93.
- [41] Villars F, Guillotin B, Amedee T, Dutoya S, Bordenave L, Bareille R, et al. Effect of HUVEC on human osteoprogenitor cell differentiation needs heterotypic gap junction communication. *Am J Physiol Cell Physiol* 2002;282:C775–85.
- [42] Vater C, Kasten P, Stiehler M. Culture media for the differentiation of mesenchymal stromal cells. *Acta Biomater* 2011;7:463–77.
- [43] Moghe PV, Berthiaume F, Ezzell RM, Toner M, Tompkins RG, Yarmush ML. Culture matrix configuration and composition in the maintenance of hepatocyte polarity and function. *Biomaterials* 1996;17:373–85.
- [44] Unger RE, Huang Q, Peters K, Protzer D, Paul D, Kirkpatrick CJ. Growth of human cells on polyethersulfone (PES) hollow fiber membranes. *Biomaterials* 2005;26:1877–84.
- [45] Unger RE, Peters K, Wolf M, Motta A, Migliaresi C, Kirkpatrick CJ. Endothelialization of a non-woven silk fibroin net for use in tissue engineering: growth and gene regulation of human endothelial cells. *Biomaterials* 2004;25:5137–46.
- [46] Barradas AMC, Fernandes HAM, Groen N, Chai YC, Schrooten J, van de Peppel J, et al. A calcium-induced signaling cascade leading to osteogenic differentiation of human bone marrow-derived mesenchymal stromal cells. *Biomaterials* 2012;33:3205–15.
- [47] Valerio P, Pereira MM, Goes AM, Leite MF. Effects of extracellular calcium concentration on the glutamate release by bioactive glass (BG60S) preincubated osteoblasts. *Biomed Mater* 2009;4:045011.
- [48] Marie PJ. The calcium-sensing receptor in bone cells: a potential therapeutic target in osteoporosis. *Bone* 2010;46:571–6.
- [49] Wang J, Ye Y, Tian H, Yang S, Jin X, Tong W, et al. In vitro osteogenesis of human adipose-derived stem cells by coculture with human umbilical vein endothelial cells. *Biochem Biophys Res Commun* 2011;412:143–9.
- [50] Simon AM, McWhorter AR. Vascular abnormalities in mice lacking the endothelial gap junction proteins connexin37 and connexin40. *Dev Biol* 2002;251:206–20.
- [51] Soucy PA, Romer LH. Endothelial cell adhesion, signaling, and morphogenesis in fibroblast-derived matrix. *Matrix Biol* 2009;28:273–83.
- [52] Deckers MM, van Bezooijen RL, van der Horst G, Hoogendam J, van Der Bent C, Papapoulos SE, et al. Bone morphogenetic proteins stimulate angiogenesis through osteoblast-derived vascular endothelial growth factor A. *Endocrinology* 2002;143:1545–53.
- [53] Furumatsu T, Shen ZN, Kawai A, Nishida K, Manabe H, Ohashi T, et al. Vascular endothelial growth factor principally acts as the main angiogenic factor in the early stage of human osteoblastogenesis. *J Biochem* 2003;133:633–9.
- [54] Stahl A, Wenger A, Weber H, Stark GB, Augustin HG, Finkenzeller G. Bi-directional cell contact-dependent regulation of gene expression between endothelial cells and osteoblasts in a three-dimensional spheroidal coculture model. *Biochem Biophys Res Commun* 2004;322:684–92.

Vascularized Bone Tissue Engineering: Approaches for Potential Improvement

Lonnis H. Nguyen, Ph.D.,^{1,2,*} Nasim Annabi, Ph.D.,^{1,2,*} Mehdi Nikkhah, Ph.D.,^{1,2}
Hojae Bae, Ph.D.,^{1,2,†} Loïc Binan, Ph.D.,³ Sangwon Park, Ph.D.,⁴ Yuning Kang, Ph.D.,⁵
Yunzhi Yang, Ph.D.,⁵ and Ali Khademhosseini, Ph.D.^{1,2,6,7}

Significant advances have been made in bone tissue engineering (TE) in the past decade. However, classical bone TE strategies have been hampered mainly due to the lack of vascularization within the engineered bone constructs, resulting in poor implant survival and integration. In an effort toward clinical success of engineered constructs, new TE concepts have arisen to develop bone substitutes that potentially mimic native bone tissue structure and function. Large tissue replacements have failed in the past due to the slow penetration of the host vasculature, leading to necrosis at the central region of the engineered tissues. For this reason, multiple microscale strategies have been developed to induce and incorporate vascular networks within engineered bone constructs before implantation in order to achieve successful integration with the host tissue. Previous attempts to engineer vascularized bone tissue only focused on the effect of a single component among the three main components of TE (scaffold, cells, or signaling cues) and have only achieved limited success. However, with efforts to improve the engineered bone tissue substitutes, bone TE approaches have become more complex by combining multiple strategies simultaneously. The driving force behind combining various TE strategies is to produce bone replacements that more closely recapitulate human physiology. Here, we review and discuss the limitations of current bone TE approaches and possible strategies to improve vascularization in bone tissue substitutes.

Introduction

BONE TISSUE ENGINEERING (TE) has emerged with the aim of producing biological substitutes for bone tissue regeneration. The need for bone constructs stems from the limited availability of donor tissues, which can be categorized as autografts, allografts, and xenografts. However, each type of donor tissue comes with its own set of limitations. For example, many difficulties are associated with autografts, such as high cost, requirement of additional surgeries, donor-site morbidity, and limiting autographs for the treatment of small defects.¹ Allografts can be used for larger defects but are limited by the possible immune rejection, disease transmission, and lower incorporation rate

compared to autografts.¹ Xenografts are rarely used since they share the same drawbacks as allografts and their physiological structures and functions do not exactly match that of human tissue.² TE strategies have been applied as promising alternatives to address the problems associated with the current therapeutic techniques and to produce bone constructs that mimic the structure of natural bone.

In an attempt toward clinical success of engineered bone constructs, tissue engineers have focused on fabricating bone tissues with similar properties (e.g., mechanical strength and microstructure) and function to naturally occurring bone. Bone tissue is composed of an external layer, referred to as cortical or compact bone, and an internal layer, referred to as cancellous or spongy bone (Fig. 1). Cortical bone makes up to

¹Harvard-MIT Division of Health Sciences and Technology, Massachusetts Institute of Technology, Cambridge, Massachusetts.

²Department of Medicine, Center for Biomedical Engineering, Brigham and Women's Hospital, Harvard Medical School, Cambridge, Massachusetts.

³Ecole Polytechnique, Palaiseau, France.

⁴Department of Prosthodontics, Chonnam National University, Gwangju, South Korea.

⁵Department of Orthopedic Surgery, Stanford University, Stanford, California.

⁶World Premier International Advanced Institute for Materials Research (WPI-AIMR), Tohoku University, Sendai, Japan.

⁷Wyss Institute for Biologically Inspired Engineering, Harvard University, Boston, Massachusetts.

*These two authors contributed equally to this work.

†Current affiliation: Department of Maxillofacial Biomedical Engineering and Institute of Oral Biology, School of Dentistry, Kyung Hee University, South Korea.

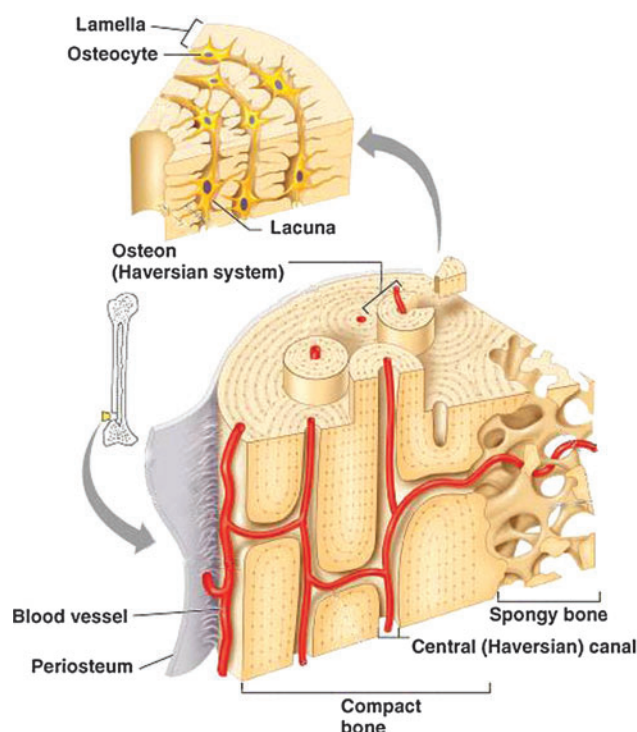


FIG. 1. Bone anatomy (Copyright © 2004 Pearson Education, Inc., publishing as Benjamin Cummings). Color images available online at www.liebertpub.com/teb

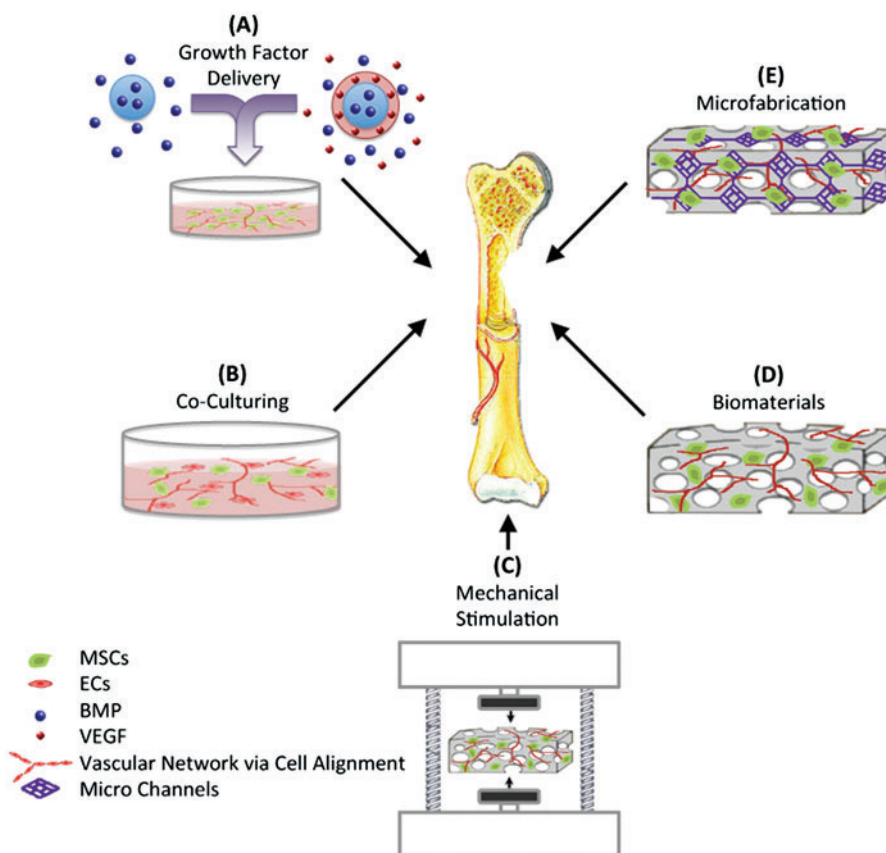
~80% of the total bone mass in adults.³ It is extremely dense, with low porosity (20%) and high mechanical strength (130–190 MPa).⁴ Cancellous bone accounts for the other 20% of the total bone mass and is highly porous (50%–90%), with ~10% of the mechanical strength of cortical bone.³ Osteons are functional units within the cortical bone structure and contain central Haversian canals, which house nerves and blood vessels.⁵ In contrast, cancellous bone does not contain osteon units, as its high porosity and surface area allows for better penetration of vasculature.⁶ Although cortical and cancellous layers are quite different in structure, they both contain a highly vascularized network. The presence of a vascular network is essential to supply nutrients and remove waste products. Therefore, it is required to incorporate a vascularized network into engineered bone substitutes in order to mimic the structure of natural bone tissue.

Despite their enormous potential for bone regeneration, current TE strategies are extremely limited by the lack of vascularization, leading to poor graft integration and failure of engineered substitutes in clinical trials. Here, we aim to discuss possible strategies to improve bone tissue regeneration by enhancement of vascularization in engineered constructs.

Strategies to Enhance Vascularization in Engineered Bone Constructs

Vascularization plays a crucial role in supplying cells with oxygen and nutrients and removing waste products from the engineered tissue constructs. The need for a vasculature is particularly important when engineering three-dimensional

FIG. 2. Various strategies to enhance vascularization in bone tissue engineering (TE). MSCs, mesenchymal stem cells; EC, endothelial cells; BMP, bone morphogenetic protein; VEGF, vascular endothelial growth factor. Color images available online at www.liebertpub.com/teb



(3D) thick tissues like the heart, liver, and kidney.⁷⁻⁹ The importance of vascularization has been also demonstrated for the engineering of other tissues, such as muscle, nerve, and bone.^{8,10,11} Various strategies have been attempted to enhance the establishment of vascular networks within engineered constructs for bone regeneration (Fig. 2). These include (A) directing cell behavior through growth factor delivery, (B) using coculturing systems, (C) applying mechanical stimulation, (D) using biomaterials with appropriate properties, and (E) incorporating microfabrication techniques.

Interactions between cells play an important role in directing their function and differentiation. *In vivo* cellular communication is mainly through a cascade of chemical cues, such as protein interactions and growth factor signaling. Growth factors are known to affect cellular proliferation, migration, and differentiation during bone repair.¹² For instance, bone morphogenetic protein-2 (BMP-2), transforming growth factor- β (TGF- β), fibroblast growth factor (FGF), platelet-derived growth factor (PDGF), insulin-like growth factor (IGF), endothelin-1, and vascular endothelial growth factor (VEGF) are involved in bone formation.¹³ BMP, PDGF, FGF, and VEGF have been shown to enhance migration of osteoprogenitor cells, while TGF- β , IGFs, and BMPs modulate their proliferation and differentiation.¹⁴ Additionally, VEGF and FGF are involved in initiating vascular growth during bone healing.¹³ The cross-talk between osteoblasts and endothelial cells (ECs) is conducted through the release of VEGF by osteoblasts, which act on ECs to promote angiogenesis,¹¹ and through the release of BMPs by ECs, which act on precursor bone cells to promote osteoblastic differentiation. In addition, FGF has been shown to stimulate proliferation and migration of ECs¹⁵ and also induce osteoblast differentiation.¹⁶ As for physical signals, cells can be stimulated either by cell-cell contact via coupling of gap junction proteins between different cell types or by externally applied stimulation such as mechanical or electrical signals. The coupling of osteocytes and ECs through gap junction proteins has been demonstrated to regulate gene expression and drive osteoblastic differentiation,¹⁷ indicating the importance of cell-cell physical contact in directing cell function.

Growth factor delivery

As mentioned in the previous section, cells respond to chemical and physical signals; thus, previous bone TE approaches have exploited this concept to control cellular behavior both *in vitro* and *in vivo*. A number of investigators have attempted to recapitulate this signaling process *in vitro* through the delivery of exogenous growth factors to direct cellular behavior. The classic approach is to deliver one growth factor by bolus injection, but this approach does not emulate the *in vivo* cascade of cellular signaling. This is because bolus injections fail to locally and efficiently deliver specific growth factors for proper modulation of cellular function. Current efforts of bolus growth factor injection at the site of injury have been limited by the rapid diffusion of the growth factors and the lack of temporal control, resulting in nonlocalized and transient cellular responses. Tomanek *et al.* evaluated the effects of bolus injection of both VEGF and bFGF on vasculogenesis. It was found that the injection of VEGF induced inappropriate neovascularization in avascular areas.¹⁸ The use of bFGF enhanced vasculogenesis, but the

vasculature was transient and disappeared at later stages.¹⁸ As an alternative method to achieve sustained release of growth factors and in turn improve on bone TE strategies, investigators explored the effects of growth factor encapsulation within degradable microparticles. Solorio *et al.* encapsulated BMP-2 within crosslinked gelatin microparticles to induce bone formation from human mesenchymal stem cells (hMSCs) through the sustained release of BMP-2.¹⁹ It was found that the release of BMP-2 from gelatin microparticles resulted in an increase of bone sialoprotein (BSP) gene expression of hMSCs.¹⁹ In another study, Formiga *et al.* demonstrated that the sustained release of VEGF from poly (lactic-co-glycolic acid) (PLGA) microparticles resulted in *in vivo* revascularization with stable vessels.²⁰ However, vasculature was not formed through the bolus injection of free VEGF, which was due to the short half-life of the protein *in vivo*.

Furthermore, the delivery of a single growth factor often fails because its isolated action does not emulate the complex process of bone regeneration *in vivo*, which involves the interaction of a large number of growth factors and cytokines.²¹ For this reason, a number of investigators have explored the effects of the combined delivery of multiple growth factors. BMPs are well established as potent osteoinductive growth factors and their delivery in combination with other growth factors has been shown to enhance bone formation *in vivo*.²¹ A study by Duneas *et al.* demonstrated that the combination of TGF- β and BMP-7 produced a synergistic effect to enhance bone formation *in vivo*.²² This synergy was also observed by Simmons *et al.* after they implanted RGD-modified alginate hydrogels containing both TGF- β 3 and BMP-2 with bone marrow stromal cells (BMSCs) in mice.²³ After 6 weeks of implantation, the combined delivery of both TGF- β 3 and BMP-2 showed significant bone formation by transplanted BMSCs. In contrast, individual delivery of TGF- β 3 or BMP-2 resulted in negligible bone formation even after 22 weeks. Interestingly, the enhancement of bone regeneration by the combined delivery of FGF and BMP is dependent on both time and dose. Kubota *et al.* combined the locally delivered BMP-2 with subcutaneous injections of FGF-4 and found that FGF increased bone formation when administered early (days 2-4), but had no effect when injected at later time points (days 6-11), demonstrating that the effect of FGF on BMP-induced bone formation is time dependent.²⁴ The dose-dependent effect of FGF when combined with BMP was observed by Nakamura *et al.* when they implanted type I collagen disks into mice that contained a constant amount of BMP-2 (5 μ g) and varying amounts of FGF-2.²⁵

The effect of simultaneous and sequential delivery on bone formation has been also investigated.²⁶⁻³¹ In one study, Raiche *et al.* found that the temporal delivery of BMP-1 and IGF-I can significantly affect alkaline phosphatase (ALP) activity during *in vitro* culture.²⁶ In this study, layered gelatin coatings were used to develop a sequential delivery system; one layer was crosslinked to encapsulate BMP-2, while the other layer contained IGF-I. The highest ALP activity was observed with the early release of BMP-2 followed by the subsequent release of IGF-I, while the simultaneous release of BMP-2 and IGF-I from both layers had no effect on the ALP activity. Other studies have also shown the effect of sequential release of BMP-2 and BMP-7 from nanocapsules of PLGA and poly(3-hydroxybutyrate-co-3-hydroxyvalerate), and PLGA scaffolds loaded with poly(4-vinyl pyridine)/alginate acid polyelectrolyte microspheres.^{28,29} It was found that

the early release of BMP-2 followed by BMP-7 suppressed rat MSC proliferation and increased osteogenic differentiation.^{28,29} These results indicate that correct growth factor combinations and delivery strategies (simultaneous and sequential delivery, single or multiple growth factor) greatly affect osteogenic differentiation and should be considered when designing delivery systems.

The studies discussed above demonstrate that the delivery of multiple growth factors can enhance bone formation. However, since blood vessel formation is tightly coupled with bone regeneration, the ideal scenario would be to deliver a cascade of multiple growth factors to simultaneously induce angiogenesis and osteogenesis in order to produce a vascularized bone tissue substitute. VEGF plays a critical role in angiogenesis during bone formation; therefore, its combined delivery, along with other growth factors, may enhance vascularization in bone tissue constructs. In one study, Richardson *et al.* found that sustained dual delivery of both VEGF and PDGF resulted in highly dense and well-established vessels compared to the bolus delivery of either of the growth factors alone.³² Patel *et al.* also demonstrated that dual delivery of VEGF and BMP-2 encapsulated in gelatin microparticles resulted in a synergistic effect, promoting both osteogenic response and blood vessel formation in an 8-mm rat cranial defect.³³ In another study, Shah *et al.* created a dual delivery system using polyelectrolyte multilayer films (PEM) fabricated through layer-by-layer assembly.³⁴ Various ratios of BMP-2 and VEGF were entrapped within the different PEM layers. It was found that VEGF was released from the PEM layers over the first 8 days, while the release of BMP-2 was sustained for 2 weeks. After implantation, the mineral density within *de novo* bone was increased by 33% in a PEM scaffold containing both BMP-2 and VEGF compared to those containing BMP-2 only. Mikos and coworkers also investigated the effects of individual and dual delivery of BMP-2 and VEGF on bone formation using a rat cranial critical-size defect.³⁵ Four weeks after implantation, dual delivery of BMP-2 and VEGF resulted in a higher percentage of bone fill compared to the delivery of BMP-2 alone. However, no significant difference was observed after 12 weeks.³⁵ These results suggest that the delivery of multiple growth factors is a possible strategy to enhance the formation of vascularized bone tissue substitutes. However, the types of growth factors to be combined, the dosage used, and the delivery method, all need to be carefully controlled in order to improve bone tissue formation, since slight alterations to any of these components can actually result in inhibition of bone regeneration. Furthermore, the limited number of studies on the combinatory delivery of multiple growth factors suggests the need of additional studies to evaluate all possible combinations and optimize concentrations, ratios, other timing, and delivery sequence.

Coculturing systems

It is well known that there is an intricate connection between osteogenesis and angiogenesis during *in vivo* bone formation. In fact, angiogenesis is a prerequisite for osteogenesis.³⁶ Therefore, the cellular interaction between osteoblasts and ECs is essential in bone formation. Wang *et al.* illustrated the important relationship between osteoblasts and ECs by coculturing human osteoblast-like cells (HOBs) with human umbilical vein endothelial cells (HUVECs).³⁷ The co-

culture of HOBs with HUVECs resulted in an increase in both ALP activity and cell numbers. They also demonstrated that the release of VEGF by HOBs can be enhanced with 1,25-dihydroxyvitamin D3 induction, but this enhancement was only observed in cocultures of HOBs with HUVECs and not in HOBs cultured alone. The expression of VEGF receptors on ECs was also enhanced during coculture with HOBs, which resulted in stimulation of ALP activity. The release of VEGF by HOBs did not directly stimulate ALP activity, but in the presence of HUVECs, ALP stimulation was observed. The results of this study confirmed the importance of the communication between osteoblasts and ECs during osteogenesis.

As this review aims to discuss possible strategies for vascular enhancement within engineered bone tissue replacements, the coculture of ECs and osteoblasts is presented as a promising alternative, due to the important relationship between these cells during bone formation, remodeling, and repair.³⁸ Recent findings have shown that the *in vivo* vascular networks produced by a single-cell population are immature and less stable compared to networks formed from coculturing systems.³⁹ The importance of a coculturing system in bone TE stems from the need to promote osteogenesis and vascularization simultaneously in order to create vascularized engineered bone tissue constructs. Yu *et al.* demonstrated the feasibility of coculturing bone marrow-derived ECs and osteoblasts in a polycaprolactone (PCL)/hydroxyapatite scaffold to promote vascularization and osteogenesis processes.⁴⁰ It was found that the presence of both cell types within the scaffolds resulted in the formation of vessel-like structures.⁴⁰ In another study, Zhou *et al.* induced MSCs to differentiate into ECs, and then cocultured MSCs and MSC-derived ECs within a porous β -tricalcium phosphate (β -TCP) ceramic biomaterial to investigate the effects of MSC-derived ECs on the proliferation and osteogenesis of MSCs. Coculturing the cells resulted in vascularized bone formation, since ECs promoted MSCs osteogenesis and accelerated local vascularization. Additionally, *de novo* bone exhibited natural mechanical properties and vascularization after 16 weeks, with stable degradation of the implanted material and repair of bone defects within the rabbit model.⁴¹ Villars *et al.* also demonstrated that coculturing of MSCs and ECs enhanced osteoblast proliferation and vascularization of engineered bone.¹⁷ It was found that VEGF was not responsible for this improvement; the physical intercommunication involving cell membrane proteins between MSCs and ECs was the driving force of the superior cellular responses.¹⁷ Kaigler *et al.* obtained similar results when they performed a comparative study that evaluated BMSCs cultured in ECs-conditioned medium, on ECs extracellular matrix (ECM), and cocultured with and without EC contact.⁴² A significant increase in osteogenic differentiation of BMSCs was observed *in vitro* only when cultured in direct contact with ECs. Additionally, greater *in vivo* bone formation was detected when ECs were co-transplanted with BMSCs than when BMSCs were transplanted alone. These findings suggest that the use of coculturing systems can potentially aid in improving bone regeneration and enhancing preformed vascular networks for bone TE purposes.

Mechanical stimulation

Mechanical force is a form of physical signaling that can affect cell functions within the body, including migration,

proliferation, enzyme secretion, and matrix orientation.^{43,44} In bone TE, it has been well established that applying external mechanical stimuli can enhance bone tissue formation.^{45,46} It has been shown that the use of bioreactors provides mechanical stimulation for cells to accelerate bone formation. They also induce fluid flow throughout the scaffold, allowing sufficient nutrient and waste exchange to increase cell viability and homogeneous distribution of cells within the biomaterial.^{47–49} Various types of bioreactors such as spinner flask, rotating wall vessel reactor, and flow perfusion have been used to apply mechanical stimulation and fluid flow to bone tissue constructs and compare their effects with static culture conditions.^{48,49} In one study, the effect of static and bioreactor cultures on PCL/TCP scaffolds seeded with human fetal MSC was investigated.⁴⁸ Compared to static culture, the use of a biaxial rotating bioreactor significantly increased proliferation and osteogenic differentiation both *in vitro* and *in vivo*, demonstrating its potential for bone TE applications.⁴⁸ In another study, a perfusion flow bioreactor was used to induce media perfusion and mechanical stimulations in a 3D culture condition for human bone mesenchymal stromal cells (hBMSC) encapsulated in a polyurethane scaffold.⁴⁷ *In vitro* studies indicated that the proliferation and differentiation of hBMSC were promoted when perfusion (10 mL/min) and on-off cyclic compressions mechanical stimulation (10% strain) were applied over 2 weeks' culture.⁴⁷ These results demonstrate that perfusion and mechanical stimulation, induced by using bioreactor, are promising approaches to enhance bone formation. Mauney *et al.* also demonstrated that the application of cyclic mechanical stimulation promoted osteogenic differentiation of MSCs within demineralized bone scaffolds.⁵⁰ Their developed bioreactor system closely mimicked the *in vivo* mechanical signals that stimulate osteoprogenitor cells to differentiate into osteoblasts within the cortical bone surface. Ignatius *et al.* also demonstrated that cyclic uniaxial mechanical strain increased multiple gene expressions that were involved in cell proliferation, matrix production, and osteoblastic differentiation.⁵¹ Kaneuji *et al.* demonstrated that static compressive force enhanced the expression of osteoprotegerin, a known inhibitor of osteoclast differentiation, which resulted in the promotion of bone growth.⁴⁶ It was found that both osteoblasts and osteocytes respond to mechanical stress by regulating osteoclastogenesis.⁴⁶ In another study, Forwood *et al.* showed that dynamic load with a magnitude of 65 N increased bone formation rate and produced the highest osteogenic response.⁵² However, they found that applying dynamic load did not affect the rate of bone formation until after 5 days of culture.⁵² Van Eijk *et al.* verified the application of the load during the first 5 days of culture had a negative effect on cell proliferation and differentiation, while after day 5, the mechanical stimulation induced alignment, proliferation, and differentiation of bone marrow cells.⁵³ These findings suggested that the temporal regulation of the applied load plays a crucial role in regulating cell responses.

The use of mechanical stimulation to modulate MSC differentiation and osteocyte behavior has been well explored. However, to improve upon this strategy it may be crucial to understand how mechanical stimulation would affect ECs and their ability to form blood vessels *in vitro*. It has been shown that the initiation and progression of angiogenesis

processes, as well as ECs function, are affected by hemodynamic forces, which are exerted by blood flow (cyclic strain and shear stress).^{54,55} For example, Von Offenbergs Sweeney *et al.* showed an increase in bovine aortic endothelial cell (BAEC) migration and tube formation as a function of applied strain,⁵⁴ while Li *et al.* found that BAEC proliferation was critically regulated by cyclic strain.⁵⁵ Additionally, Iba *et al.* demonstrated that cyclic strain influenced *in vitro* ECs alignment and elongation by a mechanism dependent on the organization and network of actin filaments.⁵⁶ Furthermore, Azuma *et al.* conducted a study to evaluate how BAECs respond to cyclic strain versus shear stress. They found a more robust and rapid activation of mechanoreceptors in response to shear stress than to cyclic strain, indicating that the type of mechanical force determines which mitogen-activated protein kinases are activated.⁵⁷ These studies provide evidence that mechanical stimuli not only affect osteogenesis but can also be utilized to initiate and regulate the process of angiogenesis and consequently lead to the formation of blood vessels.

Evidence from previous works shows that applying mechanical signals can help regulate one biological process, but like for any other *in vivo* phenomena, isolated responses do not occur. Few investigators have begun to study how mechanical stimulation would affect both osteogenesis and angiogenesis concurrently. Cheung *et al.* evaluated the relationship between fluid flow and osteocyte apoptosis and found that osteocytes, exposed to fluid flow, were protected from apoptosis.⁵⁸ Osteocyte apoptosis mainly occurred as a result of reduced interstitial fluid flow and preceded osteoclast recruitment and activity.⁵⁹ As a result, the colocalization of osteocyte apoptosis and the recruitment of osteoclasts at the remodeling site promoted angiogenesis, since the apoptosis of the osteocytes increased the release of VEGF. Cheung *et al.* also demonstrated that apoptotic osteocytes promoted EC proliferation, migration, and tubule network formation.⁵⁸ This study suggested that by regulating fluid flow, it is possible to modulate osteocyte apoptosis and promote vascularization in a VEGF-mediated manner. In another study, Li *et al.* developed a mechanical stimulator to apply periodic compressive load and evaluate VEGF delivery from alginate microparticles.⁶⁰ It was found that periodic compression accelerated VEGF release from alginate microspheres compared to noncompressed samples. Moreover, the applied load enhanced the expression of matrix metalloproteinase (MMP)-2 and -9 in HUVECs that were cultured on a demineralized bone scaffold containing VEGF alginate microspheres. The increased expression of MMPs suggested that enhanced release of VEGF under applied compressive load is crucial in HUVEC activation and angiogenesis promotion. The results of these studies illustrate the efforts toward combining TE strategies to further improve engineered constructs and to develop more complex tissue substitutes.

Utilization of suitable biomaterials

Another classical bone TE approach is to select a suitable biomaterial scaffold that provides structural support for 3D bone tissue formation.⁶¹ The properties of scaffolds can be tailored in order to induce and direct cellular attachment, proliferation, migration, and differentiation,⁶² making them prominent tools in the bone TE field. Table 1 summarizes

TABLE 1. EXAMPLES OF BIOMATERIALS USED FOR THE REGENERATION OF VASCULARIZED BONE TISSUE

Biomaterial	Pore size (μm)	Porosity (%)	Application	Refs.
PLG	250–425	—	VEGF delivery and regeneration of vascularized bone tissue	189
PLG	—	—	Sustained dual delivery of VEGF and PDGF resulted in highly dense and mature vessels	32
Starch/PCL	250	77	Human osteoblast-like cells <i>in vitro</i>	190
PLGA	25–400	95	MSC and VEC <i>in vitro</i> coculture, followed implantation in bilateral thigh defects in rat.	191
	—	—	Single hESC culture enhanced osteogenesis	192
	—	—	hESC and BMP achieved bone formation	193
	—	—	Sustained release of VEGF resulting in revascularization with stable vessels	20
Gelatin	—	—	Sustained release of BMP-2 increased BSP expression of hMSCs	19
	—	—	Dual delivery of VEGF and BMP-2 stimulated blood vessel formation and augmented osteogenic response	33
Alginate	—	—	Compressive load accelerated VEGF delivery and promoted MMP expression in HUVECs	60
Chitosan/polyester	—	—	Osteogenic differentiation of hMSCs	194
Hydroxyapatite	90–600	—	Ectopic bone formation in rat	131,195
	300–700	72–74	Vascular formation after implantation in Fascia lumbodorsalis defect in rabbit	136
PCL/hydroxyapatite	—	80	MSC and ECs <i>in vitro</i> coculture followed implantation in femur defects in mice.	196
	355–600	83	Coculture of ECs and osteoblasts promoted vascularization and osteogenesis and resulted in stable vessel-like structures	40
β -TCP	—	—	Coculture of MSC-derived ECs and MSCs induced vascularized bone formation <i>in vivo</i>	41
PLGA/ β -TCP	125–150	80–88	Rabbit calvarial defect	123
Polymeric foams containing hydroxyapatite	40–100	70–97	Rat osteoblast <i>in vitro</i>	130
Polyurethane	300–2000	85	Regeneration of bicortical defects in the iliac crest of estrogen-deficient sheep	77

PDGF, platelet-derived growth factor; BMP, bone morphogenetic protein; VEGF, vascular endothelial growth factor; ECs, endothelial cells; hMSC, human mesenchymal stem cells; BSP, bone sialoprotein; PLGA, poly (lactic-co-glycolic acid); HUVECs, human umbilical vein endothelial cells; β -TCP, β -tricalcium phosphate; PCL, polycaprolactone; MMP, matrix metalloproteinase; PLG, poly (L-lactide-co-glycolide); hESC, human embryonic stem cell.

examples of various biomaterials and their vascularization potential for bone tissue constructs.

Even though the use of biomaterial scaffolds in bone TE has shown success for bone regeneration, there are still some limitations. For example, lack of *de novo* tissue growth in 3D scaffolds remains a major limitation in clinical applications of engineered scaffolds for bone repair. The limited, peripheral bone tissue formation is mainly due to insufficient nutrient and oxygen delivery and metabolic waste removal within the 3D structure of the scaffolds.^{63,64} This is more profound under static culture conditions, where the high cell density on the outer surfaces of the scaffolds may result in diminished nutrient supply to the cells located inside the scaffolds. Consequently, the cells at the center of the constructs would be subjected to nutrient deprivation and ultimately necrosis, which hinders the success of engineered constructs for bone regeneration.^{11,40} In the absence of an intrinsic capillary network, the engineered tissues can only have a maximum thickness of 150–200 μm ; dimensions larger than this threshold may result in lack of oxygen inside the biomaterials.⁶⁵

In bone TE, biomaterial scaffolds serve as templates for bone-forming cell growth as well as the establishment of a

vascular system. Vasculature is formed through adhesion, migration, and functionality of ECs seeded within the scaffold. In fact, simultaneous *in vitro* culture of ECs and osteoblasts in a suitable scaffold can aid in the establishment of microcapillary-like networks within the constructs. The scaffold type and its properties play an important role in bone tissue formation as well as vascular network creation. The ability to fabricate scaffolds with the appropriate properties can help facilitate the formation of vasculature within the engineered bone constructs.

Biomaterial selection. Biomaterial selection is a critical factor in bone TE as the properties of scaffold mainly depend on the nature of the biomaterial. A variety of materials has been used in bone TE, including metals, ceramics, synthetic and natural polymers, and composites. The utilization of each individual material has been well explored by many investigators; however, the ability to identify the best biomaterial for bone TE applications is a difficult task, since each material has inherent drawbacks. Metals such as titanium, stainless steel, and cobalt-chromium can be used as biocompatible, strong, and inexpensive materials for bone repair. However, metals are not biodegradable and have

higher moduli than that of natural bone, which induces stress shielding.^{66,67} Ceramics and biodegradable polymers have been investigated as alternative scaffolds for bone TE applications. Bioceramics such as hydroxyapatite and β -TCP have been widely used for bone repair due to their excellent bioactivity, which is attributed to their structural and compositional similarity with the mineral phase of bone.⁶⁸ The bioactivity of ceramics facilitates the attachment of osteoprogenitor cells seeded on the surface and production of bone ECM.⁶⁹ In spite of numerous advantages, the brittleness and low mechanical properties of ceramics may result in their fracture upon applying load, making them unsuitable for the regeneration of large bone defect.^{70–72} In addition, the low degradation rate of bioceramics (e.g., hydroxyapatite) hinders the substitution of the scaffold with newly formed tissue after implantation. Although the fabrication of hydroxyapatite/ β -TCP composite scaffolds (known as biphasic calcium phosphate [BCP]) increases the degradation rate, the BCP scaffolds still remain in the body for several months, which is longer than the required time for bone healing (a few weeks).⁶⁹

Biodegradable polymers are ideal materials to use as alternatives to metals and ceramics for the development of bone TE scaffolds.⁷³ Their wide use for bone repair is due to their remarkable properties, including biocompatibility, tunable degradation, processability, and versatility.⁶⁹ Polymers are divided in two groups of natural and synthetic. Among synthetic polymers, poly (α -hydroxy) esters, such as poly (lactic acid),⁷⁴ poly (glycolic acid),⁷⁵ PLGA,⁷⁶ and polyurethanes,^{77,78} have been widely utilized for bone regeneration. Other synthetic polymers that are of interest for bone repair are poly (propylene fumarate) (PPF),^{79–82} polyanhydride,^{83,84} and poly (ethylene oxide)/poly (butylene terephthalate) copolymers.^{85,86} Synthetic biodegradable polymers have higher mechanical properties than natural polymers and can be easily processed. It is also possible to fabricate synthetic-based polymeric scaffolds with tunable properties, such mechanical stiffness and pore characteristics, to create an optimal environment for cell proliferation, vascularization, and new bone formation. However, the intrinsic hydrophobicity and lack of cell-recognition sites within the structures of some synthetic polymers obstruct cellular penetration, adhesion, and growth within the scaffold. Natural polymers can interact with cells to regulate or direct their function. However, they have lower mechanical properties compared to synthetic polymers. Common biopolymers used for bone regeneration include collagen,⁸⁷ silk fibroin,⁸⁸ chitosan,^{30,89} starch,^{90,91} hyaluronic acid,⁹² and polyhydroxyalkanoates.^{93,94}

Hydrogels are polymeric networks that have the ability to absorb and retain a large volume of water (80%–99%).⁹⁵ Hydrogels can be made from natural biodegradable polymers such collagen, chitosan, and gelatin, or synthetic polymers such as polyethylene glycol (PEG) and polyvinyl alcohol.^{96,97} Their remarkable properties, including similarities with the ECM, proper biological performance, hydrophilicity, high permeability to oxygen and nutrients, and inherent cellular interaction capabilities, make them leading candidates for engineered tissue scaffolds.⁹⁵ However, they are mechanically weak and unable to support significant loads experienced by bone tissue *in vivo*. Various methods have been applied to enhance the mechanical properties of

hydrogels, such as crosslinking (chemical, physical, or UV)^{98,99} or blending with other polymers.^{100–102}

Limitations of individual materials have led investigators toward exploring ways to improve biomaterial characteristics, such as combining natural polymers with synthetic polymers to create a balance between biological signals and mechanical properties.^{103–106} For instance, Annabi *et al.* developed a two-stage solvent-free dense gas technique to produce porous 3D structures of natural/synthetic polymeric composites.¹⁰⁷ In the first stage, a gas-foaming/salt-leaching process was used to create large pores with an average pore size of $540 \pm 21 \mu\text{m}$ in a PCL matrix. The pores of PCL scaffolds were then filled with crosslinked elastin under high pressure CO_2 to form an elastin structure (average pore size $\sim 50 \mu\text{m}$) within the macroporous PCL scaffolds. The addition of elastin within the pores of PCL scaffolds improved the cellular attachment and proliferation within the constructs. The use of PCL also increased the compressive modulus, from 0.001 MPa for the pure elastin hydrogel, to 1.3 MPa.¹⁰⁷ A study conducted by Nguyen *et al.* demonstrated that the mechanical strength of natural polymers, such as chondroitin sulfate (82.4 kPa) and hyaluronic acid (31.5 kPa), could be improved to 118 and 331 kPa, respectively, by incorporating PEG, a synthetic polymer.¹⁰⁴ Additionally, polymers have been combined with ceramics to overcome the drawbacks of each individual material and provide composites that are suitable for osteogenic applications. For example, it was reported that the compressive modulus of a hydroxyapatite scaffold increased from 0.2 to 0.5 MPa when it was coated with PCL to create a hydroxyapatite/PCL composite.¹⁰⁸ Another study by Kang *et al.* also reported that infiltration of PLGA significantly increased the compressive strength of β -TCP scaffolds from 2.9 to 4.2 MPa, and toughness from 0.2 to 1.4 MPa, while retaining an interconnected and highly porous structure.¹⁰⁹ In addition, Lickorish *et al.* found that coating a collagen scaffold with hydroxyapatite could improve the attachment and proliferation of rabbit periosteal cells due to the formation of a bioactive apatite layer on the surface of the scaffold.¹¹⁰ The combination of natural and synthetic polymers with ceramics has been also used in bone TE. Chen *et al.* developed a process to fabricate PLGA/collagen/apatite scaffolds with a porosity of 91% and pore sizes between 355 and 422 μm for bone regeneration. In this technique, a porous structure of PLGA was first fabricated by using a salt-leaching process. Collagen microsponges were then formed in the pores of PLGA scaffold, followed by apatite particulate deposition on the surface of the microsponges. The use of PLGA improved the mechanical integrity of the scaffold and incorporation of collagen resulted in the uniform deposition of apatite particles throughout the scaffold, which enhanced bone formation.¹¹¹

Scaffold properties. In bone TE, scaffolds serve as temporary structural supports for cell interactions and formation of bone ECM. Additionally, bone TE scaffolds have been used to deliver growth factors encapsulated within their structures,¹¹² and in some cases they have facilitated vascularization of neo-tissue.^{113,114} In general, more successful biomaterial scaffolds for bone TE are biodegradable, biocompatible, porous, and possess sufficient mechanical strength for load-bearing applications. The scaffold characteristics, including porosity, average pore size, and

mechanical stiffness, have been shown to influence cell survival, signaling, growth, gene expression, and phenotype.^{115–118} Many investigators have attempted to manipulate these properties to fabricate constructs, which mimic bone morphology, structure, and function.⁶⁹

The pore architecture of scaffold in terms of porosity, average pore size, and pore interconnectivity is crucial for cell survival, proliferation, and formation of 3D bone tissue *in vitro* and *in vivo*.¹¹⁹ The porosity of a scaffold can affect osteoblast proliferation and the extent of osteogenesis during bone regeneration¹²⁰; thus, manipulating the porosity of the scaffold can improve scaffold function. Kuboki *et al.* reported that osteogenesis occurred when using a porous hydroxyapatite scaffold as a BMP-2 carrier in a rat ectopic model. However, no bone formation was observed when nonporous solid hydroxyapatite particles were used as the BMP-2 carriers.¹²¹ In addition, scaffolds with highly porous surfaces enhance mechanical interconnection between the implanted biomaterial and surrounding bone tissue, resulting in higher mechanical stability at the implant/bone tissue interface.¹²² Higher porosity and larger pore sizes have been also shown to allow for *in vivo* bone ingrowth and vascularization. Roy *et al.* found that in a PLGA/ β -TCP composite scaffold with a porosity gradient from 80% to 88%, bone tissue formation was enhanced in the region with higher porosity after implantation in rabbit craniums.¹²³ Krut *et al.* also demonstrated higher proliferation of goat bone marrow stromal cells in hydroxyapatite scaffolds with 70% porosity and an average pore size of 800 μ m compared to those with 60% porosity and an average pore size of 700 μ m during a 6-day *ex vivo* culture.¹²⁴ However, *in vitro* osteogenesis has been shown to increase with lower porosity. Takahashi *et al.* fabricated nonwoven fabrics from polyethylene terephthalate (PET) with porosities ranging from 93% to 97%.¹²⁵ They reported that higher porosity (97%) allowed for sufficient oxygen and nutrient delivery within the scaffold, which resulted in an increase in the proliferation rate of rat MSCs. In contrast, MSCs cultured on PET scaffolds with lower porosity (93%) exhibited higher osteogenic differentiation.¹²⁵ These results demonstrated that scaffold porosity could be manipulated for better control and modulation of cellular behavior and function within the scaffold.

In addition to porosity, the average pore size of the scaffold greatly affects bone formation and the creation of a vascular network, and can also be manipulated to produce the desired outcomes. Pores are necessary for bone tissue formation as they allow for cell migration and ingrowth, and nutrient diffusion for cell survival. In general, scaffolds with pore sizes larger than 50 μ m can allow for both delivery of nutrients and oxygen and removal of metabolic waste, but can also result in lower cellular attachment and intracellular signaling, while scaffolds containing pore sizes smaller than 10 μ m have the opposite effects.¹²⁶ Therefore, the fabrication of scaffolds containing both macropores and micropores can be beneficial for bone formation and vasculature creation.¹²⁷ The initial study by Hulbert *et al.* demonstrated that optimum pore sizes should be larger than 100 μ m for regeneration of vascularized bone tissue.¹²⁸ In this study, calcium aluminate cylindrical pellets with 46% porosity and various pore sizes in the range of 10–200 μ m were implanted in dog femorals to investigate the effect of pore size on bone formation. They found that large pores (>200 μ m) enhanced

bone ingrowth and vascular formation, while smaller pores, in the range of 75–100 μ m, resulted in formation of unmineralized osteoid tissue.¹²⁸ Further decrease in the pore sizes of the scaffolds (<75 μ m) led to the formation of fibrous connective tissue after 12 weeks of implantation.¹²⁸ Narayan *et al.* also demonstrated that the average pore size and interpore distance of PLGA scaffold significantly influenced EC growth.¹²⁹ They reported that EC growth was enhanced on smaller pore sizes, in the range of 5–20 μ m, with lower interpore distance.¹²⁹ In another study, Akay *et al.* reported that the proliferation of primary rat osteoblasts seeded into a porous polymeric scaffold containing hydroxyapatite was enhanced when the average pore size of scaffold was less than 40 μ m.¹³⁰ Osteoblasts were shown to penetrate faster within the scaffolds containing large pores (>100 μ m); however, the extent of mineralization was not affected by the pore size.¹³⁰ Kuboki *et al.* showed that higher bone formation occurred in porous hydroxyapatite scaffolds with pore sizes in the range of 300–400 μ m after 4 weeks of implantation in rat.¹³¹ This was explained by the rapid vascularization within the implanted scaffolds, which provided a proper microenvironment for osteogenesis.¹³¹ These results indicate that the average pore size of scaffolds can be manipulated to potentially improve the formation of bone and vascular networks in bone TE.

In addition to porosity and average pore size, pore interconnectivity within scaffolds also plays an important role in bone tissue formation. Lack of pore interconnection can lead to poor nutrient and oxygen delivery as well as limited waste removal from the scaffold.¹³² This may inhibit cellular growth within the biomaterial even if it is highly porous. Gomes *et al.* studied the effect of pore interconnectivity and flow perfusion on the proliferation and osteogenic differentiation of rat BMSCs seeded on two starch-based scaffolds with different pores interconnectivities.¹³³ It was found that under perfusion flow, higher cell distribution was observed within the scaffolds with higher degree of pore interconnectivity compared to those with limited pore interconnects. Cells were not able to spread throughout the interior of the scaffold with low pore interconnectivity.¹³³ In another study, the effect of pore interconnections within silk fibroin scaffolds seeded with MSCs was investigated.¹³⁴ It was shown that the variation of pore interconnectivities had no significant effects on ALP expression and calcium deposition after 4 weeks of culture; however, cellular penetration and *in vitro* bone formation were significantly affected by scaffold interconnectivity. Silk scaffolds with highly interconnected pores allowed for homogenous mineralization and formation of bone-like tissue, while scaffolds with low degree of interconnectivity resulted in cellular growth only at the surface of the scaffolds.¹³⁴ Pamula *et al.* also showed that although gene expression levels of vinculin, β -actin, osteopontin, and osteocalcin were not affected by changing poly (L-lactide-co-glycolide) scaffold interconnectivities, faster colonization was observed in scaffolds with higher degree of interconnectivity.¹³⁵ Increasing the pore sizes and pore interconnectivities of scaffolds promoted proliferation of HOBs (MG-63) that were seeded on scaffolds up to 7 days of culture; however, these differences disappeared after 15 days of culture.¹³⁵

The average pore size and pore interconnectivity of scaffolds have been also shown to affect vascularization within

bone tissue-engineered constructs.^{136,137} Bai *et al.* used a combined template/casting technique to fabricate macroporous β -TCP scaffolds with controlled pore size and interconnections for vascularized bone tissue formation.¹³⁶ They showed that the pore architecture of the scaffold could affect vascularization when using a rabbit model. It was found that increasing the pore interconnectivity of the scaffold resulted in an increase in the size and number of the blood vessels formed within the macroporous scaffold, while an increase in scaffold pore size led to an augmentation in the size of blood vessels grown within the bioceramics. Scaffolds with pore sizes smaller than 400 μm were shown to limit the growth of blood vessels within the biomaterial, while increasing the pore size above this value had no significant effect on vascular formation, suggesting an optimized pore size of 400 μm for vascularization.¹³⁶ Ghanaati *et al.* also demonstrated that the pore size, porosity, and shape of β -TCP bone substitutes influenced the integration of the biomaterial within the defect site as well as vascularization rate, following implantation in Wistar rats.¹³⁷ The results of *in vivo* studies demonstrated that although high porosity (80%) allowed the penetration and growth of cells within the center of bone substitutes, the rate of vascularization was enhanced when the porosity of scaffold decreased from 80% to 40%. Ten days after implantation, the vascularization of scaffolds with low porosity was significantly higher than those with a high degree of porosity.¹³⁷ In another study, Klenke *et al.* studied the effect of pore size on the vascularization and osseointegration of ceramic scaffolds *in vivo*.¹³⁸ Porous ceramic scaffolds were fabricated by using a particle-leaching process with naphthalene particles followed by sintering. The fabricated ceramic scaffold had pores in the range of 40–280 μm , depending on the sizes of naphthalene particles used during scaffold preparation. It was found that increasing the pore sizes of the scaffolds promoted vascular network formation within the material after implantation in mice. Vessel formation also occurred earlier in scaffolds with pore sizes larger than 140 μm .¹³⁸ In addition, the functional capillary density, which indicated microvascular perfusion within the materials, increased when the pore sizes of the scaffold exceeded 140 μm . The volume of newly formed bone tissues within the implant was also increased two-fold when the pore sizes increased from 40 to 280 μm . These results demonstrate that the pore characteristics of the scaffolds play an important role in vascularization and osseointegration of bone substitutes.

Gradient biomaterials. Gradient biomaterials are scaffolds whose compositions and physical properties (e.g., stiffness, porosity, and topology) vary gradually and spatially.¹³⁹ A physical gradient is one characteristic that exists in several tissues, such as teeth, articular cartilage, and bone, as well as interfaces between different tissues, such as ligament-to-bone, cartilage-to-bone, and tendon-to-bone.^{139,140} Bone tissue varies from a stiff and compact external structure (porosity 5%–30%), to a spongy internal configuration (porosity 30%–90%).¹⁴¹ This gradient structure provides mechanical support to external loads while acting as a reservoir for bone marrow. Fabricating gradient scaffolds that mimic the microstructure of natural bone can potentially improve and enhance the formation of new bone tissue. In addition, the use of gradient scaffolds for bone TE can also potentially

increase the rate of vascularization and ingrowth of host vessels into the entire scaffold following implantation.

Generation of bone TE scaffolds with controlled spatial gradients provides a powerful tool for studying cell-bio-material interactions in bone TE.^{142,143} These gradient materials can improve cellular functions, including migration, signaling, proliferation, spreading, and differentiation. For example, the presence of a stiffness gradient has been shown to promote osteoblast development and function.¹²⁷ In one study, Marklein and Burdick fabricated a methacrylated hyaluronic acid scaffold with a 15-mm-long gradient in elastic modulus, ranging from 3 to 90 kPa. It was shown that hMSCs exhibited increased spreading and proliferation rates on the stiffer regions of scaffold compared to softer sections.¹⁴⁴ In another study, Oh *et al.* demonstrated that gradients in pore sizes and porosities could also influence cellular growth and bone tissue formation.¹²⁶ In this study, PCL scaffolds containing gradients in pore size ranging from 88 to 405 μm and porosity in the range of 80%–94% were fabricated. *In vitro* studies demonstrated that the growth of osteoblast cells was promoted in the regions with pore sizes in the range of 380–405 μm .¹²⁶ However, 4 weeks after implantation in rabbits, the scaffold region with 290–310 μm pore size exhibited faster bone formation.¹²⁶

To date, various methods have been applied to create gradient scaffolds for bone substitution.¹³⁹ Yang *et al.* developed a novel template-casting method to produce highly interconnected porous calcium phosphate (CaP)-graded scaffolds with controlled architecture, composition, and geometry.^{145–147} In this technique, a paraffin template was first fabricated by filling two concentric polyethylene tubes with paraffin beads of two different sizes. The tubes containing paraffin beads were subsequently heated to 50°C to induce bead coalescence and formation of a unitary mold structure. The CaP slurry was cast into the preformed paraffin template, which was followed by solidifying, drying, and sintering processes to form the porous CaP scaffold. Using this technique, a graded CaP scaffold consisting of a dense external structure (~20% porosity) and a porous central structure (70% porosity) was fabricated (Fig. 3A, B).¹⁴⁷ It was demonstrated that the graded CaP scaffold had pore architectures and mechanical properties similar to natural bone. A porous CaP scaffold loaded with BMP-2 was implanted into a nude mouse to evaluate its ability to enhance bone formation and healing. It was found that the porous scaffolds loaded with BMP-2 induced ectopic bone formation after 1 month of implantation (Fig. 3C). The fabricated porous scaffolds were also used as BMP-2 carriers to induce bone formation in a 1.5-cm bone defect in rabbit. The results of radiography and micro-CT imaging exhibited the formation of new bone tissue after 1 month (Fig. 3D–F), demonstrating the ability of fabricated scaffolds to repair various bone defect models.¹⁴⁶

In another study, PCL scaffolds with pore size and porosity gradients were formed by using a centrifuge method.¹²⁶ In this technique, a porous PCL scaffold was fabricated by centrifuging a cylindrical mold containing preformed fibril-like PCL, followed by heat-induced fibril bonding. The pore size and porosity of the fabricated scaffolds gradually increased along the longitudinal direction, due to the gradual increase of the centrifugal force along the cylindrical axis in the mold.¹²⁶ The pore size

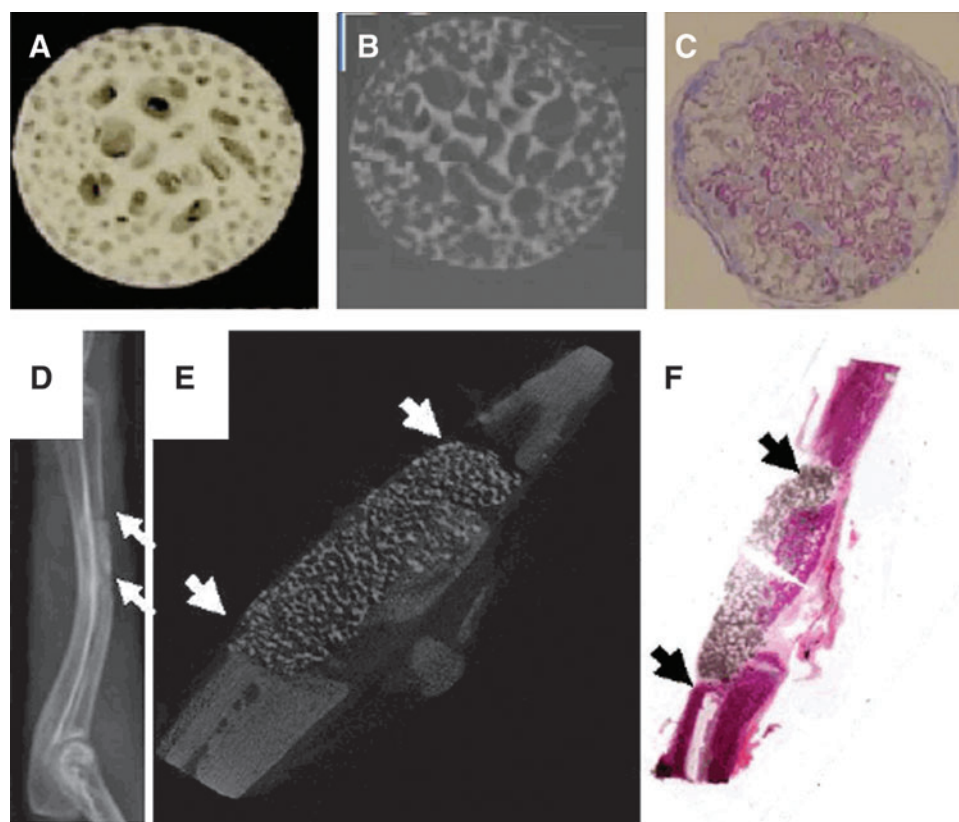


FIG. 3. Digital image (A) and two-dimensional micro-CT image (B) of calcium phosphate-graded scaffolds fabricated by using templating-casting method. The internal part of scaffold contained pores between 350 to 500 μm in diameter and the external zone contained pores between 600 and 800 μm (adapted with permission from Ref.¹⁸⁷). (C) Histology images of bone morphogenetic protein (BMP)-2-induced ectopic bone formation in porous scaffold one month after implantation in nude mouse, demonstrating that the pores of scaffold were filled with newly formed bone, which is observed as the violet stain. (D) Radiography and (E) longitudinal micro-CT images of scaffold-aided bone healing at one month after implantation in a 1.5-cm bone defect in rabbit. (F) Longitudinal HE-stained histological image of a nondecified scaffold-bone sample. Arrows indicate the scaffold. Color images available online at www.liebertpub.com/teb

gradient scaffolds were used to investigate the interaction between different cell types and scaffolds. It was found that various cell types required different pore size ranges for effective cellular growth. For example, chondrocytes and osteoblasts exhibited improved cell growth in the area of scaffold with larger pores, while fibroblast cells were shown to grow better in scaffold sections containing smaller pores.¹²⁶

The fabrication of scaffold containing gradients of pore size, porosity, and stiffness that mimic the complex architecture of bone tissue provides a powerful tool for studying cell-biomaterial interactions to accelerate bone tissue regeneration. The fabrication of these complex gradient materials is another effort toward creating bone tissue constructs, and has potential to facilitate the formation of a bone-cartilage tissue interface. It is envisioned that the fabrication and design of gradient biomaterials will open a new avenue for regenerating vascularized bone tissues.

Microfabrication techniques

The previously discussed techniques (i.e., growth factors delivery, using a coculture system, and designing of novel biomaterials) have been widely used to improve the process

of vascularization for bone TE. However, these techniques usually result in the formation of randomly organized vessel networks with poor integration capability within the host organism. Therefore, it is desirable to utilize other techniques to preform host-like vessel networks within the cell-laden biomaterials. In the following sections, we discuss different techniques that allow development of more organized vessel networks that could potentially allow for the better integration with the host tissue.

Microfabrication in bone TE. Various techniques (e.g., electrospinning, twin screw extrusion, phase separation, and salt leaching) have been used to engineer biomimetic scaffolds for bone TE applications.^{143,148–153} These techniques can be used to control the properties of scaffolds and have shown great potential for engineering bone tissue constructs. In addition, more advanced control on the cell microenvironment has been achieved through various microfabrication techniques. Using these technologies, it is possible to create microvasculature within engineered tissues to further improve integration with the host tissue.¹⁵⁴ Microscale technologies are the continuation of semiconductor and circuit technology, which comprise a wide range of processes to develop features in millimeter to submicrometer scales.¹⁵⁵

The natural microenvironment of the cells *in vivo* is composed of numerous discrete chemical, mechanical, and topographical cues at the micro- and nanoscale, which are believed to serve as signaling mechanisms to control cell function.^{156,157} Therefore, it may be possible to precisely control the cell microenvironment by integration of biology and microscale technologies in order to create engineered tissue constructs that comprise the complexity of the native tissue architectures.¹⁵⁸ To date, microscale technologies have been widely used to develop substrates, scaffolds, or biomaterials with specific properties to meet the desired criteria for bone TE applications. These technologies have also been employed in creating preformed vascular networks that can be ultimately incorporated within the biomaterials to deliver nutrition and oxygen and remove the waste products from the encapsulated cells.

Standard photolithography and soft lithography are among the common techniques that have been applied in patterning biomaterials to create cell-laden engineered tissue constructs. Standard photolithography usually requires a light-sensitive polymer solution containing a photoinitiator, a photomask layout, and a UV light source. The photomask is preprinted with the desired patterns and used to polymerize the polymer solution by exposing the patterned areas to UV light. The UV polymerization results in the cross-linking of the polymer solution to create a solid hydrogel with the desired patterns. Soft lithography techniques (i.e., microcontact printing and micromolding in capillaries) usually employ an elastomeric stamp, which is used to pattern the biomaterials with the desired geometrical features. Major advantages of soft lithography include simplicity and low cost, since these techniques do not require expensive clean room facilities. In addition, by using these techniques, it is possible to create patterns on a variety of planar or nonplanar substrates.^{155,159}

Mata *et al.* used soft lithography to create microtextured surfaces on polydimethylsiloxane (PDMS) substrates to study the behavior of human bone marrow-derived cells (hBMDCs) under osteogenic culture conditions and evaluate their osteoblastic differentiation. The substrates were comprised of microchannels with curved surfaces separated by individual ridges (Fig. 4A). Differentiation of the hBMDCs toward the osteoblastic phenotype was confirmed through staining for ALP activity. On flat surfaces, hBMDCs were oriented in random directions forming large colonies, while on PDMS microchannels, the cells, which were mostly aligned, migrated along the channel axis and formed colonies with higher aspect ratios compared to those on flat surfaces. This technique can potentially be used to improve predesigned platforms and create implants with precise topographical features for bone TE applications.

Other studies have used microgrooves^{160–163} and tapered micropits¹⁶⁴ as suitable topographies to address the current needs in bone TE. For example, Kirmizidis *et al.* used microgrooved features fabricated in polycarbonate to enhance alignment of primary calvarial rat osteoblast cells.¹⁶³ On grooves with 7 μm depth and 10, 15, and 30 μm widths, osteoblast cells exhibited a significantly improved alignment compared to flat surfaces. Notably, the cells maintained their cell–cell junctions (evaluated through connexin43 gap junction expression) and formed multilayers on 10- μm -wide grooves, confirming that the proposed microscale topographies can be potentially used in designing suitable biomaterials for orthopedic implants.¹⁶³ In a similar work, a micromolding technique was employed to create hydroxyapatite-based grooved features to analyze human osteoblast cell alignment. The finding of this work indicated that narrow grooves (20 μm width) significantly enhanced cellular orientation and alignment along their axis compared to wider grooves (40–100 μm

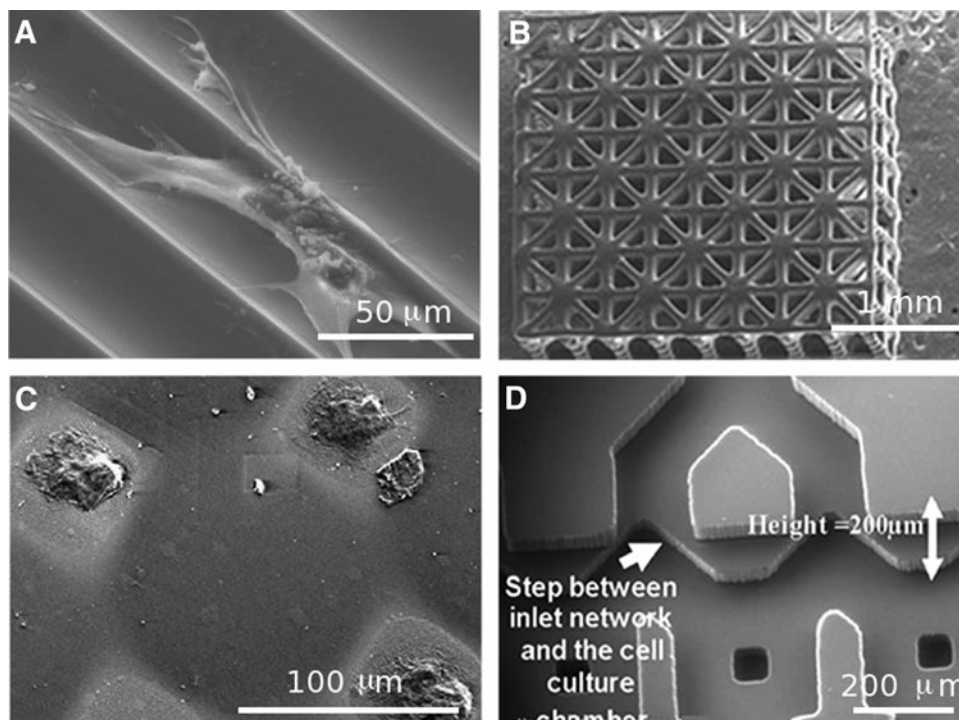


FIG. 4. SEM images of previously microfabricated platforms for bone TE applications. (A) Microfabricated PDMS channels; (B) three-dimensional scaffold fabricated with poly(propylene fumarate); (C) micropatterned polyethylene glycol (PEG) hydrogel on flat silicon surfaces; and (D) microfluidic network fabricated in polydimethylsiloxane (PDMS) (adapted with permission from Refs.^{166–168,188}).

width).¹⁶² Another study showed that on a tapered micropit topography, rat calvarial osteoblasts exhibited spindle line morphology and bridged the micropits, forming small adhesion sites, while mineralized tissue filled the area of the micropits upon *in vivo* implantation.^{163,164}

Rapid prototyping techniques have been also used to develop 3D scaffolds for bone TE applications. Mapili *et al.* demonstrated a layer-by-layer microstereolithography technique to microfabricate complex and spatially patterned poly (ethylene glycol) dimethacrylate (PEGDMA) hydrogels with desired microfeatures for bone TE applications. Using this technique, it was possible to create 3D constructs with complex architectures and spatially distributed biomolecules (i.e., fibronectin-derived arginine-glycine-aspartic acid [RGD]). *In vitro* studies demonstrated enhanced attachment of murine bone marrow-derived stromal cells on the surfaces of the PEGDMA scaffolds.¹⁶⁵ A similar microstereolithography technique was also used to pattern PPF to create a 3D interconnected scaffold for bone TE applications (Fig. 4B).¹⁶⁶ The surface of the PPF scaffold was modified using biomimetic apatite and RGD to support cellular adhesion and migration. *In vitro* studies demonstrated that apatite-RGD-coated scaffolds provided a suitable microenvironment for the proliferation of preosteoblasts (MC3T3-E1) for up to 2 weeks. In another study, Subramani *et al.* used standard photolithography and microcontact printing to create anti-adhesive patterns of PEG hydrogel on planar silicon and glass surfaces with the desired geometrical features (Fig. 4C).¹⁶⁷ They seeded rat osteoblasts on the patterned substrates and found increased proliferation within the noncoated regions. Additionally, the incorporation of the VEGF within the PEG hydrogel induced osteoblast migration, indicating that osteoblast migration can be controlled using micropatterning techniques. The ability to control cellular migration and localize cellular proliferation with the use of growth factors and micropatterned substrates provides another potential solution for the development of vascularized bone implants.

Microfluidic devices have also been shown to be potentially advantageous in the field of bone TE. Leclerc *et al.* fabricated a 3D microfluidic device by assembling two PDMS layers, one containing microholes and microchambers to support cell adhesion and the other containing a fluid network (Fig. 4D).¹⁶⁸ Mouse calvarial osteoblastic cells (MC3T3-E1) were seeded within the device and subjected to static as well as dynamic culture conditions (flow rates of 5 and 35 $\mu\text{L}/\text{min}$). The cells were able to proliferate and attach within the microfluidic device under shear stress. Notably, MC3T3s cultured under the flow rate of 5 $\mu\text{L}/\text{min}$ exhibited a 7.5-fold increase in ALP activity compared to the cells in static culture condition.¹⁶⁸ The results of this study indicated that microfluidic devices can be used as efficient platforms for bone tissue regeneration. Although these PDMS-based devices cannot be utilized as implantable TE scaffolds, these systems can serve as proof-of-concept applications.

Applying microfabrication to potentially enhance vascularization in bone TE. The previous section focused on the use of microscale technologies to create scaffolds or substrates as suitable platforms for bone TE applications. This section will focus on the potential use of microfabrication techniques to enhance vascularization in engineered bone

substitutes. Microscale technologies hold a great promise in creating vascularized networks within engineered tissue constructs.^{9,169,170} To date, numerous approaches such as micropatterning, microcontact printing, and micromolding have been widely adopted in the development of *in vitro* microscale vascularized networks.

A number of studies have used micropatterning of natural or synthetic hydrogels to enhance ECs alignment and promote angiogenesis.^{171–173} West and coworkers have been actively involved in using microfabrication technologies and PEG-diacrylate (PEGDA) hydrogels to enhance the process of vascularization for TE applications. Standard photolithography techniques and laser scanning lithography were employed to pattern PEG hydrogels in the form of strips with variable width on a layer of PEGDA.^{173–176} The surfaces of the patterned hydrogels have been modified through binding of cell-adhesive ligands (i.e., RGD), active molecules, and growth factors (i.e., VEGF) to support EC function. Their findings demonstrated that an intermediate concentration of RGD (20 $\mu\text{g}/\text{cm}^2$) induced HUVECs to undergo morphogenesis, assembling on top of each other to form cord-like structures along the patterned PEG strips.¹⁷⁵ Notably, the addition of VEGF to RGD ligands on the patterned hydrogel further enhanced tubule formation, which was verified by detecting lumens using confocal microscopy (Fig. 5A).¹⁷³ Khademhosseini and colleagues reported using methacrylated gelatin (GelMA) to investigate EC organization and alignment.^{171,177} Gelatin is an inexpensive and biocompatible polymer that can be synthesized after hydrolysis of collagen, and maintains cell binding motifs, such as RGD, along its backbone. The methacrylation of gelatin makes it photocrosslinkable, and through microfabrication technology, it is possible to create patterned geometries on cell-laden GelMA hydrogels. In their work, they demonstrated that HUVECs were able to form lumen-like ring structures on GelMA with gel concentrations of 5%, 10%, and 15%.¹⁷¹ Alignment of HUVECs was significantly enhanced within the patterned microchannels (50 μm width) compared to unpatterned regions, confirming the possibility of creating 3D vascularized networks using micropatterned GelMA.¹⁷⁷

Microcontact printing methods have been used to pattern proteins on two-dimensional surfaces in order to promote alignment and organization of ECs along the patterned regions.^{178,179} The advantage of this technique is that patterns can be generated on a number of different substrates, such as glass, silicon, and polystyrene, using proteins solutions. This would allow for the creation of patterned microvasculature structures without consideration of the substrate materials.¹⁵⁹ For example, Dike *et al.* demonstrated that both human and bovine ECs were well-connected and differentiated, forming capillary-like structures comprised of luminal cavities when grown on 10- μm -wide lanes.¹⁷⁸ In another approach, Gerecht and coworkers used microcontact printing followed by inversion of the patterned surfaces on a layer of fibrin hydrogel to promote tubulogenesis of human endothelial progenitor cells.¹⁷⁹ Fibronectin protein was patterned on glass substrates with widths in the range of 2.5 to 70 μm . Optimal cell attachment and proliferation was observed on 50 μm widths after 5 days of culture. The expression of adhesion molecules such as E-selectin and intercellular adhesion molecule-1 was significantly enhanced in response to tumor necrosis factor- α , indicating the angiogenic ability of

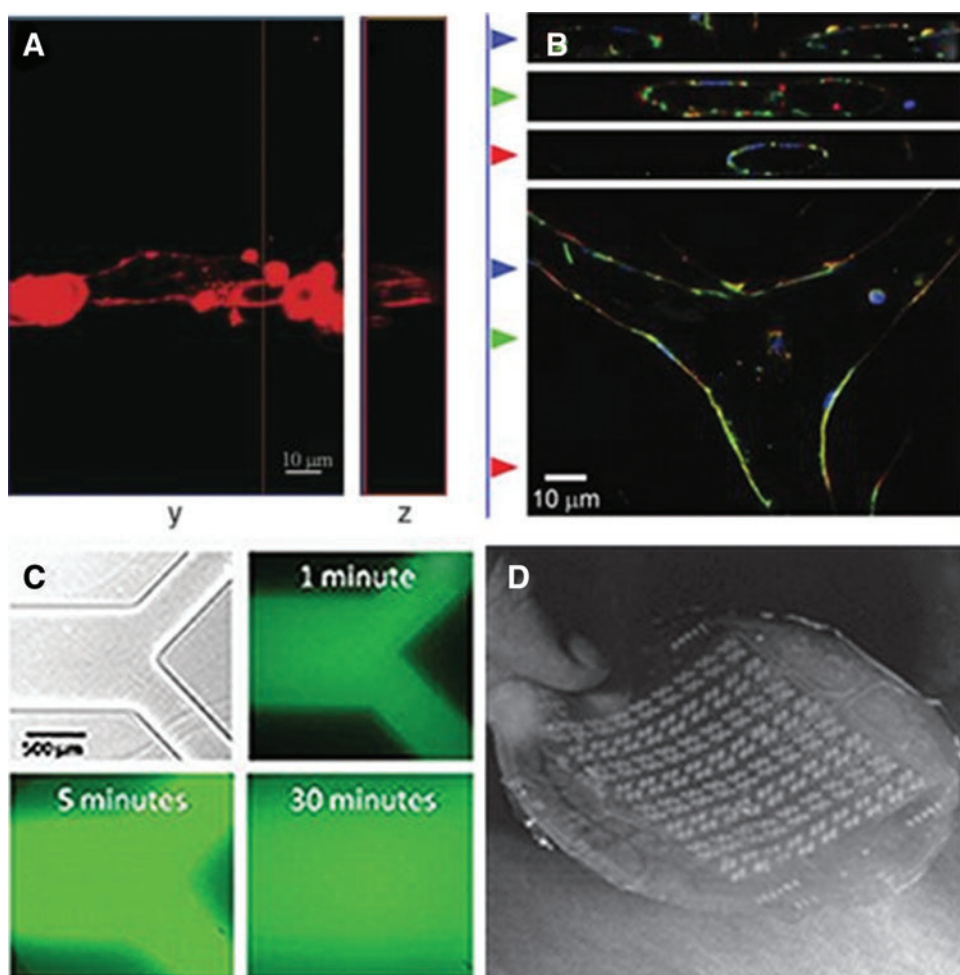


FIG. 5. (A) Top and cross-sectional confocal images of the actin filaments and tubule formation in endothelial cells (ECs) on PEG hydrogels patterned with RGDS and vascular endothelial growth factor. (B) Immunofluorescence images of ECs forming branched tubules using a micromolding technique. Actin filaments are stained in red, nuclei is stained in blue, and β -catenin is stained in green. (C) Microfluidic network fabricated in agarose hydrogels. (D) Highly branched microfluidic network fabricated in PDMS for vascularization applications (adapted with permission from Refs.^{173,180,181,185}). Color images available online at www.liebertpub.com/teb

the cells within the 50- μ m pattern widths. By addition of the fibrin gel to the patterned cells, it was possible to create 3D tubular structures comprising lumens.

Furthermore, other researchers have used micromolding techniques to spatially control EC organization and to enhance *in vitro* tubulogenesis. Raghavan *et al.* employed a micromolding technique to create cell-laden collagen gels consisting of microscale channels.¹⁸⁰ In this technique, a mold consisting of channels with the desired geometries and precoated with nonadhesive polymers was primarily fabricated in PDMS. The ECs were encapsulated within the collagen gel, and then the cell-laden gel was placed inside the channels through centrifugation followed by curing of collagen at 37°C. They observed that encapsulated ECs organized into tubes with lumens within 24–48 h.¹⁸⁰ It was also demonstrated that the tube diameter could be controlled by the collagen concentrations and channel width. Furthermore, the generation of more complex capillary architectures could be achieved by guiding the development of branches during tubule formation within the microfabricated geometry (Fig. 5B). These results illustrated the potential use of micromolding techniques to generate geometrically defined vascular networks.

In addition to micropatterning and micromolding of proteins and hydrogels, microfluidic systems have been used to develop 3D vascularized networks for TE applications. Both hydrogels^{181–183} and biocompatible, biodegradable poly-

mers^{184,185} have been used in development of microfluidic networks for vascularization purposes. In one study, soft lithography and a silicone master were used to mold the cell-embedded calcium alginate hydrogel on the desired microstructure.¹⁸³ Using this approach, it was possible to appropriately distribute the embedded microfluidic channels and uniformly exchange the soluble factors within bulk hydrogels. Khademhosseini and colleagues used a soft lithography technique to cast agarose hydrogels against a micropatterned SU-8 photoresist on a silicon substrate to create hydrogel-based microfluidic channels.¹⁸¹ Subsequently, another layer of agarose hydrogel was used to seal the channels (Fig. 5C). They demonstrated that it was possible to create microfluidic channels with variable feature sizes and high porosity, which were suitable for the creation of vascular networks. Their results showed that the cells remained viable in close proximity of the channels, confirming proper nutrient and waste exchange through the channels to the surrounding regions.

Considerable work within this field has been done by Borenstein and colleagues to develop highly branched multilayer microfluidic network using biocompatible and biodegradable polymers such as PDMS¹⁸⁵ and PLGA¹⁸⁴ in order to mimic *in vivo* microvasculatures. In their primary studies, they used a patterned silicon substrate as a mold and replica-molding technique to create highly branched microfluidic network in PDMS, which was subsequently seeded

with ECs for vascular formation (Fig. 5D).¹⁸⁵ In another study, a PDMS mold was used to create the desired microstructures out of PLGA through a melt-molding process. Multiple layers of patterned PLGA layers were bonded through thermal fusion bonding to create the desired 3D multilayer microfluidic network.¹⁸⁴

Microscale technologies have been proven to be a powerful tool in development of precise topographical features, scaffolds, and cell-laden hydrogels for bone TE applications. These technologies have been also applied to address the current challenges in vascularization of tissue constructs. Microscale technologies offer the flexibility in creating precise 3D architectures with embedded vascularized and capillary networks. For example, in a study by Moroni *et al.*, rapid prototyping computer-aided design/computer-aided manufacturing (CAD/CAM) was used to create microscale 3D scaffolds consisting of well-organized hollow fibers with controllable diameter and thickness that could be further used as a vascularized network for TE applications.¹⁸⁶ It is envisioned that by employing microscale technologies, it would be possible to address the current needs within the field of bone TE to produce a fully functional vascularized bone substitute.

Conclusions

The direction of bone TE has evolved through the years, and as the progression developed, more advanced concepts are being incorporated into the equation. Novel approaches such as dual growth factor delivery, coculturing systems, incorporation of mechanical stimulation, biomaterials with tunable properties, and microfabrication of specific microfeatures, have been proposed in bone TE field to create constructs for generation of large bone defects. However, even with the development of these strategies, challenges still remain in the inability to reproduce an engineered bone replacement that truly mimics natural bone with well-formed and stable blood vessels. The lack of vascularization in engineered bone tissue is a major obstacle that needs to be overcome in order to achieve clinical success, particularly for the regeneration of large bone defects. The absence of a vascularized network limits the maximum effective size of engineered bone tissue due to insufficient nutrients and oxygen available within the constructs. The above-mentioned strategies have been proposed to enhance vascularization in bone tissue-engineered constructs. Although each individual approach does facilitate the formation of blood vessels, no one strategy alone has been successful in producing stable and mature vascularization within a bone replacement construct. Therefore, combining these approaches can be considered as a mean of further improvement toward generating vascularized bone tissue substitutes that more closely mimic the complexity of natural bone. The resulting engineered construct ideally would aid and facilitate the natural bone-healing process *in vivo*. The ability to accomplish such a complex native-like construct will bring the field of bone TE closer to the ultimate goal of producing a prevascularized bone tissue for the treatment of bone defects. With continued research in the techniques presented here, and new advanced techniques in the future, the improved ability to develop more complex bone tissue constructs will drive investigators closer to make advances toward clinical restoration of bone tissue function.

Acknowledgments

This research has been supported by the NIH (HL092836, A.K.; EB008392, A.K.; DE019024, A.K.; HL099073, A.K.; AR057837, Y.Y.; DE021468, Y.Y.), NSF, A.K.; and DOD (W81XWH-10-1-0966, Y.Y.; W81XWH-10-200-10, Y.Y.; W81XWH-11-2-0168-P4, Y.Y.).

Disclosure Statement

No competing financial interests exist.

References

1. Salgado, A.J., Coutinho, O.P., and Reis, R.L. Bone tissue engineering: state of the art and future trends. *Macromol Biosci* **4**, 743, 2004.
2. Goldstein, S.A. Tissue engineering: functional assessment and clinical outcome. *Ann N Y Acad Sci* **961**, 183, 2002.
3. Sikavitsas, V.L., Temenoff, J.S., and Mikos, A.G. Biomaterials and bone mechanotransduction. *Biomaterials* **22**, 2581, 2001.
4. Turner, C.H., Wang, T., and Burr, D.B. Shear strength and fatigue properties of human cortical bone determined from pure shear tests. *Calcif Tissue Int* **69**, 373, 2001.
5. Hillier, M.L., and Bell, L.S. Differentiating human bone from animal bone: a review of histological methods. *J Forensic Sci* **52**, 249, 2007.
6. Rodan, G.A. Introduction to bone biology. *Bone* **13 Suppl 1**, S3, 1992.
7. He, W., Ye, L., Li, S., Liu, H., Wu, B., Wang, Q., Fu, X., Han, W., and Chen, Z. Construction of vascularized cardiac tissue from genetically modified mouse embryonic stem cells. *J Heart Lung Transplant* **31**, 204, 2012.
8. Jain, R.K., Au, P., Tam, J., Duda, D.G., and Fukumura, D. Engineering vascularized tissue. *Nat Biotechnol* **23**, 821, 2005.
9. Kaully, T., Kaufman-Francis, K., Lesman, A., and Levenberg, S. Vascularization: the conduit to viable engineered tissues. *Tissue Eng Part B Rev* **15**, 159, 2009.
10. Kermani, P., and Hempstead, B. Brain-derived neurotrophic factor: a newly described mediator of angiogenesis. *Trends Cardiovasc Med* **17**, 140, 2007.
11. Santos, M.L., and Reis, R.L. Vascularization in bone tissue engineering: physiology, current strategies, major hurdles and future challenges. *Macromol Biosci* **10**, 12, 2010.
12. Huang, Z., Nelson, E.R., Smith, R.L., and Goodman, S.B. The sequential expression profiles of growth factors from osteoprogenitors [correction of osteoprogenitors] to osteoblasts *in vitro*. *Tissue Eng* **13**, 2311, 2007.
13. Devescovi, V., Leonardi, E., Ciapetti, G., and Cenni, E. Growth factors in bone repair. *Chir Organi Mov* **92**, 161, 2008.
14. Malizos, K.N., and Papatheodorou, L.K. The healing potential of the periosteum molecular aspects. *Injury* **36 Suppl 3**, S13, 2005.
15. Collin-Osdoby, P., Rothe, L., Bekker, S., Anderson, F., Huang, Y., and Osdoby, P. Basic fibroblast growth factor stimulates osteoclast recruitment, development, and bone pit resorption in association with angiogenesis *in vivo* on the chick chorio-allantoic membrane and activates isolated avian osteoclast resorption *in vitro*. *J Bone Miner Res* **17**, 1859, 2002.
16. Kanczler, J.M., and Oreffo, R.O. Osteogenesis and angiogenesis: the potential for engineering bone. *Eur Cell Mater* **15**, 100, 2008.

17. Villars, F., Bordenave, L., Bareille, R., and Amedee, J. Effect of human endothelial cells on human bone marrow stromal cell phenotype: role of VEGF? *J Cell Biochem* **79**, 672, 2000.
18. Tomanek, R.J., Lotun, K., Clark, E.B., Suvarna, P.R., and Hu, N. VEGF and bFGF stimulate myocardial vascularization in embryonic chick. *Am J Physiol* **274**, H1620, 1998.
19. Solorio, L., Zwolinski, C., Lund, A.W., Farrell, M.J., and Stegemann, J.P. Gelatin microspheres crosslinked with genipin for local delivery of growth factors. *J Tissue Eng Regen Med* **4**, 514, 2010.
20. Formiga, F.R., Pelacho, B., Garbayo, E., Abizanda, G., Gavira, J.J., Simon-Yarza, T., Mazo, M., Tamayo, E., Jauquicoa, C., Ortiz-de-Solorzano, C., Prosper, F., and Blanco-Prieto, M.J. Sustained release of VEGF through PLGA microparticles improves vasculogenesis and tissue remodeling in an acute myocardial ischemia-reperfusion model. *J Control Release* **147**, 30, 2010.
21. Kempen, D.H., Creemers, L.B., Alblas, J., Lu, L., Verbout, A.J., Yaszemski, M.J., and Dhert, W.J. Growth factor interactions in bone regeneration. *Tissue Eng Part B Rev* **16**, 551, 2010.
22. Duneas, N., Crooks, J., and Ripamonti, U. Transforming growth factor-beta 1: induction of bone morphogenetic protein genes expression during endochondral bone formation in the baboon, and synergistic interaction with osteogenic protein-1 (BMP-7). *Growth Factors* **15**, 259, 1998.
23. Simmons, C.A., Alsberg, E., Hsiong, S., Kim, W.J., and Mooney, D.J. Dual growth factor delivery and controlled scaffold degradation enhance *in vivo* bone formation by transplanted bone marrow stromal cells. *Bone* **35**, 562, 2004.
24. Kubota, K., Iseki, S., Kuroda, S., Oida, S., Iimura, T., Duarte, W.R., Ohya, K., Ishikawa, I., and Kasugai, S. Synergistic effect of fibroblast growth factor-4 in ectopic bone formation induced by bone morphogenetic protein-2. *Bone* **31**, 465, 2002.
25. Nakamura, Y., Tensho, K., Nakaya, H., Nawata, M., Okabe, T., and Wakitani, S. Low dose fibroblast growth factor-2 (FGF-2) enhances bone morphogenetic protein-2 (BMP-2)-induced ectopic bone formation in mice. *Bone* **36**, 399, 2005.
26. Raiche, A.T., and Puleo, D.A. *In vitro* effects of combined and sequential delivery of two bone growth factors. *Biomaterials* **25**, 677, 2004.
27. Vo, T.N., Kasper, F.K., and Mikos, A.G. Strategies for controlled delivery of growth factors and cells for bone regeneration. *Adv Drug Deliv Rev* [Epub ahead of print]; DOI: 10.1016/j.addr.2012.01.016.
28. Buket Basmanav, F., Kose, G.T., and Hasirci, V. Sequential growth factor delivery from complexed microspheres for bone tissue engineering. *Biomaterials* **29**, 4195, 2008.
29. Yilgor, P., Hasirci, N., and Hasirci, V. Sequential BMP-2/BMP-7 delivery from polyester nanocapsules. *J Biomed Mater Res A* **93A**, 528, 2010.
30. Yilgor, P., Tuzlakoglu, K., Reis, R.L., Hasirci, N., and Hasirci, V. Incorporation of a sequential BMP-2/BMP-7 delivery system into chitosan-based scaffolds for bone tissue engineering. *Biomaterials* **30**, 3551, 2009.
31. Lee, K., Silva, E.A., and Mooney, D.J. Growth factor delivery-based tissue engineering: general approaches and a review of recent developments. *J R Soc Interface* **55**, 153, 2011.
32. Richardson, T.P., Peters, M.C., Ennett, A.B., and Mooney, D.J. Polymeric system for dual growth factor delivery. *Nat Biotech* **19**, 1029, 2001.
33. Patel, Z.S., Young, S., Tabata, Y., Jansen, J.A., Wong, M.E., and Mikos, A.G. Dual delivery of an angiogenic and an osteogenic growth factor for bone regeneration in a critical size defect model. *Bone* **43**, 931, 2008.
34. Shah, N.J., Macdonald, M.L., Beben, Y.M., Padera, R.F., Samuel, R.E., and Hammond, P.T. Tunable dual growth factor delivery from polyelectrolyte multilayer films. *Biomaterials* **32**, 6183, 2011.
35. Young, S., Patel Zarana, S., Kretlow James, D., Murphy Matthew, B., Mountziaris Paschalia, M., Baggett, L.S., Ueda, H., Tabata, Y., Jansen John, A., Wong, M., and Mikos Antonios, G. Dose effect of dual delivery of vascular endothelial growth factor and bone morphogenetic protein-2 on bone regeneration in a rat critical-size defect model. *Tissue Eng Part A* **15**, 2347, 2009.
36. McCarthy, I. The physiology of bone blood flow: a review. *J Bone Joint Surg Am* **88 Suppl 3**, 4, 2006.
37. Wang, D.S., Miura, M., Demura, H., and Sato, K. Anabolic effects of 1,25-dihydroxyvitamin D3 on osteoblasts are enhanced by vascular endothelial growth factor produced by osteoblasts and by growth factors produced by endothelial cells. *Endocrinol* **138**, 2953, 1997.
38. Samee, M., Kasugai, S., Kondo, H., Ohya, K., Shimokawa, H., and Kuroda, S. Bone morphogenetic protein-2 (BMP-2) and vascular endothelial growth factor (VEGF) transfection to human periosteal cells enhances osteoblast differentiation and bone formation. *J Pharmacol Sci* **108**, 18, 2008.
39. Koike, N., Fukumura, D., Gralla, O., Au, P., Schechner, J.S., and Jain, R.K. Tissue engineering: creation of long-lasting blood vessels. *Nature* **428**, 138, 2004.
40. Yu, H., VandeVord, P.J., Mao, L., Matthew, H.W., Wooley, P.H., and Yang, S.Y. Improved tissue-engineered bone regeneration by endothelial cell mediated vascularization. *Biomaterials* **30**, 508, 2009.
41. Zhou, J., Lin, H., Fang, T., Li, X., Dai, W., Uemura, T., and Dong, J. The repair of large segmental bone defects in the rabbit with vascularized tissue engineered bone. *Biomaterials* **31**, 1171, 2010.
42. Kaigler, D., Krebsbach, P.H., West, E.R., Horger, K., Huang, Y.C., and Mooney, D.J. Endothelial cell modulation of bone marrow stromal cell osteogenic potential. *FASEB J* **19**, 665, 2005.
43. Bell, E., Ivarsson, B., and Merrill, C. Production of a tissue-like structure by contraction of collagen lattices by human fibroblasts of different proliferative potential *in vitro*. *Proc Natl Acad Sci U S A* **76**, 1274, 1979.
44. Krishnan, L., Underwood, C.J., Maas, S., Ellis, B.J., Kode, T.C., Hoying, J.B., and Weiss, J.A. Effect of mechanical boundary conditions on orientation of angiogenic microvessels. *Cardiovasc Res* **78**, 324, 2008.
45. Huo, B., Lu, X.L., and Guo, X.E. Inter cellular calcium wave propagation in linear and circuit-like bone cell networks. *Philos Transact A Math Phys Eng Sci* **368**, 617, 2010.
46. Kaneuji, T., Ariyoshi, W., Okinaga, T., Toshinaga, A., Takahashi, T., and Nishihara, T. Mechanisms involved in regulation of osteoclastic differentiation by mechanical stress-loaded osteoblasts. *Biochem Biophys Res Commun* **408**, 103, 2011.
47. Liu, C., Abedian, R., Meister, R., Haasper, C., Hurschler, C., Krettek, C., von Lewinski, G., and Jagodzinski, M. Influence of perfusion and compression on the proliferation and differentiation of bone mesenchymal stromal cells seeded on polyurethane scaffolds. *Biomaterials* **33**, 1052, 2012.

48. Zhang, Z.-Y., Teoh, S.H., Chong, W.-S., Foo, T.-T., Chng, Y.-C., Choolani, M., and Chan, J. A biaxial rotating bioreactor for the culture of fetal mesenchymal stem cells for bone tissue engineering. *Biomaterials* **30**, 2694, 2009.
49. Bancroft, G.N., Sikavitsas VI, and Mikos, A.G. Design of a flow perfusion bioreactor system for bone tissue-engineering applications. *Tissue Eng Part A* **9**, 549, 2003.
50. Mauney, J.R., Sjostrom, S., Blumberg, J., Horan, R., O'Leary, J.P., Vunjak-Novakovic, G., Volloch, V., and Kaplan, D.L. Mechanical stimulation promotes osteogenic differentiation of human bone marrow stromal cells on 3-D partially demineralized bone scaffolds *in vitro*. *Calcif Tissue Int* **74**, 458, 2004.
51. Ignatius, A., Blessing, H., Liedert, A., Schmidt, C., Neidlinger-Wilke, C., Kaspar, D., Friemert, B., and Claes, L. Tissue engineering of bone: effects of mechanical strain on osteoblastic cells in type I collagen matrices. *Biomaterials* **26**, 311, 2005.
52. Forwood, M.R., Owan, I., Takano, Y., and Turner, C.H. Increased bone formation in rat tibiae after a single short period of dynamic loading *in vivo*. *Am J Physiol* **270**, E419, 1996.
53. van Eijk, F., Saris, D.B., Creemers, L.B., Riesle, J., Willems, W.J., van Blitterswijk, C.A., Verbout, A.J., and Dhert, W.J. The effect of timing of mechanical stimulation on proliferation and differentiation of goat bone marrow stem cells cultured on braided PLGA scaffolds. *Tissue Eng Part A* **14**, 1425, 2008.
54. Von Offenbergsweeney, N., Cummins, P.M., Cotter, E.J., Fitzpatrick, P.A., Birney, Y.A., Redmond, E.M., and Cahill, P.A. Cyclic strain-mediated regulation of vascular endothelial cell migration and tube formation. *Biochem Biophys Res Commun* **329**, 573, 2005.
55. Li, W., and Sumpio, B.E. Strain-induced vascular endothelial cell proliferation requires PI3K-dependent mTOR-4E-BP1 signal pathway. *Am J Physiol Heart Circ Physiol* **288**, H1591, 2005.
56. Iba, T., and Sumpio, B.E. Morphological response of human endothelial cells subjected to cyclic strain *in vitro*. *Microvasc Res* **42**, 245, 1991.
57. Azuma, N., Duzgun, S.A., Ikeda, M., Kito, H., Akasaka, N., Sasajima, T., and Sumpio, B.E. Endothelial cell response to different mechanical forces. *J Vasc Surg* **32**, 789, 2000.
58. Cheung, W.Y., Liu, C., Tonelli-Zasarsky, R.M., Simmons, C.A., and You, L. Osteocyte apoptosis is mechanically regulated and induces angiogenesis *in vitro*. *J Orthop Res* **29**, 523, 2011.
59. Aguirre, J.I., Plotkin, L.I., Stewart, S.A., Weinstein, R.S., Parfitt, A.M., Manolagas, S.C., and Bellido, T. Osteocyte apoptosis is induced by weightlessness in mice and precedes osteoclast recruitment and bone loss. *J Bone Miner Res* **21**, 605, 2006.
60. Li, Q., Hou, T., Zhao, J., and Xu, J. Vascular endothelial growth factor release from alginate microspheres under simulated physiological compressive loading and the effect on human vascular endothelial cells. *Tissue Eng Part A* **17**, 1777, 2011.
61. Rodrigues, M.T., Gomes, M.E., and Reis, R.L. Current strategies for osteochondral regeneration: from stem cells to pre-clinical approaches. *Curr Opin Biotechnol* **22**, 726, 2011.
62. Wojtowicz, A.M., Shekaran, A., Oest, M.E., Dupont, K.M., Templeman, K.L., Huttmacher, D.W., Guldberg, R.E., and Garcia, A.J. Coating of biomaterial scaffolds with the collagen-mimetic peptide GFOGER for bone defect repair. *Biomaterials* **31**, 2574, 2010.
63. Landman Kerry, A., and Cai Anna, Q. Cell proliferation and oxygen diffusion in a vascularising scaffold. *Bull Math Biol* **69**, 2405, 2007.
64. Sachlos, E., and Czernuszka, J.T. Making tissue engineering scaffolds work. *Euro Cells Mat* **5**, 29, 2003.
65. Fidkowski, C., Kaazempur-Mofrad, M.R., Borenstein, J., Vacanti, J.P., Langer, R., and Wang, Y. Endothelialized microvasculature based on a biodegradable elastomer. *Tissue Eng* **11**, 302, 2005.
66. Simon, J.A., Ricci, J.L., and Di Cesare, P.E. Bioresorbable fracture fixation in orthopedics: a comprehensive review. Part II. Clinical studies. *Am J Orthop (Belle Mead NJ)* **26**, 754, 1997.
67. Zhang, P., Hamamura, K., and Yokota, H. A brief review of bone adaptation to unloading. *J Proteomics Bioinform* **6**, 4, 2008.
68. El-Ghannam, A. Bone reconstruction: from bioceramics to tissue engineering. *Expert Rev Med Devices* **2**, 87, 2005.
69. Cordonnier, T., Sohier, J., Rosset, P., and Layrolle, P. Biomimetic materials for bone tissue engineering—state of the art and future trends. *Adv Biomater* **13**, B135, 2011.
70. Kohri, M., Miki, K., Waite, D.E., Nakajima, H., and Okabe, T. *In vitro* stability of biphasic calcium phosphate ceramics. *Biomaterials* **14**, 299, 1993.
71. Ducheyne, P. Bioceramics: material characteristics versus *in vivo* behavior. *J Biomed Mater Res* **21**, 219, 1987.
72. Rezwan, K., Chen, Q.Z., Blaker, J.J., and Boccaccini, A.R. Biodegradable and bioactive porous polymer/inorganic composite scaffolds for bone tissue engineering. *Biomaterials* **27**, 3413, 2006.
73. Agrawal, C.M., and Ray, R.B. Biodegradable polymeric scaffolds for musculoskeletal tissue engineering. *J Biomed Mater Res* **55**, 141, 2001.
74. Taboas, J.M., Maddox, R.D., Krebsbach, P.H., and Hollister, S.J. Indirect solid free form fabrication of local and global porous, biomimetic and composite 3D polymer-ceramic scaffolds. *Biomaterials* **24**, 181, 2002.
75. Agrawal, C.M., Best, J., Heckman, J.D., and Boyan, B.D. Protein release kinetics of a biodegradable implant for fracture non-unions. *J Biomed Mater* **16**, 1255, 1995.
76. Borden, M., El-Amin, S.F., Attawia, M., and Laurencin, C.T. Structural and human cellular assessment of a novel microsphere-based tissue engineered scaffold for bone repair. *J Biomed Mater* **24**, 597, 2002.
77. Gogolewski, S., Gorna, K., and Turner, A.S. Regeneration of bicortical defects in the iliac crest of estrogen-deficient sheep, using new biodegradable polyurethane bone graft substitutes. *J Biomed Mater Res A* **77A**, 802, 2006.
78. Laschke, M.W., Strohe, A., Scheuer, C., Eglin, D., Verrier, S., Alini, M., Pohlemann, T., and Menger, M.D. *In vivo* biocompatibility and vascularization of biodegradable porous polyurethane scaffolds for tissue engineering. *Acta Biomater* **5**, 1991, 2009.
79. Lewandrowski K.-U., Hile, D.D., Thompson, B.M.J., Wise, D.L., Tomford, W.W., and Trantolo, D.J. Quantitative measures of osteoinductivity of a porous poly(propylene fumarate) bone graft extender. *Tissue Eng* **9**, 85, 2003.
80. Vehof, J.W.M., Fisher, J.P., Dean, D., Van der Waerden J.-P.C.M., Spauwen, P.H.M., Mikos, A.G., and Jansen, J.A. Bone formation in transforming growth factor beta-1-coated porous poly(propylene fumarate) scaffolds. *J Biomed Mater Res* **60**, 241, 2002.

81. Fisher, J.P., Vehof, J.W.M., Dean, D., Van der Waerden J.P.C.M., Holland, T.A., Mikos, A.G., and Jansen, J.A. Soft and hard tissue response to photocrosslinked poly (propylene fumarate) scaffolds in a rabbit model. *J Biomed Mater Res* **59**, 547, 2002.
82. Fisher, J.P., Holland, T.A., Dean, D., Engel, P.S., and Mikos, A.G. Synthesis and properties of photocross-linked poly(propylene fumarate) scaffolds. *J Biomater Sci Polym Ed* **12**, 673, 2001.
83. Attawia, M.A., Uhrich, K., Herbert, K.M., Langer, R., and Laurencin, C.T. Long term osteoblast response to poly (anhydride-co-imides): a new degradable polymer for use in bone. *Proceedings of the Fifth World Biomaterials Congress*, Toronto, Canada, p. 113, 1996.
84. Ibim, S.E.M., Uhrich, K.E., Attawia, M., Shastri, V.R., El-Amin, S.F., Bronson, R., Langer, R., and Laurencin, C.T. Preliminary *in vivo* report on the osteocompatibility of poly(anhydride-co-imides) evaluated in a tibial model. *J Biomed Mater Res* **43**, 374, 1998.
85. Claase, M.B., Bruijn, J.D., Grijpma, D.W., and Feijen, J. Ectopic bone formation in cell-seeded poly(ethylene oxide)/poly(butylene terephthalate) copolymer scaffolds of varying porosity. *J Mater Sci Mater Med* **18**, 1299, 2007.
86. Kuijter, R., Bouwmeester, S.J.M., Drees M.M.W.E., Surtel, D.A.M., Terwindt-Rouwenhorst, E.A.W., Van Der Linden, A.J., Van Blitterswijk, C.A., and Bulstra, S.K. The polymer polyactive as a bone-filling substance: an experimental study in rabbits. *J Mater Sci Mater Med* **9**, 449, 1998.
87. Rocha, L.B., Goissis, G., and Rossi, M.A. Biocompatibility of anionic collagen matrix as scaffold for bone healing. *Biomaterials* **23**, 449, 2001.
88. Nazarov, R., Jin, H.J., and Kaplan, D.L. Porous 3-D scaffolds from regenerated silk fibroin. *Biomacromolecules* **5**, 718, 2004.
89. Martins, A.M., Pham, Q.P., Malafaya, P.B., Raphael, R.M., Kasper, F.K., Reis, R.L., and Mikos, A.G. Natural stimulus responsive scaffolds/cells for bone tissue engineering: influence of lysozyme upon scaffold degradation and osteogenic differentiation of cultured marrow stromal cells induced by CaP coatings. *Tissue Eng Part A* **15**, 1953, 2009.
90. Gomes, M.E., Salgado, A., and Reis, R.L. Bone tissue engineering using starch based scaffolds obtained by different methods. *NATO Sci Ser II* **86**, 221, 2002.
91. Kunjachan, V., Subramanian, A., Hanna, M., and Guan, J.J. Comparison of different fabrication techniques used for processing 3-dimensional, porous, biodegradable scaffolds from modified starch for bone tissue engineering. *Biomed Sci Instrum* **40**, 129, 2004.
92. Kim, H.D., and Valentini, R.F. Retention and activity of BMP-2 in hyaluronic acid-based scaffolds *in vitro*. *J Biomed Mater Res* **59**, 573, 2002.
93. You, M., Peng, G., Li, J., Ma, P., Wang, Z., Shu, W., Peng, S., and Chen, G.-Q. Chondrogenic differentiation of human bone marrow mesenchymal stem cells on polyhydroxyalkanoate (PHA) scaffolds coated with PHA granule binding protein PhaP fused with RGD peptide. *Biomaterials* **32**, 2305, 2011.
94. Philip, S., Keshavarz, T., and Roy, I. Polyhydroxyalkanoates: biodegradable polymers with a range of applications. *J Chem Technol Biotechnol* **82**, 233, 2007.
95. Peppas, N.A., Hilt, J.Z., Khademhosseini, A., and Langer, R. Hydrogels in biology and medicine: from molecular principles to bionanotechnology. *Adv Mater* **18**, 1345, 2006.
96. Drury, J.L., and Mooney, D.J. Hydrogels for tissue engineering: scaffold design variables and applications. *Biomaterials* **24**, 4337, 2003.
97. Burdick, J.A., and Anseth, K.S. Photoencapsulation of osteoblasts in injectable RGD-modified PEG hydrogels for bone tissue engineering. *J Biomed Mater* **23**, 4315, 2002.
98. Lee, C.R., Grodzinsky, A.J., and Spector, M. The effects of cross-linking of collagen-glycosaminoglycan scaffolds on compressive stiffness, chondrocyte-mediated contraction, proliferation and biosynthesis. *Biomaterials* **22**, 3145, 2001.
99. Park, S.N., Park, J.C., Kim, H.O., Song, M.J., and Suh, H. Characterization of porous collagen/hyaluronic acid scaffold modified by 1-ethyl-3-(3-dimethylaminopropyl)carbodiimide cross-linking. *Biomaterials* **23**, 1205, 2002.
100. Tan, W., Krishnaraj, R., and Desai, T.A. Evaluation of nanostructured composite collagen—chitosan matrices for tissue engineering. *J Tissue Eng* **7**, 203, 2001.
101. Chen, G., Ushida, T., and Tateishi, T. Development of biodegradable porous scaffolds for tissue engineering. *Mater Sci Eng C Mater Biol Appl* **17**, 63, 2001.
102. Huang, L., Nagapudi, K., Apkarian, P.R., and Chaikof, E.L. Engineered collagen—PEO nanofibers and fabrics. *J Biomater Sci Polym Ed* **12**, 979, 2001.
103. Nguyen, L.H., Kudva, A.K., Saxena, N.S., and Roy, K. Engineering articular cartilage with spatially-varying matrix composition and mechanical properties from a single stem cell population using a multi-layered hydrogel. *Biomaterials* **32**, 6946, 2011.
104. Nguyen, L.H., Kudva, A.K., Guckert, N.L., Linse, K.D., and Roy, K. Unique biomaterial compositions direct bone marrow stem cells into specific chondrocytic phenotypes corresponding to the various zones of articular cartilage. *Biomaterials* **32**, 1327, 2011.
105. Rosa, A.L., de Oliveira, P.T., and Beloti, M.M. Macroporous scaffolds associated with cells to construct a hybrid biomaterial for bone tissue engineering. *Expert Rev Med Devices* **5**, 719, 2008.
106. Oliveira, A.L., and Reis, R.L. Pre-mineralization of starch/polycaprolactone bone tissue engineering scaffolds by a calcium-silicate-based process. *J Mater Sci Mater Med* **15**, 533, 2004.
107. Annabi, N., Fathi, A., Mithieux, S.M., Weiss, A.S., and Dehghani, F. Fabrication of porous PCL/elastin composite scaffolds for tissue engineering applications. *J Supercrit Fluids* **59**, 157, 2011.
108. Kim, H.-W., Knowles, J.C., and Kim, H.-E. Hydroxyapatite/poly(ε-CL) composite coatings on hydroxyapatite porous bone scaffold for drug delivery. *Biomaterials* **25**, 1279, 2003.
109. Kang, Y., Scully, A., Young, D.A., Kim, S., Tsao, H., Sen, M., and Yang, Y. Enhanced mechanical performance and biological evaluation of a PLGA coated beta-TCP composite scaffold for load-bearing applications. *Eur Polym J* **47**, 1569, 2011.
110. Lickorish, D., Ramshaw, J.A.M., Werkmeister, J.A., Glat-tauer, V., and Howlett, C.R. Collagen-hydroxyapatite composite prepared by biomimetic process. *J Biomed Mater Res A* **68**, 19, 2004.
111. Chen, G., Ushida, T., and Tateishi, T. Poly(DL-lactic-co-glycolic acid) sponge hybridized with collagen microsponges and deposited apatite particulates. *J Biomed Mater Res* **57**, 8, 2001.
112. Groeneveld, E.H.J., Van Den Bergh, J.P.A., Holzmann, P., Ten Bruggenkate, C.M., Tuinzing, D.B., and Burger, E.H.

- Mineralization processes in demineralized bone matrix grafts in human maxillary sinus floor elevations. *J Biomed Mater Res* **48**, 393, 1999.
113. Huttmacher, D.W. Scaffolds in tissue engineering bone and cartilage. *Biomaterials* **21**, 2529, 2000.
 114. Kneser, U., Voogd, A., Ohnolz, J., Buettner, O., Stangenberg, L., Zhang, Y.H., Stark, G.B., and Schaefer, D.J. Fibrin gel-immobilized primary osteoblasts in calcium phosphate bone cement: *in vivo* evaluation with regard to application as injectable biological bone substitute. *Cells Tissues Organs* **179**, 158, 2005.
 115. Leong, K.F., Cheah, C.M., and Chua, C.K. Solid freeform fabrication of three-dimensional scaffolds for engineering replacement tissues and organs. *Biomaterials* **24**, 2363, 2003.
 116. Desai, T.A. Micro- and nanoscale structures for tissue engineering constructs. *Med Eng Phys* **22**, 595, 2001.
 117. Webster, T.J., and Ejirofor, J.U. Increased osteoblast adhesion on nanophase metals: Ti, Ti6Al4V, and CoCrMo. *Biomaterials* **25**, 4731, 2004.
 118. Popat, K.C., Daniels, R.H., Dubrow, R.S., Hardev, V., and Desai, T.A. Nanostructured surfaces for bone biotemplating applications. *Orthop Res Rev* **24**, 619, 2006.
 119. Mantila Roosa, S.M., Kempainen, J.M., Moffitt, E.N., Krebsbach, P.H., and Hollister, S.J. The pore size of polycaprolactone scaffolds has limited influence on bone regeneration in an *in vivo* model. *J Biomed Mater Res A* **92**, 359, 2010.
 120. Kasten, P., Beyen, I., Niemeyer, P., Luginbuhl, R., Bohner, M., and Richter, W. Porosity and pore size of beta-tricalcium phosphate scaffold can influence protein production and osteogenic differentiation of human mesenchymal stem cells: An *in vitro* and *in vivo* study. *Acta Biomater* **4**, 1904, 2008.
 121. Kuboki, Y., Takita, H., Kobayashi, D., Tsuruga, E., Inoue, M., Murata, M., Nagai, N., Dohi, Y., and Ohgushi, H. BMP-induced osteogenesis on the surface of hydroxyapatite with geometrically feasible and nonfeasible structures: Topology of osteogenesis. *J Biomed Mater Res* **39**, 190, 1998.
 122. Story, B.J., Wagner, W.R., Gaisser, D.M., Cook, S.D., and Rust-Dawicki, A.M. In vivo performance of a modified CSTi dental implant coating. *Int J Oral Maxillofac Implants* **13**, 749, 1998.
 123. Roy, T.D., Simon, J.L., Ricci, J.L., Rekow, E.D., Thompson, V.P., and Parsons, J.R. Performance of degradable composite bone repair products made via three-dimensional fabrication techniques. *J Biomed Mater Res* **66**, 283, 2003.
 124. Kruij, M.C., De Bruijn, J.D., Wilson, C.E., Oner, F.C., Van Blitterswijk, C.A., Verbout, A.J., and Dhert, W.J.A. Viable osteogenic cells are obligatory for tissue-engineered ectopic bone formation in goats. *Tissue Eng* **9**, 327, 2003.
 125. Takahashi, Y., and Tabata, Y. Effect of the fiber diameter and porosity of non-woven PET fabrics on the osteogenic differentiation of mesenchymal stem cells. *J Biomater Sci Polym Ed* **15**, 41, 2004.
 126. Oh, S.H., Park, I.K., Kim, J.M., and Lee, J.H. *In vitro* and *in vivo* characteristics of PCL scaffolds with pore size gradient fabricated by a centrifugation method. *Biomaterials* **28**, 1664, 2007.
 127. Karageorgiou, V., and Kaplan, D. Porosity of 3D biomaterial scaffolds and osteogenesis. *Biomaterials* **26**, 5474, 2005.
 128. Hulbert, S.F., Young, F.A., Mathews, R.S., Klawitter, J.J., Talbert, C.D., and Stelling, F.H. Potential of ceramic materials as permanently implantable skeletal prostheses. *J Biomed Mater Res* **4**, 433, 1970.
 129. Narayan, D., and Venkatraman, S.S. Effect of pore size and interpore distance on endothelial cell growth on polymers. *J Biomed Mater Res A* **87A**, 710, 2008.
 130. Akay, G., Birch, M.A., and Bokhari, M.A. Microcellular polyHIPE polymer supports osteoblast growth and bone formation *in vitro*. *J Biomed Mater* **25**, 3991, 2004.
 131. Kuboki, Y., Jin, Q., and Takita, H. Geometry of carriers controlling phenotypic expression in BMP-induced osteogenesis and chondrogenesis. *Instr Course Lect* **83 A Suppl 1**, S105, 2001.
 132. Kim, K., Yeatts, A., Dean, D., and Fisher, J.P. Stereolithographic bone scaffold design parameters: osteogenic differentiation and signal expression. *Tissue Eng Part B* **16**, 523, 2010.
 133. Gomes, M.E., Sikavitsas, V.I., Behraves, E., Reis, R.L., and Mikos, A.G. Effect of flow perfusion on the osteogenic differentiation of bone marrow stromal cells cultured on starch-based three-dimensional scaffolds. *J Biomed Mater Res* **67A**, 87, 2003.
 134. Uebersax, L., Hagenmuller, H., Hofmann, S., Gruenblatt, E., Muller, R., Vunjak-Novakovic, G., Kaplan, D.L., Merkle, H.P., and Meinel, L. Effect of scaffold design on bone morphology *in vitro*. *Tissue Eng* **12**, 3417, 2006.
 135. Pamula, E., Filova, E., Bacakova, L., Lisa, V., and Adamczyk, D. Resorbable polymeric scaffolds for bone tissue engineering: the influence of their microstructure on the growth of human osteoblast-like MG 63 cells. *J Biomed Mater Res A* **89A**, 432, 2009.
 136. Bai, F., Wang, Z., Lu, J., Liu, J., Chen, G., Lv, R., Wang, J., Lin, K., Zhang, J., and Huang, X. The correlation between the internal structure and vascularization of controllable porous bioceramic materials *in vivo*: a quantitative study. *Tissue Eng Part A* **16**, 3791, 2010.
 137. Ghanaati, S., Barbeck, M., Orth, C., Willershausen, I., Thimm, B.W., Hoffmann, C., Rasic, A., Sader, R.A., Unger, R.E., Peters, F., and Kirkpatrick, C.J. Influence of beta-tricalcium phosphate granule size and morphology on tissue reaction *in vivo*. *Acta Biomater* **6**, 4476, 2010.
 138. Klenke, F.M., Liu, Y., Yuan, H., Hunziker, E.B., Siebenrock, K.A., and Hofstetter, W. Impact of pore size on the vascularization and osseointegration of ceramic bone substitutes *in vivo*. *J Biomed Mater Res A* **85A**, 777, 2008.
 139. Sant, S., Hancock, M.J., Donnelly, J.P., Iyer, D., and Khademhosseini, A. Biomimetic gradient hydrogels for tissue engineering. *Can J Chem Eng* **88**, 899, 2010.
 140. Seidi, A., Ramalingam, M., Elloumi-Hannachi, I., Ostrovidov, S., and Khademhosseini, A. Gradient biomaterials for soft-to-hard interface tissue engineering. *Acta Biomater* **7**, 1441, 2011.
 141. Hall, S.J. *Basic Biomechanics*. Boston, MA: McGraw-Hill, 2007.
 142. Ozkan, S., Kalyon, D.M., and Yu, X. Functionally graded β -TCP/PCL nanocomposite scaffolds: *in vitro* evaluation with human fetal osteoblast cells for bone tissue engineering. *J Biomed Mater Res A* **92A**, 1007, 2010.
 143. Eriskin, C., Kalyon, D.M., and Wang, H. Functionally graded electrospun polycaprolactone and beta-tricalcium phosphate nanocomposites for tissue engineering applications. *Biomaterials* **29**, 4065, 2008.
 144. Marklein, R.A., and Burdick, J.A. Spatially controlled hydrogel mechanics to modulate stem cell interactions. *Soft Matter* **6**, 136, 2010.

145. Yang, Y., and Liu, Y. Method for making ceramic articles, including ceramic scaffolds for bone repair. US61/131, 810, 2008.
146. Yang, Y., and Liu, Y. Method for making ceramic articles, including ceramic scaffolds for bone repair. PCT/US 09/03501, 2009.
147. Liu, Y., Kim, J.-H., Young, D., Kim, S., Nishimoto, S.K., and Yang, Y. Novel template-casting technique for fabricating β -tricalcium phosphate scaffolds with high interconnectivity and mechanical strength and *in vitro* cell responses. *J Biomed Mater Res* **92A**, 997, 2010.
148. Shanti, R.M., Janjanin, S., Li, W.-J., Nesti, L.J., Mueller, M.B., Tzeng, M.B., and Tuan, R.S. In vitro adipose tissue engineering using an electrospun nanofibrous scaffold. *Ann Plast Surg* **61**, 566, 2008.
149. Jang, J.-H., Castano, O., and Kim, H.-W. Electrospun materials as potential platforms for bone tissue engineering. *Adv Drug Deliv Rev* **61**, 1065, 2009.
150. Zhang, X., Li, X., Fan, H., and Liu, X. Nano-hydroxyapatite/polymer composite scaffold for bone tissue engineering. *Key Eng Mater* **330**, 365, 2007.
151. Cevat, E., Dilhan, M.K., and Hongjun, W. A hybrid twin screw extrusion/electrospinning method to process nanoparticle-incorporated electrospun nanofibres. *Nanotechnol* **19**, 165302, 2008.
152. Ergun, A., Yu, X., Valdevit, A., Ritter, A., and Kalyon, D.M. *In vitro* analysis and mechanical properties of twin screw extruded single-layered and coextruded multilayered poly(caprolactone) scaffolds seeded with human fetal osteoblasts for bone tissue engineering. *J Biomed Mater Res A* **99A**, 354, 2011.
153. Ergun, A., Chung, R., Ward, D., Valdevit, A., Ritter, A., and Kalyon, D.M. Unitary bioresorbable cage/core bone graft substitutes for spinal arthrodesis coextruded from polycaprolactone biocomposites. *Ann Biomed Eng* **40**, 1073, 2011.
154. Andersson, H., and van den Berg, A. Microfabrication and microfluidics for tissue engineering: state of the art and future opportunities. *Lab Chip* **4**, 98, 2004.
155. Whitesides, G.M., Ostuni, E., Takayama, S., Jiang, X., and Ingber, D.E. Soft lithography in biology and biochemistry. *Annu Rev Biomed Eng* **3**, 335, 2001.
156. Goodman, S.L., Sims, P.A., and Albrecht, R.M. Three-dimensional extracellular matrix textured biomaterials. *Biomaterials* **17**, 2087, 1996.
157. Abrams, G.A., Goodman, S.L., Nealey, P.F., Franco, M., and Murphy, C.J. Nanoscale topography of the basement membrane underlying the corneal epithelium of the rhesus macaque. *Cell Tissue Res* **299**, 39, 2000.
158. Park, T.H., and Shuler, M.L. Integration of cell culture and microfabrication technology. *Biotechnol Prog* **19**, 243, 2003.
159. Kane, R.S., Takayama, S., Ostuni, E., Ingber, D.E., and Whitesides, G.M. Patterning proteins and cells using soft lithography. *Biomaterials* **20**, 2363, 1999.
160. Lu, X., and Leng, Y. Comparison of the osteoblast and myoblast behavior on hydroxyapatite microgrooves. *J Biomed Mater Res B Appl Biomater* **90B**, 438, 2009.
161. Lu, X., and Leng, Y. Quantitative analysis of osteoblast behavior on microgrooved hydroxyapatite and titanium substrata. *J Biomed Mater Res* **66A**, 677, 2003.
162. Holthaus, M.G., Stolle, J., Treccani, L., and Rezwan, K. Orientation of human osteoblasts on hydroxyapatite-based microchannels. *Acta Biomater* **8**, 394, 2012.
163. Kirmizidis, G., and Birch, M. Microfabricated grooved substrates influence cell-cell communication and osteoblast differentiation *in vitro*. *Tissue Eng Part A* **15**, 1427, 2009.
164. Hamilton, D.W., Chehroudi, B., and Brunette, D.M. Comparative response of epithelial cells and osteoblasts to microfabricated tapered pit topographies *in vitro* and *in vivo*. *Biomaterials* **28**, 2281, 2007.
165. Mapili, G., Lu, Y., Chen, S., and Roy, K. Laser-layered microfabrication of spatially patterned functionalized tissue-engineering scaffolds. *J Biomed Mater Res B Appl Biomater* **75**, 414, 2005.
166. Lan, P.X., Lee, J.W., Seol, Y.J., and Cho, D.W. Development of 3D PPF/DEF scaffolds using micro-stereolithography and surface modification. *J Mater Sci Mater Med* **20**, 271, 2009.
167. Subramani, K., and Birch, M.A. Fabrication of poly(ethylene glycol) hydrogel micropatterns with osteoinductive growth factors and evaluation of the effects on osteoblast activity and function. *Biomed Mater* **1**, 144, 2006.
168. Leclerc, E., David, B., Griscom, L., Lepioufle, B., Fujii, T., Layrolle, P., and Legallais, C. Study of osteoblastic cells in a microfluidic environment. *Biomaterials* **27**, 586, 2006.
169. Lovett, M., Lee, K., Edwards, A., and Kaplan, D.L. Vascularization strategies for tissue engineering. *Tissue Eng Part B* **15**, 353, 2009.
170. Moon, J.J., and West, J.L. Vascularization of engineered tissues: approaches to promote angiogenesis in biomaterials. *Curr Top Med Chem* **8**, 300, 2008.
171. Nichol, J.W., Koshy, S.T., Bae, H., Hwang, C.M., Yamanlar, S., and Khademhosseini, A. Cell-laden micro-engineered gelatin methacrylate hydrogels. *Biomaterials* **31**, 5536, 2010.
172. Hahn, M.S., Miller, J.S., and West, J.L. Three-dimensional biochemical and biomechanical patterning of hydrogels for guiding cell behavior. *Adv Mater* **18**, 2679, 2006.
173. Leslie-Barbick, J.E., Shen, C., Chen, C., and West, J.L. Micron-scale spatially patterned, covalently immobilized vascular endothelial growth factor on hydrogels accelerates endothelial tubulogenesis and increases cellular angiogenic responses. *Tissue Eng Part A* **17**, 221, 2011.
174. Hahn, M.S., Taite, L.J., Moon, J.J., Rowland, M.C., Ruffino, K.A., and West, J.L. Photolithographic patterning of poly(ethylene glycol) hydrogels. *Biomaterials* **27**, 2519, 2006.
175. Moon, J.J., Hahn, M.S., Kim, I., Nsiah, B.A., and West, J.L. Micropatterning of poly(ethylene glycol) diacrylate hydrogels with biomolecules to regulate and guide endothelial morphogenesis. *Tissue Eng Part A* **15**, 579, 2009.
176. Moon, J.J., Saik, J.E., Poche, R.A., Leslie-Barbick, J.E., Lee, S.H., Smith, A.A., Dickinson, M.E., and West, J.L. Biomimetic hydrogels with pro-angiogenic properties. *Biomaterials* **31**, 3840, 2010.
177. Aubin, H., Nichol, J.W., Hutson, C.B., Bae, H., Sieminski, A.L., Crokek, D.M., Akhyari, P., and Khademhosseini, A. Directed 3D cell alignment and elongation in micro-engineered hydrogels. *Biomaterials* **31**, 6941, 2010.
178. Dike, L.E., Chen, C.S., Mrksich, M., Tien, J., Whitesides, G.M., and Ingber, D.E. Geometric control of switching between growth, apoptosis, and differentiation during angiogenesis using micropatterned substrates. *In Vitro Cell Dev Biol Anim* **35**, 441, 1999.
179. Dickinson, L.E., Moura, M.E., and Gerecht, S. Guiding endothelial progenitor cell tube formation using patterned fibronectin surfaces. *Soft Matter* **6**, 5109, 2010.
180. Raghavan, S., Nelson, C.M., Baranski, J.D., Lim, E., and Chen, C.S. Geometrically controlled endothelial tubulogenesis in micropatterned gels. *Tissue Eng Part A* **16**, 2255, 2010.

181. Ling, Y., Rubin, J., Deng, Y., Huang, C., Demirci, U., Karp, J.M., and Khademhosseini, A. A cell-laden microfluidic hydrogel. *Lab Chip* **7**, 756, 2007.
182. Golden, A.P., and Tien, J. Fabrication of microfluidic hydrogels using molded gelatin as a sacrificial element. *Lab Chip* **7**, 720, 2007.
183. Choi, N.W., Cabodi, M., Held, B., Gleghorn, J.P., Bonassar, L.J., and Stroock, A.D. Microfluidic scaffolds for tissue engineering. *Nat Mater* **6**, 908, 2007.
184. King, K.R., Wang, C.C.J., Kaazempur-Mofrad, M.R., Vacanti, J.P., and Borenstein, J.T. Biodegradable microfluidics. *Adv Mater* **16**, 2007, 2004.
185. Borenstein, J.T., Terai, H., King, K.R., Weinberg, E.J., Kaazempur-Mofrad, M.R., and Vacanti, J.P. Microfabrication technology for vascularized tissue engineering. *Biomed Microdevices* **4**, 167, 2002.
186. Moroni, L., Schotel, R., Sohler, J., de Wijn, J.R., and van Blitterswijk, C.A. Polymer hollow fiber three-dimensional matrices with controllable cavity and shell thickness. *Biomaterials* **27**, 5918, 2006.
187. Yang, Y., Kang, Y., Sen, M., and Park, S. Bioceramics in tissue engineering. In: Burdick, J.A., and Mauck, R.L., ed. *Biomaterials for Tissue Engineering: A Review of the Past and Future Trends*. New York: Springer Wien New York, 2010, pp. 179.
188. Mata, A., Boehm, C., Fleischman, A.J., Muschler, G., and Roy, S. Analysis of connective tissue progenitor cell behavior on polydimethylsiloxane smooth and channel micro-textures. *Biomed Microdevices* **4**, 267, 2002.
189. Murphy, W.L., Peters, M.C., Kohn, D.H., and Mooney, D.J. Sustained release of vascular endothelial growth factor from mineralized poly(lactide-co-glycolide) scaffolds for tissue engineering. *Biomaterials* **21**, 2521, 2000.
190. Tuzlakoglu, K., Pashkuleva, I., Rodrigues, M.T., Gomes, M.E., van Lenthe, G.H., Müller, R., and Reis, R.L. A new route to produce starch-based fiber mesh scaffolds by wet spinning and subsequent surface modification as a way to improve cell attachment and proliferation. *J Biomed Mater Res A* **92A**, 369, 2010.
191. Sun, H., Qu, Z., Guo, Y., Zang, G., and Yang, B. *In vitro* and *in vivo* effects of rat kidney vascular endothelial cells on osteogenesis of rat bone marrow mesenchymal stem cells growing on polylactide-glycolic acid (PLGA) scaffolds. *Biomed Eng Online* **6**, 41, 2007.
192. Tian, X.F., Heng, B.C., Ge, Z., Lu, K., Rufaihah, A.J., Fan, V.T., Yeo, J.F., and Cao, T. Comparison of osteogenesis of human embryonic stem cells within 2D and 3D culture systems. *Scand J Clin Lab Invest* **68**, 58, 2008.
193. Kim, S., Kim, S.S., Lee, S.H., Eun Ahn, S., Gwak, S.J., Song, J.H., Kim, B.S., and Chung, H.M. *In vivo* bone formation from human embryonic stem cell-derived osteogenic cells in poly(d,l-lactic-co-glycolic acid)/hydroxyapatite composite scaffolds. *Biomaterials* **29**, 1043, 2008.
194. Costa-Pinto, A.R., Correlo, V.M., Sol, P.C., Bhattacharya, M., Charbord, P., Delorme, B., Reis, R.L., and Neves, N.M. Osteogenic differentiation of human bone marrow mesenchymal stem cells seeded on melt based chitosan scaffolds for bone tissue engineering applications. *Biomacromolecules* **10**, 2067, 2009.
195. Jin, Q.M., Takita, H., Kohgo, T., Atsumi, K., Itoh, H., and Kuboki, Y. Effects of geometry of hydroxyapatite as a cell substratum in BMP-induced ectopic bone formation. *J Biomed Mater Res* **52**, 491, 2000.
196. Yu, H., VandeVord, P.J., Gong, W., Wu, B., Song, Z., Matthew, H.W., Wooley, P.H., and Yang, S.-Y. Promotion of osteogenesis in tissue-engineered bone by pre-seeding endothelial progenitor cells-derived endothelial cells. *J Orthop Res* **26**, 1147, 2008.

Address correspondence to:

Ali Khademhosseini, Ph.D.

Harvard-MIT Division of Health Sciences and Technology
Massachusetts Institute of Technology
Cambridge, MA 02139

E-mail: alik@rics.bwh.harvard.edu

Yunzhi Yang, Ph.D.

Department of Orthopedic Surgery
Stanford University
Stanford, CA 94305

E-mail: ypyang@stanford.edu

Received: January 11, 2012

Accepted: April 18, 2012

Online Publication Date: September 4, 2012